MISSOURI S&T

CENTER FOR TRANSPORTATION INFRASTRUCTURE AND SAFETY

High-Strength Self-Consolidating Concrete (SCC) and High-Volume Fly Ash Concrete (HVFAC) for Infrastructure Elements: Implementation

Bridge A7957 – Route 50
Osage County Missouri

by

Dr. John J. Myers, P.E. (PI)
Eli S. Hernandez
Alexander Griffin
Hayder Alghazali

August 2014

A National University Transportation Center at Missouri University of Science and Technology

NUTC R315

Disclaimer

The contents of this report reflect the views of the author(s), who are responsible for the facts and the accuracy of information presented herein. This document is disseminated under the sponsorship of the Department of Transportation, University Transportation Centers Program and the Center for Transportation Infrastructure and Safety NUTC program at the Missouri University of Science and Technology, in the interest of information exchange. The U.S. Government and Center for Transportation Infrastructure and Safety assumes no liability for the contents or use thereof.

Technical Report Documentation Page

1. Report No.	2. Government Accession No.	3. Recipient's Catalog No.
NUTC R315		

4. Title and Subtitle	5. Report Date
High-Strength Self-Consolidating Concrete (SCC) and High-Volume Fly Ash Concrete (HVFAC) for Infrastructure Elements: Implementation	August 2014
	6. Performing Organization Code

7. Author/s	8. Performing Organization Report No.
Dr. John J. Myers, P.E. (PI), Eli S. Hernandez, Alexander Griffin, Hayder Alghazali	Project #00040350

9. Performing Organization Name and Address	10. Work Unit No. (TRAIS)
Center for Transportation Infrastructure and Safety/NUTC program Missouri University of Science and Technology 220 Engineering Research Lab Rolla, MO 65409	11. Contract or Grant No. DTRT06-G-0014

12. Sponsoring Organization Name and Address	13. Type of Report and Period Covered
U.S. Department of Transportation Research and Innovative Technology Administration 1200 New Jersey Avenue, SE Washington, DC 20590	Final
	14. Sponsoring Agency Code

15. Supplementary Notes

16. Abstract

Because of its unique nature, high-strength self-consolidating concrete (HS-SCC) has the potential to significantly reduce costs associated with transportation-related infrastructure, benefiting both MoDOT and the residents of Missouri. HS-SCC is a highly flowable, nonsegregating concrete that can be placed without any mechanical consolidation, and thus has the following advantages over conventional concrete: decreased labor and equipment costs during concrete placement, decreased potential for and costs to repair honeycombing and voids, increased production rates of precast and cast-in-place (CIP) elements, and improved finish and appearance of cast and free concrete surfaces.

In addition to SCC, innovative materials, such as high volume fly ash concrete (HVFAC), also provide a significant potential to produce more cost effective mix designs for CIP concrete. Since the 1930's, fly ash – a pozzolanic material – has been used as a partial replacement of portland cement in concrete to improve the material's strength and durability, while also limiting the amount of early heat generation. From an environmental perspective, replacing cement with fly ash reduces the concrete's overall carbon footprint and diverts an industrial by-product from the solid waste stream (currently, about 40 percent of fly ash is reclaimed for beneficial reuse and 60 percent is disposed of in landfills). The objective of this research is to provide an implementation test bed and showcase for the use of sustainable and extended service life concrete.

In this implementation study for Missouri Bridge A7957, a level of 50% fly ash to cement proportions was utilized as well as normal strength self-consolidating concrete (NS-SCC) and HS-SCC in the load carrying elements to showcase the use of these innovative materials.

17. Key Words	18. Distribution Statement
Bridges, self-consolidating concrete, high-volume fly ash concrete, precast girders, sustainable concrete, durability behavior, live load test, finite element modeling	No restrictions. This document is available to the public through the National Technical Information Service, Springfield, Virginia 22161.

19. Security Classification (of this report)	20. Security Classification (of this page)	21. No. Of Pages	22. Price
unclassified	unclassified	272	

Form DOT F 1700.7 (8-72)

NUTC Project 00040350

High-Strength Self-Consolidating Concrete (SCC) and High-Volume Fly Ash Concrete (HVFAC) for Infrastructure Elements: Implementation

Bridge A7957 – Route 50

Osage County, Missouri

Prepared by:

Dr. John J. Myers, P.E. (PI)

Eli S. Hernandez

Alexander Griffin

Hayder Alghazali

Missouri University of Science & Technology

Department of Civil, Architectural & Environmental Engineering

August 2014

EXECUTIVE SUMMARY

Because of its unique nature, self-consolidating concrete (SCC) has the potential to significantly reduce costs associated with transportation-related infrastructure, benefiting both MoDOT and the residents of Missouri. SCC is a highly flowable, nonsegregating concrete that can be placed without any mechanical consolidation, and thus has the following advantages over conventional concrete: decreased labor and equipment costs during concrete placement, decreased potential for and costs to repair honeycombing and voids, increased production rates of precast and cast-in-place (CIP) elements, and improved finish and appearance of cast and free concrete surfaces.

In addition to SCC, innovative materials, such as high volume fly ash concrete (HVFAC), also provide a significant potential to produce more cost effective mix designs for CIP concrete. Since the 1930's, fly ash – a pozzolanic material – has been used as a partial replacement of portland cement in concrete to improve the material's strength and durability, while also limiting the amount of early heat generation. From an environmental perspective, replacing cement with fly ash reduces the concrete's overall carbon footprint and diverts an industrial by-product from the solid waste stream (currently, about 40 percent of fly ash is reclaimed for beneficial reuse and 60 percent is disposed of in landfills).

The objective of this research is to provide an implementation test bed and showcase for the use of sustainable and extended service life concrete. In this implementation study for Missouri Bridge A7957, a level of 50% fly ash to cement proportions was utilized as well as normal strength self-consolidating concrete (NS-SCC) and HS-SCC in the load carrying elements to showcase the use of these innovative materials.

ACKNOWLEDGEMENTS

The authors would like to acknowledge the financial support for this investigation from the Missouri Department of Transportation (MoDOT) and the National University Transportation Center (NUTC) at the Missouri University of Science and Technology in Rolla. The efforts by many individuals from MoDOT throughout this project are greatly acknowledged. Special thanks are given to Jennifer Harper and Anousone Arounpradith from the Missouri Department of Transportation. The staff and technician support from the Center of Infrastructure Engineering Studies (CIES) and the Department of Civil, Architectural and Environmental Engineering (CArEE) are greatly appreciated. Support from the fabricator, County Materials Corporation, in Bonne Terre, MO and the contractor, Fred Weber, Inc., of Maryland Heights, MO is also greatly acknowledged. This project would not have been possible or accomplished without the support from so many.

TABLE OF CONTENTS

LIST OF ILLUSTRATIONS

LIST OF TABLES

NOMENCLATURE

Symbol	Description
a_g	Maximum aggregate size
A_{ps}	Area of prestressing steel
A_s	Area of longitudinal non-prestressing steel
A_v	Area of shear reinforcement at spacing s
b_w	Width of web
b_v	Effective web width
d	Distance from extreme compression fiber to centroid of longitudinal tension reinforcement
d_p	Distance from extreme compression fiber to centroid of prestressing steel
d_v	Effective shear depth
E_c	Modulus of elasticity of concrete
E_p	Modulus of elasticity of prestressing steel
E_s	Modulus of elasticity of non-prestressing steel
f'_c	Compressive strength of concrete
f'_{ci}	Compressive strength of concrete at release
f_{cl}	Compressive stress at a strain value of 0.00005
f_d	Compressive stress in concrete due to unfactored dead load at the extreme fiber of the section where tensile stress is caused by externally applied loads
f_{pc}	Compressive stress at the centroid of the concrete section due to the effective prestress force
f_{pe}	Compressive stress in concrete due to effective prestress only at extreme fiber of section where tensile stress is caused by externally applied loads
f_{po}	Locked in difference in strain between the prestressing steel and and surrounding concrete multiplied by the modulus of elasticity of the prestressing steel
f_{pu}	Specified ultimate strength of prestressing steel
f_r	Modulus of rupture

f_t	Splitting tensile strength of concrete
f_{yt}	Specified yield strength of the transverse reinforcement (ACI)
f_y	Specified yield strength of transverse reinforcement (AASHTO)
h	Depth of section
H	Relative humidity
I	Gross moment of inertia
K_1	Factor accounting for type of aggregate
k_1	Factor accounting for source of aggregate
k_2	Factor accounting for type of cementitious material
k_f	Factor accounting for concrete strength
k_{hc}	Factor accounting for humidity of concrete (creep)
k_{hs}	Factor accounting for humidity of concrete (shrinkage)
k_s	Factor for volume to surface ratio of the specimen
k_{td}	Time development factor
M_{cre}	Flexural cracking moment
M_{max}	Maximum factored moment at the section due to externally applied loads
M_u	Factored moment at section
N_u	Factored axial force at section
R	Hydration rate of concrete
s	Slump of concrete
s	Center to center spacing of transverse shear reinforcement
s_x	Cracking spacing parameter
s_{xe}	Equivalent value of s_x which allows for influence of aggregate size
t	Age of specimen
t_i	Age of specimen after load is applied
t_{la}	Concrete age at loading
V/S	Volume to surface ratio
V_c	Concrete contribution to shear resistance
V_{ci}	Nominal shear resistance when diagonal cracking results from applied shear and moment

V_{cw}	Nominal shear resistance when diagonal cracking results from high principal stresses in the web
V_d	Applied shear force at section due to unfactored dead load
V_i	Factored shear force at section due to externally applied loads
V_n	Nominal shear resistance
V_p	Vertical component of effective prestress force at section
V_s	Transverse reinforcement contribution to shear resistance
V_u	Factored shear force at section
w	Unit weight of concrete (AASHTO)
w_c	Unit weight of concrete (ACI)
y_t	Distance from centroid of concrete section to tension face
α	Air content
$\alpha_{concrete}$	Coefficient of thermal expansion of concrete
β	Factor indicating ability of diagonally cracked concrete to transmit tension
$\Delta\varepsilon_{temp}$	Measured change in strain due to temperature
ΔT	Difference in measured temperatures
ε_{cl}	Strain at 40% of the ultimate stress
ε_s	Net longitudinal strain at centroid of longitudinal reinforcement
ε_{sh}	Drying shrinkage
γ_{la}	Correction factor for age of loading
γ_s	Correction factor for slump
γ_{cc}	Correction factor for cement content
$\gamma_{V/S}$	Correction factor for volume to surface ratio
γ_α	Correction factor for air content
γ_λ	Correction factor for ambient relative humidity
γ_ψ	Correction factor for fine aggregate percentage
λ	Reduction factor for lightweight concrete
λ	Ambient relative humidity
ψ	Ratio of fine aggregate to total aggregate by weight
$\psi(t,t_i)$	Creep coefficient
ϕ	Strength reduction factor

θ	Angle of inclination of diagonal compressive stress in concrete
AASHTO	American Association of State Highway and Transportation Officials
ACI	American Concrete Institute
CA	Coarse aggregate
CC	Conventional concrete
CTE	Coefficient of thermal expansion
FA	Fine aggregate
HS-SCC	High strength self-consolidating concrete
HSC	High strength concrete
HRWR	High range water reducer
HRWRA	High range water reducing admixture
HVFAC	High volume fly-ash concrete
MSA	Maximum size of coarse aggregate
MOE	Modulus of elasticity
MOR	Modulus of rupture
NASP	North American Strand Producers Association
NS-SCC	Normal strength self-consolidating concrete
NU	Nebraska University
SCC	Self-consolidating concrete
STS	Splitting tensile strength
VWSG	Vibrating wire strain gauge

1. INTRODUCTION

1.1. BACKGROUND

Due to recent catastrophes in our nation's aging infrastructure, there is a need to develop resilient concrete mix designs for precast prestressed (PC/PS) bridges that will extend beyond the current 50 year service life.

To accomplish this goal, innovative concrete mix designs have been developed. Self-consolidating concrete (SCC) has been implemented in bridge infrastructure most notably in Japan and Europe. However, its implementation for PC/PS concrete bridges in the United States has been limited due to insufficient test bed applications. Additionally, high volume fly ash concrete (HVFAC) has been implemented at 30% replacement levels; there is little evidence of replacement levels on the order of 50% as investigated in this study.

SCC has been documented to reduce both costs associated with fabrication and long-term maintenance as well as expedite the construction process. Without a need for mechanical vibration, there is a reduction in labor cost and a reduced risk for employee injuries. However, the modifications required of the mix design to produce a flowable, nonsegregating concrete provide reluctance in the full scale application of this concrete. Reductions in both the size and proportions of coarse aggregate and an increase in the paste content hinder some mechanical properties: namely the modulus of elasticity, creep, and shrinkage with respect to conventional concrete. This in turn can lead to increased deflections and prestress losses. These material modifications, coupled with lower water to cementitious materials (w/cm) ratio, can create problems regarding the post-cracking shear behavior of high strength self-consolidating concrete (HS-SCC).

In addition to the environmental benefits of using replacement levels of fly ash in concrete, the fly ash can also reduce the heat generation during curing. The long-term strength gaining characteristics of HVFAC also correlate to a tighter concrete matrix, leading to improved durability properties.

In recent years, the use of high strength concrete (HSC), noted as a design strength equal to or greater than 8,000 psi (55 MPa), has created a demand for more economical and efficient cross sections for PC/PS concrete bridge elements. This

resulted in the development of the Nebraska University (NU) cross section at the University of Nebraska-Lincoln in Omaha, Nebraska in the early 1990's. Not only is the cross section more suitable for high strength concretes, but also easily enables the transformation of a traditional simple-span PC/PS concrete bridge to a continuous structure. As of 2006, the MoDOT began implementing the NU Series into their new bridge construction.

Following the laboratory findings at Missouri University of Science and Technology (Missouri S&T) with regards to SCC and HVFAC (Reports TRyy1103 and TRyy1110, respectively), the MoDOT proceeded to move forward with a full scale implementation of these innovative materials.

This study combines the efforts of previous work at Missouri S&T regarding normal strength self-consolidating concrete (NS-SCC), HS-SCC, and HVFAC with the NU girder series into a three span, PC/PS continuous concrete bridge along Highway 50 in Osage County, Missouri. In addition to the construction of the bridge, the shear resistance of the HS-SCC was examined in a full-scale laboratory testing using the NU girder cross section.

1.2. RESEARCH PROGRAM

1.2.1. Research Team.

Dr. John Myers, professor at Missouri S&T, served as the principal investigator (PI) for the project. Dr. Jeffrey Volz, former assistant professor at Missouri S&T, served as a co-principal investigator before leaving the university in the summer of 2013. Eli Hernandez served as the lead graduate assistant, with assistance from Alex Griffin and Hayder Alghazali. Graduate student Benjamin Gliha also helped with the instrumentation during the fabrication process of the bridge girders. Reed Norphy and Michael Janke, undergraduate students at Missouri S&T, helped with material testing and preparation. Jason Cox (Senior Research Specialist) and John Bullock (Research Laboratory Technician) at the Center for Infrastructure Engineering Studies (CIES) at Missouri S&T, helped with instrumentation and preparation of the NU girders for destructive testing. Technical help with data programming and collection and destructive girder testing was done by Brian Swift (Electronic Research Engineer) and Gary Abbott (Senior Research

Electronic Technician) from the Department of Civil, Architectural, and Environmental Engineering (CArEE) at Missouri S&T. The research was completed through careful coordination between the Missouri Department of Transportation (MoDOT), Fred Weber, Inc. of Maryland Heights, MO, and County Materials Corporation of Bonne Terre, MO. The program was funded by the MoDOT and the National University Transportation Center (NUTC) at Missouri S&T.

1.2.2. Destructive Testing of Precast-Prestressed NU Girders.

Two precast, prestressed full scale NU girders were fabricated at County Materials Corporation and tested for shear capacity at the Butler Carlton Civil Engineering Hall Structural Engineering Research Laboratory (SERL). The girders were constructed with the same cross section as was used in construction of the bridge on Highway 50 in Osage County. A 6 in. (152 mm) thick CIP concrete deck was fabricated on top of each girder to simulate the road deck on the bridge. The cross section is illustrated in Figure 1-1.

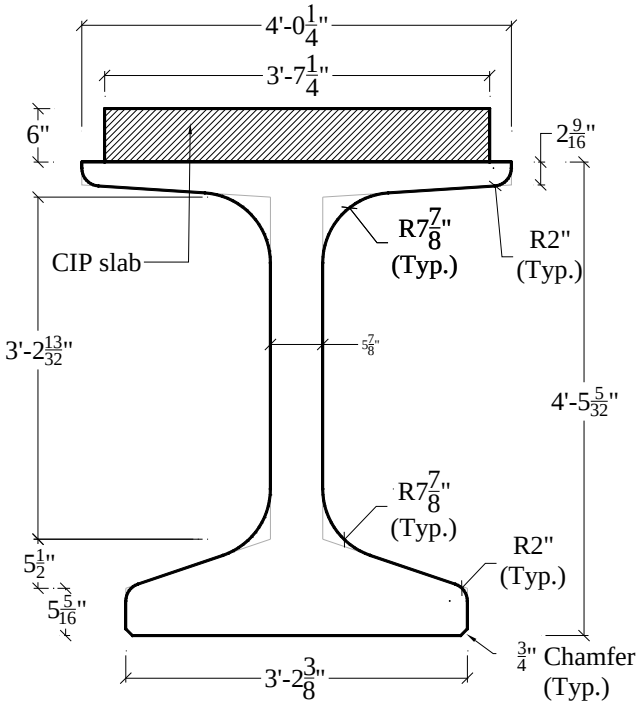

Conversion: 1 in. = 25.4 mm

Figure 1-1. Test Girder Cross Section

Both girders were 40 ft.-10 in. (12.4 m) long, with a total of 16 Grade 270 (1,862 MPa) prestressed low-relaxation prestressed tendons, 4 of which were harped.

Figure 1-2 illustrates the locations of the prestressed tendons at the end of the girder and at mid-span. Each girder had three distinct sections of shear reinforcement described in Table 1-1: a middle 10 ft. (3.05 m) region and two 15 ft. (4.57 m) end regions. Both Grade 70 ksi (483 MPa) welded wire reinforcement and Grade 60 ksi (414 MPa) mild steel bars were investigated. Each end region was tested in shear, and external strengthening was provided in the non-tested region during each test. The girders had a target design strength of 10,000 psi (68.9 MPa) and a release strength of 8,000 psi (55.2 MPa). Design drawings provided by MoDOT are located in Appendix A.

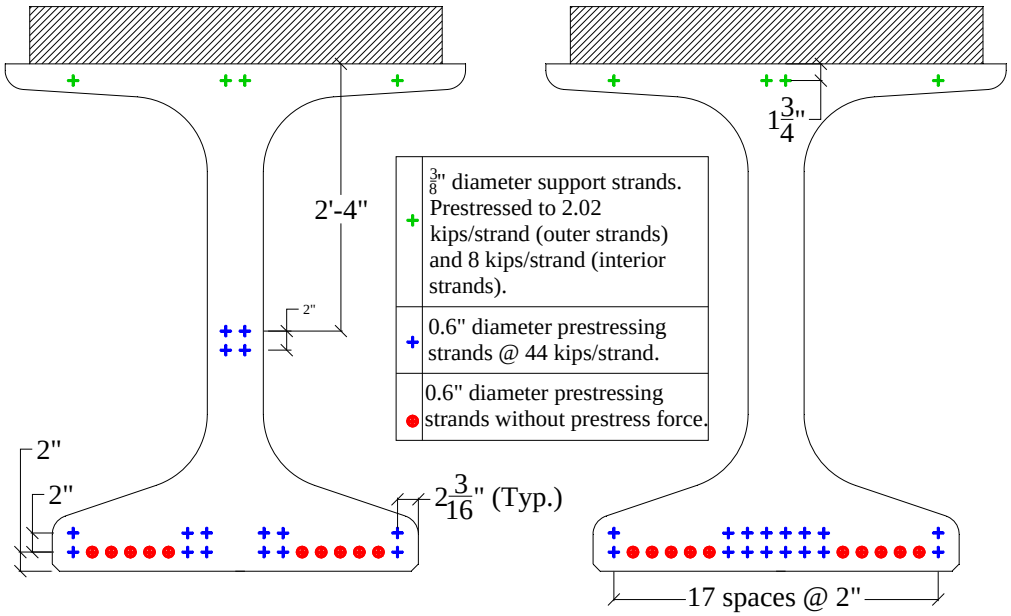

a) Ends b) Mid-span

Conversion 1 in. = 25.4 mm

Figure 1-2. NU Test Girder Strand Layout

Table 1-1. Test Girder Shear Reinforcement

Test Girder	Shear Regions		
	Region 1	Region 2	Region 3
1	D20 spaced at 12 in.	D20 spaced at 4 in.	No Shear Reinforcement
2	#5 spaced at 24 in.	#5 spaced at 12 in.	No Shear Reinforcement

1.2.3. Bridge Details.

Bridge A7957 is located along Highway 50 in Osage County shown in Figure 1-3. Latitude and longitude coordinates of the site are 38 29 39.11 N, 91 59 14.00 W. The bridge was constructed adjacent to bridge A3425 as part of a two lane expansion of Highway 50. The bridge consists of three continuous precast-prestressed concrete spans, two exterior 100 ft. (30.5 m) spans and one interior 120 ft. (36.6 m) span. Precast-prestressed concrete panels extend between spans in the transverse direction below a CIP concrete deck. Two intermediate bents and two abutments support the superstructure. The bridge has a superelevation of 2.0%. An elevation view and cross section of the bridge are shown in Figure 1-4 and Figure 1-5.

Figure 1-3. Bridge A7957 Location

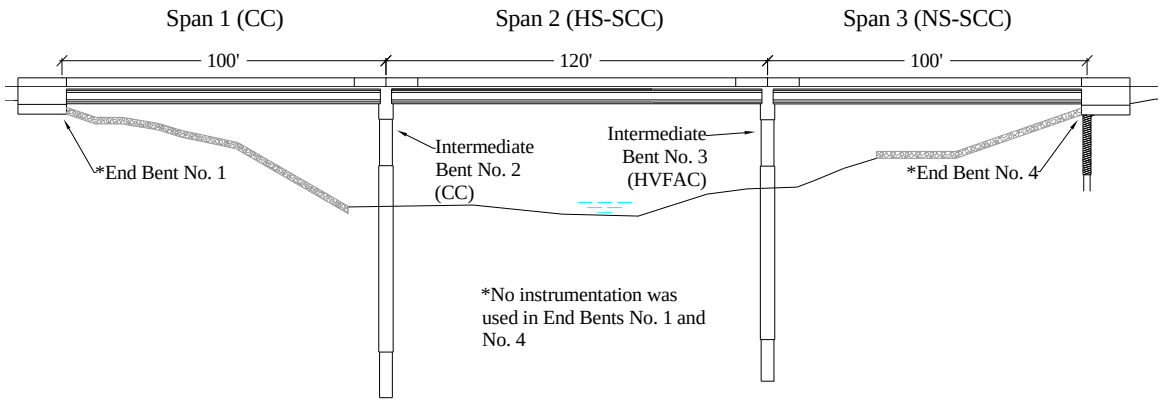

Conversion: 1 ft. = 0.3048 m

Figure 1-4. Bridge A7957 Elevation View

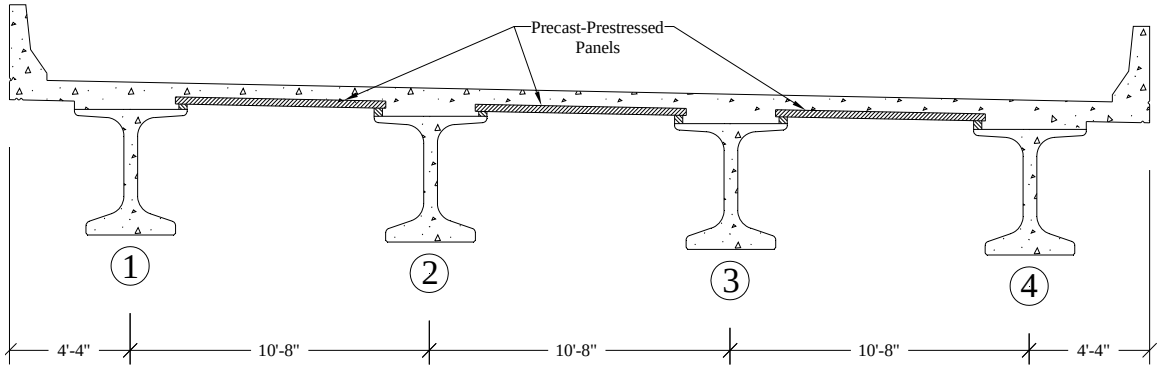

Conversion: 1 in. = 25.4 mm

Figure 1-5. Bridge A7957 Cross Section Looking East

1.2.3.1 Precast-Prestressed NU Girder.

Each span consisted of four precast-prestressed NU 53 girders. Girders in Span 1 and 3 each had 30 Grade 270 ksi (1,862 MPa) low-relaxation prestressing strands, 10 of which were harped, while span 2 consisted of 38 Grade 270 (1,862 MPa) low-relaxation prestressing strands. Cross sectional dimensions are illustrated in Figure 1-6. The strand arrangement for each span at the ends and at mid-span is displayed in Figure 1-7 and Figure 1-8. D20 welded wire reinforcement was provided for shear resistance at spacing intervals of 4 in., 8 in., and 12 in. (101.6, 203.2, and 304.8 mm, respectively) along the length of the girder. The design strength of spans 1 and 3 was 8,000 psi (55.2 MPa) with a release strength of 6,500 psi (44.8 MPa). Span 2 had a design strength of 10,000 psi (68.9 MPa) with a release strength of 8,000 psi (55.2 MPa). Design drawings provided by MoDOT can be found in Appendix A.

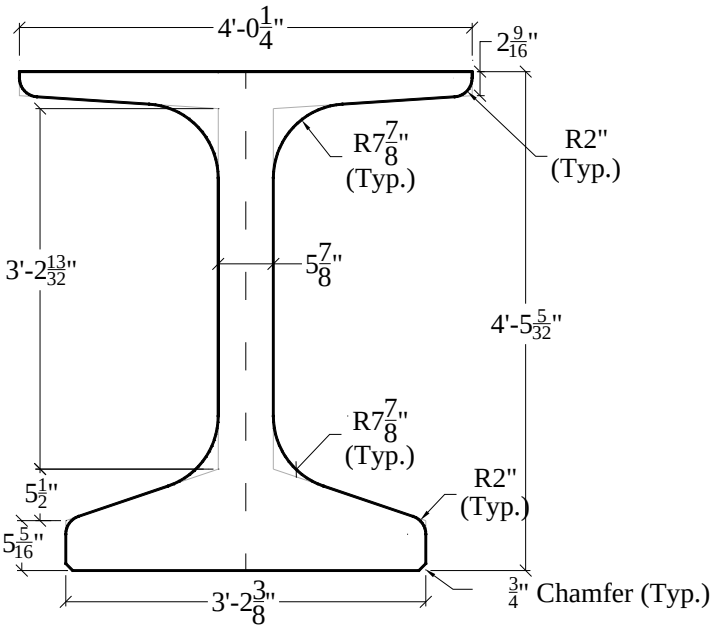

Conversion: 1 in. = 25.4 mm

Figure 1-6. NU Bridge Girder Cross Section

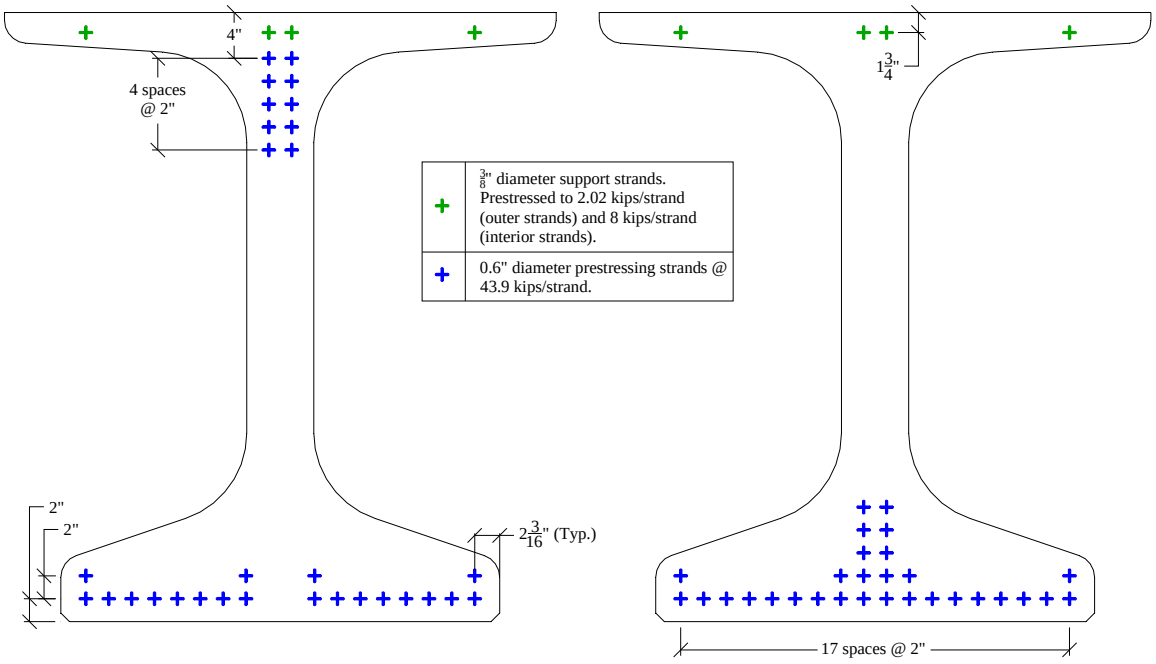

Conversion: 1 in. = 25.4 mm

a) Ends b) Mid-span

Figure 1-7. NU Girder Spans 1 & 3 Strand Layout

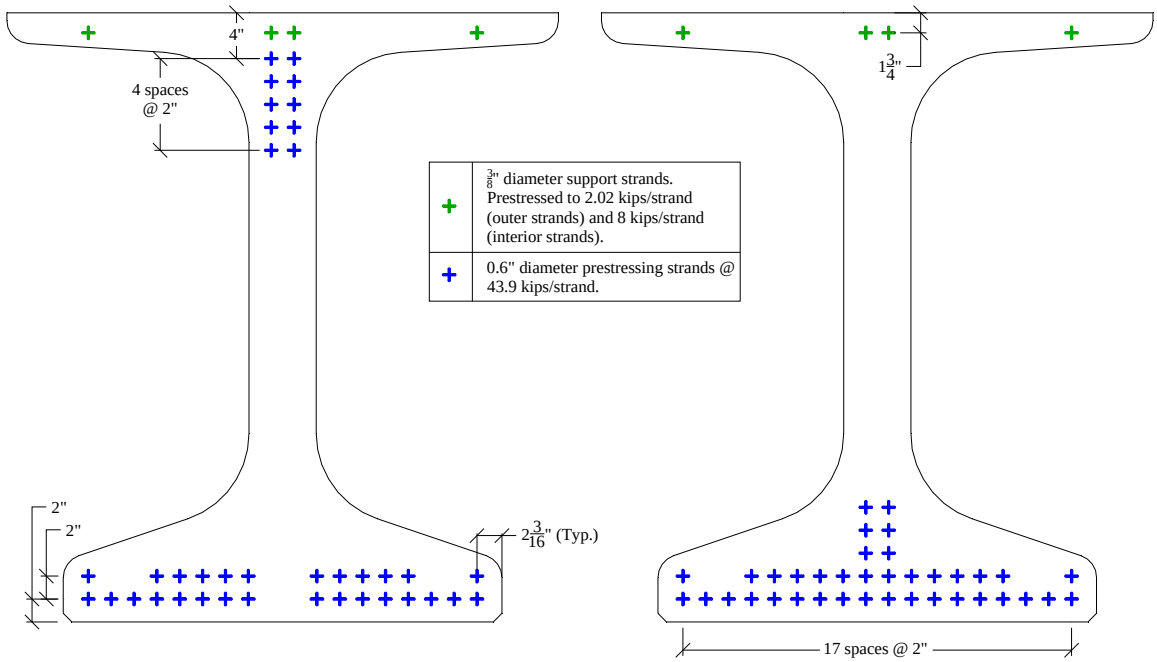

Conversion: 1 in. = 25.4 mm

a) Ends b) Mid-span

Figure 1-8. NU Girder Span 2 Strand Layout

1.2.3.2 Intermediate Bents.

Two intermediate bents identified previously in Figure 1-4 were investigated in the study. Both bents were identical with the exception of the material properties of the concrete. Intermediate bent no. 3 used HVFAC while intermediate bent no. 2 consisted of MoDOT's standard conventional concrete 'B' mix. Each intermediate bent consisted of two columns, an integral web wall and the pier cap. The columns and web wall were cast as one unit while the pier cap was cast as a second unit. The target design strength of bent 3 (HVFAC) and bent 2 was 3,000 psi (20.7 MPa). An elevation view is provided below in Figure 1-9.

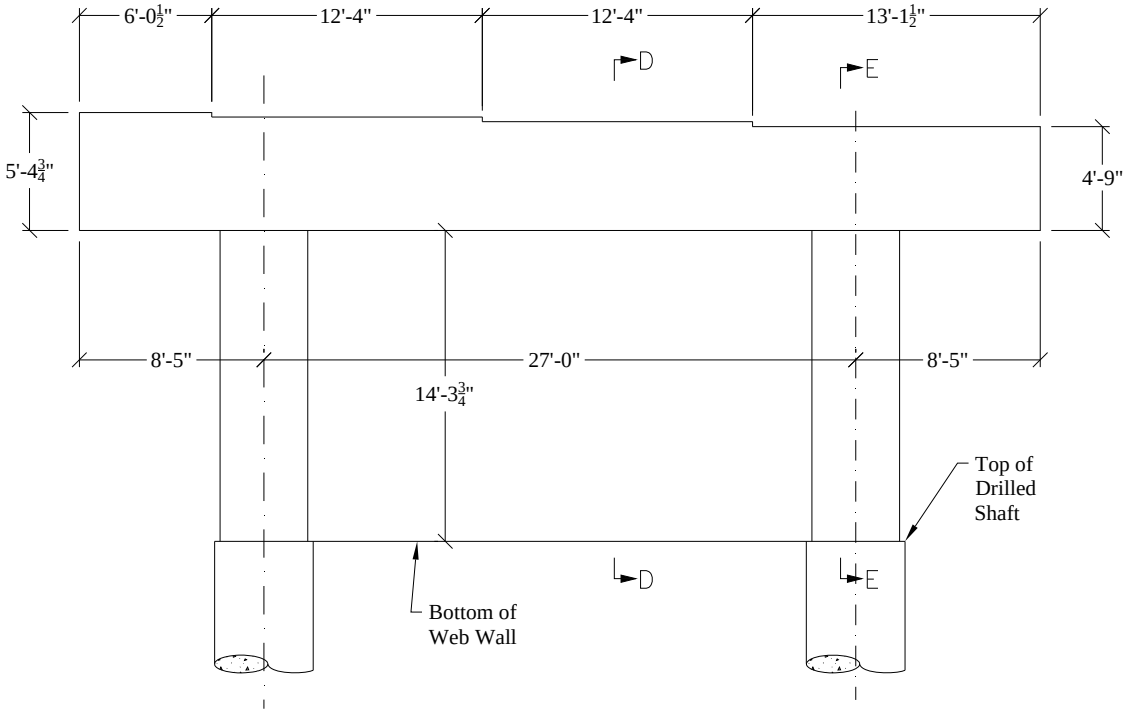

(a) East Elevation

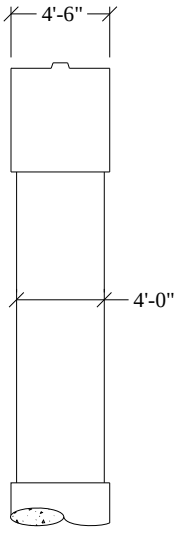

(b) Section E-E

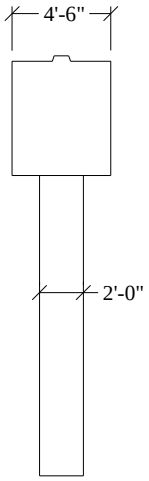

(c) Section D-D

Conversion: 1 in. = 25.4 mm

Figure 1-9. Intermediate Bent Elevation View

1.2.3.3 Bridge Elements and Numbering.

The superstructure and substructure elements of Bridge A7957 were labeled for consistency during the course of the research program. The bents were numbered 1 through 4 from west to east. Spans were labeled S1 through S3 from west to east, and girders were labeled G1 through G4 from north to south. Each girder had a unique abbreviation identifying the span number and girder number, i.e., S1-G3 for span 1-2, girder 3. Only girder lines 3 and 4 included instrumentation within the member. The numbering sequence is shown below in Figure 1-10.

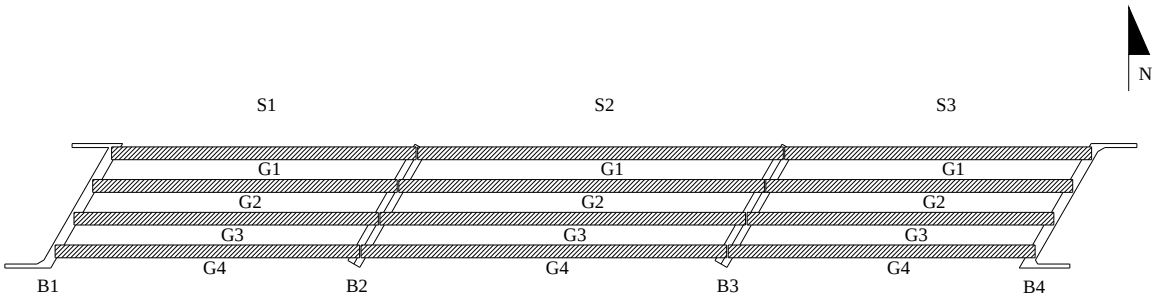

Figure 1-10. Bridge A7957 Numbering Scheme

1.3. WORK PLAN

A work plan was drafted for this research program to outline the major tasks involved in the project. Ten major tasks were identified in the work plan for *MoDOT FRP Proposal Number: TRyy123*6. The tasks are listed here with the original instrumentation plan in Appendix B.

1. Pre-Construction Planning and Coordination
2. Development of Bridge Instrumentation Plan and Load Testing Plan (Bridge A7957)
    - Addressed in Section 5.3
3. Mix Design and Quality Control Procedures/Quality Assurance – Trial Mixes
    - Addressed in Section 5.1 with results located in Section 6.1.1
4. Shear Testing and Evaluation of HS-SCC Precast NU Girders
    - Addressed in Section 5.2 with results located in Section 6.2
5. Precast-Prestressed Plant Specimen Instrumentation and Fabrication
    - Addressed in Section 5.3 and 5.5
6. Field Cast-In-Place Elements and Instrumentation

- Addressed in Section 5.3

7. Hardened Properties of Plant and Field Produced Concrete
    - Results located in Section 6.1
8. Bridge Load Testing and Monitoring/Evaluation of Experimental Load Testing Results
    - To be included in final MoDOT report
9. Reporting/Technology Transfer
10. Value to MoDOT and Stakeholders to Implementing SCC/HVFAC
    - To be included in final MoDOT report

1.4. SCOPE OF THE REPORT

This report includes the instrumentation, fabrication, construction, and load testing plan of bridge A7957 in Osage County Missouri. First, three trial mixes of HVFAC, NS-SCC, and HS-SCC were batched and collected for quality assurance of the following mechanical properties: compressive strength, modulus of elasticity, and splitting tensile strength. After the trial mix specimens were collected and tested, two precast-prestressed HS-SCC NU 53 girders were tested in shear to validate the shear resistance with ACI and AASHTO design codes. For Bridge A7957, HVFAC and CC (MoDOT's class B mixture) were used in the substructure (columns, web walls, and pier caps) to compare the strength gaining characteristics and hydration profiles via thermocouple wire. Each of the three spans of the bridge was unique: the first span (span 1-2) utilized CC (MoDOT's class A-1 mixture), the second span (span 2-3) HS-SCC, and the third span (span 3-4) NS-SCC. The in-situ performance of the bridge girders was investigated using vibrating wire strain gauges (VWSG) and a high performance Total Station (TS). The serviceability and structural performance were monitored and evaluated from fabrication to service conditions via a load test. Additional load test(s) will be performed to study the long-term behavior of the concrete members. Furthermore, material properties were collected from the three concretes and compared including: compressive strength, modulus of elasticity, modulus of rupture, shrinkage, creep, and coefficient of thermal expansion. Freeze-thaw, chloride penetration, and abrasion resistance tests were also performed on the concrete of the CIP deck (MoDOT modified

class B-2 mixture). More details about the MoDOT's standard concrete mixtures are given in Section 2.6. During the course of this research, the MoDOT's mixes class A-1 and class B were referred to as conventional concrete (CC) mixes when they were compared to their counterpart mixes: NS-SCC, HS-SCC and HVFAC.

1.5. ORGANIZATION OF THE REPORT

The report is organized into six sections. Section 1 contains an overview of the research program including the shear testing of the NU girders as well as general bridge details and numbering sequence. The instrumentation plan is also described as referenced from Appendix B of the MoDOT RFP Proposal Number: TRyy1236.

A literature review of SCC, HS-SCC, and HVFAC, and MoDOT's mix designs used in the study is addressed in section 2. Shear behavior and properties of HS-SCC are included.

Section 3 contains the material testing program. A plethora of tests were conducted on the different concretes investigated during the program from compressive strength to creep and shrinkage to abrasion resistance.

The measurement types and systems are listed in section 4. Concrete temperatures and strains and member deflections were recorded. Among others, vibrating wire strain gauges (VWSG) were the primary instrumentation used during the program. The data collection system is also included in section 4.

Section 5 describes the chronological progression of events in the research program. The trial mixes were first conducted, followed by the destructive shear testing of the NU girders, and finally the member instrumentation and fabrication. The construction of the bridge is documented regarding girder erection, the CIP deck, approach slabs, and safety barriers. The load test plan is also included followed by problems that were encountered in the study.

The preliminary results of the study are documented in Section 6. All material test results for the various concretes with the exception of creep tests are documented. The results of the shear testing of the NU girders are included and compared with ACI and AASHTO predictions. Preliminary conclusions are drawn and an overview of the final report is discussed.

2. LITERATURE REVIEW

2.1. SCC

2.1.1. Definition.

According to ACI 237R-07, self-consolidating concrete (SCC) is a highly flowable, non-segregating concrete that can spread into place, fill the formwork and encapsulate the reinforcement without any mechanical vibration. SCC has numerous advantages over conventional concrete (CC) which includes:

- Reduce equipment, labor, and associated cost;
- Less need for screeding operations to ensure flat surface (self-leveling characteristics);
- Is cast with desired mechanical properties which is independent of the skill of the vibrating crew;
- Accelerated construction;
- Facilitates filling complex formwork or members with congested reinforcement;
- Decrease employee injuries;
- Permits more flexible reinforcement detailing and design; and
- Creates smooth, aesthetically appealing surfaces free of honeycombing and signs of bleeding and discoloration.

All of these benefits can be obtained through the use of conventional concrete materials and admixtures and, in some cases, with high viscosity-modifying admixture (VMA).

2.1.2. Fresh Material Properties.

The definition of SCC includes properties that are related to the fresh state of the concrete. Terms as flowable, nonsegregating, and fill refer to standardized tests that have been developed with definable quantitative measurements and suggested ranges.

Table 2-1, taken from NCHRP Report 628 (also ACI 237R 2007), summarizes the fresh properties of interest that were utilized for this implementation project. In addition, the associated test methods (standard and non-standard), suggested test result targets, and

recommendations related to whether these tests should be conducted for routine quality control or as part of an SCC mix design program are presented.

Table 2-1. Suggested Fresh Property Tests (Mix Design and Quality Control)

Property	Test Method	Target Values	Design	QC
Filling ability	Slump flow T-50 (ASTM C1611)	23.5-29 in (600-735 mm) 1.5-6 s (upright cone position)	√	√
Passing ability	J-Ring flow (ASTM C1621)	21.5-26 in (545-660 mm) 0-3 in. (0-75 mm)	√	√
Filling capacity	Slump flow and J-Ring flow tests			√
Static stability	Column segregation (ASTM C 1610)	Column segregation index (C.O.V.) ≤ 5%. Percent static segregation (S) ≤ 15%	√	
Air volume	AAHTO T 152	4% - 7% depending on exposure conditions, MSA, and type of HRWRA.	√	√

MSA: Maximum size of coarse aggregate

An important aspect of the suggested SCC fresh concrete quality control tests is that these can be satisfied by a combination of ASTM standardized tests, namely the slump flow, J-ring flow and the air content tests. The slump flow and J-ring tests are simple and have demonstrated repeatability. In addition, both tests have to be conducted within 6 minutes to be in conformance with the standard (ASTM C1621 2009).

The slump flow test is a measure of mixture filling ability, and it is performed similarly to the conventional slump test using the standard ASTM C143/C 143M slump cone. Instead of measuring the slumping distance vertically, the mean spread of the resulting concrete patty is measured horizontally. The value obtained is recorded as the slump flow (ACI 237R 2007).

The J-ring comprises a ring of reinforcing bars that will fit around the base of a standard ASTM C 143/C 143M slump cone. The slump cone is filled with concrete and then lifted in the same way a slump flow test is conducted. The final spread of the concrete is measured, and the difference between the conventional slump flow and the J-ring slump flow values is calculated (ACI 237R 2007).

The column segregation test, as prescribed in ASTM C1610, evaluates the static stability of a concrete mixture by quantifying aggregate segregation. A 26 in. (610 mm) high column is filled with concrete. The concrete is allowed to sit for 15 minutes after placement. The column has three parts that are removed individually. The concrete from the top and bottom sections is washed over a No. 4 (4.75 mm) sieve, and the retained aggregate is weighed. A nonsegregating mixture will have consistent aggregate mass distribution between the top and bottom sections. A segregating mixture will have a higher concentration of aggregate in the lower section (ACI 237R 2007).

SCC mixtures used in PC/PS concrete girders should displayed a slump flow value of 23.5 to 29 in. (600-735 mm). In addition, a J-Ring flow value within a range of 21.5 to 26.0 in. (545 to 660 mm), and a difference in slump flow and J-Ring flow values lower than 4 in. (100 mm) should be displayed. Regardless of the MSA, stable SCC should develop a column segregation index (C.O.V.) less than 5% and percent static segregation lower than 15% (Khayat and Mitchell 2009).

Viscosity modifying admixtures (VMA) can be used to reduce the impact of material variability and improve the robustness of the designed SCC. However, it is important to prevent using VMA as a substitute of a well-formulated mix design or poor quality constituents. In addition, a careful selection of constituent materials, and a continuous quality assurance program (EFNARC 2006) are necessary.

Table 2-2 presents some slump flow test values as well as slump flow minus J-ring flow test values recommended by NCHRP that are based on the intended application of SCC (Khayat and Mitchell 2009). The fresh characteristics of SCC are described in terms of the two simple tests described early, namely the slump flow and J-ring tests. In 2006, Hwang concluded that the filling capacity is best described by a combination of passing ability and non-restricted deformability test (Hwang et al. 2006) such as the two shown in Table 2-2.

Table 2-2. Workability Values of SCC Used in Precast/Prestressed Applications

		Slump flow, in			Slump flow – J-ring flow, in		
Relative Values		23.5-25	25-27.5	27.5-29	3-4	2-3	≤2
Low	Reinforcement density	■				■	
Medium			■			■	
High				■			■
Small	Shape intricacy	■				■	
Moderate			■			■	
Congested				■			■
Shallow	Depth	■			■		
Moderate			■			■	
Deep			■				■
Short	Length	■				■	
Moderate			■			■	
Long			■				■
Thin	Thickness		■				■
Moderate			■			■	
Thick		■				■	
Low	Coarse Aggregate			■			■
Medium				■		■	
High		■			■		

2.1.3. Hardened Material Properties.

The mixture proportions may be adjusted to obtain a SCC concrete with similar or better hardened properties than those of a conventional concrete mixture. The following sections give an insight of the most important aspects that influence key mechanical properties when the SCC mixture is being developed.

2.1.3.1 Compressive strength.

The strength of SCC mixtures is highly affected by the water to cementitious material (w/cm) ratio, age, powder content (cement and supplementary cementitious

materials), curing conditions, admixtures used, aggregate gradation and surface texture (Mindess et al. 2003). SCC mixtures usually require a high flowable concrete with enough cohesion to improve the stability of the mixture. This requires SCC concrete mixtures to have a lower w/cm when compared to traditional concrete mixtures. As a result of using a lower w/cm (typically between 0.32 and 0.40), higher compressive strengths are attained. The enhanced compressive strength is the result of the lack of vibration and reduction of bleeding and segregation that promotes a more uniform microstructure and less porous interface zone between the aggregate, paste and embedded reinforcement (ACI 237R 2007).

2.1.3.2 Modulus of elasticity.

The modulus of elasticity (MOE) in concrete is affected by the compressive strength, aggregate type and content, and unit weight of concrete. SCC concrete mixtures typically have a decrease in the MOE because of the lower coarse aggregate and higher paste proportions utilized in their production. Various researchers have reported that for equal compressive strength, the elastic modulus of SCC can be as much as 10 to 15% lower than that of conventional concrete with similar compressive strength (ACI 237R 2007). Because MOE controls the response of RC and PC elements to load as well as the camber, creep and shrinkage, it is mandatory to quantify and understand the reduction in MOE for the mixtures in use.

2.1.3.3 Tensile strength.

The tensile strength of concrete is determine by two separate tests: modulus of rupture (MOR) test (determined in accordance to ASTM C 78 or C 293), and splitting tensile strength (STS) test (determined in accordance to ASTM C 496). The tensile strength of SCC also depends on the w/cm, coarse aggregate volume, and the quality of the interface between aggregate and cement paste. Some researchers have reported that SCC may exhibit higher tensile strength than conventional concrete with similar batch proportions (ACI 237R 2007).

2.1.3.4 Creep and shrinkage.

Creep and shrinkage are mostly influenced by the coarse aggregate volume and stiffness, rigidity of the cement paste and concrete, curing time, curing method, temperature, relative humidity, and concrete age at time of load application. Creep and

shrinkage of SCC is affected by the mixture composition, paste volume and aggregate content. The high paste volumes and reduction in the aggregate content used in SCC mixtures results in a greater potential for shrinkage and creep. Shrinkage has been reported to be similar to or lower than that of CC with similar compressive strength. Creep is expected to be similar for SCC and CC with similar mixture proportions. When SCC is proportioned with a greater paste volume, a higher creep is exhibited than it is for a CC with similar compressive strength. In addition, Persson (1999), reported that for mature SCC and CC with similar properties, the creep coefficient was compatible when the strength at load application was similar and held constant (ACI 237R 2007).

2.2. HS-SCC

2.2.1. Definition.

High strength self-consolidating concrete uses the benefits of SCC with the added strength gain of HSC. ACI 363 defines high strength concrete as concrete with a specified concrete compressive strength for design of 8,000 psi (55 MPa) or greater (ACI 363 2010). Additionally, consideration must be taken when applying design equations in the ACI 318 code and AASHTO LRFD Bridge Design Specifications as many empirical relations were developed from data with compressive strengths less than 8,000 psi (ACI 318 2011, AASHTO 2012). A review of the mechanical and shear properties of this innovative material is presented.

2.2.2. Fresh Material Properties.

The plastic state of HS-SCC is expected to be similar to that of NS-SCC. The reduced w/cm ratio in HS-SCC can lead to greater static stability (ACI 237 2007).

2.2.3. Hardened Material Properties.

2.2.3.1 Compressive strength.

The use of high-range water reducing admixtures (HRWRA) in HS-SCC mixes increases the compressive strength of equivalent HSC mixes (Myers et al. 2012). The HRWRA disperses the cement particles, which increases the proportion of cement particles available for hydration. Myers et al. (2012) also noted that the effect of the HRWRA increases as the compressive strength increases. This can be attributed to the lower w/cm ratio in high strength concrete mixes. Aforementioned results consisted of

dolomitic limestone coarse aggregate and a CA content of 48%, matching that used in this study. ACI 237R-07 also notes that, for a given w/cm ratio, SCC can achieve greater compressive strength than CC due to the reduction in bleeding and segregation resulting from mechanical vibration. Without vibration, SCC can achieve a more uniform microstructure with a less porous interfacial bond zone between the paste and aggregate (ACI 237R 2007).

2.2.3.2 Modulus of elasticity.

An understanding of the elastic modulus of HS-SCC is necessary to more accurately predict camber, deflections, shrinkage, creep, and prestress losses. The MOE of HS-SCC has typically been found to be less than that of conventional high-strength concrete. The reduction in stiffness can be attributed to the smaller percentage and size of the coarse aggregate. Additionally, the larger paste content in HS-SCC theoretically leads to a reduction in the modulus of elasticity. In 2007, Domone discovered that the reduction in MOE for SCC can vary from 40% to 5% for low and high strength concretes, respectively (Domone 2007). The reduction diminishes with compressive strength since high strength concretes already rely on the strength of the paste for stiffness. Various studies indicate that the AASHTO model more accurately predicts the MOE for SCC with crushed aggregate over ACI 363 and ACI 318 models (Khayat and Mitchell 2009; Long et al. 2013). Both ACI 363 and ACI 318 tend to underestimate the modulus of elasticity (Long et al. 2013).

2.2.3.3 Tensile strength.

The tensile strength of concrete is measured in two ways: splitting tensile strength (STS) test and modulus of rupture (MOR) test following ASTMs C496 and C78, respectively (ASTM C 496 2011, ASTM C 78 2010). The flexural strength depends on the w/cm ratio, coarse aggregate volume and the quality of the interface between the aggregate and cement paste. ACI 237 states that for a given set of mixture proportions, the flexural strength of SCC may be higher. However, Myers et al. (2012) found comparable results between HSC and HS-SCC in terms of MOR and STS tests.

2.2.3.4 Creep and shrinkage.

The creep and shrinkage of HS-SCC is expected to be greater than that of its high-strength concrete (HSC) counterpart for similar compressive strength, a result of the

smaller percentage and size of coarse aggregate as well as increased binder content of HS-SCC (Khayat and Mitchell 2009). Khayat and Mitchell found that for a given w/cm ratio, SCC exhibited 10-20% higher creep and 30% higher shrinkage than the HSC control mix. Additionally, for a given w/cm ratio, an increase in the binder content leads to an increase in drying shrinkage; this supports the trend that SCC mixes exhibit increased drying shrinkage than HSC. ACI 209 and AASHTO 2007 models underestimated both the drying shrinkage and creep for SCC mixes with Type I Portland cement (Khayat and Mitchell 2009).

In contrast, Myers et al. (2012) discovered that at a given w/cm ratio, HS-SCC exhibited less shrinkage and creep compared to HSC. This trend is confirmed at the University of Texas at Austin where the creep of HS-SCC was approximately 30% less than that of HSC when limestone was used. However, there was no difference in creep between the two mixes when river gravel aggregate was incorporated. The stiffness of the aggregate also contributes to the extent of creep in both conventional and SCC mixes. It was also noted that the AASHTO 2006 model best predicted the creep of the SCC mixtures containing limestone aggregate (Trejo et al. 2008). A more extensive parametric study should be undertaken to evaluate the effects of aggregate type, content and size in addition to the w/cm ratio and binder content.

2.2.4. Hydration Profile.

Due to the increased paste content in HS-SCC, these mixes experience greater temperature gradients during curing. ACI 363 states that a temperature rise of 11 to 15°F per 100 lb/yd^3 (10 to 14°C per 100 kg/m^3) cement is expected in HSC depending on the geometry of the structural element (ACI 363 2010). Myers and Carrasquillo discovered that hydration temperatures above 170°F (76.7°C) can lead to microcracking within the concrete, hindering strength and durability properties (Myers and Carrasquillo 1998).

2.2.5. Shear Characteristics.

A principal reason for hesitation in the implementation of HS-SCC lies in its reduced shear performance. The mechanisms which contribute to the shear strength of conventional prestressed concrete are listed as follows (Frosch and Wolf 2003):

- Uncracked concrete and the flexural compression zone. Shear is transferred through inclined principle tensile and compressive stresses.

- Aggregate interlock. As a crack forms around the aggregate, the protruded section creates a friction force that prevents slippage of the crack.
- Dowel action of longitudinal reinforcement. The reinforcement provides a vertical tension force that prevents slippage of the concrete.
- Residual tensile stresses across cracks. For hairline cracks, less than 0.006 in. (0.15 mm), the concrete can still bridge tensile stresses. However, this contribution is limited.

In the case of HS-SCC, modifications on material proportions, namely the reduced content and size of coarse aggregate, hinder the ability of the concrete to transmit shear stresses through aggregate interlock. Furthermore, when limestone aggregates are used in a HSC application, the failure plane can propagate through the aggregate particles, rather than at the paste-aggregate interface zone.

2.2.5.1 Push off test.

A collection of researchers have studied the shear response of HS-SCC in push off tests. This is a widely recognized test, used and refined by Mattock (1969 and 1972), Reinhardt (1981), Walraven (1981 and 1994), and (Sells 2012).

Sells discovered that the coarse aggregate fraction and concrete type (HS-SCC vs. HSC) showed little impact on the shear resistance of the specimens. There was a slight trend that showed reduced shear stress for a given crack opening for higher strength concretes. The smoother failure plane in the high strength specimens explains the results. However, there was no distinguishable difference in shear stress at a given crack opening between the HS-SCC and HSC mixes for a given aggregate type.

The most distinguishable findings related to the aggregate type. The limestone aggregate carried significantly less shear stress across a crack opening than the river gravel. Thus, the river gravel exhibited greater aggregate interlock (Sells 2012).

Kim et al observed similar trends regarding push off tests of high and low strength SCC and CC mixes. Push off tests revealed a decreasing contribution of aggregate interlock at high compressive strength level, and an increased contribution of river gravel over limestone aggregates. There was also statistically significant data which showed the volume of coarse aggregate influences the contribution of aggregate interlock.

Additionally, the researchers noted a lower fraction reduction factor, c, and friction coefficient, μ, for HS-SCC than HSC at maximum shear stress. The fraction reduction factor accounts for the reduced contact area at a crack due to particle fracturing. The smaller volume of coarse aggregate in HS-SCC explains this trend (Kim et al. 2010).

2.2.5.2 Mid-scale and full-scale beam tests.

There is limited evidence regarding beam shear testing on HS-SCC. In the case of SCC, there are mixed results concerning the ultimate shear capacity with respect to CC. Hassan et al. (2010) reported that SCC beams showed reduced shear resistance and ductility compared to their CC counterparts. Their results supported theory in which the ultimate shear stress decreases with an increase in the effective beam depth. Lin and Chen found that for an equivalent CA content, SCC beams had increased shear resistance; however, for typical SCC beams in which the CA content is lower than a CC mix for a given compressive strength, the shear resistance was found to be less than the CC beam (Lin and Chen 2012).

Sells conducted shear tests on mid-size precast-prestressed rectangular beams. His tests included high and low strength SCC and CC beams. The SCC and HS-SCC beams experienced increased deflections over the CC beams. This could be attributed to the lower modulus of elasticity reported in the SCC mixtures. The failure loads for the HS-SCC beams exceeded the predicted failure from ACI 318, AASHTO 2007, and modified compression field theory (MCFT) estimates. The normalized shear stress for the HS-SCC beams slightly outperformed that of the HSC mix shown in Figure 2-1. The HS-SCC mix is denoted by S10-48L and the HSC mix by C10-5L. The two HS-SCC beams exhibited less variation at ultimate failure loads than the HSC beams (Sells 2012). This could be attributed to the robustness of the SCC mixtures.

Full scale structural performance testing on AASHTO Type II girders was completed by Khayat and Mitchell. Four girders were fabricated from 8,000 and 10,000 psi (55 and 69 MPa, respectively) SCC as well as CC. The researchers noted the following in terms of shear performance (Khayat and Mitchell 2009):

- All four girders exceeded the nominal shear resistance according AASHTO 2007 specifications. However, the HS-SCC maximal shear load was 6.5% less than that of the 10,000 psi (69 MPa) CC girder.

- Both the HSC and HS-SCC girders experienced initial shear cracking at similar loads.
- The HS-SCC girders exhibited less ductility prior to shear failure.
- The reduced ductility and shear resistance associated with the SCC mixtures could be attributed to the reduction in coarse aggregate volume, thereby reducing the energy absorbing characteristic of aggregate interlock.

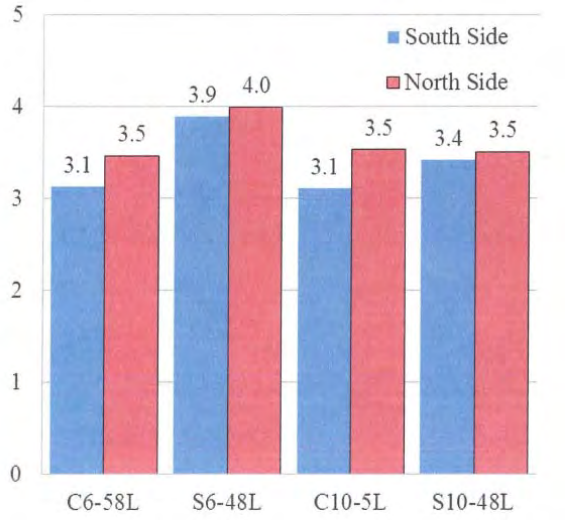

Figure 2-1. HS-SCC vs. HSC Ultimate Shear Stress (Sells 2012)

2.3. PREVIOUS PROJECTS USING SCC AND HS-SCC

Self-consolidating concrete has been widely implemented across Japan, Europe and the United States. ACI 237 cites sixteen references linked to the use of SCC in both the precast and cast-in-place industry. The production in the precast industry in the United States raised from 17,000 yd^3 in 2000 to 2.3 million yd^3 in 2003 and continues to climb to this day (ACI 237 2007). The use of SCC has been widespread; however, the implementation of HS-SCC in structural applications is extremely limited. Examples of the implementation of SCC include:

Shin-kiba Ohashi Bridge, Japan. SCC was used in the production of the cable stay bridge towers (Okamura and Ouchi 2003).

Ritto Bridge, Japan. Due to congested steel reinforcement and the need for high earthquake resistance, SCC was chosen for the pier construction. The specified compressive strength of the SCC mixture was 7,250 psi (50 MPa) (Ouchi et al. 2003).

Higashi-Oozu Viaduct, Japan. SCC was chosen to produce the precast-prestressed T-girders to alleviate noise complaints from vibration of the concrete and to create a smoother finished surface. The specified compressive strength used in the T-girders was 7,250 psi (50 MPa) (Ouchi et al. 2003).

Soda Lanken Project, Sweden. Difficulties in compaction of conventional concrete in rock lining, wall sections and arch sections in the tunnel led to project managers choosing SCC. The decision also provided an increased aesthetic appearance. The 28-day cube compressive strength ranged from 10,000 to 11,600 psi (70-80 MPa) (Ouchi et al. 2003).

Pedestrian Bridges, Rolla, Missouri. An implementation project comparing the use of HSC and HS-SCC concrete was conducted on two pedestrian bridges in Rolla, MO. Both the hardened properties and time-dependent deformations were studied via load tests. This was the only discovered project implementing HS-SCC in a bridge application (Myers and Bloch 2011).

Tauranga Harbour Link, Tauranga, New Zealand. Self-consolidating concrete was chosen to expand the multi-span existing bridge at the Port of Tauranga. The expansion was completed in the fall of 2010. SCC was chosen to achieve the goal 100 year design life in a harsh marine environment. Durability models predicted a useful design life ranging from 103 to 156 years depending on the structural element and level of clear cover. The design strength of the pretensioned beams was 8700 psi (60 MPa); however, to achieve the desired durability properties, the two SCC mix designs developed for the project had 28 day design cylindrical compressive strengths of 10,400 psi and 12,600 psi (71.5 and 87.0 MPa), respectively. By incorporating HS-SCC, the cost advantage for the design build team was 20% of the bid price, or $20 million dollars. This project provides a prime example of the cost savings associated with SCC (McSaveney et al. 2011).

2.4. HVFAC

2.4.1. Definition.

High volume fly ash (HVFA) concrete has been typically defined as concrete mixtures that contain more than 30% fly ash by mass of cementitious material (Volz et al. 2012; Naik et al. 1995). Other authors have defined HVFA concrete mixtures as having more than 50% fly ash by mass of cementitious material with a low water content of w/cm <0.40 (Reiner and Rens 2006).

2.4.2. Fresh Material Properties.

2.4.2.1 Workability.

Bouzoubaa et al. (2010) evaluated the effects of varying the fly ash contents and the required dosage of HRWRA on the concrete mixtures' slump. The results indicated that the mixtures prepared with unground fly ash required less HRWRA to obtain a target slump than the mix that had been interground with the cement. An increment in the required HRWRA was primarily due to the larger fineness of the interground fly ash.

Bouzoubaa et al. (2007) studied the variation of the mass replacement of cement (30%, 40%, and 50%) by fly ash. Three different concrete mixes with compressive strength of: 2.9, 5.8 and 8.7 ksi (20, 40, and 60 MPa, respectively) were obtained by varying the cement content. By increasing the fly ash content, the water requirement to attain a given slump decreased, and consequently the w/cm decreased.

2.4.2.2 Air content.

Bouzoubaa et al. (2001) also investigated the effect of varying the fly ash content on the concrete mix's air content. In the case of fly ash interground with cement, the results indicated that a higher dosage of air entraining agent was required than when the mix was prepared with unground fly ash. The reason was due to the increase of the fineness of the interground fly ash.

Bilodeau et al. (1994) reported that the amount of air entraining agent required to attain the desired air content was greatly influenced by both the fly ash and the cement used in the mix. Different dosages were necessary due to the carbon, alkali contents, and fineness of the fly ash as well as the alkali content of the cement used.

2.4.2.3 Setting time.

It has been observed that the initial and final setting times are arbitrarily defined in test methods, and they do not mark a specific physical or chemical change in the cement paste (Mehta and Montiero 1993). However, the initial setting time defines the limit of handling, and the final setting time marks the beginning of development of mechanical strength.

In addition, Bouzoubaa et al. (2001) reported that the setting times for HVFA concrete mixtures were 30 minutes to 3½ hours longer than those of the baseline mixes. The fly ash mixes used in this study consisted of 45% by mass of cement, and 55% by mass of a Class F fly ash.

2.4.3. Hardened Material Properties.

2.4.3.1 Compressive strength.

The compressive strength of HVFA concrete typically suffers in the short term as highly reactive cement is replaced with less reactive fly ash. Bouzoubaa et al. (2001) reported that 55% Class F fly ash mixtures achieved around half the strength of conventional concrete mixes at one day. The fly ash mixtures began to match or exceeded the strength of the control mixes between 14 and 28 days. In addition, substantial strength gains occurred at one year.

Galeota et al. (1995) conducted a maturity study to determine the difference in strength gains by using Class F fly ash to obtained mixes at 30%, 40%, and 50% replacement by mass of cement with fly ash. The results showed a strength development delay behind their control mix counterpart. This difference between the HVFA mixtures and the control mix diminished as the specimens age, and at one year of age, the 40% fly ash mix has exceeded the control mix in compressive strength.

In terms of the long-term effects of high volumes of both Class C and Class F fly ash on concrete mixtures, it was observed that increasing volumes of both types of fly ash resulted in a similar decrease in early strengths. However, Class F fly ashes show a better long-term strength gain correlation with increased fly ash volume. Due to the pozzolanic activity given by the higher calcium content in Class C fly ashes, Class C fly ashes performed better at early age strength gains than Class F fly ashes (Naik et al. 2003).

2.4.3.2 Modulus of elasticity.

Rivest et al. (2004) reported that the modulus of elasticity for HVFA concrete mixes was generally higher than for control concretes made with Type I and Type II cement. This was related to the content of unreacted glassy fly ash particles acting as a very fine aggregate rather than hydration products, thereby, increasing the rigidity of the concrete. Additionally, the filler effect of the fly ash contributes to a stronger transition zone that contributes to increase the rigidity of the concrete.

2.4.3.3 Hydration profile.

An important aspect to be considered when large volumes of cement are replaced with fly ash is the effect produced on the hydration curve of the cementitious system. Some researchers have investigated this effect when Type I and II cement was replaced with 20% of Class C and Class F fly ash (Wang et al. 2006). Class C fly ash helped reduce the heat release and delay the peak of the hydration curve which effectively retarded the set of the concrete mixture. Additionally, Class F fly ash only provoked a reduction of the heat release. When a substitution of fly ash was coupled with an addition of a water reducer (WR) and a retarding admixture, the Class C mixes were significantly affected compared to any other combination. The addition of these two admixtures caused a delay of the hydration for an extended time (Wang 2006a).

2.5. CONVENTIONAL CONCRETE

A brief review of the durability properties that were investigated for the CIP deck of Bridge A7957 is presented.

2.5.1. Freeze-thaw Resistance.

An exposure to cycles of freezing and thawing is considered a sever exposure condition on the concrete. Air entrainment has been used since the 1930s to improve the resistance to freezing and thawing. Stark (1989) found that long freeze-thaw cycles more severe than freeze-thaw cycles for same number of cycles, even where air void spacing factors were no greater than 0.008 in (0.2 mm). Sun et al. (2002) showed that there is a large difference in the freeze-thaw effects of a specimen in water and one in NaCl solution. Also, concrete in chloride loses weight faster and reaches the failure threshold

earlier than concrete in water. The loss of weight is mainly due to surface scaling which was found to be twice as fast in NaCl solution as it was in water, Sun et al. (2002).

2.5.2. Abrasion Resistance.

Abrasion is wearing due to repeated rubbing or frictional processes. For pavements, abrasion results from traffic wear. Laplante et al. (1991) indicated that concrete resistance to abrasion is strongly influenced by the relative abrasion resistance of its constituent materials such as coarse aggregates and mortar. Where concretes with trap rock or granite as aggregates exhibit higher abrasion resistance compared to the "softer" limestone aggregate concretes. On other hand, Nanni (1989) showed that compressive strength is a poor parameter to evaluate abrasion because of the influence of surface finishing and curing conditions. In general, proper finishing and curing practices are known to enhance the abrasion resistance of concrete considerably.

2.6. MODOT STANDARD CONCRETE MIXES

The Missouri Department of Transportation (MoDOT) specifies four concrete class mix designs for use in new bridge construction. The four mixes according to section 751.4.1 of MoDOT's Engineering Policy Guide (EPG) are as follows (MoDOT 2011):

- A-1. Used for prestressed concrete girders including precast panels.
- B. Typically used for the above-ground substructure elements.
- B-1. Used for barrier curbs and substructure elements needing additional compressive strength.
- B-2. Used for slabs, and subsurface structural elements.

All four of the above mixes were used during the course of this research program in addition to a NS-SCC mix with a design compressive strength of 8,000 psi (55.2 MPa), a HS-SCC mix with a design strength of 10,000 psi (68.9MPa), and a HVFAC with a specified design strength of 3,000 psi. Mix designs for the bridge elements investigated are discussed in Section 5.

3. MATERIAL TESTING PROGRAM

3.1. INTRODUCTION

To provide more accurate results and get a comparison of CC, HVFAC, NS-SCC, and HS-SCC, material and mechanical tests were conducted. In this section, the compressive strength, modulus of elasticity, modulus of rupture, splitting tensile strength, shrinkage, creep, freeze-thaw, ponding chloride concentration, and coefficient of thermal expansion tests were determined.

3.1.1. Member Cast.

The precast girders and deck panels were fabricated at County Materials Corporation, located in Bonne Terre, MO. The bents and deck slab were cast-in-place (CIP). The deck slab was cast from the east to the west side of the deck after erection of PC/PS girders at the site.

To ensure that the concrete has quality control/quality assurance (QC/QA), all girders and panels specimens were cast next to the girders and deck panels to have them experience similar temperature and atmospheric condition of ambient weather of the precast concrete plant. The specimens of the bents, deck slab, and safety barriers were fabricated at the jobsite. The specimens are shown in Figure 3-1.

a) Precast Girder QC/QA Specimens b) Deck Slab QC/QA Specimens

Figure 3-1. QC/QA Specimens Placement at Precast Plant and Jobsite

3.1.2. Curing Conditions.

For the first days the girders, deck panels, and CIP member specimens were field cured where they were left close to the members to have same member condition. After releasing the prestressing strands for the precast member, the QC/QA specimens were taken to Rolla, MO. The Compressive strength, modules of elasticity, splitting tensile, and modulus of rupture were stored outside a storage area on campus which had similar environmental conditions as the member in the precast concrete plant yard. The shrinkage, creep, and coefficient of thermal expansion specimens were placed within an enclosed temperature controlled environment. The chloride ponding and abrasion resistance specimens were kept in a 70°F (21.1 °C) room. This room is called ASTM moist curing room which had a temperature of 70 F (21.1 °C) and a humidity of 100%. Figure 3-2 displays the location of the material specimens during storage.

a) Summer Storage b) Winter Storage

Figure 3-2. Storage of QC/QA Specimens at Missouri S&T

3.1.3. Testing Program Overview.

Table 3-1 and Table 3-2 summarize the material testing program for the testing of fresh properties and collection of QC/QA specimens.

Table 3-1. Summary of Fresh Properties of Material Testing Program

Test	ASTM Standard	Mix Type
Slump	C143	CC,HVFAC
Cylinders	C31	CC,SCC,HVFAC
Air content	C231	CC,SCC,HVFAC
MOR beams	C31	CC,SCC
Creep molds	C470	CC,SCC
Segregation column	C1610	SCC
Slump flow	C1611	SCC
Passing ability (J-ring)	C1621	SCC

Table 3-2. Summary of Hardened Properties of Material Testing Program

Tests	Test Method	Specimens	Material
Compressive Strength	ASTM C39 -12	4 x 8 in. (100 x 200 mm) cylinders	A,B,C,D,E,F,G, H,I
Modulus of Elasticity	ASTM C469 -10		A,B,C,D,E,H,I
Splitting Tensile Strength	ASTM C496 -11		B,C
Modulus of Rupture	ASTM C78 -10e1	6 x 6 x 21/24 in. (150 x 150 x 500/600 mm) beams	D,E
Creep	ASTM C512 -10	4 x 24 in. (100 x 600 mm) cylinders	E
Shrinkage	ASTM C157 -08		
Freeze-Thaw Durability	AASHTO T161-12	3.5 x 4.5 x 16 in. (90 x 115 x 400 mm) beams	H
Chloride Ponding	ASTM C1543-10	18 x 18 x 4 in. (460 x 460 x 100 mm) square specimen	H

A: HVFAC Trial Mix
B: HS-SCC Trial Mix
C: NS-SCC Trial Mix
D: HS-SCC Test Girders
E: Bridge Girders
F: Intermediate Bents
G: Precast Panels
H: CIP Bridge Deck
I: Safety Barriers

3.2. COMPRESSIVE STRENGTH

The compressive strength test was measured according to ASTM C39-12 "Standard Test Method for Compressive Strength of Cylindrical Concrete Specimens." This standard requires a cylinder equal to 4 x 8 in. (100 x 200 mm) long. Each specimen was capped using a high-strength, sulfur-based capping compound before being placed into a compressive testing machine. The specimens were tested by using the Tinius-Olsen testing machine at the Construction Materials Load Frame Laboratory located in the

Butler-Carlton Civil Engineering Hall of the Missouri S&T, Rolla, MO. Figure 3-3 shows the testing machine and specimens after the test.

a) Tinius-Olsen Testing Machine

b) Compressive Specimens after Test

Figure 3-3. Compressive Strength Test

3.3. MODULUS OF ELASTICITY

The modulus of elasticity of the concrete is considered as a function of the modulus of elasticity of aggregates and cement matrix and their relative proportions. The modulus of elasticity is one of the important mechanical properties of concrete. So, to determine serviceability and performance of the HVFAC, NS- SCC, and HS-SCC, the MOE is required. ASTM C469 -10 “Standard Test Method for Static Modulus of Elasticity and Poisson’s Ratio of Concrete in Compression” was used to determine MOE using 4 x 8 in. (100 x 200 mm) cylinders. All specimens were tested with the Tinius-Olsen testing Machine at the Construction Materials Load Frame Laboratory located in the Butler-Carlton Civil Engineering Hall at Missouri S&T, Rolla, MO. To determine the MOE, the compressive stress, f_{cl}, that is produced when the strain reaches 0.00005 in/in and the strain, ε_{cl}, at 40% of the ultimate stress, f'_c, are required. The modulus of elasticity was calculated by $(0.4f'_c - f_{cl})/(\varepsilon_{cl} - 0.00005)$. The testing apparatus is displayed in Figure 3-4.

Figure 3-4. MOE Test Set Up

3.4. SPLITTING TENSILE STRENGTH

ASTM C496-11 “Standard Test Method for Splitting Tensile Strength of Cylindrical Concrete Specimens” was used to determine the splitting tensile strength. Cylindrical specimens, 4 x 8 in. (100 x 200 mm), were used for splitting tensile tests. The specimens were steam cured. The tests were done with the Tinius-Olsen testing machine at the Construction Materials Load Frame Laboratory located in the Butler-Carlton Civil Engineering Hall at Missouri S&T, Rolla, MO. In order to run this test, wooden strips were utilized to induce the stress locations required in the ASTM. The test setup is shown in Figure 3-5. The specimens were loaded at a continuous rate of 100 to 200 psi per minute (0.7 to 1.4 MPa per minute) until failure. Table 3-3 shows the testing apparatus and set up.

Figure 3-5. Typical Splitting Tensile Test Set Up

Table 3-3. Specimens for Splitting Tensile Test

NS-SCC Trial Mix	HS-SCC Trial Mix
1 day (3 Cylinders) 7 days (3 Cylinders) 28 days (3 Cylinders)	3 day (3 Cylinders) 7 days (3 Cylinders) 28 days (3 Cylinders)
Pour Date: 1/30/2013	Pour Date: 3/8/2013
Total Cylinders: 18	

3.5. MODULUS OF RUPTURE

The flexural strength of concrete is determined by calculating the concrete's modulus of rupture. ASTM C78 -10e1 "Standard Test Method for Flexural Strength of Concrete (Using Simple Beam with Third- Point loading)" was used to perform modulus of rupture test. The specimen tested was a 6 x 6 x 24 in. (150 x 150 x 600 mm) beam. The test was completed at Butler-Carlton Hall at the Missouri S&T in Rolla, MO, using a Tinius-Olsen testing machine. The specimens were loaded continuously at a rate of 125 and 175 psi per minute (0.86 and 1.21 MPa per minute). Test set up can be seen in Figure 3-6.

Figure 3-6. Modulus of Rupture Test Set Up

3.6. SHRINKAGE AND CREEP

Creep and shrinkage can be critical factors for design of structural members due to the length change by time dependent deformation. A modified version of ASTM C512 (2010) “Standard Test Method for Creep of Concrete in Compression” was performed to determine the creep of 4 x 24 in. (100 x 600 mm) concrete cylinders loaded to 40 percent of the design strength of 10,000 psi and 8000 psi (68.9 MPa and 55.2 MPa). In addition, the same cylinders were used to determine the shrinkage of the specimens using a modified version of ASTM C157 (2008) “Standard Test Method for Length Change of Hardened Hydraulic-Cement Mortar and Concrete.” The concrete specimens are similar to the cylinders used by Myers’ research on high performance concrete (Myers 1998). The molds preparation and test of creep and shrinkage followed the same procedure that was done in Myers’s research on HSC and HS-SCC (Myers and Bloch 2010).

a) Creep and Shrinkage Specimens

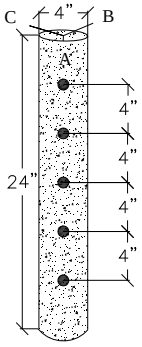

b) DEMEC Points Installation

Conversion: 1 in =24.5 mm

Figure 3-7. Creep & Shrinkage Specimen & DEMEC Point Arrangements

Figure 3-7 displays the cylindrical specimens and the location of the various DEMEC points used to determine the strain of the specimens. Each specimen was placed in 4 x 24 in. (100 x 600 mm) polyvinyl chloride (PVC) pipes. Within 24 hours of placement, the specimens were de-molded and DEMEC points were outfitted with five-minute quick set epoxy on the specimens and preliminary readings were taken. Nine locations on each cylinder could be read to determine the change in strain over that length. The average of all of the readings was computed to be the total strain of the

specimen. Table 3-4 lists the specimens made to determine the creep and shrinkage of CC, NS-SCC, and HS-SCC.

Table 3-4. Creep & Shrinkage Specimens

Material	CC	NS-SCC	HS-SCC
Placed	7/29/2013	8/6/2013	8/13/2013
Shrinkage	1,2,3	1,2,3	1,2,3
Creep	1,2,3	1,2,3	1,2,3
CC: 6 cylinders NS-SCC: 6 cylinders HS-SCC: 6 cylinders		Total: 18 cylinders	

Specimens were read every day for the first two weeks, every two days for the next week, once a week for the first month, and then every month for a full year, thereafter. The specimens were stored and monitored in the Engineering Research Lab (ERL) Structural Engineering Laboratory to keep the specimens within an area that would maintain an average relative humidity of 50% and a temperature around 70 °F (21.1°C). However, fluctuations in humidity and temperature did occur on days when the loading dock door was opened and closed for large scale specimen delivery and removal. The creep specimens were loaded after the bridge erection when the bridge experienced loading applied by the deck panels. While waiting for the bridges to be erected, the specimens were sulfur capped to provide a smooth surface that would be in uniform contact with the load frame. In addition, the load frames were assembled. The frames loaded the specimens at 40% of the target load, and the springs had an average radius of 7.7 in. (195 mm) and an approximate stiffness of 10.25 k/in (1.795 kN/mm). After the CIP deck was placed (October 21, 2013), the creep specimens were loaded in the creep frames (October 23, 2013). In order to load the specimens, a jack and load cell were required to be positioned under the load frame on a jack plate. After the creep specimen was centered within the frame, the jack increased the load to the required stress level of 4,000 psi (27.6 MPa) in the case of the 10,000 psi (68.9 MPa) concrete specimens. In the case of the 8,000 psi (55.2 MPa) concrete specimens, the jack load applied was 3,200 psi

(22 MPa). Once the required axial load was obtained, the bolts were tightened and the jack was removed. In Figure 3-8, a representative schematic is provided for the creep load frame utilized for the 4,000 psi (27.6 MPa) stress level.

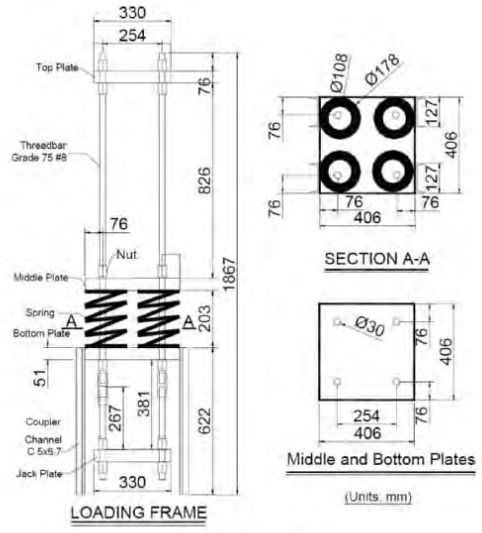

(Myers and Yang, 2005)

Conversion: 1 in. = 25.4 mm

Figure 3-8. Schematic of Creep Loading Frame

a) Creep Frames in High Bay Laboratory b) Creep Cylinder Loaded in Creep Frame

Figure 3-9. Creep Loading Frame & Specimens.

This schematic was provided by Myers and Yang in their research on HPC girders and used in the creep load frame assembly since the same creep frames were

implemented in their research (Myers and Yang 2005). Readings were taken in the same interval as those of the shrinkage specimens. Figure 3-9 displays images of the apparatuses used to apply the required sustained load to the creep specimens.

3.7. COEFFICIENT OF THERMAL EXPANSION

The coefficient of thermal expansion (CTE) in concrete is the measure of how concrete changes in volume in response to changes in temperature. The CTE of concrete is defined as the rate at which concrete contracts or expands as temperature changes. The following method was used to determine the CTE (Myers and Bloch 2011). A shrinkage specimen was taken from each concrete mixture. The test was completed 6 months after curing to ensure that shrinkage strain was not contributing to the change in length of the specimen. Initial strain and temperature readings were taken on each specimen utilizing the DEMEC gauge and a laser surface thermometer. The temperature was taken at the top, middle, and bottom of each specimen. Each specimen was placed into a freezer set at -25°C (-13°F). The freezer is shown in Figure 3-10. After 24 hours, each specimen was taken out and strain and temperature readings were immediately taken.

a) CTE Specimen

b) Specimen Inside the Refrigerator

Figure 3-10. Coefficient of Thermal Expansion (CTE) Test at Missouri S&T

Due to the rapid temperature change of the specimens while taking the strain readings, an average temperature was determined using the temperature immediately after the specimens were removed from the freezer and after strain readings were taken.

Calculation of the CTE is provided in equation 3.1, where $\alpha_{concrete}$ is the CTE of the concrete mixture, $\Delta\varepsilon_{temp}$ is the change in strain measured, and ΔT is the difference in measured temperatures.

$$\alpha_{concrete} = \frac{\Delta_{\varepsilon}\, temp}{\Delta T} \tag{3.1}$$

3.8. FREEZE-THAW DURABILITY

The resistance to freezing and thawing of the concrete was performed in accordance with AASHTO T161 “Standard Method of Test for Resistance of Concrete to Rapid Freezing and Thawing.” Procedure B was used. Stainless steel molds 3.5 in. (89 mm) in width, 4.5 in. (114 mm) in height, and 16 in. (406 mm) in length were used to fabricate specimens as shown in Figure 3-11.

Figure 3-11. Freezing and Thawing Specimen Molds

A specialized bolt was installed at the ends of each mold through a threaded hold in the end of each mold. After the specimens were de-molded, the end of this bolt protruded from both ends of the prism. The embedded bolt gives a mechanism to measure the length change of the concrete prism as it is subjected to freezing and thawing cycles.

The beams were wet cured for 35 days in lime water. All rapid freezing and thawing tests were performed by MoDOT employees of the Construction & Materials Division in Jefferson City, Missouri. The F-T test process can be seen in Figure 3-12.

a) Preparing F-T Specimens

b) Specimens during Curing

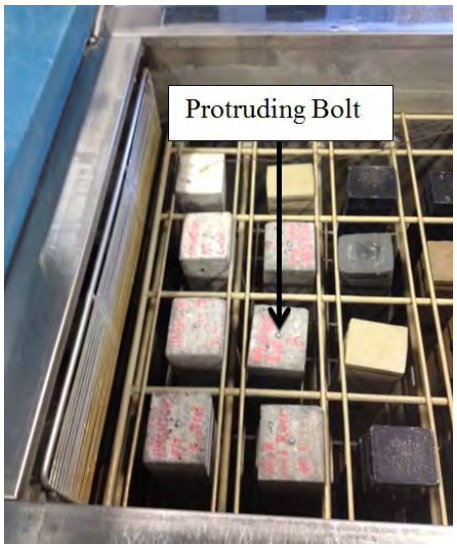

c) Freezing and Thawing Test Machine

d) Inside the MoDOT Construction & Materials Laboratory

Figure 3-12. Freezing and Thawing Test

3.9. CHLORIDE PONDING

In reinforced concrete bridges, one of the major forms of environmental attack is chloride ingress, which leads to corrosion of the reinforcement steel and a subsequent reduction in the strength and serviceability of a structure. Also, during winter season, de-icing salts are used to dissolve snow and ice from bridge decks. The chlorides in the de-icing penetrate to the concrete causing problems. The ability of chloride ions to penetrate

the concrete must then be known for design as well as quality control purpose. Therefore, in order to assess chloride penetration, A ponding test was conducted. ASTM C1543-10 “Standard Test Method for Determining the Penetration of Chloride Ion into Concrete by Ponding” was used to fabricate the concrete specimens for the ponding test. Three specimens were made as shown in Figure 3-13.

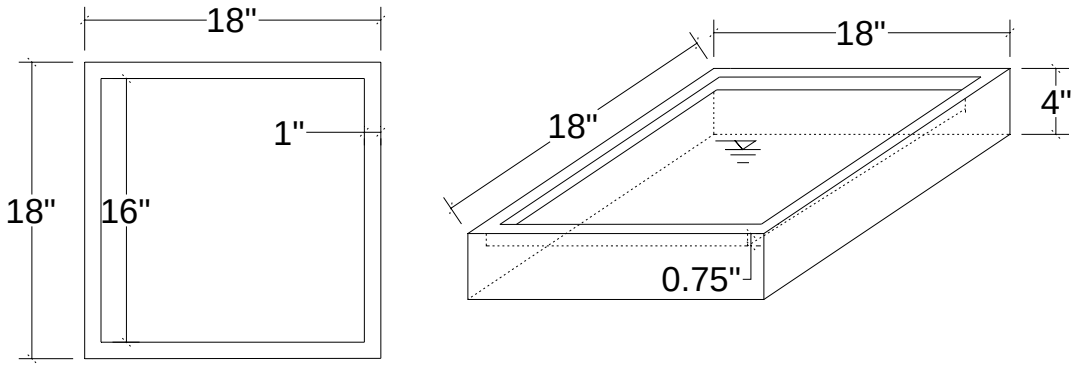

Conversion: 1 in. = 25.4 mm

Figure 3-13. Ponding Test Specimen Dimensions

After 24 hours from having placed the concrete into the deck, the specimens were de-molded and placed in a moist curing room at 100% relative humidity. After 14 days of moist curing, the specimens were transported to a temperature and humidity controlled environment where they were cured at 75 °F (23.8°C) and 65% relative humidity for another 14 days. At 28 days of curing, the ponding test was started. A 5% by weight chloride solution was placed into the ponding specimens and covered with plastic sheeting. The sheets were secured with plastic bands to prevent evaporation of the chloride solution.

Figure 3-14 shows the specimens after the chloride solution was placing and covered with a plastic sheet. The specimens were periodically monitored to ensure that the proper depth of chloride solution was maintained at the specified depth by adding additional fresh solution. After 60 days of ponding, the solution was removed and fresh solution was added and the plastic sheet was replaced with a new one. The test is still under ponding, therefore, after 60 days, the ponding solution was removed to allow the specimens surface to dry. After drying is completed, salt crystals are removed from the

surface by brushing with a wire brush. A typical sample will be taken from the specimens and the test will be completed according to ASTM C1543-10 requirements.

Figure 3-14. Ponding Specimens

3.10. ABRASION RESISTANCE

ASTM C944 “Standard Test Method for Abrasion Resistance of Concrete or Mortar Surfaces by the Rotating Cutter Method” was used to determined abrasion resistance. Three 12 x 12 x 3 in. (305 x 305 x 75 mm) specimens were cast from the deck slab concrete in a 2 x 3 in. (50 x 75 mm) mold made of wooden sections and attached to a plywood base. Concrete was placed and external vibration was used. Specimens were moist cured until testing at 28 days age. The test was conducted at the Butler-Carlton Civil Engineering Hall in the High Bay Laboratory at Missouri S&T. Figure 3-15 shows the specimens during and after completion the abrasion test.

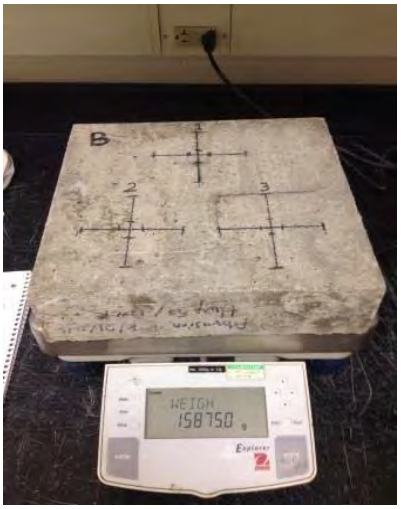

a) Specimen before the Test

b) Specimen during the Test

c) Specimen Set Up

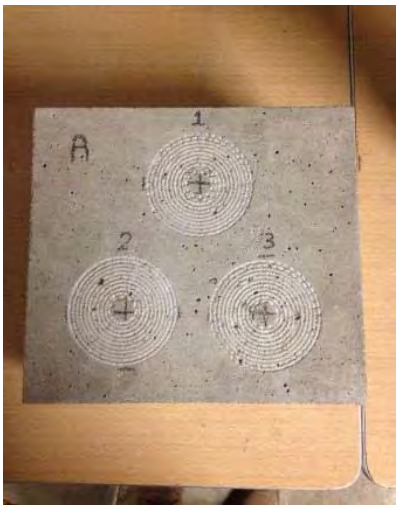

d) Specimen after the Test

Figure 3-15. Abrasion Test

3.11. NASP BOND TEST

The NASP bond test was conducted following a procedure that was developed by Russell at Oklahoma State University in 2006. The test aims to assess the bonding abilities of seven wire prestressing strand with concrete. Strand with 0.6 in diameter was used and cut to 32 in lengths. The molds were constructed with 18-in (457 mm) long sections of 5 in. (127 mm) outside diameter, 1/8-in thick (3 mm) steel tubing. The sections of tube were welded to 6 x 6 x 0.25 in. (152 x 152 x 6 mm) steel plates with a 5/8 in. (16 mm) diameter hole in the center. A 1.75 in. (45 mm) section of inverted 2 x 2 in. (51 x 51 mm) angle was welded onto the side of the tube at the open end to allow for

the attachment of an LVDT during testing. Figure 3-16a shows the NASP specimens. Three specimens for NS-SCC and three for CC were tested. The test was completed at the Butler-Carlton Civil Engineering Hall in the High Bay Laboratory using the MTS-880 testing machine. The free end slip of the specimen was monitored by an LVDT mounted on the specimen. The specimens were loaded at a rate of 0.1 in/minute until the test was completed. The NASP result value is the load that is required to displace the free end by 0.1 in. Figure 3-16b shows the NASP test.

a) NASP Specimens

b) NASP Test Set up

Figure 3-16. NASP Bond Test

3.12. SUMMARY

In this section, a material testing program for the concrete types investigated was developed. Tested hardened properties included compressive strength, modulus of elasticity, splitting strength, rapid chloride ponding, freeze- thaw, creep, shrinkage, and coefficient of thermal expansion. Table 3-5 below summarizes the test program for Bridge A7957.

Table 3-5. Summary of Material Testing Program

Time	Bents		Girders			Panels**	Deck*	Barriers*
	HVFAC*	CC*	Span1	Span2	Span3			
			CC**	HS-SCC**	NS-SCC**			
Release	C	C	C, E	C, E	C, E	C		
3 days	C	C	C, E	C, E	C, E	C	C,E	
7 days	C	C	C, E	C, E	C, E	C	C,E	C,E
14 days	C	C	C, E	C, E	C, E			
28 days	C	C	C, E, R	C, E, R	C, E, R	C	C,E	C,E
56 days	C	C	C, E	C, E	C, E	C	C,E	C,E
1st Load Test			C, E, R	C, E, R	C, E, R	C	C,E	C,E
2nd Load Test			C, E, R	C, E, R	C, E, R	C	C,E	C,E
1 year	C	C	C, E	C, E	C, E	C	C,E	C,E
Additional			CTE	CTE	CTE		AB***, P***, FT***	
Continuous			CR, SH	CR, SH	CR, SH			

*Field curing

**Member curing

***ASTM specified curing

C - compressive strength

E - modulus of elasticity

R - modulus of rupture

FT - freeze-thaw

CTE - coefficient of thermal expansion

CR - creep

SH - shrinkage

AB - abrasion resistance

P - ponding

4. MEASUREMENT SYSTEMS

4.1. MEASUREMENT TYPES

Three central measurement types were collected throughout the research program including concrete strains, concrete temperatures, and girder camber and deflection. Prestressing tendon strains as well as the concrete corrosion process were also investigated. Table 4-1 lists the gauges used and the data obtained for each measurement type.

Table 4-1. Measurement Types

Measurement Type	Measurement System	Data Collected
Concrete Strains	• Vibrating Wire Strain Gauges • Demountable Mechanical Strain Gauges	• Stress-strain response • Development length of prestress force • Prestress losses
Concrete Temperatures	• Thermocouples • Thermistors	• Hydration profiles • Strain corrections due to thermal effects • Deflection corrections due to thermal effects • Seasonal temperature variations
Girder Response Properties	• Precise Surveying System	• Camber • Time dependent deflections (creep) • Service life deflections
Prestressed Tendon Strains	• Electrical Resistance Strain Gauges • Loadcell	• Tendon stresses • Verification of initial prestress force
Corrosion	• RFID Corrosion Sensor	• Onset of corrosion

4.1.1. Concrete Temperatures.

Concrete temperatures were collected in both the intermediate bents and bridge girders. Thermocouples were embedded in the pier cap, columns and web wall of the

intermediate bents to measure the hydration profile within the first 48 hours of concrete curing. A thermocouple wire was attached outside of the formwork during data collection to measure the ambient temperature through the curing process. Within the bridge girders, each vibrating wire strain gauge (VWSG) included a built in thermistor to correct the measured strain and to record hydration temperatures. The hydration temperature measurements were of value during the casting and early service life of the bridge girders. In span 2, girders 3 & 4 were instrumented with VWSG at mid-span and at both ends. Girders 3 & 4 in spans 1 and 3 were instrumented with VWSG at mid-span and at the end closest to the intermediate bent.

4.1.2. Concrete Strains.

Concrete strains were measured in selected prestressed girders and panels and the cast-in-place (CIP) deck. A combination of VWSGs and a Demountable Mechanical Strain Gauge with exterior fixed discs referred to as “DEMEC points” were used with the NU girders, and VWSGs were embedded in two of the precast panels and across the CIP deck. By embedding up to five VWSG in the girder and two VWSG in the CIP deck at a given section, the strain profile could be accurately determined. This was accomplished at the mid-span location of each instrumented girder and at sections above the intermediate bent supports. Strains in the transverse direction of the bridge were also measured in the precast panels and CIP deck. Long-term creep and shrinkage effects could also be measured using the VWSGs. Furthermore, the DEMEC system was used to measure the transfer of force from the prestressing tendons to the girder.

4.1.3. Girder Deflection and Camber.

The camber and time-dependent deflection of each instrumented girder was obtained at the pre-cast plant shortly after fabrication. At the plant, deflection measurements were made at the ends, mid-span and quarter points of each member. In-service deflections were also measured during the live load test at five equidistant locations (including mid-span) along the bottom of each girder along line 3.

Additionally, mid-span deflections were also recorded for girder lines 1, 2 and 4 of each span. The measured camber and deflections were used to assess the in-situ serviceability performance of the girders from fabrication through in-service conditions.

4.2. MEASUREMENT SYSTEMS

4.2.1. Loadcell.

A 100 kip (44.8 kN) loadcell was attached to one prestressing strand during the fabrication of girder S2-G4 as shown in Figure 4-1. The loadcell was used to check the applied load to each prestressing tendon.

Figure 4-1. Loadcell

4.2.2. Thermocouples.

A thermocouple is a temperature sensing device that produces a voltage that is transmitted as a measure of temperature. Thermocouples are junctions of specific metals (wires) which have a predictable and repeated relation between voltage and temperature. These wires are coupled simply by tightly twisting thermocouple wire. Figure 4-2 shows these wires.

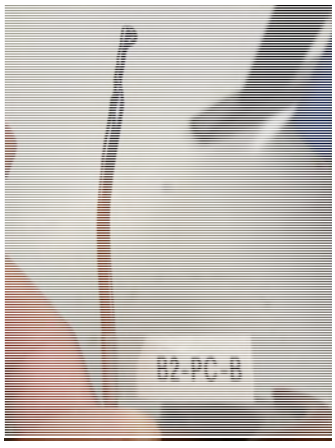

Figure 4-2. Thermocouple

Thermocouple model TT-T-20-TWSH from OMEGA In. was used in this project. Figure 4-3 shows the meaning of this term. The temperature range is reported to be 450 to 500 °F (-267 to 260 °C) by the manufacturer. The accuracy of measurements was stated to be ± 1.8 °F (± 1.0 °C) for the thermocouple used.

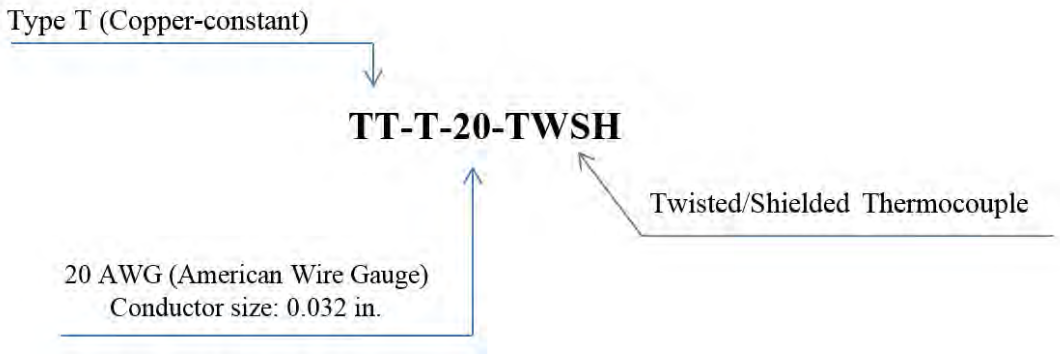

Figure 4-3. Definition of TT-T-20-TWSH

4.2.3. Vibrating Wire Strain Gauges.

A vibrating wire strain gauge is used for monitoring strain in concrete caused by stress variations. The sensor is installed by placing the gauge at a location in the structure (normally tied to rebar with soft iron or plastic wire) suitable to accurately pass loads from the cured concrete into the gauge. Each strain gauge consists of two end blocks with a tensioned steel wire between them. As the concrete surface that encompasses the strain gauge undergoes strain, the end blocks will move relative to each other. The tension in the wire between the blocks will change accordingly, thus altering the resonant frequency of the wire. Vibrating wire readout is utilized to generate voltage pulses in the magnet/coil assembly located at the center of the strain gauge. The magnet/coil assembly plucks the wire and measures the resulting resonant frequency of vibration. The VWSGs used in this project were EM-5 series manufactured by Roctest, Inc. shown in Figure 4-4.

The EM-5 has an adjustable 3000 microstrain range with an accuracy of 1 microstrain. This is the usable microstrain limit of the EM-5 VWSG. The gauge has a built in thermistor to record concrete temperatures ranging from -122 °F to 140 °F (-50 °C to 60 °C). Embedded VWSGs were selected for this project because of their durability and have been found to be reliable for several years in field conditions (Myers and Yang, 2005). 86 VWSGs were used at specific points of interest.

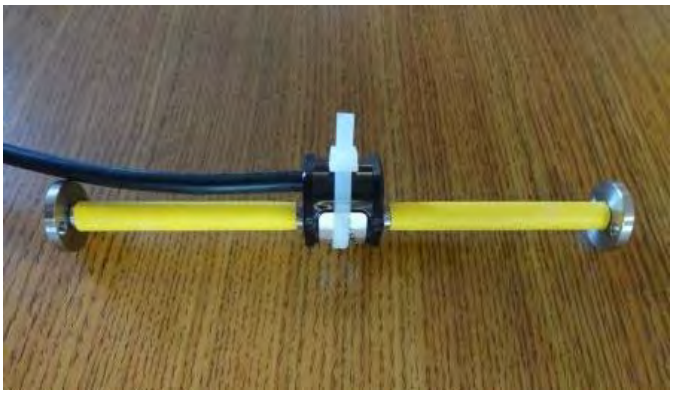

Figure 4-4. Vibrating Wire Strain Gauge

4.2.4. Electrical Resistance Strain Gauges.

A linear strain gauge, model EA-06-125BT-120-LE by Micro Measurements, was used in the test girders. The gauge has a constantan foil with a tough, flexible, polyimide backing (EA), with pre-attached leads and encapsulation (LE). The gauge has a resistance of 120 ± 0.15% ohms and an usable temperature range of -100° to +350°F (-75° to +175°C). The gauge has an overall length of 0.37 in. (9.4 mm) and an overall width of 0.16 in. (4.1 mm). Two gauges were applied to each girder at mid-span: one in each of the two bottom rows of prestressed tendons. The gauges were used to monitor the stress in the prestressing tendons during the course of the shear testing. The gauge is shown in Figure 4-5 prior to installation.

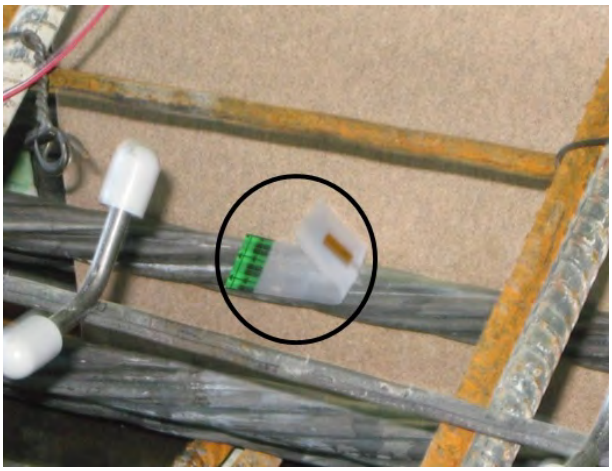

Figure 4-5. Electrical Resistive Strain Gauge

4.2.5. Demountable Mechanical Strain Gauges.

The demountable mechanical strain gauge (DEMEC) is used for determining the linear deformation caused on two reference points fixed on a loading member. The system utilizes a standard digital gauge that is attached and supported by a bar. One end is fixed, the other can move on a pivot. The digital gauge measures the movement of the pivot. A reference bar is used to position pre-drilled stainless steel discs which are attached to the locations with a five-minute quick set epoxy. After the discs set to the location, initial readings are taken. The conical points of the gauge are inserted into the holes in the discs and the reading on the dial gauge noted. In this way, strain changes in the structure are converted into a change in the reading on the dial gauge. The gauge has been designed so that only minor temperature corrections are required for changes in ambient temperature, and an Invar reference bar is provided for this purpose. Figure 4-6 shows the DEMEC gauge and the reference bar.

Figure 4-6. The DEMEC Gauge and Reference Bar

To determine the change in strain, $\Delta\varepsilon$ (microstrain), from one reading to the next, Equation 4.1 was used.

$$\Delta\varepsilon = G\big((R_i - R_0) - (D_i - D_0)\big) \qquad (4.1)$$

Terms used in this equation are defined as followed: G is the gauge factor as shown in Figure 4-7, 0.400 x 10^{-5} strain per division (4 microstrains), D_o is the datum reading on the reference bar, D_i is the subsequent reading on the reference bar, R_o is the datum reading on the tested material, and R_i is the subsequent reading on the tested material.

Figure 4-7. Gauge Factor Used for Shrinkage and Creep Calculations

4.2.6. High Performance Total Station System.

At the precast plant, a laser-based High Performance Total Station system was used to obtain vertical deflection data before and after the release of the prestressing force acting on the PC girders. The total station (TS) employed to monitor the camber of the PC/PS girders was a Leica TCA2003 (Figure 4-8).

Figure 4-8. Total Station (Leica TCA2003)

The TS equipment was set atop a secure tripod with an unobstructed view of the prisms (targets) that were placed on the top flange of the girders. Additionally, two prisms were set atop secure tripods located between the PC/PS girder and the TS. These additional prisms were used as reference targets that help verify that the TS had not experienced any additional relative movement before and after the strands release. Five prisms were set on steel plates installed atop the flange of the girders at 5 different locations: 1.0 ft (0.30 m) from the ends and at sections located at L/4 and L/2 from each end.

The TS, also called as Robotic Tacheometry System (RTS), (Hernandez et al. 2006), obtains three-dimensional coordinates of every target by measuring the horizontal and vertical angle as well as the distance between the TS and prisms. The instrument was configured to take three readings per recorded measurement. This was done internally by four diodes that optically read a fine bar code set on a glass ring inside the instrument. During monitoring, the equipment continuously reads the bar codes on the horizontal and vertical planes by sending a laser ray to reflecting the targets (Figure 4-9) mounted on the structure to be monitored. By means of triangulation with the fixed reference points placed outside the PC girders, the total station allows to determine how much the element has moved in a three-dimensional array with an accuracy of 0.5 arc-seconds on angular measurements and 1mm+1ppm (1 in = 25.4 mm) on distance measurements.

Figure 4-9. Reflecting Prisms Mounted on PC/PS Girders (Precast Plant)

The Leica TCA2003 is very accurate through the use of robotics, and this feature allows the instrument to rotate on the horizontal and vertical axes by itself. The system automatically recognized and locked onto targets that were manually entered by the user

at the beginning of the test. The Leica TCA2003 automatically relocated the targets and obtained their coordinates. Because of the high sensitivity of the equipment to movement and vibration, its robotic capability helps eliminate any human error through less physical contact during operation.

The Leica TCA2003 was also used to obtain the vertical deflections of the bridge at different sections located along the longitudinal axis of the PC/PS girders. The first part of the first series of non-destructive load tests was conducted in April 2014 to evaluate the live-load response of the bridge during serviceability loading. The second part of the first series of load tests has been scheduled to be conducted in August 2014. The results obtained during this first series of load test will be presented in the final report that will be submitted to MoDOT in January 2016.

4.2.7. Radio Frequency Identification (RFID) based Corrosion Sensor.

A RFID based corrosion sensor was employed to detect the chloride salt concentration that initiates the onset of corrosion within the reinforcing steel of the CIP RC deck. Figure 4-10 shows the sensor employed in this implementation project. The body of the sensor is about the size of a quarter (Myers and Hernandez 2014). The sensor houses an internal circuit board that registers voltage variations of the wire links shown in Figure 4-10. This sensor does not rate the mass loss or corrosion rate of reinforcing steel. Instead, each external iron wire acts as a trigger mechanism that fails when the content of chloride ingress reaches a critical value in the sensor's surrounding concrete.

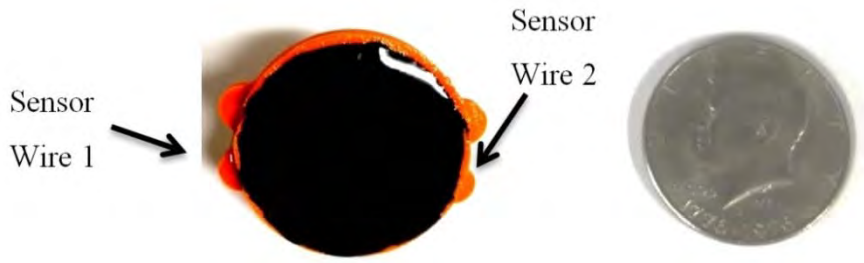

Figure 4-10. RFID Based Corrosion Sensors

The wires' diameters are 0.065 mm (thinner link) and 0.100 mm (thicker link), respectively. This second generation of the sensor allows detecting two critical chloride concentration values. The thinner wire detects the chloride content that initiates the

corrosion, and the second detects a chloride concentration that produces an important loss of the reinforcing steel area within the CIP RC deck. Additional information about the RFID corrosion sensor and its implementation on this project can be found in Myers and Hernandez (2014).

4.3. DATA ACQUISITION

4.3.1. Data Acquisition System.

Three data acquisition systems (DAS) were used for strain and temperature data collection during the fabrication and construction of Bridge A7957. These DAS were custom-built by the researchers at Missouri S&T. The first built DAS was a compact RIO system, and the two remaining DAS were Campbell Scientific CR800 boxes that work wirelessly.

4.3.1.1 Compact RIO.

The compact RIO system (Figure 4-11) with a NI9214 High Accuracy Thermocouple module was used for temperature data collection during the construction of the bents along with a 90 Watt solar panel. Four thermocouples were connected to the Compact RIO DAS during concrete placement of the web wall and pier cap of each bent. The thermocouples collected data for at least 23 hours during and after concrete placement. These sensors provided a temperature profile development for each part of the bents.

Figure 4-11. Compact RIO System and 90 Watt Solar Panel

4.3.1.2 Campbell Scientific CR800.

During the girders fabrication, erection and construction, the VWSG were connected to either of two Campbell Scientific CR800 DAS that have AVW200 and AVW206 VWSG reading modules. Following the erection of the girders, these two CR800 DAS were anchored to the interior side of the intermediate bent pier caps for long-term monitoring. A cellular antenna, also anchored to the interior side of the bent 2 pier cap, was used to send the data from the CR800s in real time back to the researchers at Missouri S&T during fabrication of the precast PC girders and the different stages of the bridge construction. Figure 4-12 through Figure 4-14 show the data acquisition systems and their components.

CR800 DAS

CR800 Modules

Figure 4-12. Campbell Scientific CR800

The number of channels needed during the fabrication of each instrumented girder is presented in Table 4-2.

Table 4-2. Gauges Needed During Fabrication of PC Girders (Precast Plant)

Span	Member	Gauges		DAS Type	Total of Channels
1-2 (CC)	Girder 3 Girder 4	VWSG + Thermistor	9	CR800	9
2-3 (HS-SCC)	Girder 3 Girder 4	VWSG + Thermistor	13	CR800	13
3-4 (NS-SCC)	Girder 3 Girder 4	VWSG + Thermistor	9	CR800	9

The number of channels used to monitor the bents during their construction is presented in Table 4-3.

Table 4-3. Gauges Needed During Construction of Bents

Bent	Member	Gauges		DAS Type	Total No. of Channels
2 (CC)	Web Wall	Thermocouple	4	Compact RIO	8
	Pier Cap		4		
3 (HVFAC)	Web Wall	Thermocouple	4	Compact RIO	8
	Pier Cap		4		

The number of channels needed during the different construction stages and long-term monitoring of Bridge A7957 is presented in Table 4-4.

Table 4-4. Channels Needed During the Long-Term Monitoring of Bridge A7957

Part	Gauges		DAS Type	Total of Channels
PC/PS Girders (Longitudinal VWSG)	VWSG + Thermistor	62	CR800	62
CIP Deck (Longitudinal VWSG)	VWSG + Thermistor	20	CR800	20
CIP Deck (Transverse VWSG)	VWSG + Thermistor	2	CR800	2
PC/PS Panels (Transverse VWSG)	VWSG + Thermistor	2	CR800	2
Total channels for long-term monitoring:				86

The components of the two DAS boxes are shown in the diagrams of Figure 4-13 and Figure 4-14.

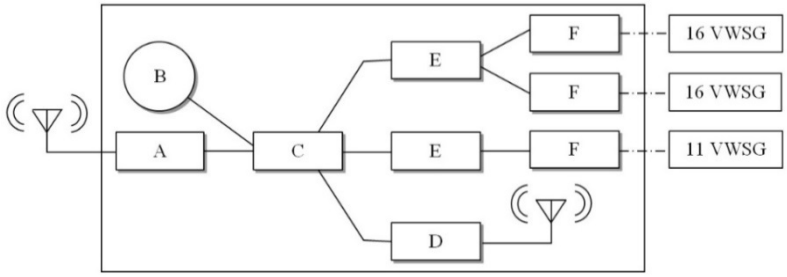

Figure 4-13. Components of DAS Box 1

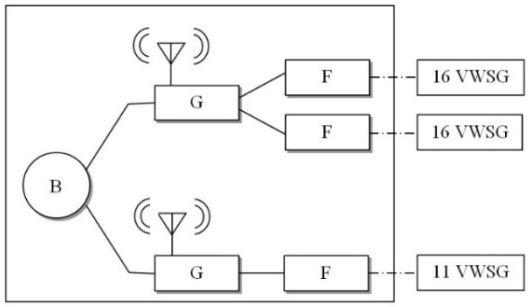

Figure 4-14. Components of DAS Box 2

Where:

A: Sierra Raven XT (wireless modem with high boost antenna)

B: 12V solar panel with backup battery

C: CR800 (logger)

D: RF401 radio transceiver (send/receive)

E: AVW200 (2-port VW reader, serial connection)

F: AM16/32 B (16/32 channel multiplexer)

G: AVW206 (2 port VW reader, wireless)

Within each CR800 DAS box, the first two multiplexer modules host 16 VWSGs, and the third module hosts 11 VWSG. A total of 43 VWSG can be connected to each CR800 DAS.

4.3.2. Programming and Data Collection.

A portable personal computer (Dell Latitude E6520 Laptop) and the CR800Series software package supplied with LoggerNet 4.1 by Campbell Scientific were used for programming and collecting stored data. The data, obtained at the different construction stages and during the long-term monitoring of Bridge A7957, can also be downloaded wirelessly to this portable personal computer that is installed in the research laboratory (Figure 4-15).

a) CR800 DAS Box Installed on Bent 3

b) CR800 Modules and VWSGs

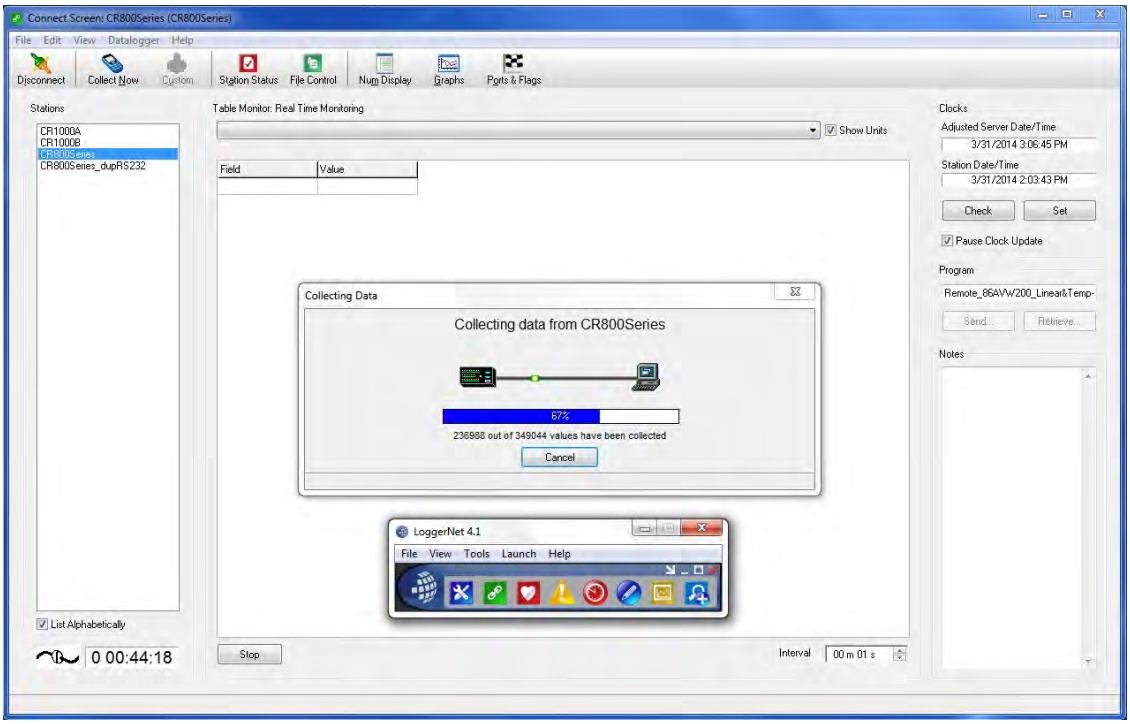

c) CR800 DAS Software with LoggerNet 4.1

Figure 4-15. Data Acquisition System Installed on Bridge A7957

4.3.3. RFID Corrosion Sensor Data Acquisition.

4.3.3.1 Data acquisition hardware.

The data acquisition hardware consists of a Dell Latitude E6520 Laptop, with an Intel® Core™ i7-2620M CPU, 2.7 GHz Processor, and a 15-in HD Monitor (Figure 4-16a), and an RFID scanning system (Figure 4-16b). The RFID scanning system has three main components: an RS-232 Serial to USB adaptor cable, a GP25 proximity RFID reader (model EM4200/4102), and a battery box (Myers and Hernandez 2014).

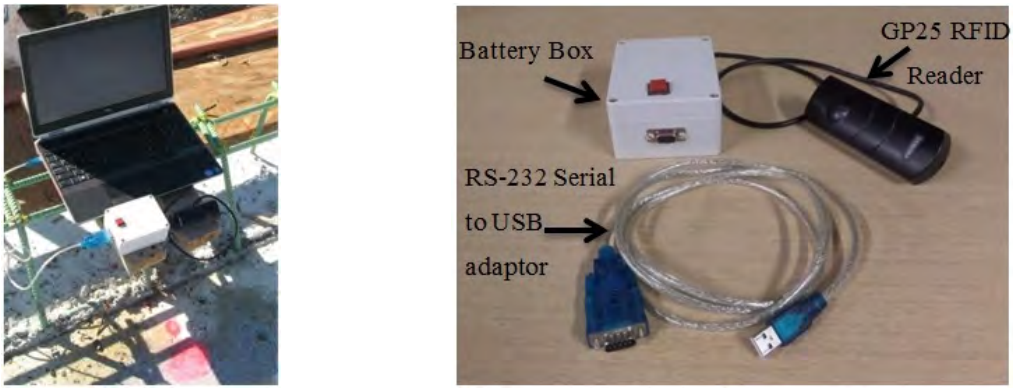

a) Dell Laptop b) RFID Scanning System

Figure 4-16. RFID Data Acquisition Hardware

The GP25 RFID reader is a low frequency component, high-performance, proximity reader featuring a long range data acquisition that can be used within a distance of 4 in (100 mm) from the corrosion sensor. In addition, this unit was configured to the interface format Clock/Data and RS-232 serial ASCII output. The battery box houses eight 1.5-volt AA batteries that supply power to the RFID reader.

4.3.3.2 Data acquisition software.

The data acquisition software is the user's interface that controls and orders the RFID reader what information to read and how to collect it from the RFID sensor tag. LabVIEW™ (2013) was the graphical programming language used to write and compile the software "Serial Reader.vi" that controls the DAS equipment. Figure 4-17 shows the user's interface of "Serial Reader.vi" that is utilized to control the RFID reader and to receive the output data from the sensor tag in the form of RFID code IDs.

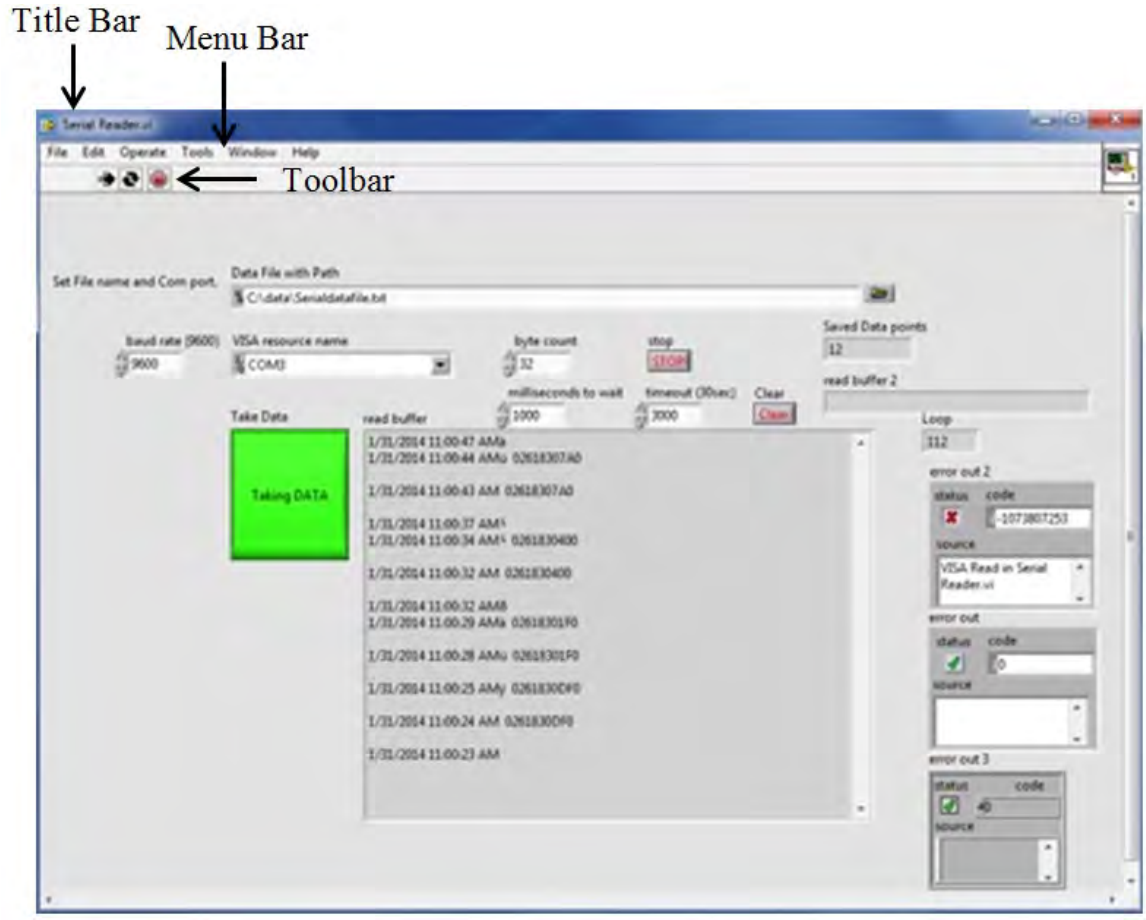

Figure 4-17. RFID DAS Software (User's Interface)

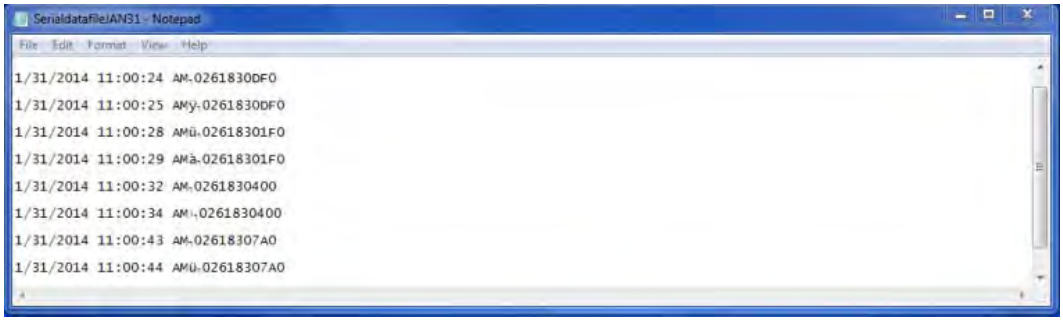

Figure 4-18. RFID Sensor's Output File

Figure 4-18 shows an output file written by the data acquisition software "Serial Reader.vi". The RFID reader collects an RFID code each time the sensor is scanned and sends the reading to "Serial Reader.vi" and is written into an output file (.txt format). The file can be edited by any commercial word processor (Myers and Hernandez 2014).

The first, second and third columns of the data file represent the date, time, and RFID codes obtained by the RFID data acquisition system. Figure 4-19 displays a typical RFID code.

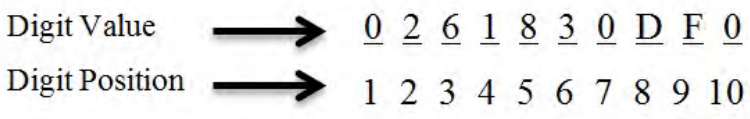

Figure 4-19. Typical RFID Code

From the RFID ID code of Figure 4-19, the following information is extracted:

a) Digits 1 and 2 represent the revision number of the RFID tag. For this case, the "02" indicates the RFID sensor belongs to the second prototype generation
b) Digits 3 through 9 contain a fixed tag's ID, in other words, this is the sensor's serial or identification. For this reading, the tag's ID is: **61830DF**
c) Digit 10 is the decoded response that the RFID tag sends through the reader to the data acquisition software. It indicates the status of the sensors' wire links. This digit can take four different values. A value equal to zero (0) means that both iron wires are intact; therefore, no critical chloride content is surrounding the sensor. A value of one (1) or two (2) means that the thinner or thicker iron wire has failed, respectively (i.e. the resistance measured by the sensor is greater or equal than about 500 ohm). Finally, a value of 4 means that both sensors' link wires have failed.

5. RESEARCH PROGRAM PLANS & PROCEDURES

5.1. TRIAL MIXES

Before the fabrication of the bridge elements or test girders could begin, trial mixes had to be developed to validate the fresh and hardened properties of the various concretes used in the research program. The three mixes investigated during this phase of the project were high-volume fly-ash concrete (HVFAC), high strength self-consolidating concrete (HS-SCC), and normal strength self-consolidating concrete (NS-SCC). All three mixes were developed by MoDOT based on previous research at Missouri S&T (Myers et al. 2012; Volz et al. 2012).

5.1.1. HVFAC.

The mix design was based off of MoDOT's B mix with 50% fly ash replacement. The official mix ID is 13CDHVFA003. The mix had a design water to cementitious material ratio (w/cm) of 0.33 and a design air content of 6.0%. The target compressive strength was 3,000 psi (20.7 MPa). The mix design is shown below in Table 5-1. The high volume fly-ash concrete was batched on January 8, 2013 at Osage County Industries in Linn, Missouri (Figure 5-1a) with MoDOT representatives present. Concrete slump and air content were measured before specimen collection. Nine 4 x 8 in. (100 x 200 mm) cylinders were collected for compressive strength testing at 7 and 28 days. Osage County Industries collected cylinders for compressive strength testing at 1, 2, 3, 4, 7, and 28 days.

a) Batching b) Sampling

Figure 5-1. HVFAC Trial Mix at Osage County Industries

Figure 5-1b shows the test cylinders collected by the Osage County Industries and Missouri S&T.

Table 5-1. HVFAC Trial Mix Design

Type	Material	Design Weight (lb/yd^3)	Batched Weight (lb/yd^3)
Coarse Aggregate	Choteau-Burlington-Cedar Valley – Gradation D Ledges 1A, 1B, 1, 2, 3	1750	1780
Fine Aggregate	Missouri River/Class A	1242	1269
Cementitious Material	Portland Cement – Type I/II	325	325
	Fly Ash – Class C	325	325
Water	--	213	213
Chemical Admixtures	Air Entraining Agent	0.2-2.0 oz/yd^3	5.0 oz/yd^3
	Water Reducer	2.0-6.0 oz/cwt	2.0 oz/cwt
	Accelerator	0-32.0 oz/cwt	16.0 oz/cwt
w/cm	--	0.33	0.33

Conversions: 1 lb/yd^3 = 0.5933 kg/m^3, 1.0 oz/yd^3 = 0.03708 kg/m^3, 1.0 oz/cwt = 6.5 oz/yd^3

5.1.2. HS-SCC.

The high strength self-consolidating concrete (HS-SCC) mix was batched on January 30, 2013 at County Materials Corporation in Bonne Terre, Missouri. The mix ID is 13SECSPE001, with the mix design shown in Table 5-2. The w/cm ratio was 0.329 with a target air content of 5.0%. The percentage of coarse aggregate in the mix was 48%; significant reductions in the coarse aggregate content would compromise the stiffness and shear behavior of the mix. The mix's fresh properties were tested following ASTM standards and included: air content, slump flow, passing ability (J-Ring), and static segregation. Figure 5-2 exhibits these tests. Eighteen 4 x 8 in. (100 x 200 mm) cylinders were cast for testing of compressive strength, modulus of elasticity, and splitting tensile strength as illustrated in Figure 5-3. The cylinders were stream cured at 120°F (49°C) for approximately 24 hours to simulate the curing conditions during the precast-prestressed girder fabrication process.

a) Segregation Column

b) Air Content

c) J-Ring (Passing Ability)

d) Slump Flow

Figure 5-2. HS-SCC Trial Mix Fresh Property Tests

Figure 5-3. HS-SCC Trial Mix Specimens

Table 5-2. HS-SCC Trial Mix Design

Type	Material	Weight (lb/yd^3)
Coarse Aggregate	Leadbelt 1/2" Dolomite	1340
Fine Aggregate	Mississippi River Sand	1433
Cementitious Material	Portland Cement Type I	850
Water	--	280
Chemical Admixtures	Air Entraining Agent	17 oz/yd^3
	High Range Water Reducer	76.5 oz/yd^3
	Retarder	25.5 oz/yd^3
w/cm	--	0.329

Conversions: 1 lb/yd^3 = 0.5933 kg/m^3, 1.0 oz/yd^3 = 0.03708 kg/m^3

5.1.3. NS-SCC.

The normal strength self-consolidating concrete (NS-SCC) mix was batched on March 8, 2013 at County Materials Corporation in Bonne Terre, Missouri. The mix ID is 13SECSPE002, with the mix design shown in Table 5-3. The w/cm ratio, target air content, and coarse aggregate content were 0.346, 5.0%, and 51%, respectively.

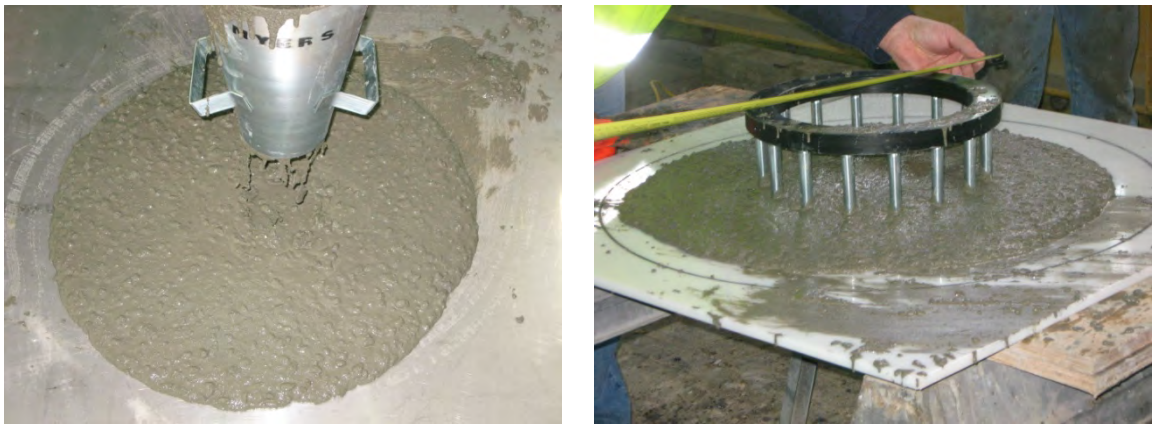

a) Slump Flow b) J-Ring (Passing Ability)

Figure 5-4. NS-SCC Trial Mix Fresh Property Tests

The mix had a target compressive strength at 28 days of 8,000 psi (55.2 MPa) and a target release strength of 6,500 psi (44.8 MPa). The mix's fresh properties were tested following ASTM standards and included: air content, slump flow, passing ability (J-Ring), and static segregation. Figure 5-4 exhibits two of these tests. Eighteen 4 x 8 in. (100 x 200 mm) cylinders were cast for testing of compressive strength, modulus of elasticity, and splitting tensile strength. The cylinders were steam cured at 120°F (49°C) for approximately 72 hours to simulate the curing conditions during the precast-prestressed girder fabrication process.

Table 5-3. NS-SCC Trial Mix Design

Type	Material	Weight (lb/yd^3)
Coarse Aggregate	Leadbelt 1/2" Dolomite	1476
Fine Aggregate	Mississippi River Sand	1433
Cementitious Material	Portland Cement Type I	750
Water	--	260
Chemical Admixtures	Air Entraining Agent	17 oz/yd^3
	High Range Water Reducer	67.5 oz/yd^3
	Retarder	25.5 oz/yd^3
w/cm	--	0.346

Conversions: 1 lb/yd^3 = 0.5933 kg/m^3, 1.0 oz/yd^3 = 0.03708 kg/m^3

5.2. NU SHEAR TEST GIRDERS

5.2.1. Introduction.

The objective of this task was to evaluate the shear capacity of the HS-SCC mix in a full scale application using the NU 53 girder. The girders were designed by MoDOT and were identical to those used in bridge A7957. Two girders were tested, identified as test girder 1 (TG1) and test girder 2 (TG2), and both welded wire reinforcement and mild steel bars were investigated as the primary method of shear reinforcement. A 6 in. (152

mm) thick cast-in-place (CIP) deck was poured in the laboratory to simulate a bridge deck. Table 5-4 describes the progression of activities that occurred in this task. All testing was performed at the Butler Carlton Hall Structural Engineering Research Laboratory (SERL) at Missouri S&T in Rolla, Missouri.

Table 5-4. NU Test Girders Progression of Events

Description of Activity	Date
Fabrication of TG1 and TG2	3/8/2013
Delivery of TG1 to Missouri S&T SERL	3/20/2013
CIP deck poured	3/28/2013
Testing of reinforced shear region (TG1-T1)	4/22/2013
Testing of unreinforced shear region (TG1-T2)	4/29/2013
Demolition and removal of TG1	5/2/2013
Delivery of TG2 to Missouri S&T SERL	5/8/2013
CIP deck poured	5/10/2013
Testing of reinforced shear region (TG2-T1)	5/24/2013
Testing of unreinforced shear region (TG2-T2)	6/3/2013
Demolition and removal of TG2	6/4/2013

5.2.2. Design Details.

Both girders were 40 ft.-10 in. (12.4 m) long, with 16 Grade 270 (1,862 MPa) prestressed low-relaxation prestressed tendons, 4 of which were harped. An additional 10 strands were added for increased flexural resistance. However, to prevent excessive tensile stresses in the top concrete fibers at release, these additional strands were not prestressed. Figure 1-1 and Figure 1-2 are presented again as Figure 5-5 and Figure 5-6, which define the cross sectional dimensions and strand arrangement of the test girders. Each girder had three distinct sections of shear reinforcement described in Table 5-5 and illustrated in Figure 5-8: a middle 10 ft. (3.05 m) region and two 15 ft. (4.57 m) end regions. Test girder 1 consisted of welded wire reinforcement (WWR) and TG2

contained mild steel bars (MS) as the primary method of shear reinforcement. Four pairs of #6 (mild steel bars were used within the bearing regions of the test girders.

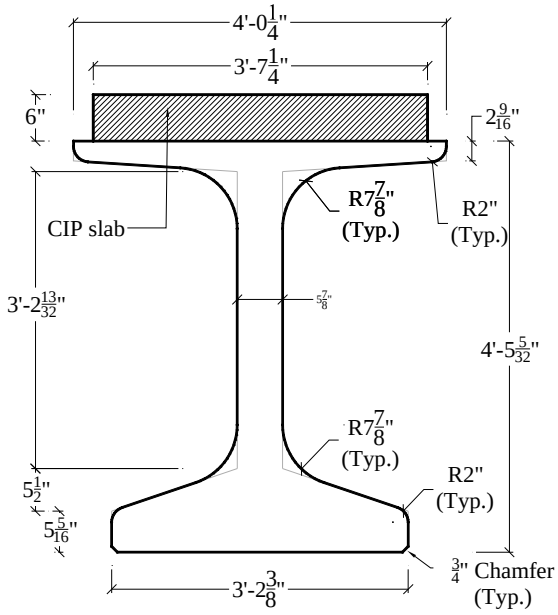

Conversion: 1 in. = 25.4 mm

Figure 5-5. Test Girder Cross Section

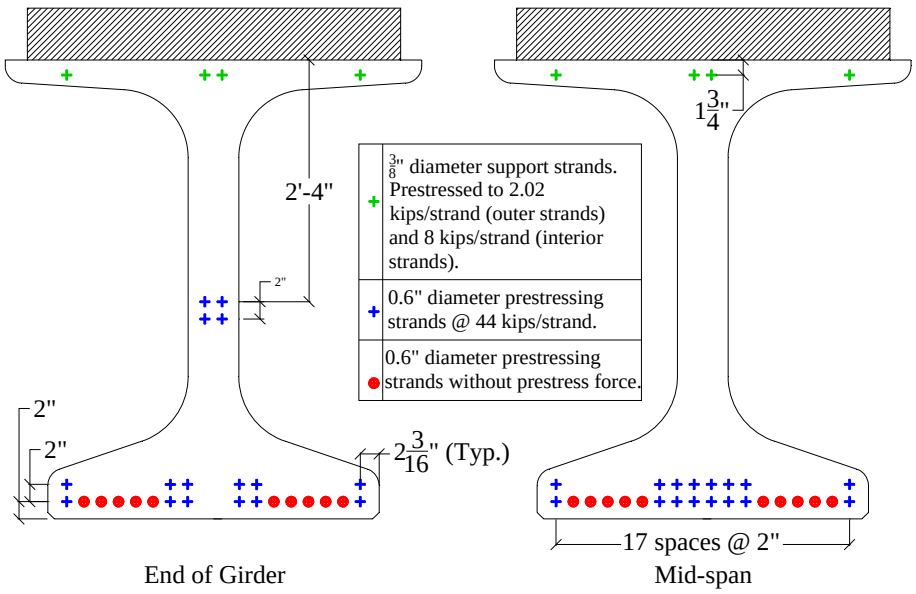

a) Ends b) Mid-span

Conversion: 1 in. = 25.4 mm

Figure 5-6. NU Test Girder Strand Layout

In order for the girder to act as a composite section with the cast-in-place (CIP) slab, shear studs were installed at 8 in. (203 mm) on center (o.c.) in region 3 as shown in Figure 5-7. The welded wire reinforcement had a yield strength of 70 ksi (517 MPa) and an ultimate tensile strength of 80 ksi (552 MPa) in accordance with AASHTO M 221 (ASTM A 1064 2012). The mild steel bars in test girder 2 had a yield strength of 60 ksi (414 MPa) and an ultimate tensile strength of 90 ksi (621 MPa) following AASHTO M 31 (ASTM A 615 2012). Each end region was tested in shear, and external strengthening was provided in the non-tested region during each test. Design drawings provided by MoDOT are located in Appendix A.

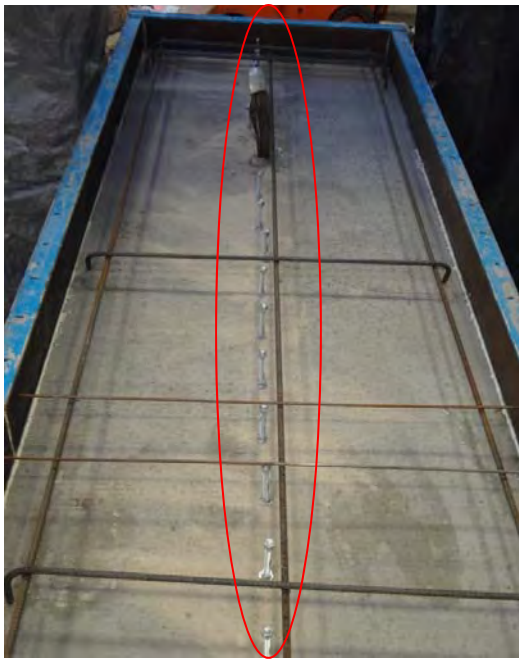

Figure 5-7. Shear Studs in Region 3

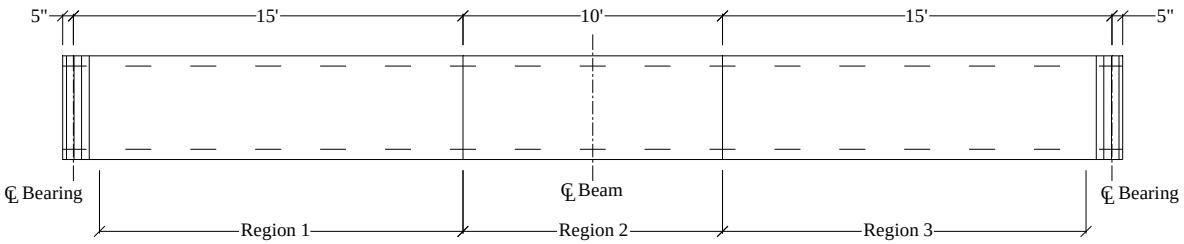

Conversion: 1 in. = 25.4 mm

Figure 5-8. Shear Reinforcement Layout

Table 5-5. Test Girder Shear Reinforcement

Welded Wire Reinforcement (TG1)						
Region 1			Region 2			Region 3
Bar Size	Spacing	Length	Bar Size	Spacing	Length	No Shear Reinforcement
D20	12"	14'-0"	D20	4"	10'-0"	
Mild Steel Bars Reinforcement (TG2)						
Region 1			Region 2			Region 3
Bar Size	Spacing	Length	Bar Size	Spacing	Length	No Shear Reinforcement
#5	24"	14'-0"	#5	12"	10"-0"	

Conversion: 1 in. = 25.4 mm

5.2.3. Fabrication.

The test girders were fabricated at County Materials Corporation on March 8, 2013. The following sections describe the actions taken by Missouri S&T and County Materials Corporation during the fabrication of the test girders.

5.2.3.1 Strain gauges.

Electrical resistive strain gauges (model EA-06-125BT-120-LE by Micro Measurements) as described in Section 4.2.4 were adhered onto the bottom two layers of prestressing tendons at mid-span of each test girder as shown in Figure 5-9. A standard M-Coat F Coating Kit by Vishay Measurements was used to adhere and protect the gauges from the concrete.

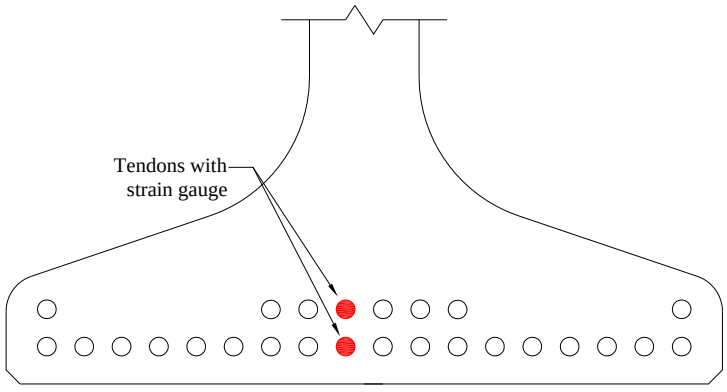

Figure 5-9. Location of Strain Gauges

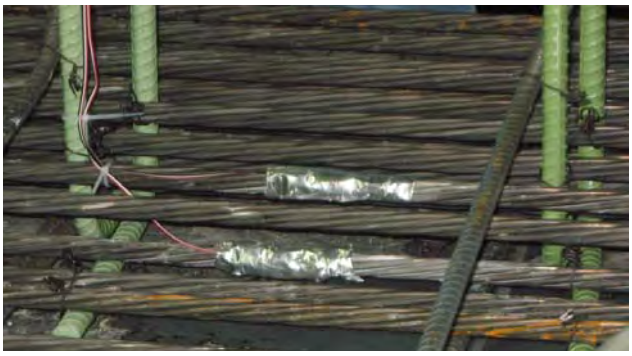

Figure 5-10. Strain Gauge Installation

The tendons were wiped clean, sanded, and then the gauges were applied with Teflon® tape and a rubber sealant. The leads were then soldered to the electrical wire. A neoprene rubber puddy material was molded around the gauge and subsequently wrapped with aluminum tape. A final transparent layer of a nitrile rubber coating was added around the aluminum tape for additional protection from moisture. The completed installation of the gauges is illustrated in Figure 5-10.

5.2.3.2 Mix design.

The mix design for the test girders was identical to that described in Section 5.1.2 during the HS-SCC trial mix.

Table 5-6. Test Girder Mix Design

Type	Material	Weight (lb/yd^3)
Coarse Aggregate	Leadbelt 1/2" Dolomite	1340
Fine Aggregate	Mississippi River Sand	1433
Cementitious Material	Portland Cement Type I	850
Water	--	280
Chemical Admixtures	Air Entraining Agent	17 oz/yd^3
	High Range Water Reducer	76.5 oz/yd^3
	Retarder	25.5 oz/yd^3
w/cm	--	0.329

Conversions: 1 lb/yd^3 = 0.5933 kg/m^3, 1.0 oz/yd^3 = 0.03708 kg/m^3

The mix design is repeated above in Table 5-6 for convenience. The mix had a 28 day design strength of 10,000 psi (68.9 MPa) and a target release strength of 8,000 psi (55.2 MPa). The target air content was 5.0%.

5.2.3.3 Concrete Batching.

The test girders were poured consecutively in four continuous batches; test girder 2 was batched first with test girder 1 batched second as shown in Figure 5-11. Air content, slump flow, and passing ability (J-ring) were performed on batches 1 and 3 (Figure 5-12).

Figure 5-11. Fabrication of Test Girders

5.2.3.4 Specimen collection.

QC/QA specimens were collected for testing of hardened concrete properties through the curing process as well as on shear test days. Eighteen 4 x 8 in. (100 x 200 mm) cylinders and 8 modulus of rupture (MOR) beams measuring 6 x 6 x 24 in. (152 x 152 x 610 mm) were collected (Figure 5-13). All 18 cylinders were sampled from batch 1, while the modulus of rupture beams were split between batches 1 and 3. The test girders and QC/QA specimens were steam cured at 120°F (49°C) for approximately 72 hours prior to release.

a) J-Ring (Passing Ability)

b) Slump Flow

c) QC/QA Cylinders and Segregation Column

Figure 5-12. Test Girder Fresh Properties

a) MOR Beams

b) Cylinders

Figure 5-13. Test Girder QC/QA Specimens

5.2.4. Storage and Delivery.

The test girders were stored in the yard below in Figure 5-14 at County Materials Corporation until delivered to the Butler Carlton Hall Structural Engineering Research Laboratory at Missouri S&T. The girders were delivered to Missouri S&T on a semi tractor-trailer bed. Test girder 1 was delivered on March 20, 2013, and test girder 2 was delivered on May 8, 2013. Figure 5-15 illustrates the delivery process at Missouri S&T.

a) West End of Storage Yard b) East End of Storage Yard

Figure 5-14. Storage Yard at County Materials Corporation

Figure 5-15. Delivery Process at Missouri S&T

5.2.5. Testing Preparation.

After the girder was delivered to the lab, researchers at Missouri S&T needed to install a cast-in-place (CIP) deck to simulate the bridge deck in Bridge A7957. After the deck was allowed to cure, external strengthening was affixed to the girder. The strengthening was used in regions that were not tested in shear. The girder was painted white and an 8 x 8 in. (203 x 203 mm) grid was drawn in the testing regions illustrated in Figure 5-16. Column gridlines were labeled 1 through 25 and row gridlines were labeled A though J.

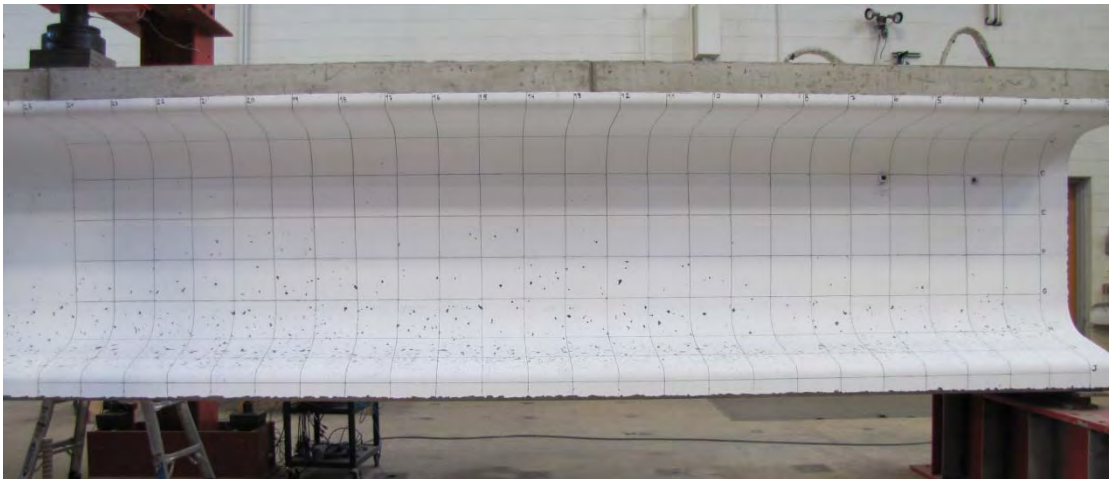

Figure 5-16. Crack Monitoring Grid

5.2.5.1 CIP deck.

The deck was 6 in. (152 mm) thick and spanned the entire width of the top flange (minus the thickness of the formwork) for a total width of 43.25 in. (1.10 m). The longitudinal reinforcement included three rows of #4 (no. 13) bars with a 5 ft. (1.52 m) splice at mid-span. Five no. 4 stirrups were placed at third points of the girder to support the longitudinal reinforcement. Two #4 (no. 13) stirrups were placed at each end with two intermediate stirrups. Clear cover for the reinforcement was 1.5 in. (38 mm) on all sides and 1.0 in (25 mm) on the top. The deck reinforcement layout is shown in Figure 5-17 with the formwork in Figure 5-18.

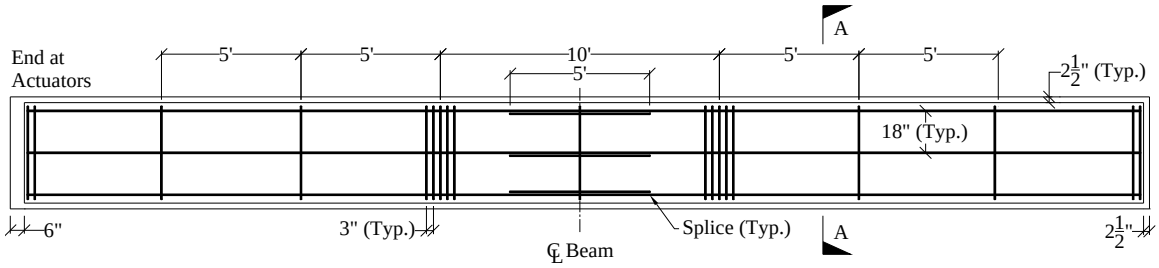

Conversion: 1 in. = 25.4 mm

a) Plan

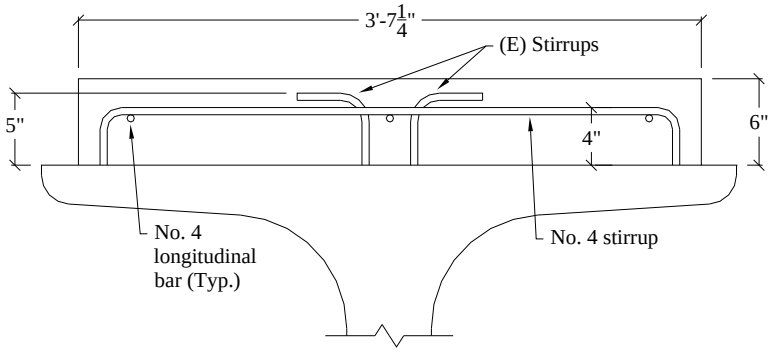

Conversion: 1 in. = 25.4 mm

Section A-A

Figure 5-17. CIP Deck Reinforcement Layout

Figure 5-18. CIP Deck Preparation

5.2.5.1.1 Mix design.

The deck mix design was based off of MoDOT's modified B-2 mix, identification no. 12CDMB2A087. The deck mixes were batched by Ozark Ready Mix Company, Inc. of Rolla, Missouri. The mix design for both girder decks is shown below in Table 5-7; amounts in () indicate values used in test girder 2 deck mix. The mix had a design w/cm ratio of 0.37 with a target air content and slump of 6.0% and 6.0 in. (152 mm), respectively. MoDOT's modified B-2 mix has a target 28 day compressive strength of 4,000 psi (27.6 MPa).

Table 5-7. Test Girder CIP Deck Mix Design

Type	Material	Weight (lb/yd^3)
Coarse Aggregate	Jefferson City 1" Dolomite	1895
Fine Aggregate	Missouri River Sand	1170
Cementitious Material	Portland Cement Type I	450
	Fly Ash Type C	150
Water	--	220
Chemical Admixtures	Air Entraining Agent	4.6 (6.2) oz/yd^3
	Mid Range Water Reducer	60 oz/yd^3
w/cm	--	0.37

Conversions: 1 lb/yd^3 = 0.5933 kg/m^3, 1.0 oz/yd^3 = 0.03708 kg/m^3

5.2.5.1.2 Specimen collection.

The decks were poured on March 28, 2013 and May 10, 2013 for TG1 and TG2, respectively. The decks were poured at the Structural Engineering Research Laboratory in Butler Carlton Hall at Missouri S&T. Figure 5-19 shows representative images of the pours. Twenty-one 4 x 8 in. (100 x 200 mm) cylinders were collected for compressive strength testing as illustrated in Figure 5-20.

a) CIP Deck Pour

b) Finishing of CIP Deck

Figure 5-19. Test Girder CIP Deck Pour

Figure 5-20. Test Girder CIP Deck QC/QA Specimens

After pouring, the deck was tarped for 14 days (Figure 5-21). The QC/QA cylinders were also placed beneath the tarp to simulate the curing conditions of the deck. Due to time constraints for testing in the laboratory, the second test girder deck was tarped for 7 days and then subsequently coated with a transparent paint sealant to lock in moisture. Without the tarp in place for the second week, the preparation time of the second test girder was accelerated.

Figure 5-21. Tarping of CIP Deck

5.2.5.2 External strengthening.

After the tarp was removed from the test girder, external strengthening was applied to the girder in the non-tested region (Figure 5-22). Since the amount of shear reinforcement in the middle 10 ft. (3.05 m) – see Table 5-5 – was double or more than that in the tested region, external strengthening was not applied in the central region. External strengthening was applied approximately every 2 ft. (610 mm) from the adjacent support as indicated in Figure 5-23. Notches were cut in the top flange of the girder for the actuators and Dywidag bars.

a) Strengthening for Test #1 b) Strengthening for Test #2

Figure 5-22. External Strengthening

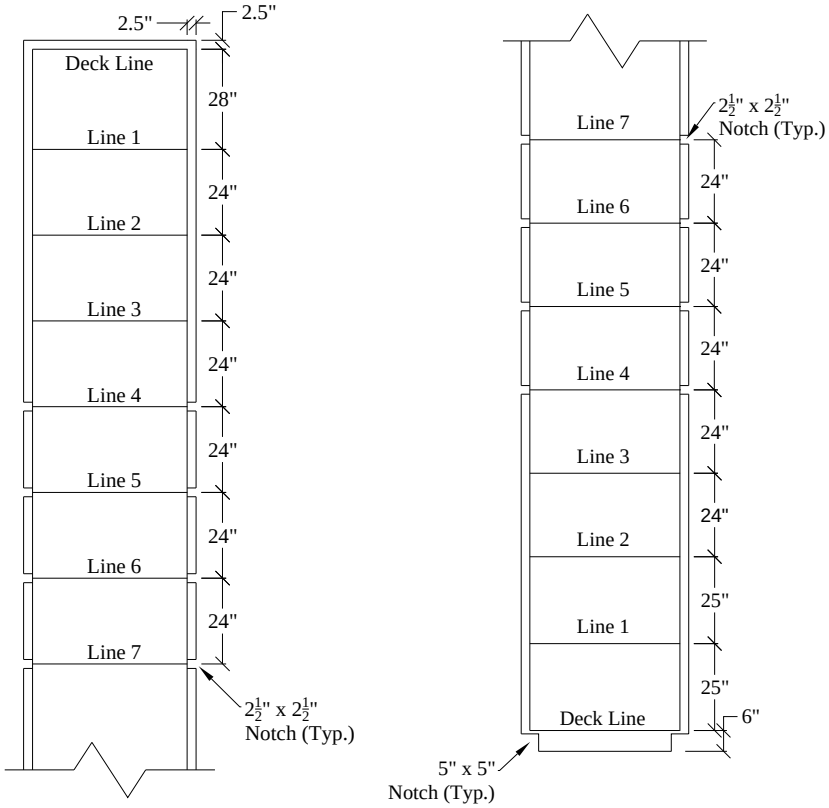

Conversion: 1 in. = 25.4 mm

a) North End b) South End

Figure 5-23. External Strengthening Layout

Each stiffener line consisted of a top and bottom beam, consisting of two C-Shape channel sections welded together by ½ in. (12.7 mm) thick plates. Stiffeners were also welded to the channels to prevent a buckling failure of the web. They were connected by two #14 (no. 43) Dywidag bars with a yield strength of 75 ksi (517 MPa). The channel sections ranged in from size C10x30 towards the interior of the girder to size C15x50 at the supports. A schematic of the strengthening system is shown in Figure 5-24.

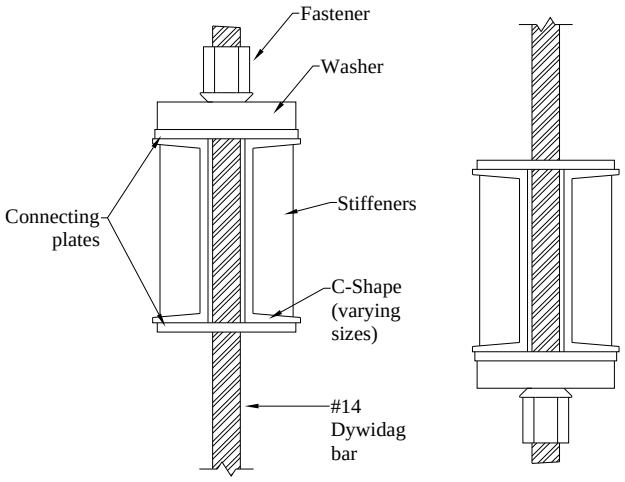

a) Top Side b) Bottom Side

Figure 5-24. External Strengthening Schematic

5.2.6. Test Setup.

The girders were tested under 3 point loading, displayed in Figure 5-25. Two 110 kip (490 kN) capacity actuators were used to apply load to the girder by lifting upward at the south end, creating a downward acting reaction force from the reaction frame. A 500 kip load cell was used to record the load from the reaction frame. The actuators alone did not supply sufficient force during the test. After they reached capacity, a 400 kip (1780 kN) capacity hydraulic jack, situated approximately 12 in. (305 mm) on the interior side of the load frame, was used to apply additional load. After test #1, the reaction frame (Figure 5-26c) was moved 9 feet to the south to test the unreinforced section of the girder. Due to the laboratory strong floor anchor holes located every 3 ft. (914 mm), the test length varied from 16 ft. (4.88 m) for the first test to 15 ft. (4.57 m) for the second test.

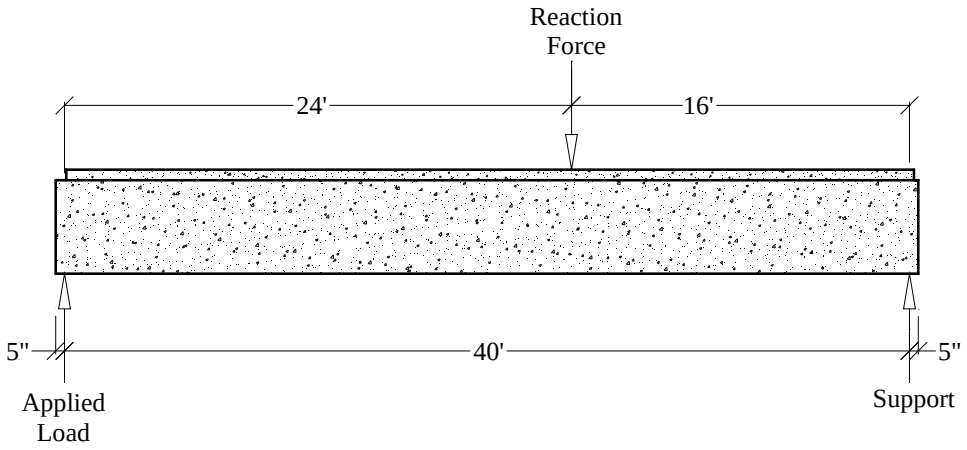

Conversion: 1 ft. = 0.3048 m

a) Test #1 (Reinforced Side)

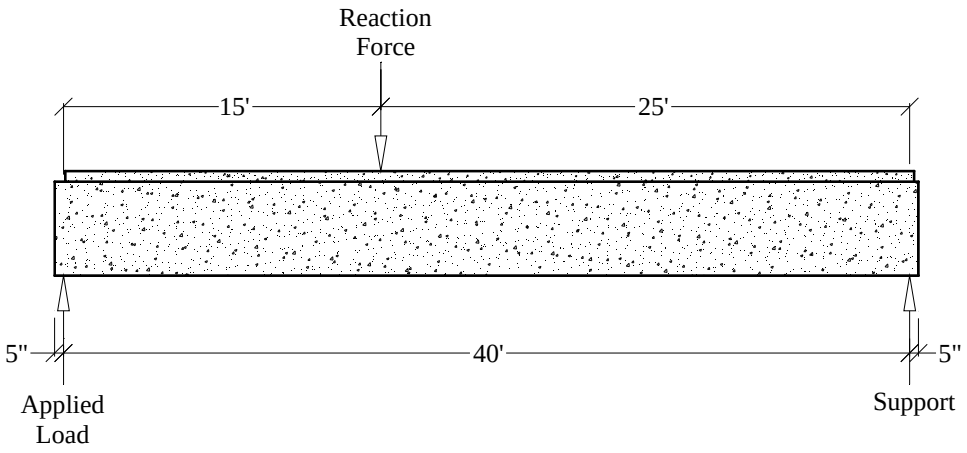

Conversion: 1 ft. = 0.3048 m

b) Test #2 (Unreinforced Side)

Figure 5-25. Test Setup Schematic

The test set-up is shown in Figure 5-26. The girder rested on two W24x176 I-beams; one at the north end and the other 5 ft. (1.52 m) from the south end. The load frame and reaction frame consisted of two W30x90 beams welded together and supported by W14x90 columns.

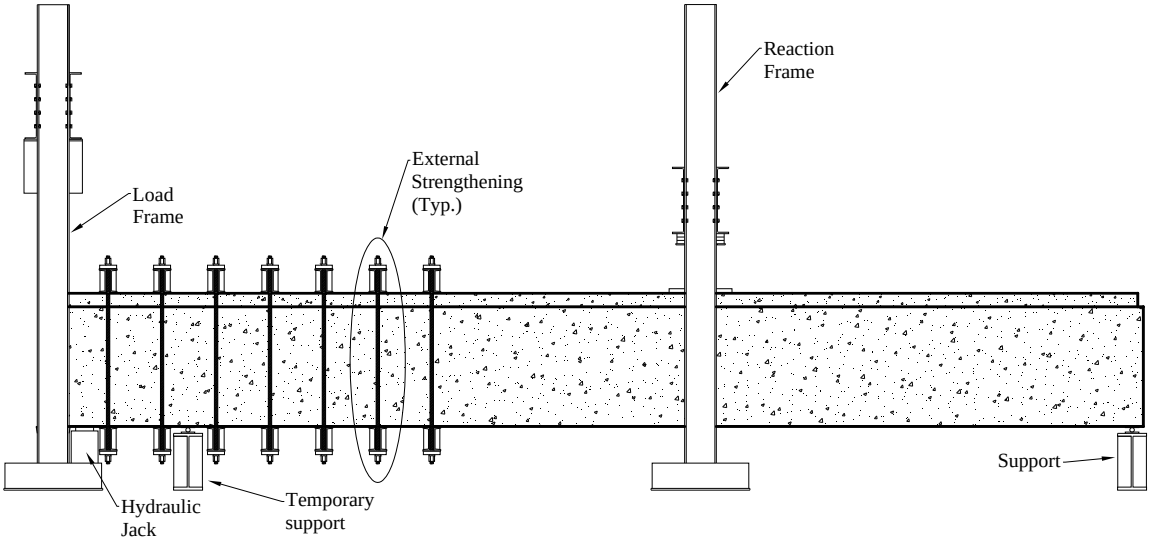

a) Setup for Test #1

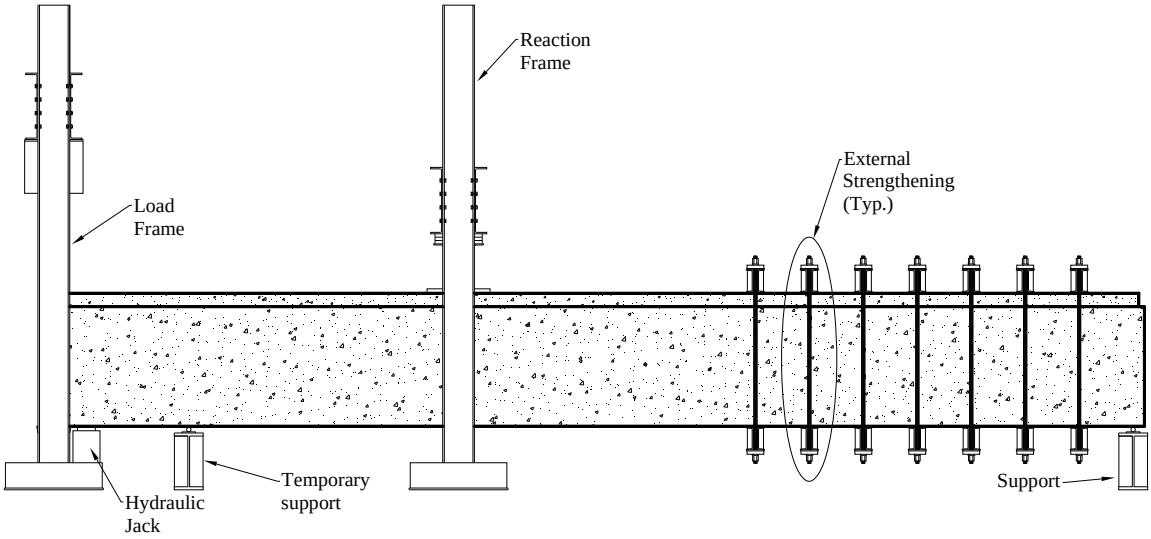

b) Setup for Test #2

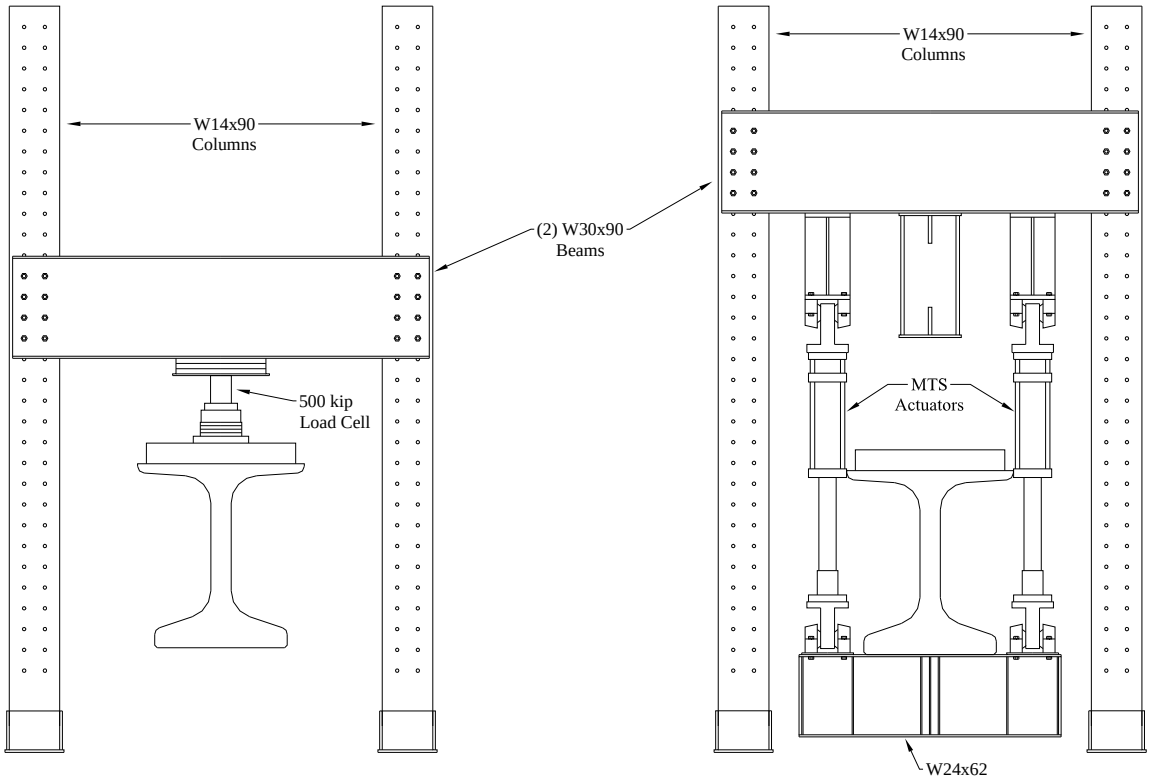

c) Reaction Frame d) Load Frame

Figure 5-26. Overall Test Setup

5.2.7. Test Procedure.

The testing schedule is displayed previously in Table 5-4. The shear reinforced region was tested first due to the ductile failure nature, and for the girder to still retain a majority of its stiffness properties for the second test. After the first test concluded, the reaction frame was moved to the south 9 ft. (2.75 m) and the external strengthening was moved to the opposite end.

The test underwent displacement controlled loading. The actuators lifted the girder at the south end at a rate of 0.1 in/min (2.5 mm/min). Loading continued until approximately 75 kips (334 kN) were read from the load cell at the reaction frame. The girders were then examined for cracks. An additional 20 kips of load was added and the girder was then checked for cracking. This procedure was repeated until the first sign of cracking. Loading ceased and cracks were marked every 0.2 in. (5.1 mm) of deflection at the actuators. Prior to flexural cracking, this increment of 0.2 in. (5.1 mm) corresponded

to an increase in shear of approximately 20 kips (89 kN). After flexural cracking, a 0.2 in. deflection correlated to an increase in shear of roughly 10 kips (44.5 kN).

Once the actuators reached capacity, the 400 kip hydraulic jack was manually operated as seen in Figure 5-27. The displacement of the actuators was closely monitored while operating the jack to meet the 0.1 in./min loading rate.

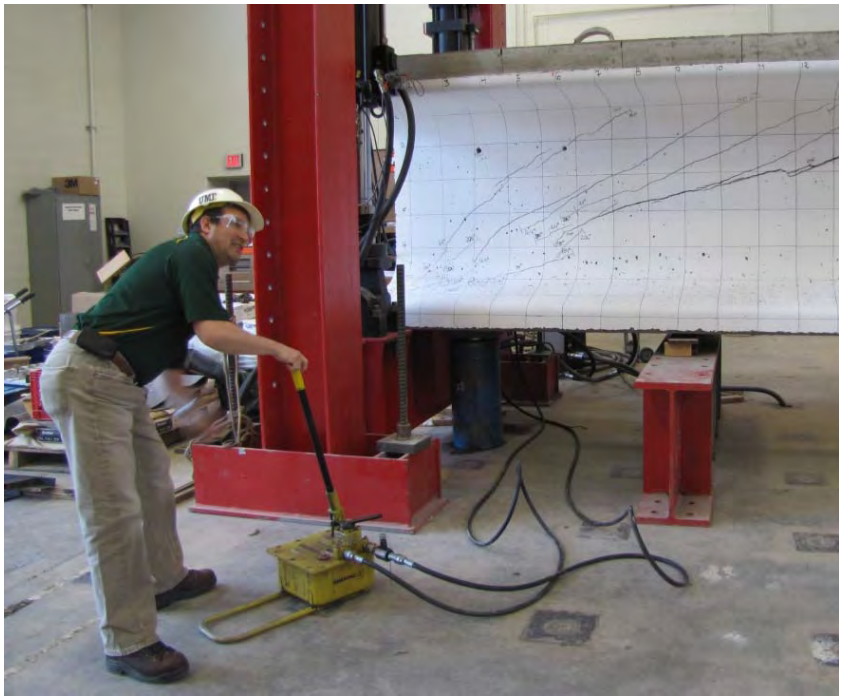

Figure 5-27. 400 kip Hydraulic Jack

The first test, consisting of shear reinforcement, was not tested to complete failure. Despite the external strengthening that was applied at the opposite end of the girder, hairline cracks still developed in this region as shown in Figure 5-28. The Dywidag bars elongated, which resulted in hairline cracking in the externally strengthened region. To prevent excessive damage in this region during the first test, the region with shear reinforcement was not loaded to failure.

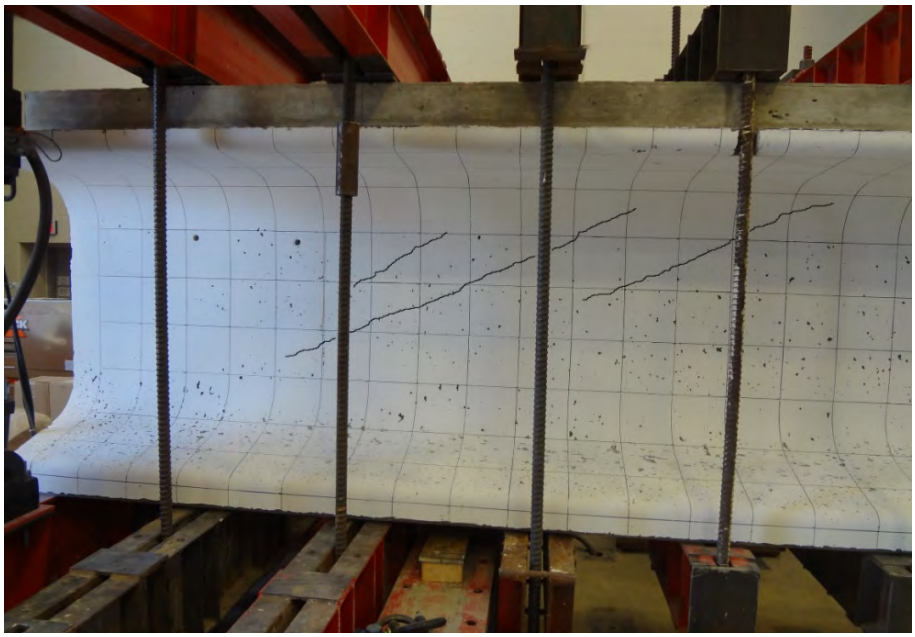

Figure 5-28. Cracks in Non-Tested Region (Cracks traced for clarity)

The second test (no shear reinforcement) was tested following the same rate and procedures as the first test. However, this region was tested to failure to obtain the ultimate shear capacity of the section; this corresponded to the shear capacity of the concrete not in the presence of shear reinforcement. Following the completion of testing, the girders were demolished into three sections and hauled out of the SERL in Butler-Carlton Hall illustrated in Figure 5-29.

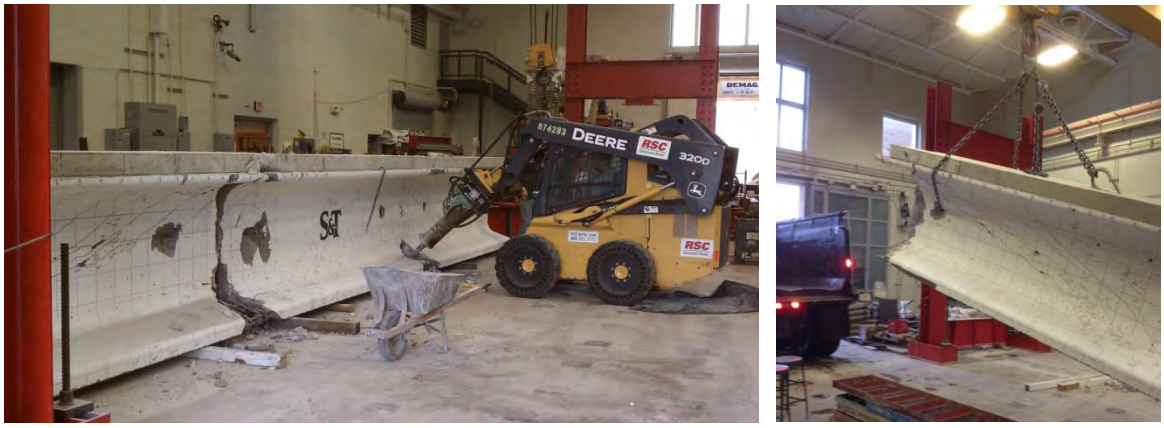

a) Demolition of Test Girder b) Removal of Test Girder

Figure 5-29. Demolition and Removal of Test Girders

5.3. INSTRUMENTATION PLAN AND FIELD PREPARATION

5.3.1. Equipment and Gauges.

The instrumentation equipment and gauges employed on this implementation project are summarized in Table 5-8. Two data acquisition systems were assembled for the girders' data collection. The VWSG can provide a strain profile through the cross section of the PC girders as well as temperature profiles. A total of 86 VWSG with thermistors were embedded in the PC/PS girders, PC/PS panels and CIP deck of Bridge A7957.

Table 4-4 presents the number of VWSG installed within the different components of Bridge A7957. A compact RIO acquisition system was assembled for temperature data collection during and after the bents' concrete placement. A total of 16 thermocouples were connected to the compact RIO acquisition system. Two electrical resistance strain gauges were used for each girder tested in the laboratory. At the precast plant, a TS equipment was used to obtain the camber deflections of the PC/PS girders as described in sections 4.1.3 and 4.2.6.

Table 5-8. Instrumentation Equipment and Gauges

EQUIPMENT & GAUGES	QUANTITY	DESCRIPTION
CR800 DAS	2	Collecting data from VWSG
Compact Rio	1	Collecting data from thermocouples
Thermocouples	16	Monitoring temperature
Vibrating wire strain gauges (VWSG)	86	Monitoring strain and temperature
Electrical resistance strain gauges (ERSG)	4	Monitoring strain
Total Station (TS)	1	Monitoring deflection

5.3.2. Instrumentation Location.

In the precast plant, six out of twelve PC/PS girders were instrumented at the cluster locations displayed in Figure 5-30. A total of 86 VWSG with built-in thermistors,

type EM-5, manufactured by Roctest Inc., were employed to monitor the stress variation as well as temperature changes in the girders, panels and CIP deck from fabrication through service life. The VWSG were installed prior to casting of the PC girders and were limited to girder lines 3 and 4 of the bridge (Figure 5-30). The CIP deck was instrumented at 16 different locations before concrete placement.

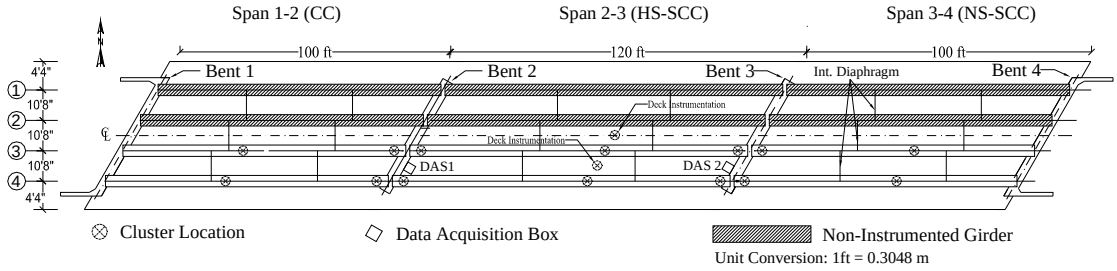

Figure 5-30. Bridge A7957's Instrumented Girders and Clusters' Locations

5.3.3. Gauge Numbering and Identification.

A complete identification of each gauge was performed to minimize confusion when installing and analyzing the data. The gauge identification designations are listed in Table 5-9 and Table 5-10.

Table 5-9. Girders, Panels and Deck's Gauge Identification Designations

ITEMS	IDENTIFICATION			
Embedded Gauge Number	Type		Range	Named
	Deck VW		See Appendix C	(1-2)
	Girder VW		See Appendix C	(1-7)
	Girder ER		N/A	(1-2)
Girders and Decks Designation	Sm		S=Span; m=Span #	
	Gn		G= Girder; n= Girder #	
	Dmn		D= Deck; m, n= Girder line #	
Embedded Gauge Depth (Mid-span and Near Support Sections)	TD*: M7, W5, E5		Top Deck# (6 in. Above Bottom Fiber)	
	BD*: M6		Bottom Deck (2 in. Above Bottom Fiber)	
	TF*: M5, W4, E4		Top Flange (2 in. Below Top Fiber)	
	CGC*: M4, W3, E3		Center of Gravity of Composite Beam Section	
	CGU/CGI*: M3		Center Gravity of Noncomposite Beam Section	
	CGS*: M2, W2, E2		Center of Gravity of Pretensioned Strands	
	BF*: M1, W1, E1		Bottom Flange (2 in. Above Bottom Fiber)	
Embedded Gauge Depth (Deck's Mid-span)	M2		Top Deck# (4½ in. above Bottom Fiber)	
	M1		Mid Height of PC Panel	
Embedded Gauge Depth (Lab Test Girders)	TF*: M2		Top Flange (2 in. Below Top Fiber)	
	BF*: M1		Bottom Flange (2 in. Above Bottom Fiber)	
Longitudinal Location of Gauges	W		Near Girder's West Support	
	M		Girder's Mid-span	
	E		Near Girder's East Support	
Gauge Type	Embedded Gauges	VW	Vibrating Wire Strain Gauge, VWSG	
		TR	Thermistor (Integral with VWSG)	
		ER	Electrical Resistance Strain Gauge	
	Other Sensor	TS	Total Station	
DAS	CR800		DAS BOX 1	DAS BOX 2

*: VWSG depth according to instrumentation plan (Appendix B).

#: The original depth locations proposed in the instrumentation plan (Appendix B) were adjusted to precast plant conditions.

Table 5-10. Bent's Gauge Identification Designations

ITEMS	IDENTIFICATION		
Embedded Gauge Number	Type	Range	Named
	Bent TC	N/A	2-3
Bent Designation	Bm	B=Bent; m=Bent #	
Web Wall Designation	NC	NC= North Column's Center Line	
	SC	SC= South Column's Center Line	
	NW	NW= Web Wall 's North Side	
	SW	SW= Web Wall 's South Side	
Pier Cap Designation	PC	Pier Cap	
	B	Bottom	
	M	Mid Height	
	T	Top	
	MT	Ambient Temperature	
Gauge Type	TC	Thermocouple	
DAS	Compact RIO		

5.3.4. Gauge Locations.

Within each girder of span (1-2) and span (3-4), the instrumentation clusters were located at two cross-sections. The first cross-section was located at mid-span, and the second was at 2ft (610 mm) from the centerline of bents 2 and 3, respectively. For span (2-3), the instrumentation clusters were located at three different locations: one at mid-span, and the remaining two at approximately 2 ft. (610 mm) from each support centerline. The locations at which the VWSG were installed are specified in Table 5-9. Figure 5-31 shows the cluster locations and layers at which the sensors were installed (mid-span and near the supports). More details about the instrumentation are presented in Appendices B and C.

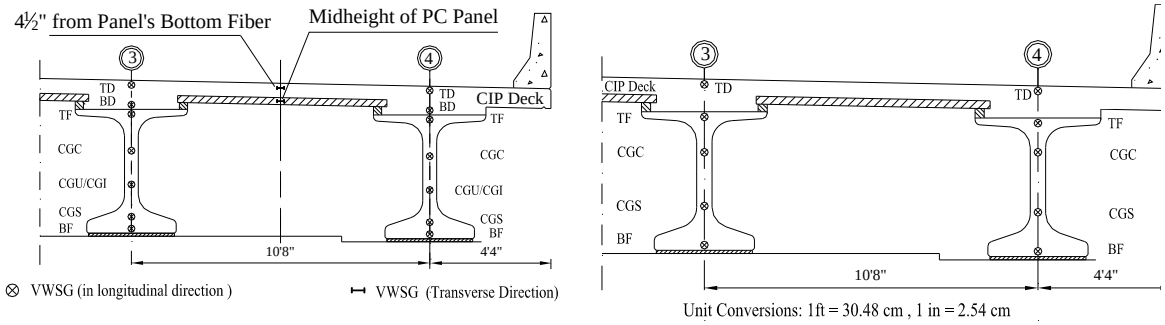

(a) Mid-span b) Near Support

Figure 5-31. VWSG Installation Detail through the Different Girders' Sections

5.3.5. Embedded Gauges Preparation.

All sensors were prepared in the Structural Engineering Research Laboratory at Missouri S&T prior to installation in the field. The first step consisted in cutting the thermocouples to the specified length of the different sections of the interior bents (web wall and pier cap).

Figure 5-32. Thermocouple Preparation Prior to Field Installation

To prepare the thermocouple sensors, the two wires at one end were twisted and welded. Afterwards, the same end was coated with a rubber coating (Performix Plasti Dip®) for protection. Additionally, the sensors were labeled according to information specified in Table 5-10. Additional details about the locations where the thermocouples

were installed and the corresponding label used for each of them are given in Table 5-10 and Figure 5-34. The VWSG did not require a significant work preparation. To prevent any damage on the VWSG's body, a zip tie was fastened around its body as shown in Figure 5-33a. Afterwards, all the wires were numbered and labeled (Figure 5-33b) according to the information listed in Table 5-9. Finally, the VWSG were grouped depending on the section they were going to be installed within the PC girders and CIP deck.

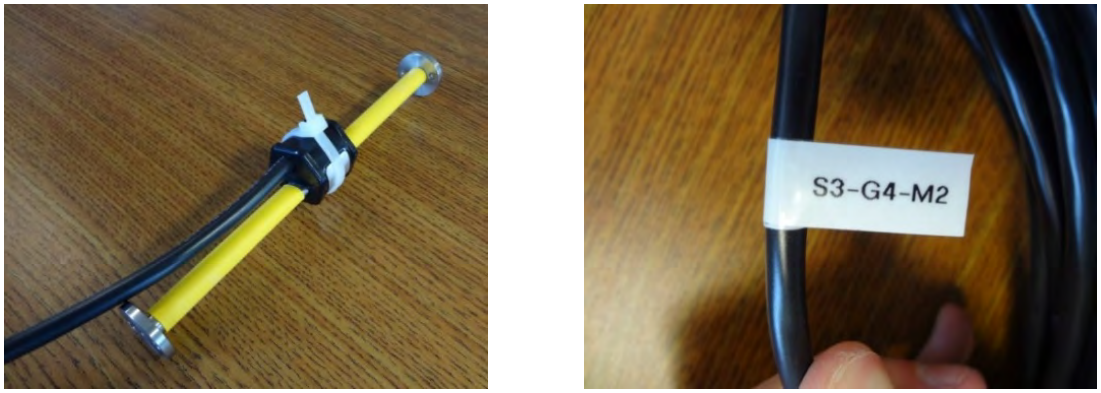

a) VWSG Secured with Zip Tie b) VWSG Labeled for Field Installation

Figure 5-33. VWSG Preparation Prior to Field Installation

5.3.6. Field Installation.

5.3.6.1 Intermediate bents.

Thermocouple sensors were installed within bents 2 and 3 to read temperature data during and after casting.

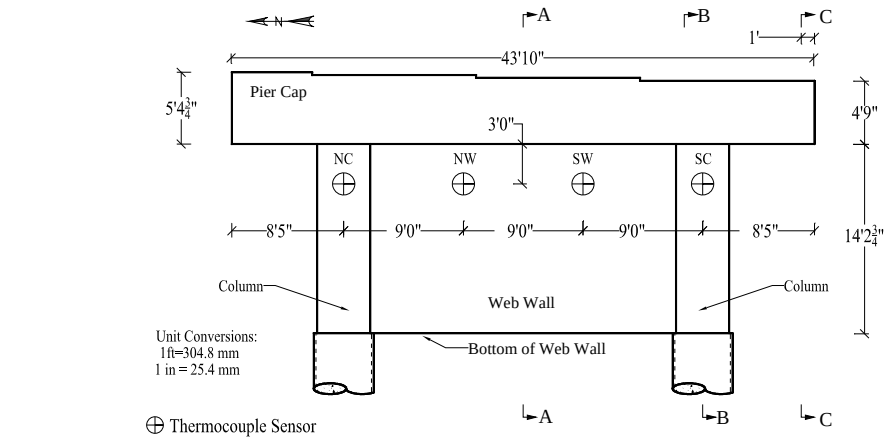

a) Bent Elevation

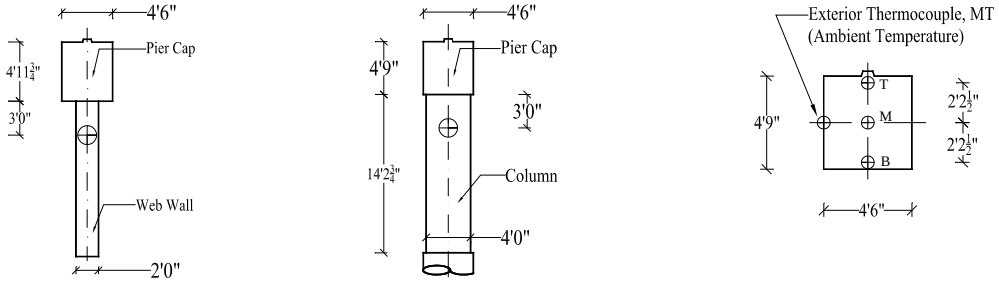

b) Section A-A c) Section B-B d) Section C-C

Figure 5-34. Thermocouple Sensors Installation Details

Additionally, the ambient temperature was recorded to adjust for any differences between the materials used in both bents when they were subjected to similar environmental conditions. For each bent, a thermocouple was installed at the center line of each column 3 ft. (0.91 m) from the bottom edge of the pier cap (Figure 5-34a and Figure 5-34c). A second set of thermocouples were placed in the web wall 9 ft. (2.74 m) from the center line of each column (Figure 5-34a and Figure 5-34b) in the same horizontal plane. At section C (Figure 5-34a), located 1 ft. (0.30 m) from the south end of the pier cap, one exterior and three interior thermocouples were installed according to the

detail shown in Figure 5-34d. Figure 5-35 shows the installation procedure of the thermocouple sensors within the bents' web wall.

Figure 5-35. Thermocouples Installation on Bent 2's Web Wall

The thermocouples were strapped around the reinforcing steel by zip ties to avoid any possible damage of the sensors during concrete placement. Figure 5-36 shows some of the thermocouples installed at specified bent sections.

a) Column (B3-NC)

b) Web Wall (B3-SW)

Figure 5-36. Thermocouples Installed at Specified Bent Sections

5.3.6.2 Precast prestressed girders.

After all the strands were tensioned, usually about one or two days prior to casting, placement of the shear reinforcement was conducted by the fabricator. The placement of embedded VWSG within the prestressed girders was performed after this procedure because the steel reinforcement was used as a framework for the gauges.

Figure 5-37a shows the process of placing a VWSG within a section located near the end of a girder. Gauges located at a mid-span section are shown in Figure 5-37b. After the installation was completed, the gauges were connected to one of the DAS boxes as shown in Figure 5-38.

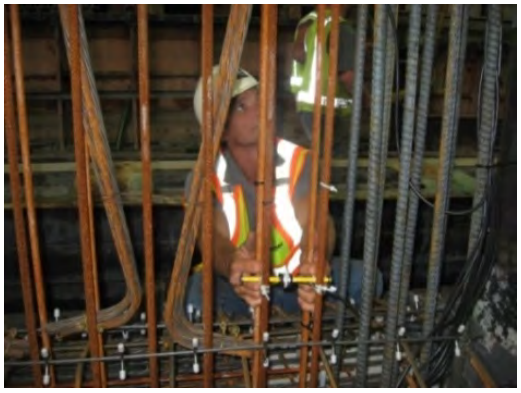

a) VWSG Installation at Specified Depth

b) VWSG Installed at Specified Sections

Figure 5-37. VWSG Installation within PC Girders at Precast Plant

a) DAS Box 1

b) Antenna Installation to DAS Box 1

Figure 5-38. VWSGs Connected to DAS Box

DAS box 1 was employed as the main acquisition system while DAS box 2 worked as the auxiliary acquisition system (Figure 5-38 and Figure 5-39). When the secondary box was used, it was always necessary to employ the main box to allow remote communication of the data to the lab. In such a case, the DAS box 1 was installed aside the PC girder as shown in Figure 5-39a.

a) CR800 DAS Box 1 (Main DAS)

b) DAS Box 2 (Secondary DAS)

Figure 5-39. VWSG Connected to DAS at Precast Plant

After concrete reached the required compressive strength necessary for release, the prestressing force was released and the VWSG were allowed to collect the strain variation for at least one hour. Finally, the girders were moved to the yard for storage until being delivered to the bridge site.

5.3.7. Precast prestressed panels.

A VWSG was installed within two PC/PS panels at the precast plant. These panels were placed at the mid-span section of span 2-3, between girder lines 2 and 3 and girder lines 3 and 4, respectively. Once the panels were set on the girders, the two VWSG remained perpendicularly oriented to the girders' longitudinal axis (according to the details of Figure 5-30 and Figure 5-31a). Figure 5-40 shows the detail of a VWSG installed at mid-height of the precast panels.

a) Before Concrete Placement

b) After Concrete Placement

Figure 5-40. VWSG Installed within PC/PS Panels

5.3.7.1 CIP deck.

A total of twenty two VWSG were installed within the CIP RC deck. Twenty of them were installed along the girders' longitudinal direction as specified in Figure 5-31a. Figure 5-41 shows the two PC/PS panels that were instrumented with VWSG along the perpendicular direction of the bridge. Figure 5-42 shows details of the VWSG employed within the CIP deck at mid-span and near-support sections.

Figure 5-41. Instrumented PC/PS Panels

The two last VWSG were transversely placed at 4.5 in (114 mm) from the bottom of the instrumented panels. One was located between girder lines 2 and 3, and the second between girder lines 3 and 4 (Figure 5-31a). DAS box 1 and DAS box 2 were situated on the interior sides of bent 2 and bent 3 pier caps. The 86 VWSG were split into two groups of 43 sensors that were connected to each DAS box (Figure 5-43). More details about the VWSG connected to each CR800 DAS box are given in Appendix C. After all the VWSG were placed within the deck, the CR800 DAS were anchored to the interior faces of the bents' pier caps.

a) Mid-span Section

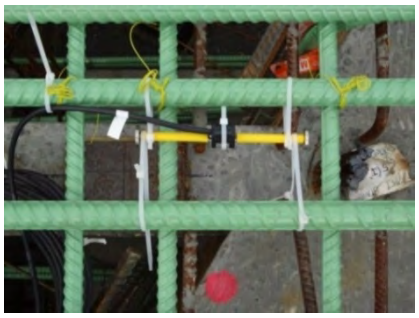

b) Near Support Section

Figure 5-42. VWSG Installed on CIP RC Deck

Figure 5-43. Bridge A7957 VWSG Instrumentation

5.3.8. DEMEC Points.

A small predrilled stainless steel disks as shown in Figure 5-44 were adhered to the surface of specimens with five minutes quick set epoxy. They were arranged in three vertical lines of five points, 120° apart and from this arrangement nine reading can be taken per specimen by inserting the DEMEC gauge in the DEMEC point and then the reading is taken. The average of all readings can be used to obtain the shrinkage strain in the specimen.

Figure 5-44. Stainless Steel DEMEC points

5.3.9. RFID Corrosion Sensors.

Two RFID corrosion sensors (Figure 4-10), identified in Figure 5-45 as RFID corrosion sensors 1 and 2, were embedded at two different locations within the south side of the CIP RC deck. The purpose of the sensors is to detect two critical chloride

concentration levels at each location. The first value of chloride concentration will mark the onset of corrosion. The second value will be used to establish a correlation between the chloride ingress and the area of reinforcing steel that might be lost at that moment.

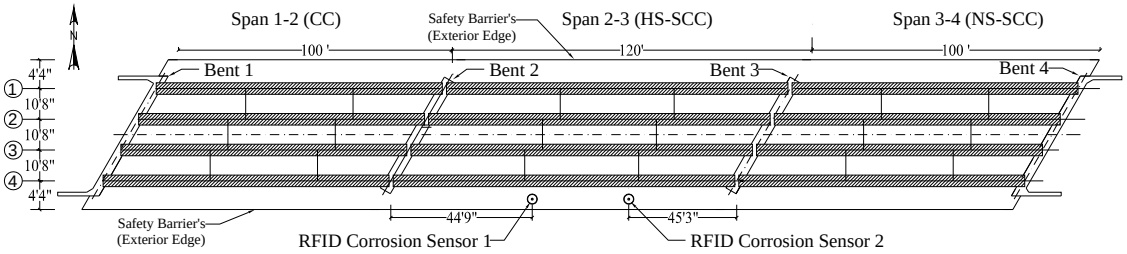

Figure 5-45. Bridge A7957 RFID Corrosion Sensors Installation (Plan View)

Table 5-11 presents the location's coordinates within the RC deck where the sensors were installed. Corrosion sensor 1 was placed 44 ft. 9 in. (13.7m) from the center line of bent 2 (Figure 5-45), along the direction of the safety barriers' longitudinal axis. This sensor was located 0.25 in. (0.6 cm) from the top surface of the deck, and at a distance of 22.0 in. (55.9 cm) from the exterior edge of the safety barrier (Figure 5-46).

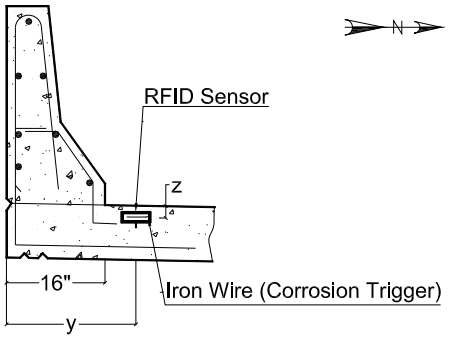

Figure 5-46. Bridge A7957 RFID Corrosion Sensors Installation (Elevation)

The second sensor was set 45 ft. 3 in. from the center line of bent 3, along the direction of safety barrier's principal axis. This sensor was separated 0.50 in. (1.3 cm) from the top surface of the deck and placed at a distance of 18.25 in. (46.4 cm) from the exterior edge of the safety barrier (as reported in Table 5-11).

Table 5-11. RFID Sensors' Coordinates through CIP RC Deck of Bridge A7957

Sensor No	*Y*	*Z*
1	22"	¼"
2	18 ¼"	½"

Figure 5-47 shows an RFID corrosion sensor installed within the CIP RC deck of Bridge A7957 before concrete placement.

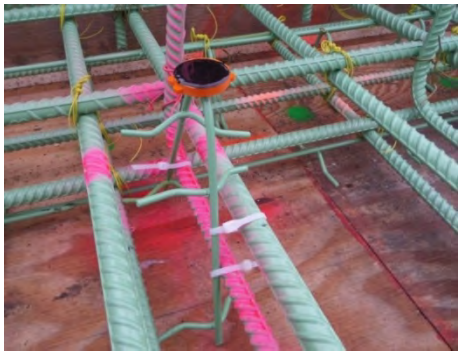

Figure 5-47. RFID Installed on CIP RC Deck (Before Concrete Placement)

5.3.10. Steel Plate Installation for Total Station Data Collection.

Twenty four steel plates were fixed along the girders of Bridge A7957 at the locations shown in Figure 5-48.

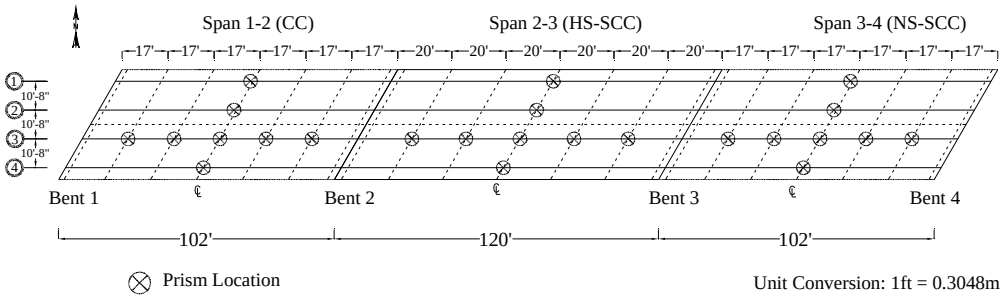

Figure 5-48. Prisms Layout for TS Data Collection

Before the diagnostic live load test was conducted, the TS prisms were magnetically mounted on the plate locations shown in Figure 5-48. The coordinates of these targets are read before, during and after the bridge is loaded, and then the deflection

of the points shown in Figure 5-48 is computed. More information about the trucks configurations during a load test is shown in Appendix D. The information that was obtained during the first series of load tests will be used to establish a benchmark of the bridge structure response under in-service conditions. As mention in section 4.2.6, the second part of the first series of load tests will be conducted in August 2014.

For each span, the steel plates were situated at L/6, L/3, L/2, 2/3L and 5/6L. L is the length of the span measured between the bents center lines. The steel plates were fixed to the bottom of the girder with an epoxy adhesive (Loctite® Metal & Concrete Gray Epoxy) which set within 5 minutes. Figure 5-49 shows the installation of a steel plate underneath the bottom flange of one of the girders situated in span 2-3.

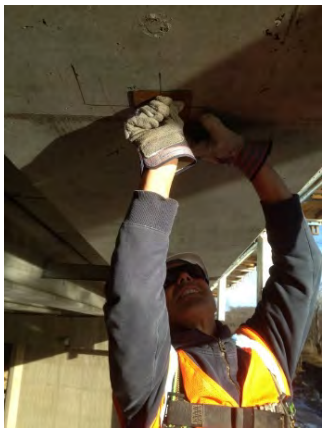

a) Steel Plate Installation

b) Steel Plate Fixed (Girder's Bottom Flange)

Figure 5-49. Steel Plate Installation for Deflection Data Collection with TS

5.4. INTERMEDIATE BENT CONSTRUCTION

The first phase of the construction monitoring process of bridge A7957 included the two intermediate bents. Bent no. 2 consisted of MoDOT's standard B mix while bent no. 3 was designed using MoDOT's B-2 mix with a 50% fly ash replacement level. The concrete temperature development profiles were recorded and analyzed between the two mixes.

Each bent was constructed in two phases. First, the columns and web wall were poured. After sufficient strength was achieved, the pier cap was cast. Table 5-12 displays the construction schedule for the intermediate bents.

Table 5-12. Intermediate Bents Construction Schedule

Activity	Date
Instrumentation of bent 3 columns and web wall	6/28/2013
Pour of bent 3 columns and web wall	7/3/2013
Instrumentation of bent 2 columns and web wall	7/11/2013
Pour of bent 2 columns and web wall	7/12/2013
Instrumentation of bent 3 pier cap	7/23/2013
Pour of bent 3 pier cap	7/25/2013
Instrumentation of bent 2 pier cap	7/29/2013
Pour of bent 2 pier cap	7/30/2013

5.4.1. Mix Designs.

Two mix designs were used in the intermediate bents. Bent 2 consisted of MoDOT's class B mix while bent 3 consisted of the same class B mix, modified with 50% fly ash replacement; mix IDs for bents 2 and 3 are 12CDB00A084 and 13CDHFVA003, respectively. Both mixes were batched by Osage County Concrete of Linn, MO. The design compressive strength for bents 2 and 3 was 3,000 psi (20.7 MPa). The mix designs are presented in Table 5-13. Air content and slump tests were performed prior to each pour. Twenty-four 4 x 8 in. (100 x 200 mm) cylinders were collected for maturity studies of the compressive strength at 1, 3, 7, 14, 28, and 56 days as shown in Figure 5-50. The cylinders were field cured both at the job site as well as Missouri S&T to simulate the exposure conditions of the bridge substructure elements.

Figure 5-50. Intermediate Bent QC/QA Specimens

Table 5-13. Intermediate Bents Mix Designs

Type	Material	Bent 2 (lb/yd^3)	Bent 3 (lb/yd^3)
Coarse Aggregate	Choteau-Burlington-Cedar Valley – Gradation D Ledges 1A, 1B, 1, 2, 3	1840	1750
Fine Aggregate	Missouri River/Class A	1225	1242
Cementitious Material	Portland Cement – Type I/II	425	325
	Fly Ash – Class C	105	325
Water	--	248	213
Chemical Admixtures	Air Entraining Agent	6 oz/yd^3	6.5 oz/yd^3
	Water Reducer	11 oz/yd^3	13 oz/yd^3
w/cm	--	0.45	0.33
Design Air Content (%)	--	6.0	6.0

Conversions: 1 lb/yd^3 = 0.5933 kg/m^3, 1.0 oz/yd^3 = 0.03708 kg/m^3

5.4.2. Data Collection.

Temperature data was recorded during each of the four castings of the intermediate bents identified previously in Table 5-12. After the thermocouples were installed, they were hooked up to the Compact RIO system. For the construction of the columns and web walls, the solar panel was connected after the pour was complete; the solar panel was connected before the pour of the pier caps. Data was collected for

approximately 24-48 hours from the start of each pour. Figure 5-51 shows the DAS during the intermediate bent construction.

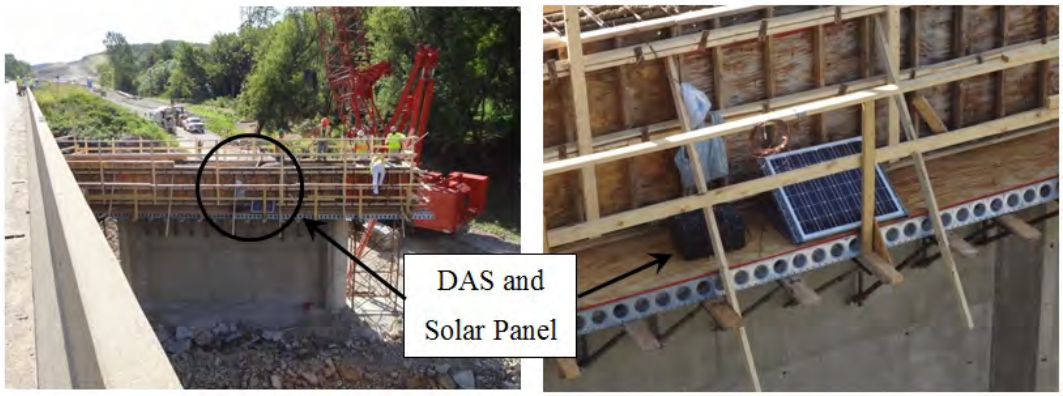

a) Bent 3 Pier Cap

b) Bent 2 Pier Cap c) Bent 3 Columns and Web Wall

Figure 5-51. Data Collection at Intermediate Bents

5.5. PC/PS GIRDERS AND PANELS FABRICATION

The second stage of the construction process included monitoring the fabrication of two precast PC girders per span and two precast panels placed at the locations shown in Figure 5-30.

A preconstruction planning meeting was held on November 16th, 2012, at Missouri S&T. The concrete producer, fabricator, contractor, and Missouri S&T researchers participated to clarify any details specific to the construction of the bridge and its components. The bridge girders and panels were fabricated from July 26th through Aug 22nd, 2013 at the County Materials Corporation precast plant in Bonne Terre, MO. For the three spans, the PC/PS girders located on lines 3 and 4 (Figure 5-30) were

selected to be monitored during their fabrication. Table 5-14 lists the construction timeline and the estimated steam curing time for the precast PC/PS girders and panels of Bridge A7957.

Table 5-14. PC/PS Girders Construction Timeline

Activities	Date
Instrumentation of span 1-2 girder 4 (S1-G4)	7/26/13
Pour of S1-G4 (steam cured for 16 hours)	7/29/13
Release of S1-G4	7/30/13
Instrumentation of span 1-2 girder 3 (S1-G3)	7/31/13
Pour of S1-G3 (steam cured for 16 hours)	8/1/13
Release of S1-G3, Instrumentation of span 3-4 girder 4 (S3-G4)	8/2/13
Pour of S3-G4 (steam cured for 38 hours)	8/3/13
Release of S3-G4, Instrumentation of span 3-4 girder 3 (S3-G3)	8/5/13
Pour of S3-G3 (steam cured for 16 hours)	8/6/13
Release of S3-G3, Instrumentation of span 2-3 girder 4 (S2-G4)	8/7/13
Pour of S2-G4 (steam cured for 88 hours)	8/8/13
Release of S2-G4,	8/12/13
Instrumentation of span 2-3 girder 3 (S2-G3), Pour of S2-G3 (steam cured for 38 hours)	8/13/13
Release of S2-G3	8/15/13
Instrumentation of precast PC panels Pour of instrumented PC/PS panels (steam cured for 15 hours)	8/21/13
Release of PC/PS panels	8/22/13

5.5.1. Mix Designs.

Three different concrete mixtures were utilized in the fabrication of the girders. The girders of the first span (span 1-2) were fabricated using a conventional concrete

(CC) mixture with a specified strength of 8,000 psi (55.2 MPa). The concrete mix ID of the first span girders was 110A10A002CM. The girders in the second span (span 2-3), fabricated with HS-SCC, have a target compressive strength of 10,000 psi (68.9 MPa). The mix ID of the girders of this span was 13SECSPE001. The third span (span 3-4) used girders fabricated of NS-SCC with a specified compressive strength of 8,000 psi (55.2 MPa). The mix ID corresponding to the girders of the last span was 13SECSPE002.

a) Slump flow and J-Ring Tests

b) Column Segregation

Figure 5-52. Fresh Property Tests (Concrete Mixtures of Spans 2-3 and 3-4)

The mix designs are listed in Table 5-15. Air content and slump flow tests were conducted prior to each pour of the girders of span 1-2. In the case of the girders of spans 2-3 and 3-4, air content, slump flow, column segregation, and J-ring flow tests were also performed before concrete placement. Thirty 4 x 8 in (100 mm x 200 mm) cylinders were collected to conduct maturity studies on the compressive strength at 1, 3, 7, 14, 28, 56, load test 1, 1 year, and load tests 2 and 3. Furthermore, six 6 x 6 x 21 in (150 x 150 x 525 mm) beam specimens were made for each instrumented girder to obtain the flexural strength of concrete at 28 days and at the time when the live load tests 1 and 2 are executed. Two 4 x 24 in (100 x 600 mm) creep, shrinkage and coefficient of thermal expansion (CTE) specimens were fabricated prior to casting of S1-G4, S3-G3, and S2-G3. Figure 5-52 shows the fresh property tests conducted on the PC/PS girders of spans 2-3 and 3-4. Figure 5-53 shows the specimens collected during the fabrication of one of the girders mentioned previously.

Table 5-15. PC/PS Girders Concrete Mixture Comparison

Type	Material	Span 1-2 (CC)* (lb/yd3)	Span 2-3 (HS-SCC) (lb/yd3)	Span 3-4 (NS-SCC) (lb/yd3)
Coarse Aggregate	Lead Belt, Park Hills Stone Masonry Grade E Dolomite	1780#	1340§	1476§
Fine Aggregate	Weber, Cristal City Sand/Class A Ledges 4-1	1085	1433	1433
Cement	Portland Cement – Type I (Holcim, Ste. Genevieve Plant)	800	850	750
Water	---	256	280	260
Chemical Admixtures	Air Entraining Agent	(1-5) oz/yd3	17.0 oz/yd3	17.0 oz/yd3
	Type D Water Reducer (Recover)	(1-3) oz/yd3	76.5 oz/yd3	67.5 oz/yd3
	Type F High Range Water Reducer (Adva Cast 575)	(9-18) oz/yd3	25.5 oz/yd3	25.5 oz/yd3
w/c	---	0.32	0.33	0.35
Design Air Content (%)	---	5.5	5.0	5.0

*: CC corresponds to MoDOT's class A-1 mix.

#: MSA was limited to ¾".

§: MSA was limited to ½".

The PC/PS panels were fabricated with a MoDOT class A-1 mix. The design compressive strength of the mixture was 6,000 psi (41.4 MPa). Eighteen cylinders 4 x 8 in. (100 mm x 200 mm) were cast to conduct compressive strength tests at 1day, 28 days, load test 1, 1 year, load test 2, and load test 3. The cylinders were field cured both at the job site as well as at Missouri S&T to simulate the same exposure conditions of the bridge girder elements.

Figure 5-53. PC/PS Girders QC/QA Specimens

5.5.2. Data Collection.

The two CR800 DAS were taken to County Materials, the fabricators' precast plant, in Bonne Terre, Missouri, to record data from the VWSG. The VWSG were connected to the CR800 DAS prior to casting, and temperature and strain readings were recorded from the pour until after release of the PC girders. Data was collected for at least one hour after the strands were released. Figure 5-54 shows the DAS boxes reading data during the fabrication of one of the girders.

Figure 5-54. Data Collection During the PC/PS Girders Fabrication

After releasing the tendons (Figure 5-55), deflection data was recorded to obtain the camber of the girders (Figure 4-8).

Figure 5-55. Release of PC/PS Girder

Finally, the girders were moved to the yard for storage until they were shipped and delivered to the bridge jobsite (Figure 5-56).

Figure 5-56. Girders Storage at Precast Plant

5.6. BRIDGE CONSTRUCTION

This stage of the project included monitoring the temperature and stresses of the different superstructure components of the bridge according to the instrumentation plan. The different monitoring phases included the girders erection, concrete placement within the CIP RC deck, and safety barriers.

5.6.1. Girders Erection.

On September 24th, 2013, the first eight PC girders were shipped and placed on spans 1-2 and 2-3. Figure 5-57 shows some of the girders being delivered to the bridge jobsite. One HS-SCC and one NS-SCC PC/PS girder were selected to be monitored during their erection.

Figure 5-57. Shipping of the PC Girders to the Bridge Jobsite

Before the girders were lifted and set onto their final locations, CR800 DAS box 1 was strapped to the top flange of the girder as shown in Figure 5-58. The VWSG were connected to the DAS (Figure 5-58) to measure strain and temperature data until approximately one hour after the erection of the girders.

Figure 5-58. VWSG Sensors Connected to CR800 DAS

Figure 5-59 shows girder 4 of span 2-3 (HS-SCC) during the erection (September 24th, 2013). The data was read from the VWSG sensors placed at mid-span and near the east support sections.

Figure 5-59. Lifting of HS-SCC PC Girder 4 (Span 2-3)

Figure 5-60 shows the PC girders of the first two spans placed atop their supports. This activity was accomplished on September 24th, 2013.

Figure 5-60. Conventional Concrete and HS-SCC PC Girders Placed on Supports

On September 25th, 2013, the last four PC/PS girders were shipped and placed on span 3-4. The VWSG sensors installed at mid-span and near the west-end sections of girder 4 collected data during the erection. Figure 5-61 shows the lifting and erection of the girder.

a) NS-SCC PC/PS Girder 4 with DAS b) PC/PS Girders Placed on Their Supports

Figure 5-61. Lifting and Setting of NS-SCC PC Girders

5.6.2. CIP RC Deck.

After the PC girders were erected, the contractor started setting the steel diaphragms and precast concrete panels as shown in Figure 5-62. Steel channels C15x33.9 were employed as the intermediate steel diaphragms that transversely connect the PC girders (Figure 5-62).

Figure 5-62. Diaphragm and PC/PS Panels Erection

The deck's reinforcing steel was placed, and the rest of the VWSG sensors were set within the girder's mid-span and near support sections according to the instrumentation plan (Figure 5-30 and Figure 5-31).

a) VWSG Wires Passed through Formwork b) VWSG Collected Through PVC Pipe

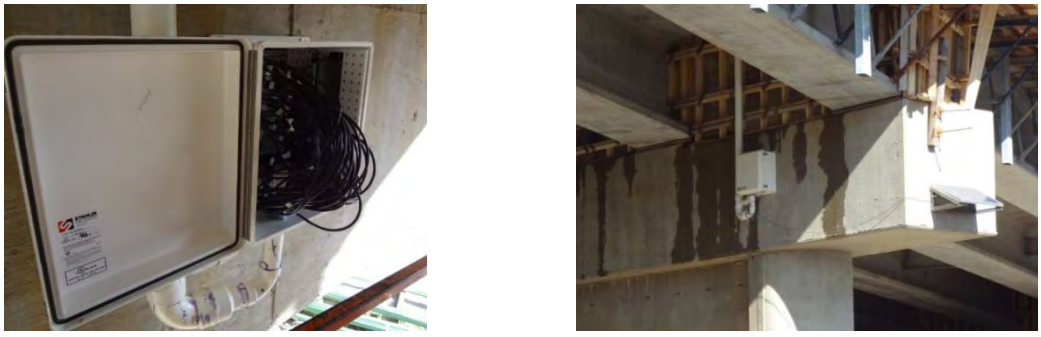

c) VWSG Wires Connected to CR800 DAS Modules d) CR800 DAS Anchored to Bent 3 Pier Cap

Figure 5-63. Installation of VWSG within CIP Deck and CR800 DAS Boxes

Figure 5-63a and Figure 5-63b show how the VWSG wires were gathered and passed through a PVC pipe. Finally, the wires were hooked up to the CR800 DAS boxes that were previously anchored on the interior faces of bents 2 and 3 (Figure 5-63c and Figure 5-63d).

Figure 5-64. Concrete Placement on Intermediate RC Diaphragm

The intermediate bents RC diaphragms were cast before the CIP RC deck (Figure 5-64). This procedure was executed to give continuity to the RC and PC bridge super structure elements.

After the RC diaphragms were cast, the contractor poured the RC deck. Figure 5-65 shows the equipment employed during the concrete placement and some of the crew members finishing the surface of the CIP deck.

Figure 5-65. Concrete Placement on CIP RC Deck

RFID corrosion sensors 1 and 2, were placed in the locations described in Section 5.3.9. These sensors were set within the CIP RC deck right after the concrete finishing equipment worked the concrete surface located above the locations selected to be instrumented. Figure 5-66 shows one of the corrosion sensors embedded within the south side of Bridge A7957. More details about the installation of the RFID corrosion sensors on Bridge A7957 can be found in Myers and Hernandez (2014).

Figure 5-66. RFID Corrosion Sensor Embedded within CIP Deck

Figure 5-67 displays the final appearance of the CIP RC deck of Bridge A7957 after concrete was placed in October 21, 2014.

Figure 5-67. Finished Surface of CIP RC Deck

5.6.2.1 Mix design.

A MoDOT modified B-2 concrete mixture (identified as mix 12CDMB2A087) with a specified design strength of 4,000 psi (27.6 MPa) was employed to cast the RC deck. The deck was poured on October 21st, 2013. Osage County Concrete of Linn, MO, produced the concrete mix. The mix proportions are listed in Table 5-16.

Table 5-16. CIP RC Deck's Concrete Mix Proportions

Type	Material	Design Weight (lb/yd^3)	Batched Weight (lb/yd^3)
Coarse Aggregate	Capital Quarries Holt Summit, MO	1895	1932
Fine Aggregate	Natural Sand Class A Capital Sand. Jefferson City, MO	1170	1214
Cementitious Material	Portland Cement – Type I/II Continental Hannibal, MO	450	450
	Fly Ash – Class C Headwaters	150	150
Chemical Admixtures	Air Entraining Agent Daravair 1400	4.5 oz/yd^3	4.5 oz/yd^3
	Water Reducer Type A Adva140	2.0 oz/cwt	2.0 oz/cwt
Water	--	220	175
w/cm	--	0.37	0.29

Conversions: 1 lb/yd3 = 0.5933 kg/m3, 1.0 oz/yd3 = 0.03708 kg/m3, 1.0 oz/cwt = 6.5 oz/yd3

Concrete temperature, air content and slump tests were conducted prior to casting the deck. Twenty four 4 x 8 in. (100 mm x 200 mm) concrete cylinders (Figure 5-68) were collected to obtain the compressive strength at different ages (3, 7, 14, 28, 56, load test 1, 1 year, and load test 2). Three 12 x 12 x 3 in. (305 x 305 mm x 76 mm) abrasion test specimens (Figure 3-15), and three 3.5 x 4.5 x16 in. (89 x 114.3 x 406.4 mm) freeze-thaw specimens (Figure 3-12) were also fabricated. Finally, five ponding specimens were collected according to the detail of Figure 3-13 and Figure 3-14. RFID corrosion sensors 3 and 4 were installed in only two ponding specimens (Figure 5-69).

a) Compression Test Specimens

b) Freeze-Thaw, Abrasion and Ponding Test Molds

c) Curing Freeze-Thaw, Abrasion and Ponding Test Specimens

Figure 5-68. CIP Deck QC/QA Specimens Collected During Concrete Placement

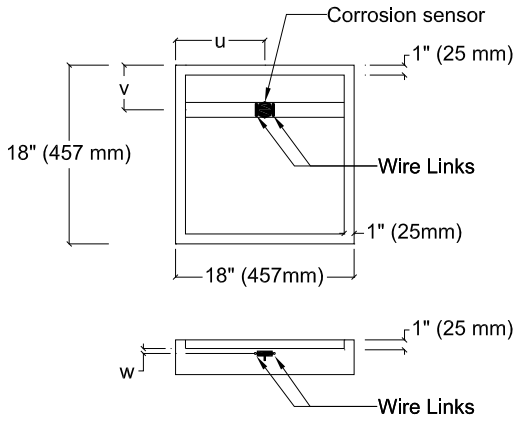

Figure 5-69. Detail of RFID Corrosion Sensor Installed in Ponding Test Specimens

The coordinates of the location where the RFID corrosion sensors were installed within the ponding specimens are listed in Table 5-17.

Table 5-17. RFID Sensors' ID Coordinate Locations within Ponding Specimens

Sensor ID	*RFID ID*	*Specimen ID*	*u (in.)*	*v (in.)*	*w (in.)*
3	61830DF	C-SEN2-001-F	9	4½	¼
4	618301F	C-SEN2-002-F	9	4½	½

u, v, w : Coordinates that define the location of the RFID tag sensors within the ponding specimens (Figure 5-69).

Conversion: 1 in. = 25 mm

5.6.2.2 Data collection.

On October 17th, 2013, the eighty six VWSG sensors were fixed to both CR800 DAS according to the instrumentation plan and details of Figure 5-30 and Figure 5-31. Since this date, these sensors have been continuously collecting temperature and strain data within the superstructure elements of Bridge A7957. Temperature and strain data corresponding to the cast of the RC deck, approach slabs, and safety barriers are available and will be used to compare any trends in the responses of the different super structure elements.

5.6.3. Approach Slab Concrete Placement.

The approach slabs were poured on December 4, 2013. No compression cylinders were made by the researchers during the casting of this part of the structure. However, temperature and strain data was recorded by the sensors embedded within the structure.

5.6.4. Safety Barrier Curbs.

The safety barriers concrete were poured on December 19, 2013. Fifteen 4 x 8 in. (100 mm x 200 mm) concrete cylinders were collected during the concrete placement on this part of the structure. The compressive strength was programmed to be obtained at different ages (7, 28, 56, load test 1, and 1 year). Figure 5-70 shows the final view of Bridge A7957 after it was completed.

Figure 5-70. Bridge A7957 Completed

5.7. LOAD TEST PLAN

Bridge A7957 is the first superstructure bridge implementing NS-SCC, HS-SCC and HVFAC in Missouri. The bridge was instrumented with embedded strain gauges and thermocouples to monitor the short and long-term response of the structure from construction through service life. To investigate the overall behavior of the bridge under live load, a first static load test was developed and planned. The first part of the load test lasted two days and was completed in April 2014. The second part of the first load test will be conducted in August 2014.

5.7.1. Load Test Plan.

Girder strains and deflections were the mechanical variables monitored during the load test. An instrumentation program was developed to identify trends in the observed behavior (as noted in Section 5.3.1 through 5.3.4). A data acquisition system (CR800 DAS1 and CR800 DAS 2) with sufficient channels was designed and assembled for the project (Section 4.3.1.2). At the cluster locations shown in Figure 5-71, 86 VWSG were employed to acquire the strain rate within the bridge caused by the varying live load conditions.

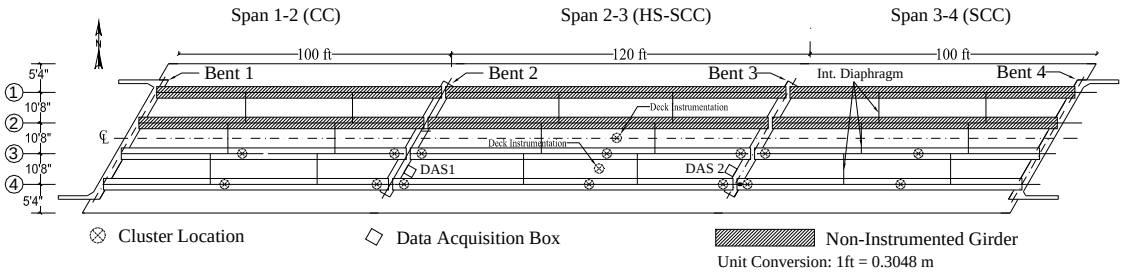

Figure 5-71. VWSG Data Collection During Load Test 1(DAS1 and DAS2)

A Leica TCA2003 total station (Section 4.2.6) was employed to record deflection measurements at the locations identified as surveying points in Figure 5-72. In addition, inclinometers were place on the deck to obtain the slope deformation at the locations indicated in Figure 5-72.

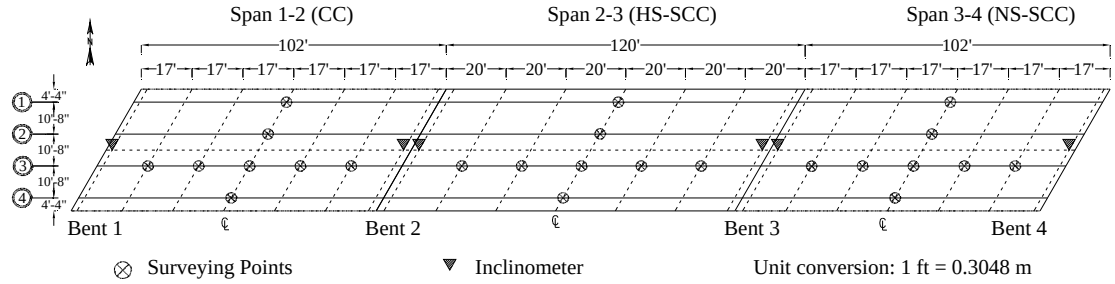

Figure 5-72. Sensor Locations for Live Load Test

5.7.2. Load Cases.

Six MoDOT dump trucks with similar configuration were utilized during the first load test (Figure 5-73). Twenty different static load cases were planned for the first diagnostic load test. The different truck configurations used on each load test case are described in Appendix D. Due to difficult weather conditions during the first day of the static load test, only the first thirteen load cases were accomplished. The second part of the load test, which includes the last seven load cases, has been scheduled to be executed in August 2014.

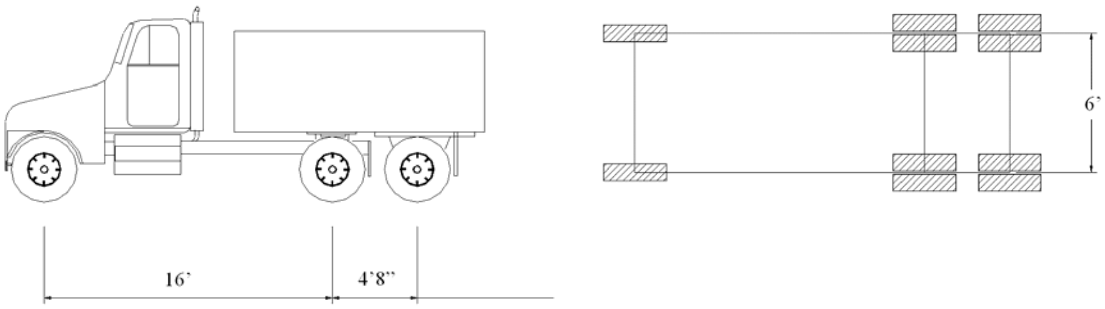

Figure 5-73. MoDOT Dump Truck Utilized for Diagnostic Load Tests

5.8. PROBLEMS ENCOUNTERED

The instrumentation at the precast plant for the girders was installed successfully and took approximately 4 hours per girder. The instrumentation installed at the bridge site including the CIP deck and routing of wiring was also installed successfully taking approximately 3 days. However, there were some problems encountered throughout the instrumentation program. At the precast plant, one VWSG was accidentally broken during placement within the section located at girder 3's mid-span of span 2-3 (HS-SCC), layer TF (Table 5-9). This sensor, labeled as "S2-G3-M5", was connected to CR800 DAS 2. No data was collected during fabrication for this sensor. At the bridge site, the sensor placed at the mid-span section of girder 4 (span 1-2), layer CGC presented a failure after it was connected to the CR800 DAS1 secured to the interior face of bent 2. This sensor, labeled as"S1-G4-M4", did not collect any data before and after the deck was poured.

6. RESEARCH PROGRAM RESULTS

6.1. MATERIAL TEST RESULTS

The following section contains preliminary material results from the trial mixes and QC/QA specimens from the bridge substructure and superstructure elements. Also included are the hydration profiles from the intermediate bents.

6.1.1. Trial Mixes.

6.1.1.1 HVFAC.

6.1.1.1.1 Fresh properties.

The HVFAC trial mix was batched on January 8, 2013 at Osage County Materials in Linn, MO. Fresh properties of the mix were reported and are listed in Table 6-1. The air content closely matches the design air content of 6.0%. The lower slump value compared to the HVFAC mixes in the intermediate bents (Table 6-1) could be explained by the colder weather and concrete temperatures during the trial mix batching.

Table 6-1. HVFAC Trial Mix Fresh Properties

Air Temp. (°F/°C)	64/18
Concrete Temp. (°F/°C)	64/18
Slump (in.)	2.5
Air Content (%)	5.3

Conversions: 1 in. = 25.4 mm

6.1.1.1.2 Hardened properties.

The researchers conducted compressive strength and modulus of elasticity tests on the HVFAC trial mix at 7 and 28 days. The contractor, Fred Weber, Inc., also collected compressive strength results at 1, 2, 3, 4, 7, and 28 days. The rate of strength gain for HVFAC is expected to be slower than that of CC. Compressive strengths at 56 days are typically reported to address this trend; however, for the trial mix investigated, a 56 day test was not conducted. Results for the peak compressive stress, f'_c, are shown in Table 6-2. Slight variations between the university and contractor in compressive strength

occurred, possibly due to curing conditions, end capping conditions, and the selected load rate from ASTM C39 (ASTM C 39 2012).

Table 6-2. HVFAC Trial Mix Compressive Strength

Concrete Age (days)	Compressive Strength (psi)	
	Contractor	University
1	100	N/A
2	1000	N/A
3	2330	N/A
4	3070	N/A
7	4440	3977
28	6240	5967

Conversion: 1000 psi = 6.895 MPa

Measured values for the modulus of elasticity at the time of testing were compared with empirical estimates from ACI 318-11 and AASHTO 2012. These empirical formulas account for the unit weight of concrete (w_c) (pcf for ACI, kcf for AASHTO), compressive strength (f'_c) (psi for ACI, ksi for AASHTO), and the type of aggregate (K_1). Since additional testing was not performed on the dolomitic limestone aggregate, K_1 was taken as 1.0. Empirical equations for MOE from ACI 318-11 and AASHTO 2012 are provided in Equations 6.1 and 6.2, respectively (ACI 318-11, AASHTO 2012).

$$E_c = 33 w_c^{1.5} \sqrt{f'_c} \quad (6.1)$$

$$E_c = 33{,}000 K_1 w_c^{1.5} \sqrt{f'_c} \quad (6.2)$$

ACI uses units of pounds and feet while the AASHTO formula uses kips and feet. The variable, K_1, is a correction factor for source of aggregate, and is typically taken as 1.0, unless determined by physical testing (AASHTO 2012). Measured and predicted values for the modulus of elasticity in units of psi for the HVFAC trial mix are listed in Table 6-3. Both the ACI and AASHTO predictions underestimated the MOE. The modulus of elasticity of concrete can have significant variability due to concrete strength,

concrete age, aggregate and cement properties, rate of loading, type and size of specimen, and the definition of the elastic modulus, be it initial, tangent, or secant modulus (Pauw 1960).

Table 6-3. HVFAC Trial Mix Measured and Predicted Modulus of Elasticity

Age (days)	Calculated	ACI Prediction	AASHTO Prediction
7	4,137,169	3,550,527	3,550,527
28	4,766,590	4,349,036	4,349,036

Conversion: 1000 psi = 6.895 MPa

6.1.1.2 HS-SCC.

6.1.1.2.1 Fresh properties.

Fresh properties from the HS-SCC trial mix conducted at County Materials Corporation on January 31, 2013 are provided below in Table 6-4. The slump flow and passing ability were on the low end of typical SCC mixtures, in part due to the colder temperatures (ACI 237 2007). The segregation percentage was 0.0% as there was a slightly larger amount of coarse aggregate in the top third as opposed to the bottom third of the column.

Table 6-4. HS-SCC Trial Mix Fresh Properties

Air Temp. (°F/°C)		46/8
Concrete Temp. (°F/°C)		65/18
Air Content (%)		5.6
Slump Flow (in.)		21
J-Ring (in.)		19
Segregation Column	Top (lb.)	8.96
	Bottom (lb.)	8.88
	S (%)	0.00

Conversions: 1 in. = 25.4 mm, 1 lb. = 0.4536 kg

6.1.1.2.2 Hardened properties.

Compressive strength, modulus of elasticity, and splitting tensile strength (STS) tests were performed at 1, 7, and 28 days. The average results are presented in Table 6-5. The modulus of elasticity was compared to empirical estimates from ACI 318-11 and ACI 363R-10 graphically displayed in Figure 6-1. The ACI 318-11(Equation 6.1) model is typically not reliable for concrete strengths in excess of 8,000 psi (55 MPa) because of the data it is based on (ACI 318 2011). The ACI 363R-10 model proposed by Martinez et al. (1982) (Equation 6.3) was implemented as a lower bound for HSC concrete for concrete strengths ranging from 3,000 to 12,000 psi (20.7 to 82.7 MPa) (ACI 363 2010). In the case of HS-SCC, it provides a reasonably accurate estimate. Tomosawa et al. proposed a separate ACI 363R-10 model (Equation 6.4) which accounts for the aggregate source as well as type of cementitious material; it provides a lower-bound estimate for HS-SCC. For the listed equations, E_c is the modulus of elasticity (psi), f'_c is the compressive strength of concrete (psi), and w is the concrete unit weight (pcf). The variable k_1 is taken as 1.2 for crushed limestone and calcined bauxite aggregates; 0.95 for crushed quartzite, crushed andesite, crushed basalt, crushed clay slate, and crushed cobble stone aggregates; and 1.0 for other aggregates. The variable k_2 is taken as 0.95 for silica fume, slag cement, and fly ash fume; 1.10 for fly ash; and 1.0 for other types of admixtures (ACI 363 2010). The dolomite and Portland cement used in the HS-SCC trial mix correspond to k_1 and k_2 values of 1.0 and 1.0, respectively.

$$E_c = 40{,}000\sqrt{f'_c} + 10^6 \tag{6.3}$$

$$E_c = 4.86 * 10^6 k_1 k_2 \left(w/150\right)^2 \left(f'_c/8700\right)^{(1/3)} \tag{6.4}$$

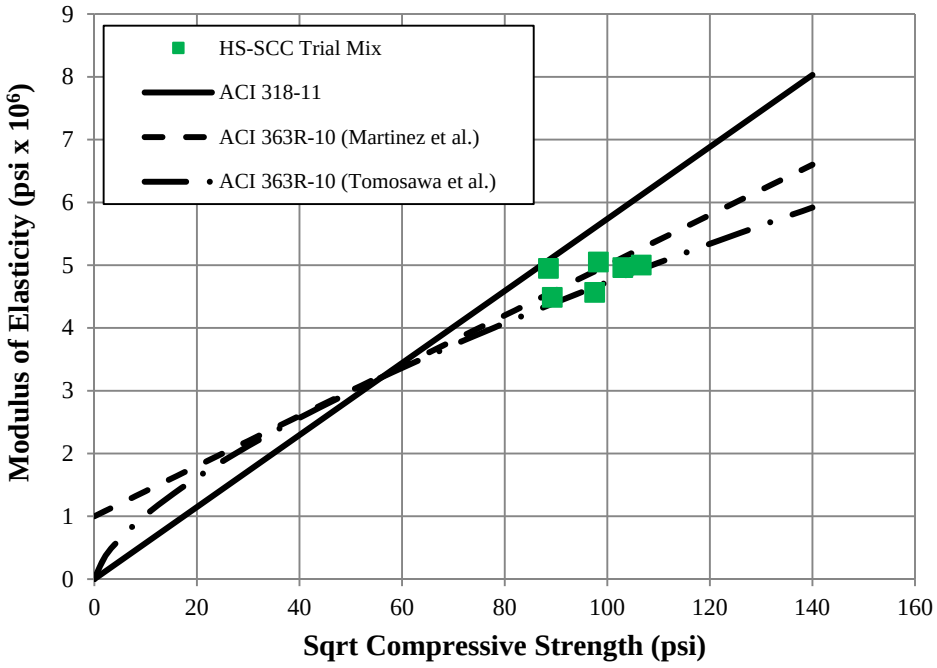

Conversion: 1000 psi = 6.895 MPa

Figure 6-1. HS-SCC Trial Mix Modulus of Elasticity vs. Compressive Strength

Table 6-5. HS-SCC Trial Mix Hardened Properties

Age of Concrete (days)	Compressive Strength (psi)	Modulus of Elasticity (psi)	Splitting Tensile Strength (psi)
1	7,996	4,527,561	567
7	9,658	4,977,283	579
28	10,957	5,008,516	537

Conversion: 1000 psi = 6.895 MPa

The splitting tensile strengths of the HS-SCC were compared to empirical estimates from ACI-318-11 (Equation 6.5) and ACI 363R-10 as shown in Figure 6-2. Equation 6.2 below, proposed by Carrasquillo et al. (1981) in ACI 363R-10, is valid for concrete strengths ranging from 3,000 to 12,000 psi (21 to 83 MPa). Myers and Carrasquillo suggested Equation 6.7 from ACI 363R-10 specifically for member-cured dolomitic limestone (ACI 363 2010). For Equations 6.5-6.7, f_t is the splitting tensile strength (psi), and f'_c is the compressive stress of concrete (psi).

$$f_t = 6.7\sqrt{f'_c} \quad (6.5)$$

$$f_t = 7.4\sqrt{f'_c} \quad (6.6)$$

$$f_t = 8.66\sqrt{f'_c} \quad (6.7)$$

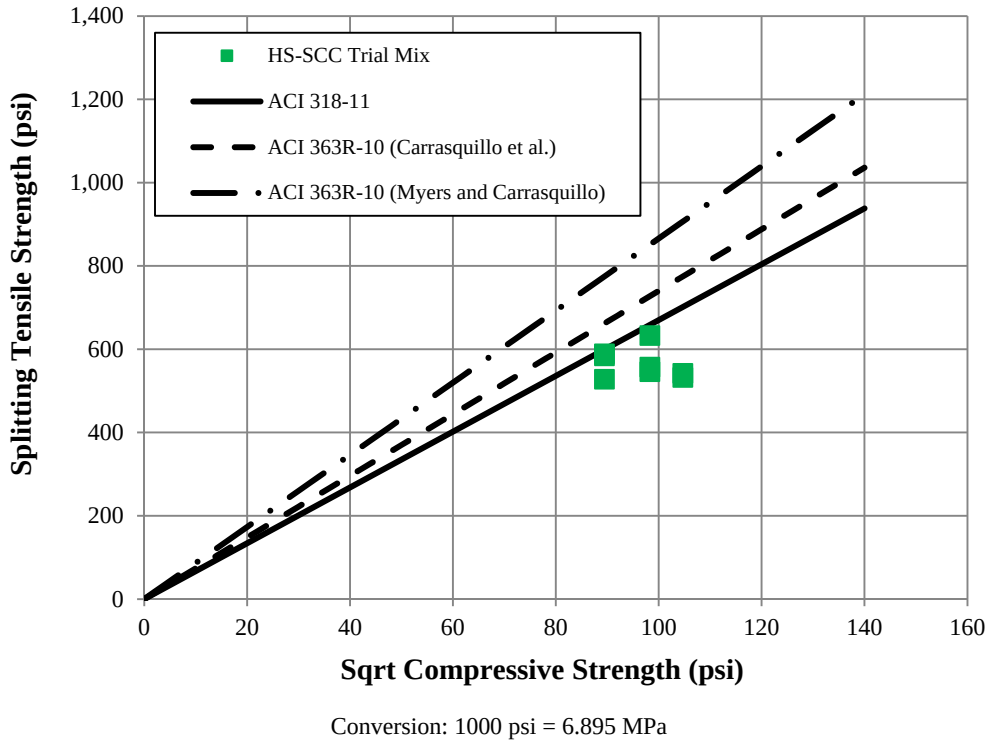

Conversion: 1000 psi = 6.895 MPa

Figure 6-2. HS-SCC Trial Mix Splitting Tensile Strength vs. Compressive Strength

The ACI 318-11 model more closely correlates to the data obtained. The STS has been shown to have significant variability depending on the aggregates, paste, and interface zone (Wight and MacGregor 2005). However, post-failure images of STS testing reveal that the failure plane extended through the aggregate (Figure 6-3). Thus the bond between the aggregates and paste is greater than the strength of the aggregate themselves. Furthermore, Myers et al. (2012) found no variability between HSC and HS-SCC with dolomitic limestone, and both mixtures fell below the ACI 318-11 prediction.

Figure 6-3. Splitting Tensile Strength Failure Plane

6.1.1.3 NS-SCC.

6.1.1.3.1 Fresh properties.

The NS-SCC trial mix was batched on March 8, 2013 at County Materials Corporation in Bonne Terre, MO. Fresh properties recorded are listed in Table 6-6. The slump flow and passing ability are larger than those measured during the HS-SCC trial mix in part due to the warmer temperatures and higher w/cm ratio. ACI 237r-07 recommends a maximum segregation percentage of 10%; the segregation of 8.2% met this value. Khayat and Mitchell (2009) found that an increase in the w/cm ratio of SCC mixes leads to a reduction in static stability and thus increased segregation. The w/cm ratios of the HS-SCC and NS-SCC were 0.33 and 0.35, respectively, which support that trend.

Table 6-6. NS-SCC Trial Mix Fresh Properties

Air Temp. (°F/°C)		53/12
Concrete Temp.		not recorded
Air Content (%)		8.2
Slump Flow (in.)		25
J-Ring (in.)		25
Segregation Column	Top (lb.)	8.66
	Bottom (lb.)	9.41
	S (%)	8.20

Conversions: 1 in. = 25.4 mm, 1 lb. = 0.4536 kg

6.1.1.3.2 Hardened properties.

The resulting average hardened mechanical properties of the NS-SCC mix including compressive strength, modulus of elasticity, and splitting tensile strength are displayed in Table 6-7.

Table 6-7. NS-SCC Trial Mix Hardened Properties

Concrete Age (days)	Compressive Strength (psi)	Modulus of Elasticity (psi)	Splitting Tensile Strength (psi)
3	7497	4,513,258	454
7	8163	4,539,066	489
28	9179	4,717,905	633

Conversion: 1000 psi = 6.895 MPa

The modulus of elasticity and splitting tensile strength were compared against ACI 318-11 and ACI 363R-10 equations previously mentioned in Sections 6.1.1.1.2 and 6.1.1.2.2 and are illustrated in Figure 6-4 and Figure 6-5, respectively.

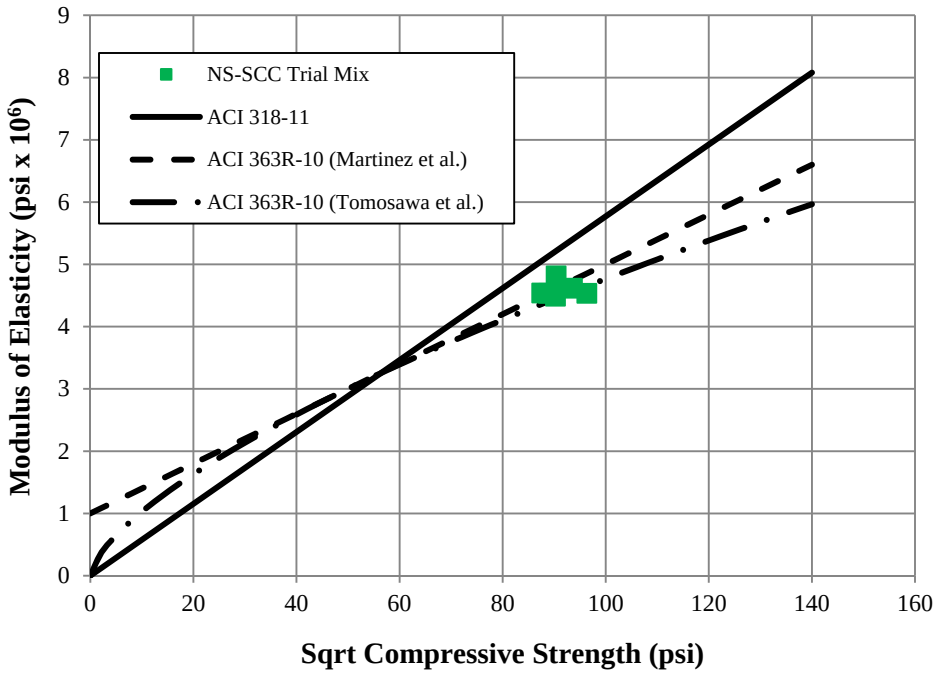

Conversion: 1000 psi = 6.895 MPa

Figure 6-4. NS-SCC Trial Mix Modulus of Elasticity vs. Compressive Strength

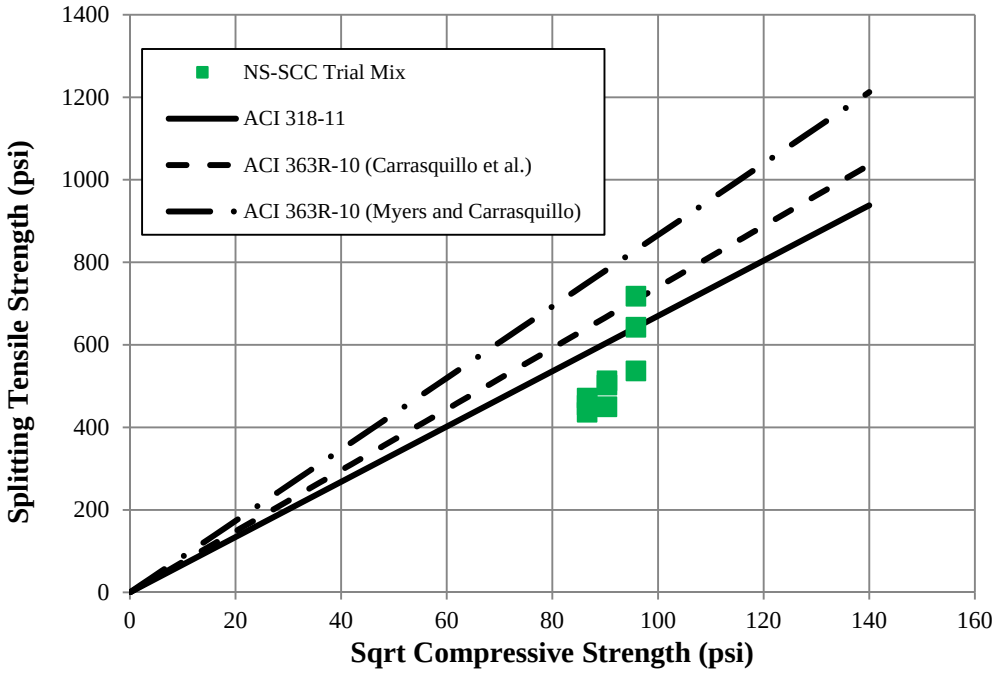

Conversion: 1000 psi = 6.895 MPa

Figure 6-5. NS-SCC Trial Mix Splitting Tensile Strength vs. Compressive Strength

The MOE of the NS-SCC mix straddles the ACI 363R-10 equation proposed by Martinez et al., and can be conservatively estimated by the ACI 363R-10 estimate suggested by Tomosawa et al. These observations are similar to those from the HS-SCC trial mix.

In general, all three splitting tensile strength models overestimate the STS, with the ACI model being the best predictor. As expected, there is considerable variability in STS test results. The variations in aggregate sources could explain the variation between the test results and the ACI 363R-10 (Myers and Carrasquillo) equation, which was suggested for dolomitic limestone.

6.1.2. Intermediate Bents (HVFAC).

The intermediate bents were constructed in four phases previously presented in Table 5-12. Fresh properties were recorded and QC/QA specimens were collected for maturity studies of compressive strength. Lastly, the hydration profiles from each structural element were collected via the Compact RIO data acquisition system.

6.1.2.1 Fresh properties.

The intermediate bents were constructed during the month of July 2013. Fresh properties, including air content and slump, were performed prior to each pour for the intermediate bents and are listed in Table 6-8.

Table 6-8. Intermediate Bents Fresh Properties

	Bent 2 Web Wall	Bent 2 Pier Cap	Bent 3 Web Wall	Bent 3 Pier Cap
Air Temp. (°F/°C)	79/26	70/21	76/24	67/19
Concrete Temp. (°F/°C)	78/26	75/24	79/26	79/26
Slump (in.)	4	5.5	5.75	3
Air Content (%)	5.6	7.6	6.6	5.5

Conversions: 1 in. = 25.4 mm

6.1.2.2 Hardened properties.

The time development of the compressive strength is illustrated in Figure 6-6. Bent 3 had a 28 day design compressive strength of 4,000 psi (28 MPa) while bent 2's specified compressive strength was 3,000 psi (21 MPa). Trendlines were applied to the tested data from each pour to develop a sense of the long-term strength gaining characteristics of each mix. The HFVAC mixes do not appear to level off to the extent of the CC mix, evidence of the high replacement level of fly ash. Testing of the two mixes at later ages (1 year and 2 years) will be conducted and included in the final MoDOT report to identify long-term strength gaining characteristics of the HVFAC concrete mix.

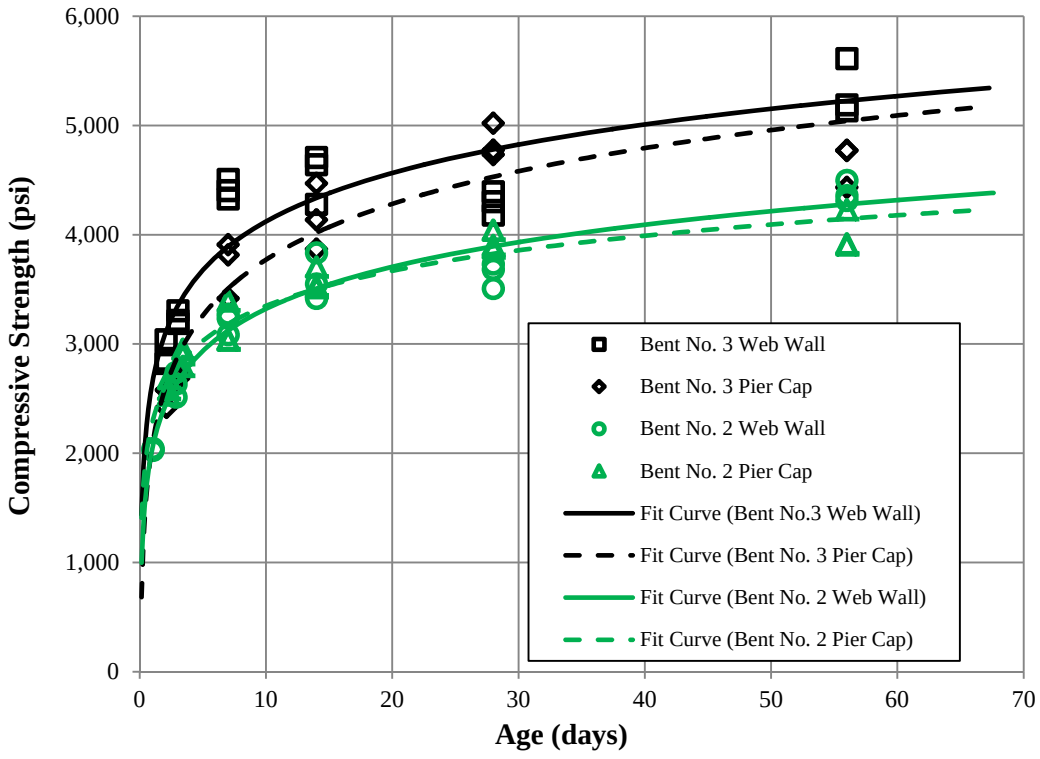

Conversion: 1000 psi = 6.895 MPa

Figure 6-6. Intermediate Bents Compressive Strength vs. Age

6.1.2.3 Hydration profiles.

The temperature development profiles were recorded from the start of each pour using thermocouple wires. The locations of the embedded thermocouples were presented in Section 5.3.6. Figure 6-7 presents hydration profiles from the construction of the columns and web wall. Figure 6-8 illustrates the temperature development in the pier caps. The trends in the columns and web walls of the two bents indicate that a 50% fly ash replacement has a negligible effect on setting time, but reduces the amount of heat released and the time at which the peak of the hydration curve occurs. These observations support the findings of Wang et al. (2006). When examining the heat generation in the pier caps, similar trends are noted with the exception that the peak of the hydration curve is delayed with respect to the conventional concrete mix.

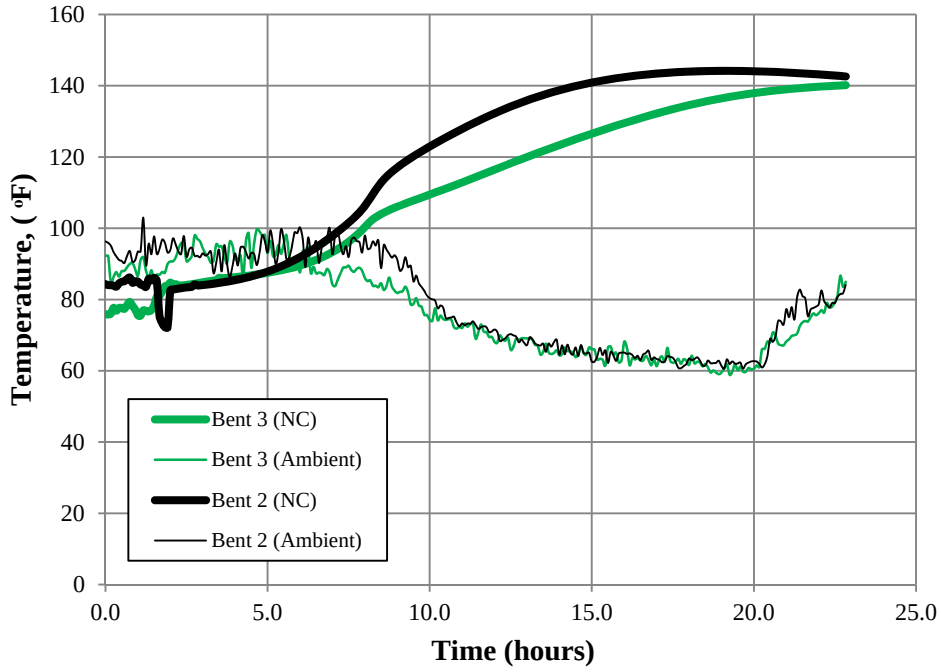

a) North Column

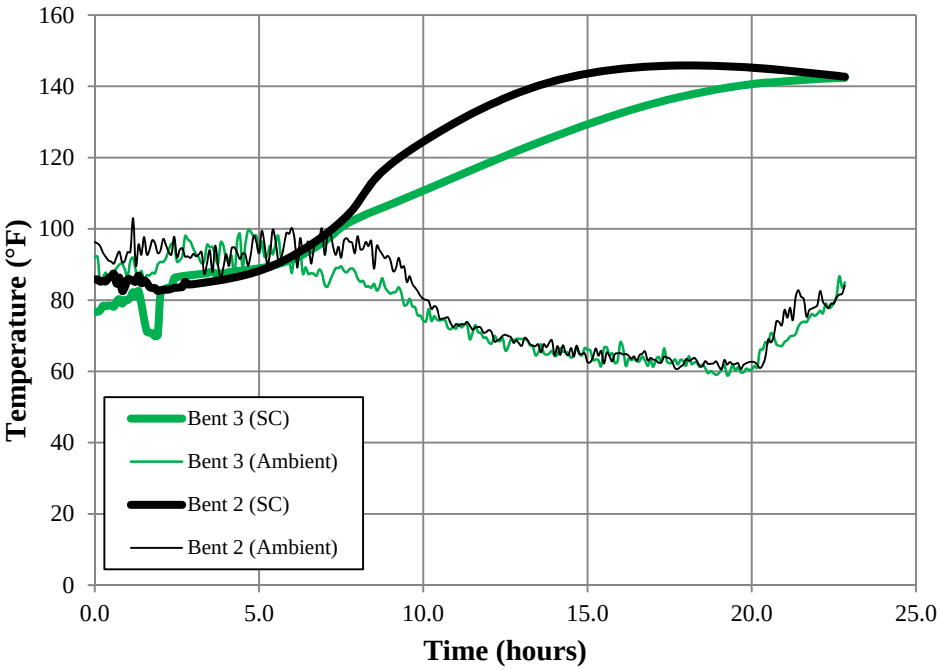

b) South Column

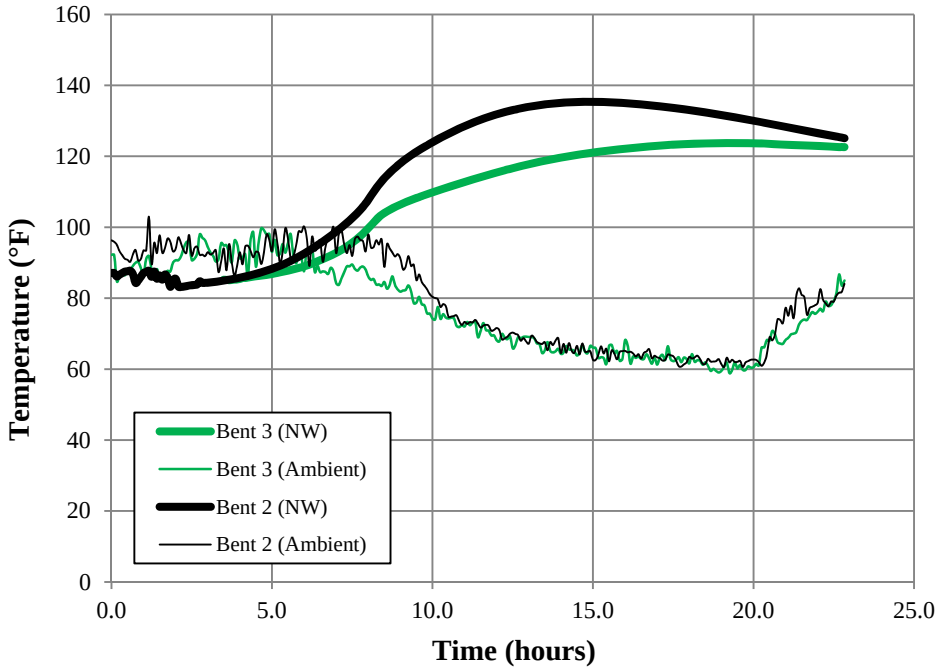

c) North Web Wall

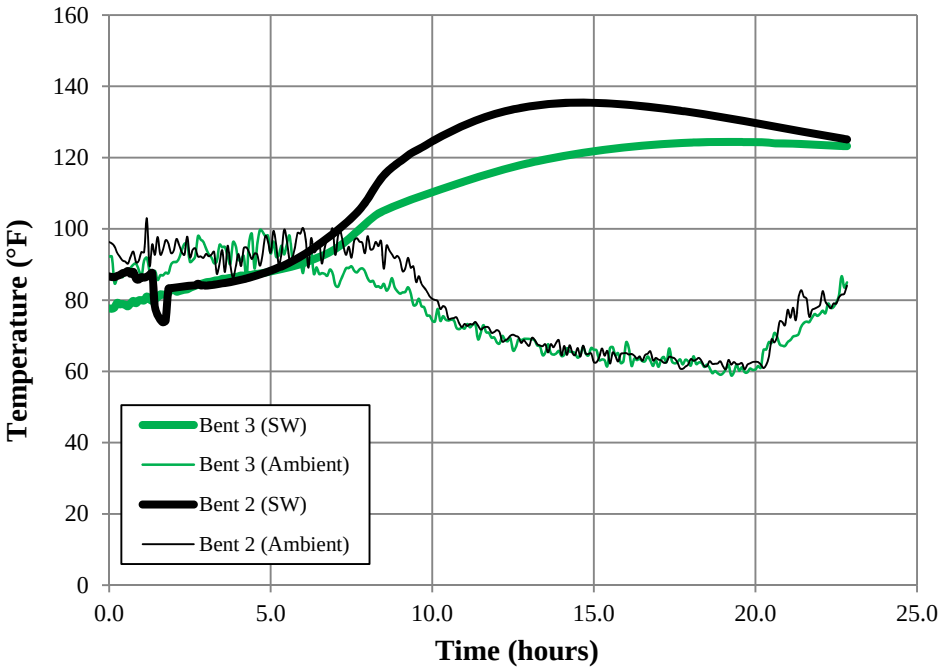

d) South Web Wall

Conversion: °C = (°F)(5/9)+32

Figure 6-7. Intermediate Bents Hydration Profiles: Columns and Web Wall

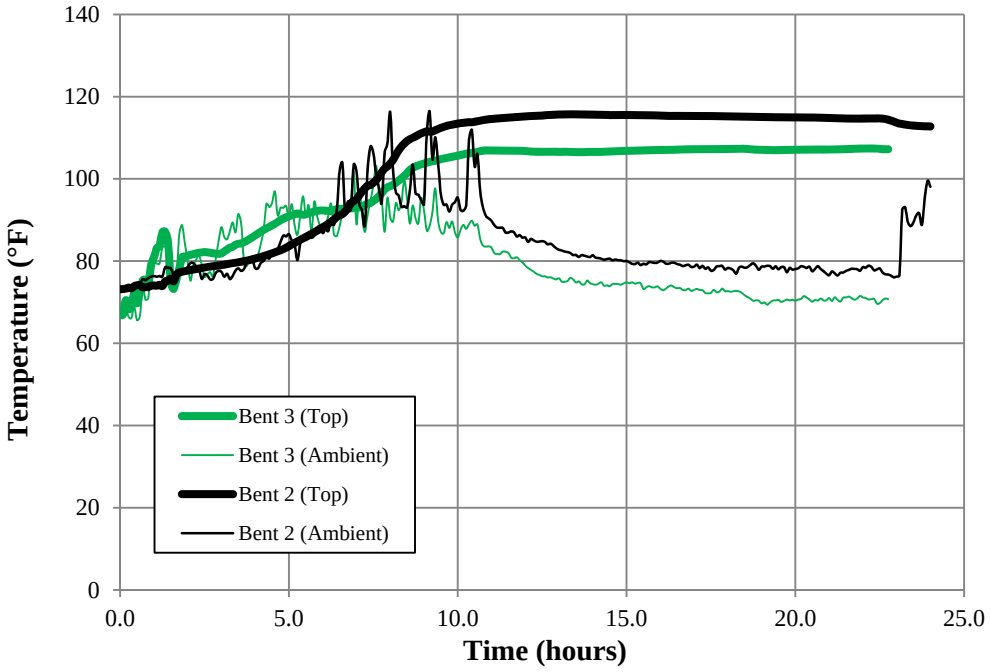

a) Top of Pier Cap

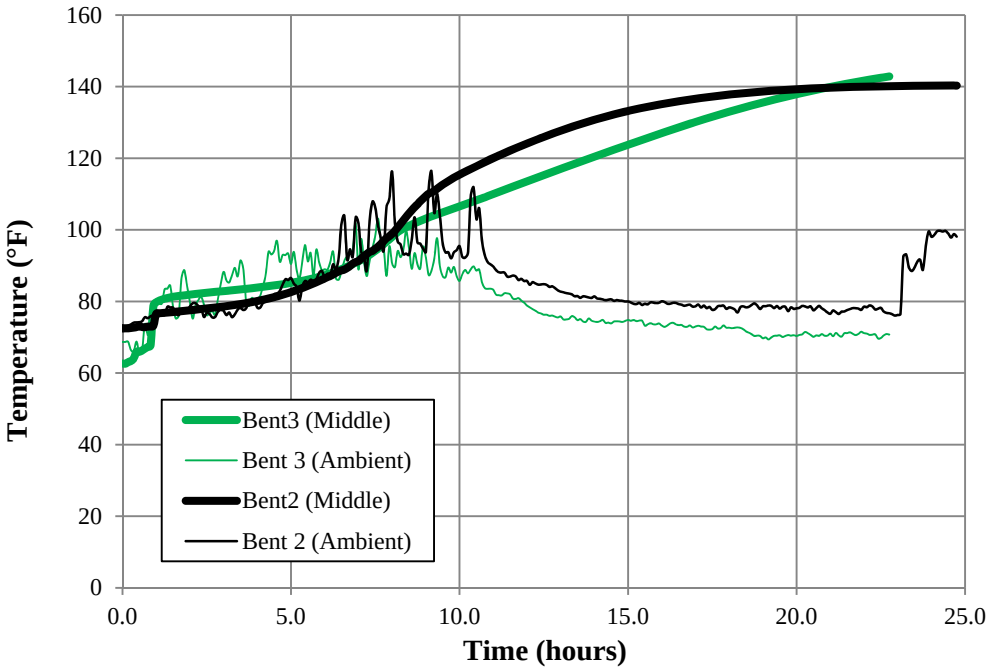

b) Middle of Pier Cap

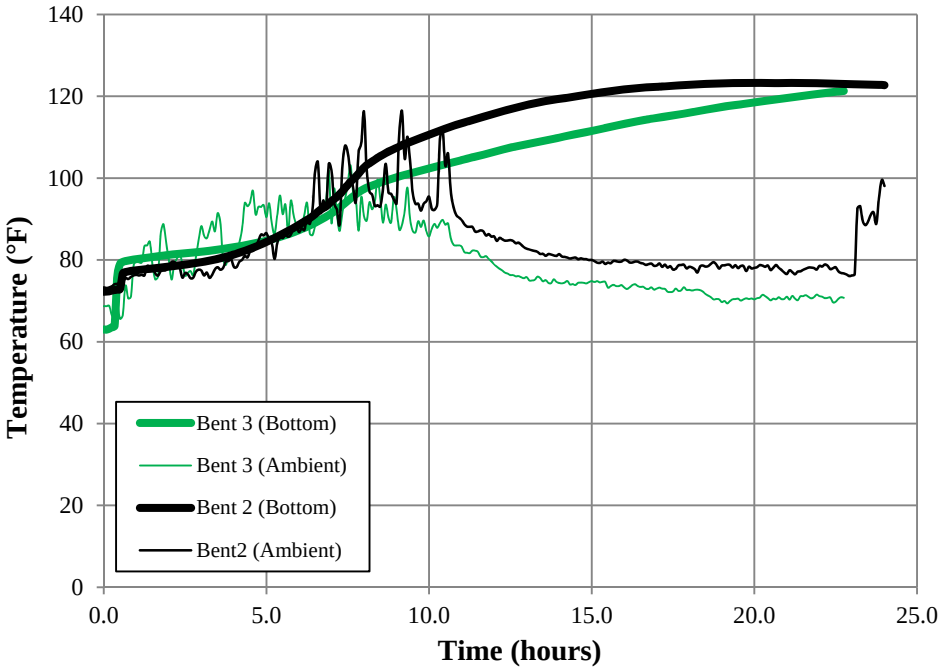

c) Bottom of Pier Cap

Conversion: °C = (°F)(5/9)+32

Figure 6-8. Intermediate Bents Hydration Profiles: Pier Cap

The hydration rate is defined as the temperature rise per 100 lbs (45.4 kg) of cementitious material per cubic yard, defined in Equation 6.8. The difference in temperature (peak concrete temperature minus initial concrete temperature) in each profile was calculated and divided by the amount of cementitious material per cubic yard in the respective mixture. The amount of cementitious material per cubic yard in bents 2 and 3 was 530 and 650, respectively. Table 6-9 lists the hydration rates at each of the investigated locations for bents 2 and 3.

$$R = \frac{Peak\ Temperature - Initial\ Temperature}{100\ lbs.cementitious\ material\ per\ yd^3} \quad (6.8)$$

Approximately 23 hours after pour of the bent 3 pier cap, the DAS was accidentally disconnected when the formwork was removed by the contractor. Missouri S&T did not return to the construction site until 2 days after the pour, and consequently hydration data from roughly 23-48 hours after casting was lost. However, temperature development profiles from the other intermediate bent pours leveled off after roughly 20-

26 hours, thus bent 3 was nearing the peak of the hydration process when the DAS was disconnected.

In Figure 6-8, the temperature rise in the top and bottom of the pier cap for bent 3 appear to be leveling off, and thus the hydration rates will be very similar to that if additional data was collected. However, for the thermocouple located at the middle of the pier cap in bent 3 (Figure 6-8b), the temperature rise does not appear to level off, and so the hydration rate was not calculated.

The high fly ash replacement significantly reduced the heat generation within the intermediate bents. The percent reduction in the heat of hydration process was calculated as a percentage of the intermediate bent 2 as shown in Table 6-9. There was a 24-43% reduction in heat generation when a 50% fly ash replacement level was used.

Table 6-9. Intermediate Bents Hydration Rates

	Hydration Rates				
	Bent 2		Bent 3		Percent Reduction
Location	(°F/cwt)	(°C/cwt)	(°F/cwt)	(°C/cwt)	
North Column	11.47	6.37	8.67	4.82	24.4
South Column	11.77	6.54	8.63	4.79	26.7
North Web Wall	9.77	5.43	5.93	3.29	39.3
South Web Wall	9.71	5.39	6.31	3.51	35.0
Top Pier Cap	7.68	4.86	4.37	2.43	43.1
Middle Pier Cap	12.32	6.85	N/A	N/A	N/A
Bottom Pier Cap	9.11	5.06	6.51	3.61	28.6

6.1.3. Bridge Girders.

6.1.3.1 Fresh properties.

The PC/PS girders were constructed during July 29th through August 13th 2013 (Table 5-14). Fresh properties, including air content, slump, and temperature were performed prior to each pour of the girders fabricated with conventional concrete. Slump flow, J-Ring and segregation column tests were conducted for the NS-SCC and HS-SCC girders. The fresh properties for the instrumented girders of the three spans are listed in Table 6-10.

Table 6-10. PC/PS Girders Fresh Properties

		Span 1 Girder 4	Span 1 Girder 3	Span 3 Girder 4	Span 3 Girder 3	Span 2 Girder 4	Span 2 Girder 3
Air Temp. (°F/°C)		71/22	71/22	78/26	74/23	76/24	78/26
Concrete Temp. (°F/°C)		72/22	72/22	83/28	81/27	83/28	84/29
Slump (in.)		9	9	N/A	N/A	N/A	N/A
Air Content (%)		6.9	6.9	8.3	5.4	8.3	7.9
Slump Flow (in.)		N/A	N/A	27	25	23	27
J-Ring (in.)		N/A	N/A	25	24	24	26.5
Segregation Column	Top (lb.)	N/A	N/A	7.70	-	8.85	-
	Bottom (lb.)			7.49	-	8.90	-
	S (%)			0.00	-	0.56	-

Conversions: 1 in. = 25.4 mm, 1 lb. = 0.4536 kg

6.1.3.2 Compressive strength.

The development of the compressive strength through time is displayed in Figure 6-9. Spans 1-2 (CC) and 3-4 (NS-SCC) girders had a 28-day specified compressive strength of 8,000 psi (55.2 MPa) while Span 2-3's design compressive strength was 10,000 psi (68.9 MPa).

Trendlines were plotted for the tested data of each pour. Figure 6-9a presents a strength development comparison of the girders in span 1-2 (CC) and span 3-4 (NS-SCC). In both cases the compressive strength developed at 28 days was higher than the design compressive strength. Figure 6-9b displays the compressive strength development in the case of the girders of span 2-3 (HS-SCC). At 28 days, the HS-SCC girders reached a higher compressive strength than the specified compressive strength. Testing of the two

mixes at later ages (1 year and 2 years) will be conducted and included in the final MoDOT report to identify long-term strength gaining characteristics of the NS-SCC and HS-SCC concrete mixes.

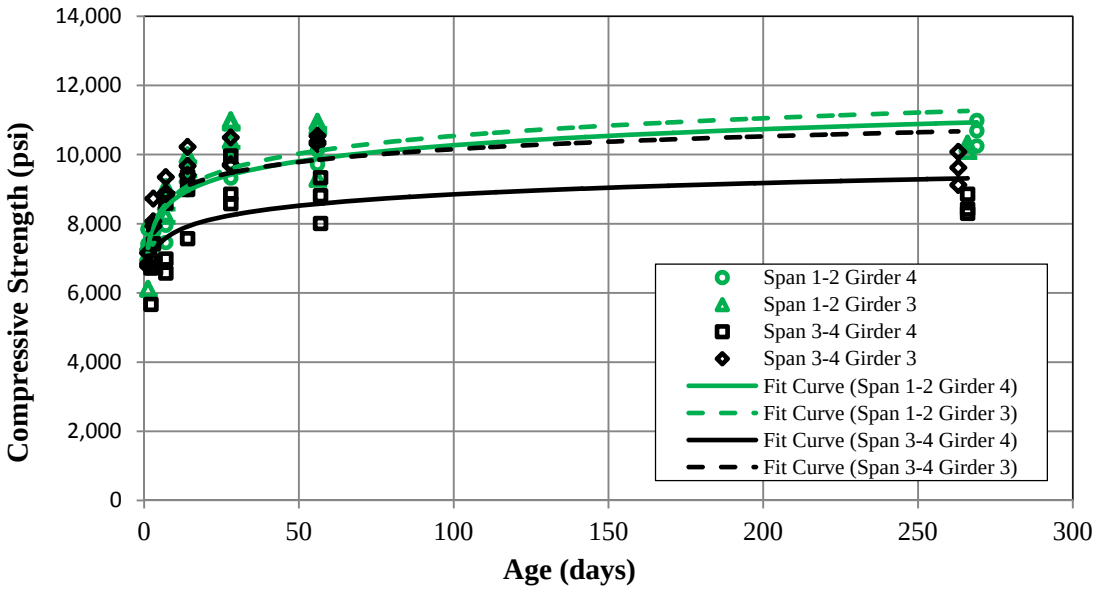

a) CC vs. NS-SCC PC/PS Girders

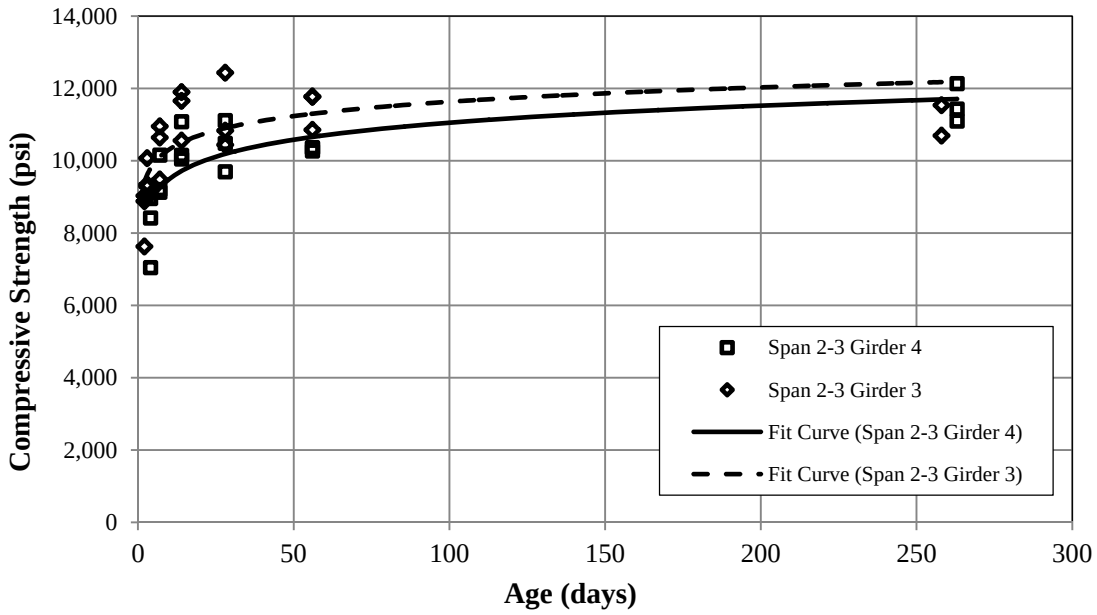

b) CC vs. HS-SCC PC/PS Girders

Conversion: 1000 psi = 6.895 MPa

Figure 6-9. PC/PS Girders Compressive Strength vs. Age

6.1.3.3 Modulus of elasticity.

The modulus of elasticity data was plotted against the square root of compressive strength shown in Figure 6-10. The data was compared to ACI 318-11 (Equation 6.1), and ACI 363R-10 (Equations 6.3 and 6.4) estimates. Similar trends are observed when the three different concrete mixes used are compared. The ACI 363R-10 model proposed by Martinez et al. (1982) provides an accurate estimate for the MOE of the three mixes employed to fabricate the girders, while the Tomosawa et al. (1993) equation of ACI 363R-10 is a lower bound predictor. The ACI 318-11 equation in the majority of the tests conducted overestimates the modulus of elasticity.

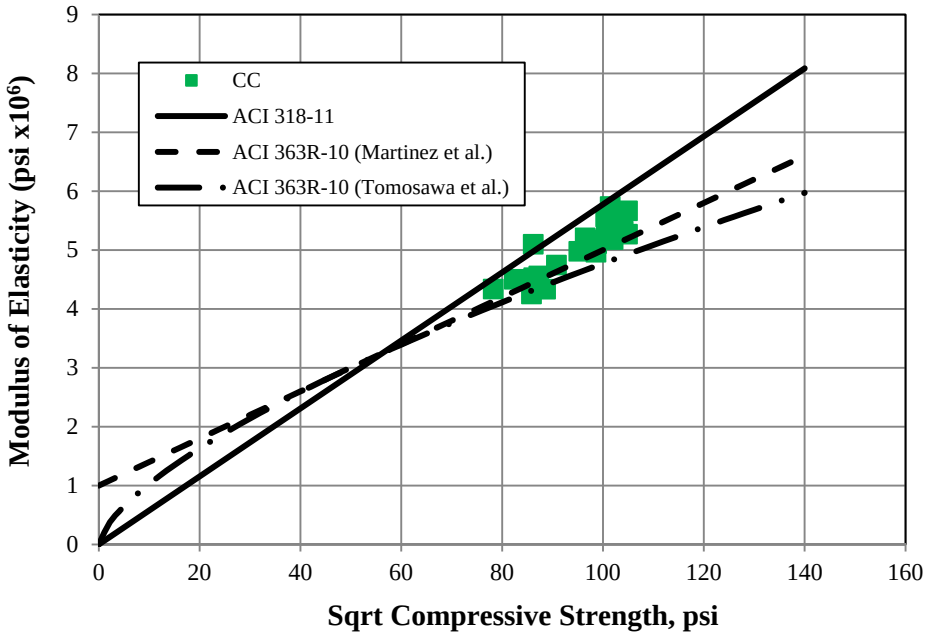

a) Span 1-2 Girders (Conventional Concrete)

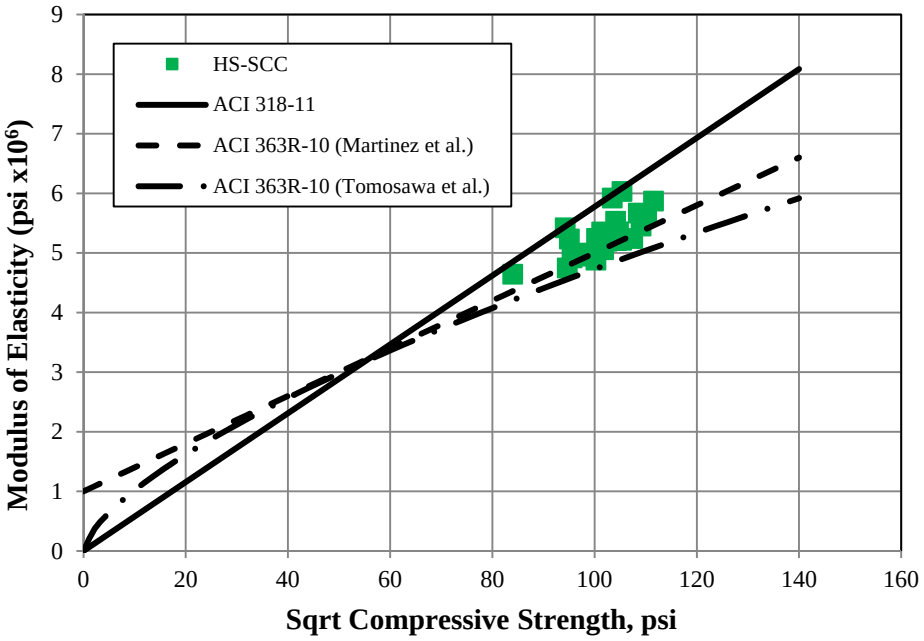

b) Span 2-3 Girders (High-Strength Self-Consolidating Concrete)

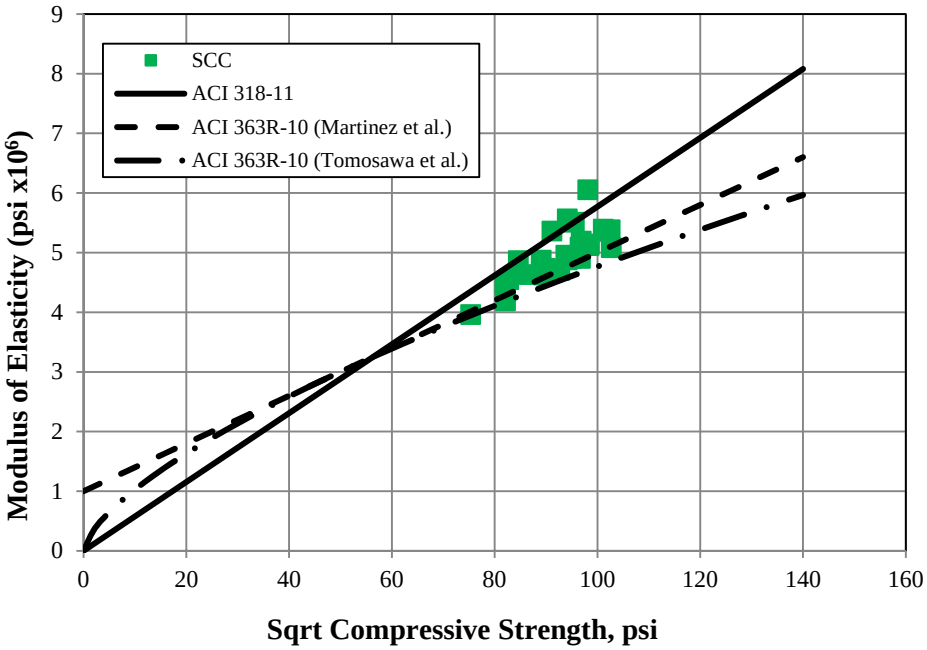

c) Span 3-4 (Self-Consolidating Concrete)

Conversion: 1000 psi = 6.895 MPa

Figure 6-10. PC/PS Girders Modulus of Elasticity vs. Compressive Strength

6.1.3.4 Modulus of rupture.

For each span, two tests per girder (girders 3 and 4) were conducted at 28 days and on the same day when the first live load test was conducted on the bridge. Figure 6-11 presents the modulus of rupture versus the square root of compressive strength for the 8 tests run per mix. Despite the validity of the ACI 318-11 empirical model for concrete strengths up to approximately 8,000 psi (55.2 MPa), it appropriately estimates the MOR for the three mixes used. The HSC model in ACI 363R-10 significantly overestimates the MOR. The reduction of the MOR, compared to the ACI 363R-10 model, in the case of the girders fabricated with HS-SCC is associated to the smaller volume of coarse aggregate used in the mix.

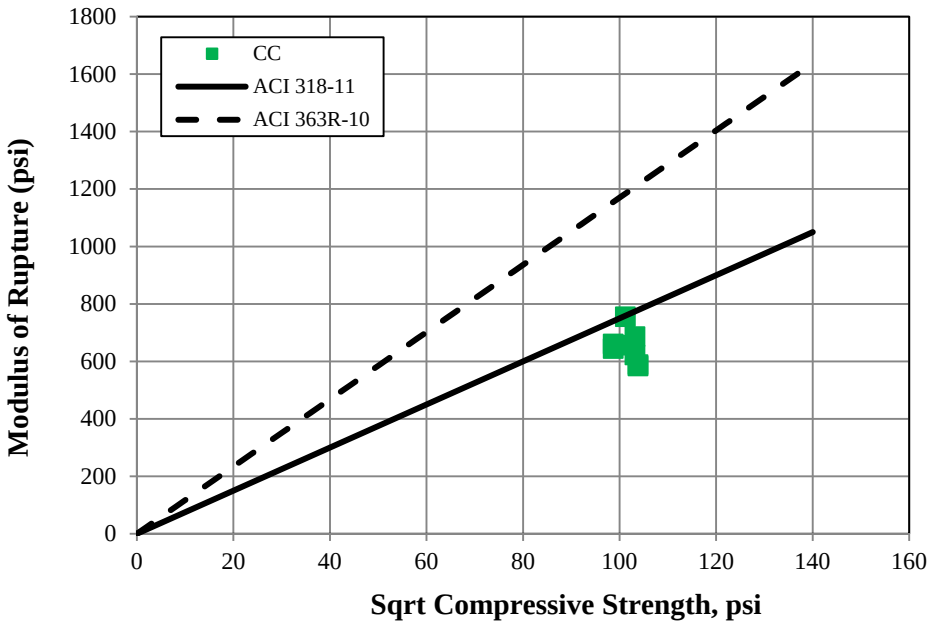

a) Span 1-2 Girders (Conventional Concrete)

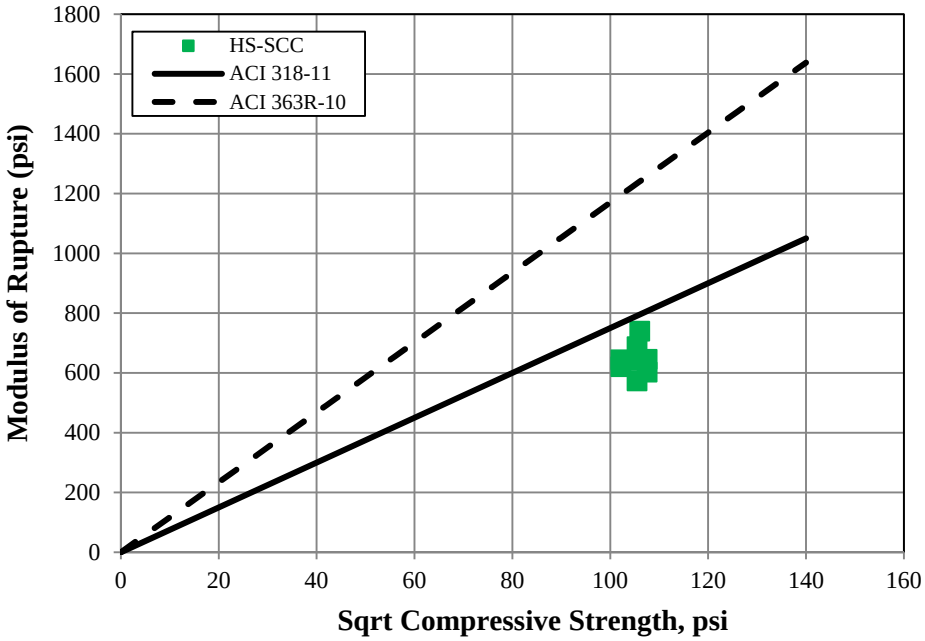

b) Span 2-3 Girders (High-Strength Self-Consolidating Concrete)

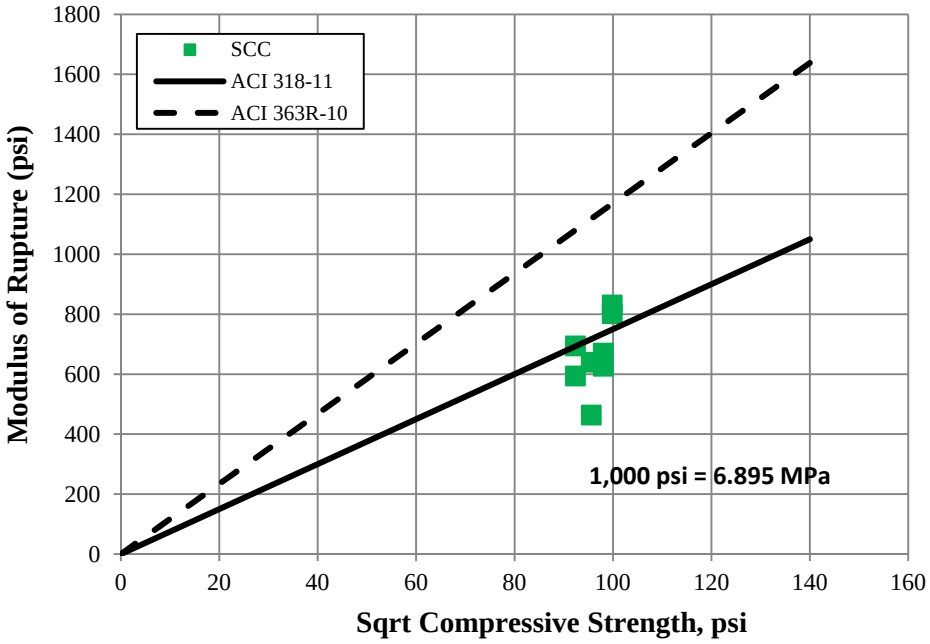

c) Span 3-4 (Self-Consolidating Concrete)

Conversion: 1000 psi = 6.895 MPa

Figure 6-11. PC/PS Girders Modulus of Rupture vs. Compressive Strength

6.1.3.5 Coefficient of thermal expansion.

The coefficient of thermal expansion (CTE) is defined as the rate at which concrete contracts or expands with temperature changes. The CTE gives the amount of strain variation within a structure that occurs from changes in temperature. Since coarse aggregate makes up the bulk of concrete, the coarse aggregate's CTE is the most influential factor in concrete's CTE, as well as quantity of aggregate in the mix. The CTE was obtained for one specimen of each mixture. As it is shown in Table 6-11 and Figure 6-12, the CC exhibited a reduced thermal change compared to the other mixtures due to the quantity of coarse aggregate in the mix.

Table 6-11. Measured Coefficient of Thermal Expansion

Mixture	Placement Date	Coefficient of Thermal Expansion	
		με/°F	με/°C
CC (Span 1-2)	7/29/2013	4.97	8.94
HS-SCC (Span 2-3)	8/13/2013	5.51	9.91
NS-SCC (Span 3-4)	8/6/2013	6.28	11.3

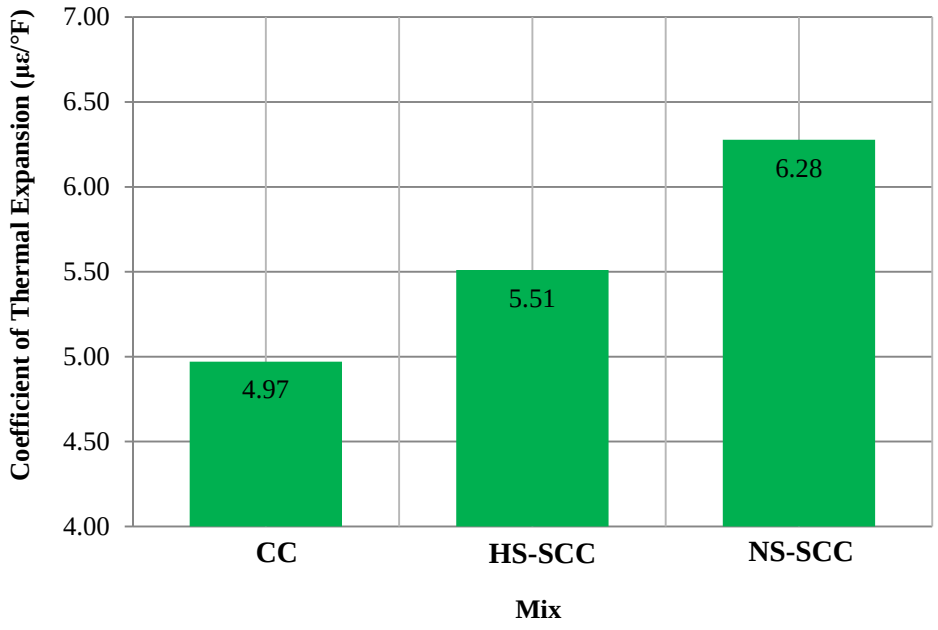

Figure 6-12. Coefficient of Thermal Expansion

6.1.3.6 Creep.

ACI 209 (2005) defines creep as the time dependent increase in strain under a sustained constant load that takes place after the initial strain at loading. In case of concrete, the constant stress is due to the prestress force, self-weight, and superimposed dead loads. Table 6-12 summarizes the loads applied to the creep specimens. Table 6-13 provides the results that include creep strain, creep coefficient, and specific creep.

Table 6-12. Creep Test Summary

Mixture	Casting Date	Curing Type	Design Compressive Strength (ksi)	Loading Force (kip)	Stress Level (ksi)
CC (Span 1-2)	7/29/2013	Steam Curing	8	20	3.2
HS-SCC (Span 2-3)	8/13/2013	Steam Curing	10	25	4
NS-SCC (Span 3-4)	8/6/2013	Steam Curing	8	20	3.2

Conversions: 1 ksi = 6.89476 MPa, 1 kip = 4.4482 kN

The data presented in Table 6-14 show that the HS-SCC underwent a greater amount of creep than NS-SCC and CC. This is due to the fact that its ratio of sand to total aggregate content is greater than the ratio present in both of NS-SCC and CC. In other words, the percentage of coarse aggregate in HS-SCC is less than in NS-SCC and CC.

The values of HS-SCC, NS-SCC, and CC were compared to empirical models. The models implemented were AASHTO LRFD (2007), ACI 209 (1997), and a method recommended by NCHRP 628 for determining the creep of self-consolidating concrete. The AASHTO LRFD (2007) model for determining creep of CC was updated by NCHRP 426 (Tadros et al. 2003). The empirical model is presented in Equations 6.9 to 6.13 below.

Table 6-13. Creep Results.

Creep Strain (microstrain)				
Mixture	Days After Loading			
	3	28	56	120
CC	87.944	106.944	116.088	125.76
HS-SCC	126.505	160.62	169.75	192.2
NS-SCC	88.337	104.372	114.644	119.46
Percentage of 120 Day Creep				
CC	69.99	84.79	92.3	100
HS-SCC	65.78	83.52	88.27	100
NS-SCC	73.73	87.11	95.69	100
Measured Creep Coefficient				
CC	1.08	1.31	1.43	1.55
HS-SCC	1.11	1.40	1.48	1.68
NS-SCC	1.10	1.30	1.43	1.49
Specific Creep (με/psi)				
CC	0.03	0.035	0.0375	0.04
HS-SCC	0.032	0.040	0.043	0.048
NS-SCC	0.028	0.034	0.037	0.039

$$\psi\,(t,t_i) = 1.9 k_s k_{hc} k_f k_{td} t_i^{-0.118} \times A \tag{6.9}$$

$$k_s = 1.45 - 0.13\left(\frac{V}{S}\right) \geq 0.0 \tag{6.10}$$

$$k_{hc} = 1.56 - 0.008H \tag{6.11}$$

$$k_f = \frac{5}{1+f'_{ci}} \tag{6.12}$$

$$k_{td} = \left(\frac{t}{61-4f'_{ci}}\right) \tag{6.13}$$

Where:

$\psi(t,t_i)$: creep coefficient

k_s: factor for volume to surface ratio of the specimen

k_{hc}: factor for humidity for creep

k_f: factor for the concrete strength

k_{td}: factor for time development

V/S: volume to surface ratio(in.)

H: relative humidity (%)

f'_{ci}: compressive strength at release (psi)

t_i: age (days) in which the load is applied

t: concrete maturity age (days)

The ACI 209 (2008) model developed for conventional concrete creep is shown in Equations 6.14 to 6.22 below.

$$\nu_u = 2.35\gamma_c \quad (6.14)$$

$$\gamma_{cr} = \gamma_{la}\gamma_\lambda\gamma_{v/s}\gamma_s\gamma_\psi\gamma_\alpha \quad (6.15)$$

$$\gamma_{la} = 1.25(t_{la})^{-0.118} \text{ for moist cured concrete} \quad (6.16)$$

$$\gamma_{la} = 1.13(t_{la})^{-0.094} \text{ for steam cured concrete} \quad (6.17)$$

$$\gamma_\lambda = 1.27 - 0.0067\lambda \quad (6.18)$$

$$\gamma_{v/s} = 2/3(1 + 1.13e^{-0.54(\frac{v}{s})}) \quad (6.19)$$

$$\gamma_s = 0.82 + 0.067s \quad (6.20)$$

$$\gamma_\psi = 0.88 + 0.0024\psi \quad (6.21)$$

$$\gamma_\alpha = 0.46 + 0.09\alpha \leq 1.0 \quad (6.22)$$

Where:

γ_{la}: correction factor for the age of loading

γ_λ: correction factor for ambient relative humidity

$\gamma_{v/s}$:correction factor for the volume to surface ratio

γ_s: correction factor for the slump

γ_ψ: correction factor for fine aggregate percentage

γ_α: correction factor for air content

t_{la}: concrete age at loading (days)

λ: ambient relative humidity (%)

V/S: volume to surface ratio (in.)

s: slump (in.)

ψ: ratio of fine aggregate to total aggregate by weight (%)

α: air content (%)

NCHRP 628 (Khayat and Mitchell 2009) developed a modified expression for AASHTO LRFD (2007) to determine the creep of SCC. This expression is presented in Equations 6.23 to 6.27. The expression utilizes the same variables as the AASHTO LRFD expression except A is a factor for the cement type; A is 1.19 for Type I/II cement and 1.35 for Type III with 20% fly ash binder. In addition, all variables in this method are in the metric (SI) system; therefore, V/S is in mm and f'_{ci} is in MPa.

$$\psi\,(t,t_i) = 1.9k_s k_{hc} k_f k_{td} t_i^{-0.118} \times A \tag{6.23}$$

$$k_s = 1.45 - 0.13\left(\frac{V}{S}\right) \geq 0.0 \tag{6.24}$$

$$k_{hc} = 1.56 - 0.008H \tag{6.25}$$

$$k_f = \frac{35}{7+f'_{ci}} \tag{6.26}$$

$$k_{td} = \left(\frac{t}{61-0.58f'_{ci}+t}\right) \tag{6.27}$$

Table 6-14 shows the measured to theoretical creep values for CC, HS-SCC, and NS-SCC. As can be concluded from the table, CC, HS-SCC, and NS-SCC measured creep coefficients at 120 days were lower than the predicted values using AASHTO (2007), higher than values determined by ACI 209 model, and lower than predicted values obtained by NCHRP 628. The test is still under progress. More data will be collected and more details will be presented in the final MoDOT report.

Table 6-14. Measured & Predicted Creep Coefficient at 120 days

Material	CC	HS-SCC	NS-SCC
Measured	1.55	1.68	1.49
AASHTO LRFD 2007	1.88	1.8	1.95
ACI 209-08	0.73	0.82	0.73
NCHRP 628	2.06	1.97	2.14

6.1.3.7 Shrinkage.

The shrinkage of concrete is the decrease in volume of hardened concrete with time which includes drying shrinkage, autogenous shrinkage, and carbonation. The shrinkage monitored by the specimens was drying shrinkage. Drying shrinkage is unrelated to load application or thermal effects. The amount of water contained in most concrete mixes is more than is needed for the complete hydration of the cementitious materials. This excess water leaches to the surface and evaporates as a function of time. As the excess water makes it to the surface and evaporates the concrete structure is reduced in volume. The rate of volume reduction occurs initially at a high rate and later diminishes with time. This is due to both the lack of excess water and increase in stiffness as the concrete cures. The results for the drying shrinkage data are presented in Tables 1.3, 1.4, and 1.5. Furthermore, the empirical results derived from shrinkage equations recommended by AASHTO (2007), ACI 209R (2008), and NCHRP Report 628 developed by Khayat and Mitchell (2009) for modifications to the AASHTO LRFD (2004) for SCC are documented within the tables.

The AASHTO LRFD (2007) developed for HSC by Tadros et al. (2003). The empirical model is presented in Equation 6.28 to 6.32.

$$\varepsilon_{sh} = k_s k_{hs} k_f k_{td} 0.48 \times 10^{-3} \tag{6.28}$$

$$k_s = \left[\frac{t}{\frac{26e^{0.36\left(\frac{V}{S}\right)}+t}{\frac{t}{45+t}}}\right]\left[\frac{1064-94\left(\frac{V}{S}\right)}{923}\right], \quad \frac{V}{S} \leq 6.0\ in \tag{6.29}$$

$$k_{hs} = 2 - 0.014H \tag{6.30}$$

$$k_f = \frac{5}{1+f'_{ci}} \tag{6.31}$$

$$k_{td} = \left(\frac{t}{61-4f'_{ci}}\right) \quad (6.32)$$

Where:

ε_{sh}: drying shrinkage

k_s: factor for volume-to-surface ratio of the specimen for shrinkage

k_{hs}: factor for humidity for shrinkage

k_f: factor for the concrete strength

k_{td}: factor for time development

V/S: volume to surface ratio (in.)

H: relative humidity (%)

f'_{ci}: compressive strength at release (psi)

t: concrete maturity age (days)

The ACI 209 (1997) model developed for conventional concrete shrinkage is displayed in Equations 6.33 to 6.42.

$$(\varepsilon_{sh})_u = 780\gamma_{sh} \times 10^{-6} \quad (6.33)$$

$$\gamma_{sh} = \gamma_\lambda \gamma_{V/S} \gamma_S \gamma_\psi \gamma_c \gamma_\alpha \quad (6.34)$$

$$\gamma_\lambda = 1.4 - 0.0102\lambda \; for \; 40 \leq \lambda \leq 80 \quad (6.35)$$

$$\gamma_\lambda = 3 - 0.030\lambda \; for \; 80 \leq \lambda \leq 100 \quad (6.36)$$

$$\gamma_{\frac{V}{S}} = 1.2e^{-\frac{0.12V}{S}} \quad (6.37)$$

$$\gamma_S = 0.89 + 0.041s \quad (6.38)$$

$$\gamma_c = 0.75 + 0.00036c \quad (6.39)$$

$$\gamma_\psi = 0.3 + 0.014\psi \; for \; \psi \leq 50\% \quad (6.40)$$

$$\gamma_\psi = 0.9 + 0.002\psi \; for \; \psi > 50\% \quad (6.41)$$

$$\gamma_\alpha = 0.95 + 0.008\alpha \; for \; \alpha \leq 1.0 \quad (6.42)$$

Where:

γ_λ: correction factor for ambient relative humidity

$\gamma_{V/S}$: correction factor for the volume to surface ratio

γ_s: correction factor for the slump

γ_{cc}: correction factor for cement content

γ_ψ: correction factor for fine aggregate percentage

γ_α: correction factor for air content.

λ: ambient relative humidity (%).

V/S: volume to surface ratio (in.)

s: slump (in.)

ψ: ratio of fine aggregate to total aggregate by weight (%)

c: cement content (lbs/ft^3)

α: air content (%)

NCHRP 628 (Khayat and Mitchell 2009) developed a modified expression for AASHTO LRFD (2004) model to determine the shrinkage of SCC. This expression is presented in Equations 6.43 to 6.45. The expression utilizes the same variables as the AASHTO LRFD expression, except A is a factor for the cement type. A is 0.918 for Type I/II cement and 1.065 for Type III with 20% fly ash binder. In addition, all variables in this method are in the metric (SI) system; therefore, V/S is in mm.

$$\varepsilon_{sh} = k_s k_{hs} \left(\frac{t}{55+t}\right) 0.56 \times 10^{-3} \times \text{A (steam cured)} \quad (6.43)$$

$$k_s = \left[\frac{t}{\frac{26e^{0.0142\left(\frac{V}{S}\right)}+t}{\frac{t}{45+t}}}\right]\left[\frac{1064-3.7\left(\frac{V}{S}\right)}{923}\right], \quad \frac{V}{S} \leq 6.0\ in \quad (6.44)$$

$$k_{hs} = 2 - 0.014H \quad (6.45)$$

Tables 6-15 through 6-17 summarize the measured shrinkage strain at different days compared to prediction models. As can be seen from Tables 6-15 through 6-17, AASHTO 2007 provides a closer estimate for CC, HS-SCC, and NS-SCC after 28 days. NCHRP 628 and ACI 209 overestimate the amount of shrinkage strain after 28 days. This test is still under progress; more data will be collected and additional details will be presented in the final MoDOT report.

Table 6-15. CC Shrinkage Strain

Method	Shrinkage Strain (με)				
	7 days	14 days	28 days	56 days	180 days
Measured Shrinkage Strain	-136	-165	-165	-166	-175.5
AASHTO 2007	-85	-140	-206	-269	-339
NCHRP Report 628	-94	-164	-265.5	-383.5	-555
ACI 209R-08	-134	-229.8	-357	-495	-673

Table 6-16. HS-SCC Shrinkage Strain

Method	Shrinkage Strain (με)				
	7 days	14 days	28 days	56 days	180 days
Measured Shrinkage Strain	-144	-166.5	-187	-198	-201.56
AASHTO 2007	-85	-138	-199	-254.6	-312.7
NCHRP Report 628	-82	-147	-244.5	-365.6	-555
ACI 209R-08	-137.7	-236	-367	-508	-691

Table 6-17. NS-SCC Shrinkage Strain

Method	Shrinkage Strain (με)				
	7 days	14 days	28 days	56 days	180 days
Measured Shrinkage Strain	-138.5	-139	-143	-159	-180
AASHTO 2007	-86	-143	-214	-284	-364
NCHRP Report 628	-82	-147	-244.5	-365	-555
ACI 209R-08	-132	-225.8	-351	-486	-661

6.1.4. NASP Pullout Tests.

The NASP test aims to assess the bonding abilities of seven wire prestressing strands in concrete. The pullout specimens were fabricated with the concrete mixes employed to cast the PC girders of spans 1-2 (CC) and 3-4 (NS-SCC) of Bridge A7957. Table 6-18 summarizes the NASP test results. There was little difference in bond performance between NS-SCC and CC at 0.001 in (0.025 mm) of strand slip. However CC exhibits higher bond performance than NS-SCC at 0.1 in (2.54 mm) of strand slip. Since the loads had been normalized with respect to concrete strength, this difference is most likely due to other factors, such as a higher fine aggregate content in the NS-SCC mix than CC. In addition, that might have caused a less adhesion between the strand and concrete which leads to a lower slip load.

Table 6-18. Concrete NASP Results

Mix	Day	Specimen ID	√f'c (√psi)	Load/√f'c at Slip of 0.001 in				Load/√f'c at Slip of 0.1 in			
				Load/√f'c (lb/√psi)	Avarge (lb/√psi)	Std. Dev. (lb/√psi)	COV.	Load/√f'c (lb/√psi)	Avarge (lb/√psi)	Std. Dev. (lb/√psi)	COV.
NS-SCC	28 days	SCC-1	104.96	82.9	93.14	18	19%	131.74	122.59	9	7%
		SCC-2		77.9				110.44			
		SCC-3		118.6				125.59			
CC	28 days	A-1-1	105.35	75.74	90.73	17	19%	152.72	151.14	6	4%
		A-1-2		81.61				157.12			
		A-1-3		114.85				143.59			

Conversion: 1 lb. = 4.45 N, 1 in. = 2.54 mm

6.1.5. Deck.

6.1.5.1 Fresh properties.

The CIP RC deck was cast on October 21st 2013 (Section 5.6.2). Fresh properties were recorded for batches 1 through 3 and are presented in Table 6-19.

Table 6-19. Modified B-2 Concrete Mix Fresh Properties

	Batch 1	Batch 2	Batch 3
Air Temp. (°F/°C)	49/9	49/9	50/10
Concrete Temp. (°F/°C)	62/17	64/18	63/17
Slump (in.)	6.0	5.5	5.75
Air Content (%)	7.0	6.2	8.3

Conversions: 1 in. = 25.4 mm

6.1.5.2 Compressive strength.

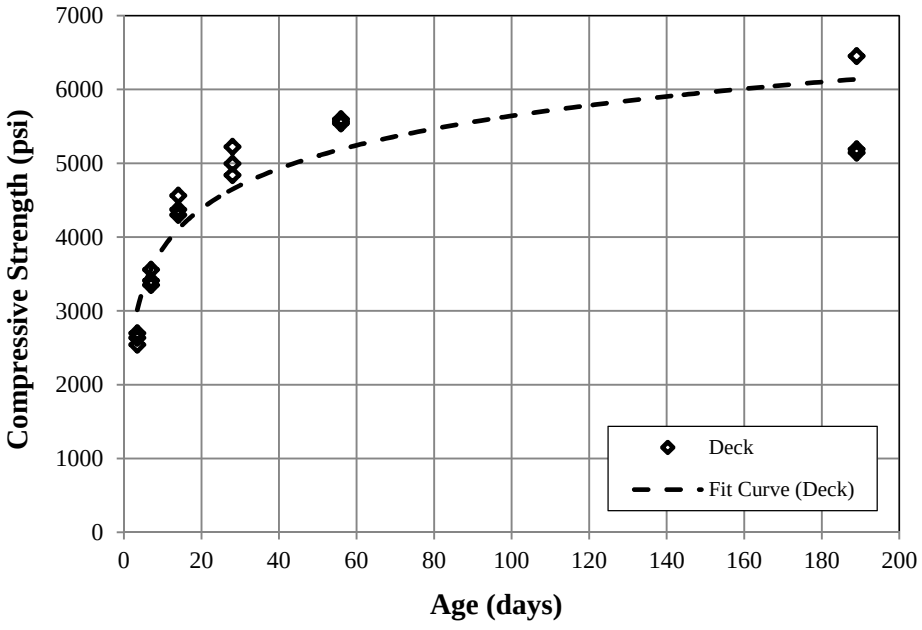

Conversion: 1000 psi = 6.895 MPa

Figure 6-13. Deck Compressive Strength vs. Age

Compressive strength tests were conducted at 3, 7, 14, 28, 56 days, and when the first live load test was executed. The compressive strength is plotted in Figure 6-13. The results obtained after 14 days exceeded the target strength of 4,000 psi (27.6 MPa) specified by MoDOT.

6.1.5.3 Abrasion resistance.

The abrasion resistance results are illustrated in Figure 6-14 and Figure 6-15. The results obtained are consistent with trends found in previous studies. Figure 6-16 shows the specimen after the abrasion test.

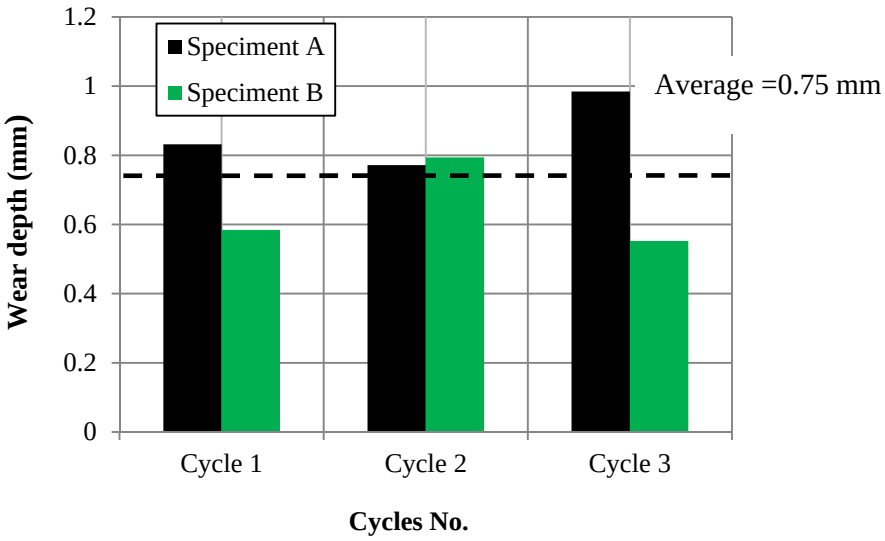

Figure 6-14. Depth of Wear Results

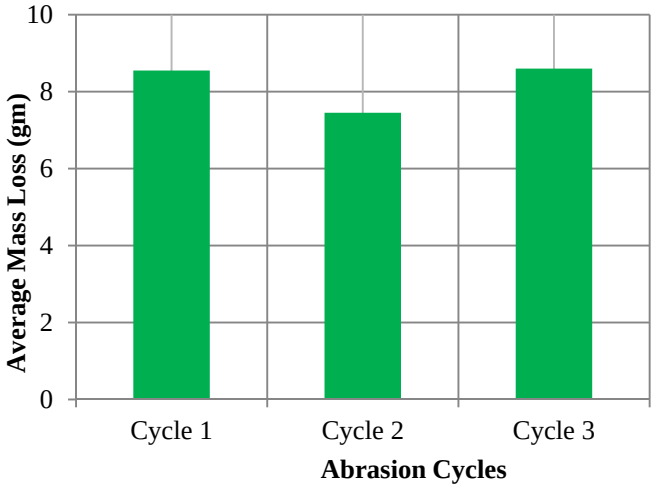

Figure 6-15. Average Mass Loss Results

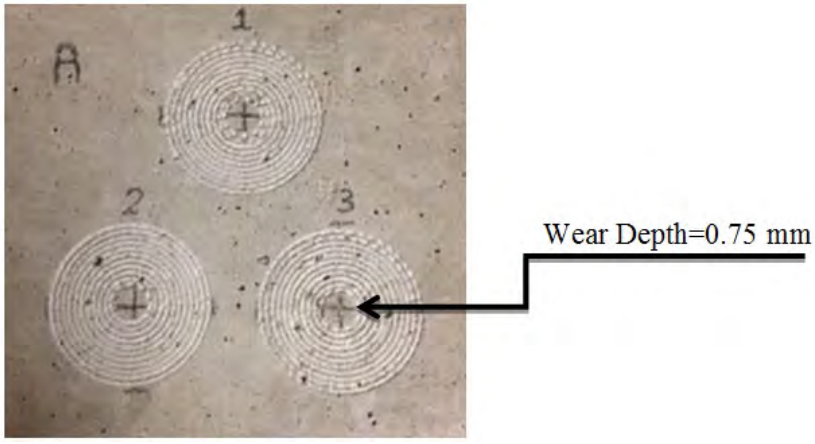

Figure 6-16. Specimen after Abrasion Test

6.1.5.4 Freeze and Thaw Resistance.

The freeze-thaw resistance was investigated for deck concrete. The test results for each specimen are presented in Table 6-20 which illustrates the durability factor for every beam for the test specimens.

Table 6-20. Freeze and Thaw Results

Beam No.	Casting Date	Durability Factor
1	10/21/2013	84.6
2	10/21/2013	88.4
3	10/21/2013	87.9
Average		87.0

6.1.6. Safety Barriers.

6.1.6.1 Compressive strength.

The safety barriers were was cast on December 19th, 2013 (Section 5.6.4). Fresh properties were not recorded by the researchers. Compressive strength tests were executed at 7, 28, 56 days and when live load test 1 was conducted. The compressive strength against age is presented in Figure 6-17. The results obtained after 7 days exceeded the design strength of 4,000 psi (27.6 MPa) specified by MoDOT (Class B-2 mix).

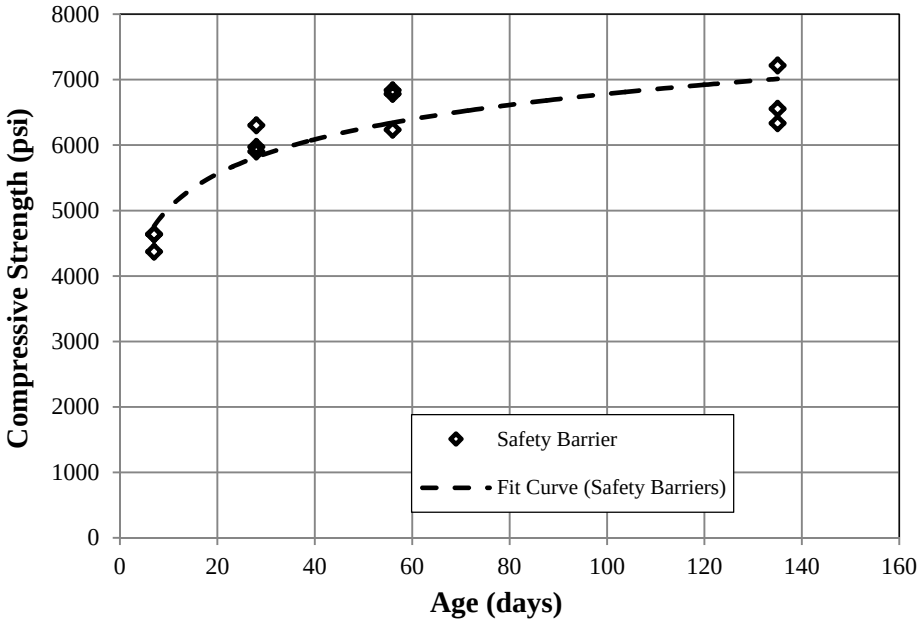

Conversion: 1000 psi = 6.895 MPa

Figure 6-17. Deck Compressive Strength vs. Age

6.2. NU GIRDER SHEAR TESTING RESULTS

The following section includes the material test results and destructive shear test results of the precast prestressed NU girders performed at the Structural Engineering Research Laboratory (SERL) at Missouri S&T.

6.2.1. Material Properties.

6.2.1.1 Test girders.

6.2.1.1.1 Fresh properties.

The test girders were poured consecutively in four continuous batches at County Materials Corporation in Bonne Terre, MO on March 8, 2013. Fresh properties were recorded for batches 1 and 3 and are displayed in Table 6-21. The segregation percentage of 7.4% performed on batch 1 meets the ACI 237r-07 maximum recommended value of 10.0% (ACI 237 2007).

6.2.1.1.2 Hardened properties.

Compressive strength and modulus of elasticity tests were performed at release (3 days), 28 days and on days when laboratory shear testing was performed. Modulus of rupture beams were also tested on days when shear testing was performed. The

compressive strength was plotted against specimen age in Figure 6-18. MoDOT recorded compressive strength test results at release (3 days) of 10,490 and 10,660 psi (72.3 and 73.5 MPa) for TG1 and TG2, respectively. Their results exceeded the target release strength of 8,000 psi (55.2 MPa). The difference compared to Missouri S&T's average at 3 days of 7,942 psi (54.8 MPa) could be attributed to the method of capping as well as the testing machine.

Table 6-21. Test Girder Fresh Properties

		Batch 1 (TG2)	Batch 3 (TG1)
Air		6.3%	4.2%
Slump Flow (in.)		24.5	25
J-Ring (in.)		22	25
Concrete Temp. (°F/°C)		65/18	65/18
Air Temp. (°F/°C)		51/11	51/11
Segregation Column	Top (lb.)	6.14	N/A
	Bottom (lb.)	6.61	N/A
	S (%)	7.4	N/A

Conversions: 1 in. = 25.4 mm, 1 lb. = 0.4536 kg

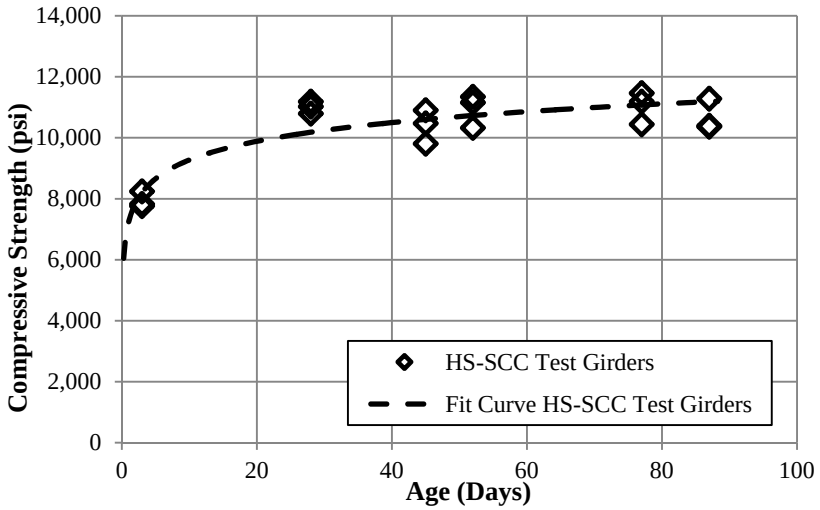

Conversion: 1000 psi = 6.895 MPa

Figure 6-18. HS-SCC Test Girders Compressive Strength vs. Age

The modulus of elasticity data was graphed against the square root of compressive strength shown in Figure 6-19. The data was compared to ACI 318-11 (Equation 6.1) and ACI 363R-10 (Equations 6.3 and 6.4) estimates. Similar trends are observed when compared to the HS-SCC trial mix. The ACI 363R-10 suggested by Martinez et al. (1982) equation provides an accurate estimate for the MOE of HS-SCC, while the Tomosawa et al. (1993) equation of ACI 363R-10 is an accurate lower bound predictor for HS-SCC. The ACI 318-11 equation overestimates the modulus of elasticity.

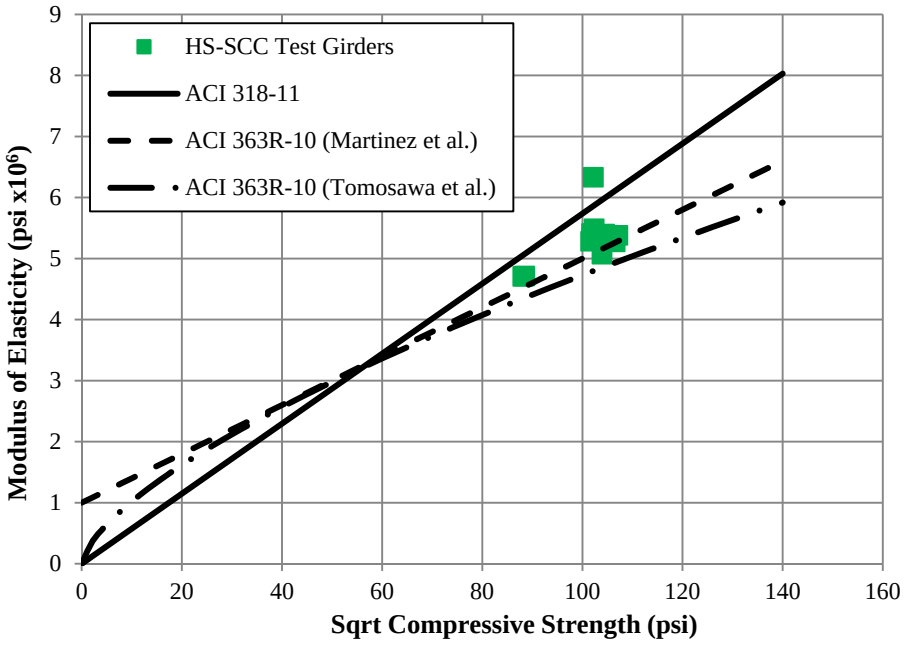

Conversion: 1000 psi = 6.895 MPa

Figure 6-19. HS-SCC Test Girders Modulus of Elasticity vs. Compressive Strength

The modulus of rupture for HS-SCC was compared to empirical estimates provided by ACI 318-11(Equation 6.46) and ACI 363R-10 (Equation 6.47). In the below expressions, f_r is the modulus of rupture (psi), λ is a reduction factor for lightweight concrete, and f'_c is the compressive strength of concrete (psi). The AASHTO 2012 model is identical to the ACI 318-11 model with the exception of the units considered; AASHTO deals with ksi while ACI regularly uses psi (ACI 318-11, AASHTO 2012). For this reason, the AASHTO 2012 equation for modulus of rupture was not considered for comparisons. The HSC model proposed by Carrasquillo et al. (1982) considered compressive strengths ranging from 3,000 to 12,000 psi (20.7 to 82.7 MPa).

$$f_r = 7.5\lambda\sqrt{f'_c} \quad (6.46)$$

$$f_r = 11.7\sqrt{f'_c} \quad (6.47)$$

Figure 6-20 displays the modulus of rupture versus the square root of compressive strength for the 8 tests run. Despite the validity of the ACI 318-11 empirical model for concrete strengths up to approximately 8,000 psi (55.2 MPa), it appropriately estimates the MOR for HS-SCC. The HSC model in ACI 363R-10 significantly overestimates the MOR. The reduced MOR of the HS-SCC mix with respect to the ACI 363R-10 equation for HSC could be attributed to the reduction in the coarse aggregate volume.

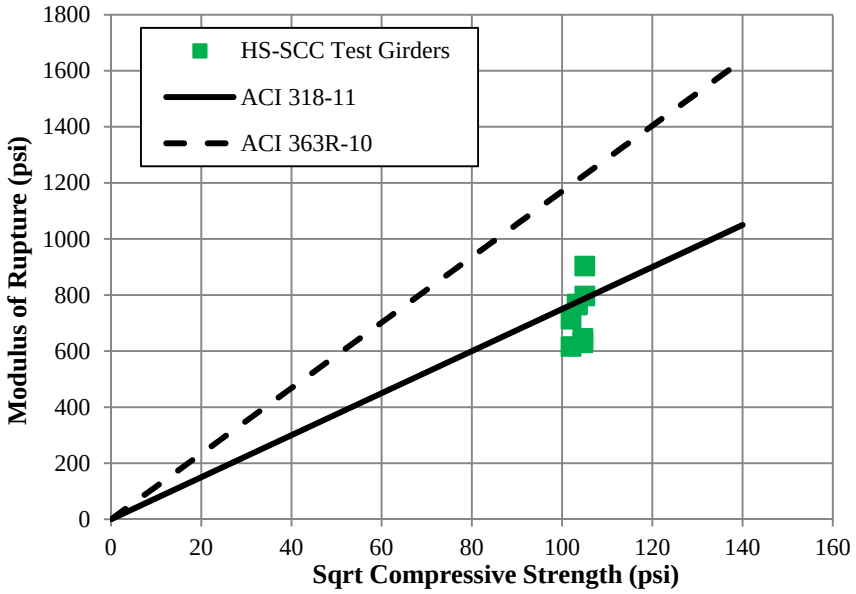

Conversion: 1000 psi = 6.895 MPa

Figure 6-20. HS-SCC Test Girders Modulus of Rupture vs. Compressive Strength

6.2.1.2 CIP deck.

6.2.1.2.1 Fresh properties.

Fresh properties were collected for the CIP deck that was poured on each test girder; however, the fresh properties were not recorded from the first pour. Both mixes consisted of the same mix design, and consequently, fresh properties should not differ significantly. Table 6-22 lists the fresh properties from the CIP deck on TG2.

Table 6-22. TG2 CIP Deck Fresh Properties

Air Temp. (°F/°C)	65/18
Concrete Temp.	not recorded
Air Content (%)	12.0
Slump (in.)	6.5

Conversion: 1 in. = 25.4 mm

6.2.1.2.2 Hardened properties.

The CIP deck was designed off of MoDOT's modified B-2 mix design: mix ID 12CDMB2A087. The design compressive strength at 28 days was 4,000 psi (27.6 MPa). The mix was batched by Ozark Ready Mix Company, Inc. in Rolla, Missouri. Only compressive strength testing was conducted on the deck QC/QA cylinders. Average results at 3, 7, 14, 21, 28, and at shear testing days are listed in Table 6-23 with strength generation over time plotted in Figure 6-21. There is considerable variability in the results between the two batches despite the identical mix designs. This trend has been observed in previous encounters with the local ready mix supplier in Rolla, MO. Addition of excess water could raise the w/cm ratio, thus reducing the compressive strength of the mixture to less than that of MoDOT's modified B-2 mix design.

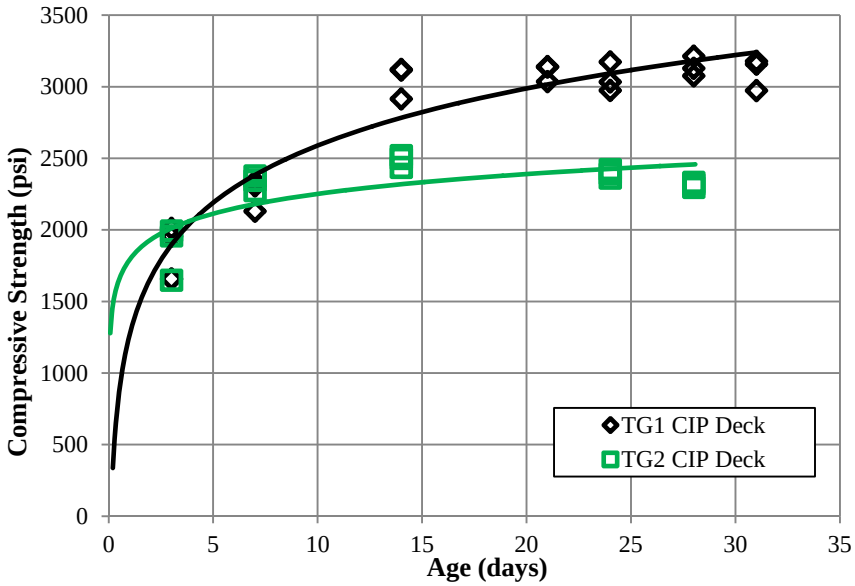

Conversion: 1000 psi = 6.895 MPa

Figure 6-21. HS-SCC Test Girders CIP Deck Compressive Strength vs. Age

Table 6-23. Compressive Strength of HS-SCC Test Girders CIP Deck

Age (days)	3	7	14	21	24	28	31
TG1	1875	2258	3051	3105	3061*	3140	3103#
TG2	1867	2333	2485*	N/A	2392#	2316	N/A

*: Test results performed on day of shear testing for test #1

#: Test results performed on day of shear testing for test #2

6.2.2. Shear Testing Results

The ultimate loads from each shear test were compared to both the nominal and factored shear resistances from ACI 318-11 and AASHTO 2012 LRFD Bridge Design Specifications. A brief review of each prediction equation is presented followed by results from the destructive shear testing.

6.2.2.1 ACI.

The ACI Building Code Requirements for Structural Concrete (2011) states the nominal shear strength (V_n) of a prestressed concrete member as the summation of the concrete contribution to shear (V_c) and the steel contribution to shear (V_s) shown in Equation 6.48. The factored shear strength (ϕV_n) is then determined by multiplying the nominal shear resistance by a strength reduction factor (ϕ), which must exceed the ultimate shear force due to external loads (Equation 6.49). The strength reduction factor for shear in ACI 318-11 Section 9.3.2.3 is listed as 0.75. The ultimate shear force (V_u) is said to act at a distance $h/2$ from the support, where h is the height of the member.

$$V_n = V_C + V_S \tag{6.48}$$

$$\phi V_n \geq V_u \tag{6.49}$$

The ACI 318-11 building code provides two methods for computing the concrete contribution to shear of prestressed concrete members. The first is a simplified procedure (Equation 11-9 in ACI 318-11) for members with an effective prestress force not less than 40 percent of the tensile strength of the flexural reinforcement. It is most applicable for members subject to uniform loading. The simplified procedure is presented below in Equation 6.50 (ACI 318 2011). In the below expression, V_c is the concrete contribution to

shear (lb.), λ is a reduction factor for lightweight concrete, f'_c is the compressive strength of concrete (psi), V_u is the factored shear force at the section (lb.), M_u is the factored moment at the section (in.-lb.), d is the distance from the extreme compression fiber to the centroid of the longitudinal tension reinforcement (in.), and b_w is the width of the web (in.).

$$V_C = \left(0.6\lambda\sqrt{f'_C} + 700\left(\frac{V_u d_p}{M_u}\right)\right) b_w d \qquad (6.50)$$

The second procedure is a detailed calculation of the shear resistance which accounts for both web-shear cracking (V_{cw}) and flexure-shear cracking (V_{ci}) shown in Figure 6-22. To obtain more accurate results, this study compared results to the second (detailed) procedure. The shear contribution provided by the concrete is taken as the lesser of V_{cw} and V_{ci}. The critical section investigated was a distance $h/2$ from the support as stated in ACI 318-11. Equations 11-10 and 11-12 in ACI 318-11 are used to determine the shear force to cause flexure-shear and web-shear cracking, respectively. The equations for web-shear and flexure-shear cracking are shown in Equation 6.51 and 6.52. The cracking moment required in Equation 6.52 is listed as Equation 6.53 (ACI 318 2011). For the listed expressions, f_{pc} is the compressive stress at the centroid of the concrete section due to the effective prestress force (psi), d_p is the distance from the extreme compression fiber to the centroid of the prestressing steel (in.), V_p is the vertical component of the effective prestress force at the section (lb.), V_d is the shear force at the section due to unfactored dead load (lb.), V_i is the factored shear force at the section due to externally applied loads (lb.), M_{cre} is the flexural cracking moment (in.-lb.), M_{max} is the maximum factored moment at the section due to externally applied loads (in.-lb.), I is the gross moment of inertia, y_t is the distance from the centroid to the tension face (in.), f_{pe} is the compressive stress in concrete due to effective prestress only at the extreme fiber of the section where tensile stress is caused by externally applied loads (psi), and f_d is the stress due to the unfactored dead load at the extreme fiber of the section where tensile stress is caused by externally applied loads (psi).

$$V_{cw} = \left(3.5\lambda\sqrt{f'_C} + 0.3f_{pc}\right)b_w d_p + V_p \quad (6.51)$$

$$V_{ci} = 0.6\lambda\sqrt{f'_C}b_w d_p + V_d + \left(\frac{V_i M_{cre}}{M_{max}}\right) \quad (6.52)$$

$$M_{cre} = \left(\frac{I}{y_t}\right)\left(6\lambda\sqrt{f'_C} + f_{pe} - f_d\right) \quad (6.53)$$

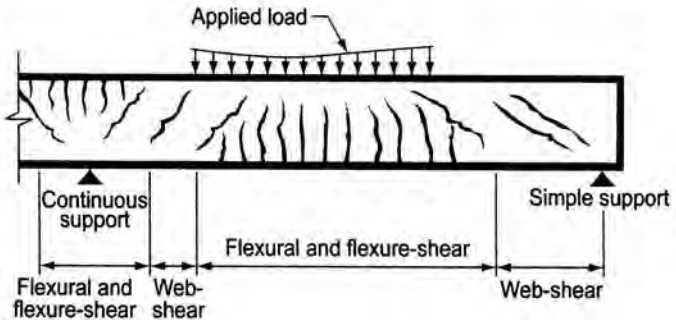

Figure 6-22. Schematic of Web-Shear and Flexure-Shear Cracking

The nominal shear strength provided by transverse reinforcement is calculated from ACI 318-11 equation 11-15 for both reinforced and prestressed concrete. This equation is valid when the shear reinforcement is perpendicular to the axis of the member. The equation is presented below as Equation 6.54, where V_s is the shear contribution from the shear reinforcement (lb.), A_v is the area of shear reinforcement at spacing s (in.^{2}), f_{yt} is the specified yield strength of the transverse reinforcement (psi), d is the distance from the extreme compression fiber to the centroid of the longitudinal tension reinforcement (in.), and *s* is the center to center spacing of the transverse reinforcement (in.).

$$V_s = \frac{A_v f_{yt} d}{s} \quad (6.54)$$

The load-deflection response was recorded during each test. The deflection at the south end of the girder (at the actuators) was recorded during each test. The shear force was then plotted against this deflection. Figure 6-23 and Figure 6-24 display the load-deflection response for the shear reinforced sections (test #1) and non-reinforced sections (test #2), respectively.

The shear reinforced region was not tested to complete failure as mentioned in Section 5.2.7. As a result, the nominal shear strength (V_n) following ACI 318-11 was not plotted, but rather the factored shear strength (ϕV_n). Regardless, both types of shear reinforcement (welded wire reinforcement and mild steel bars) exceed the factored shear resistance from ACI 318-11. The different factored shear resistance between the WWR and MS of Figure 6-23 can be contributed to the cross sectional area and spacing of the transverse reinforcement.

From Figure 6-24, there is considerable variability between the ultimate shear forces of the two girders. This observation is not unusual, as the shear strength of concrete is still not a fully understood concept. Test girder 1 exceeds both the nominal and factored shear strength predicted by ACI 318-11. Test girder 2 falls just short of the nominal capacity, but exceeds the calculated factored shear strength following ACI 318-11. Table 6-24 summarizes ultimate shears compared to ACI prediction equations.

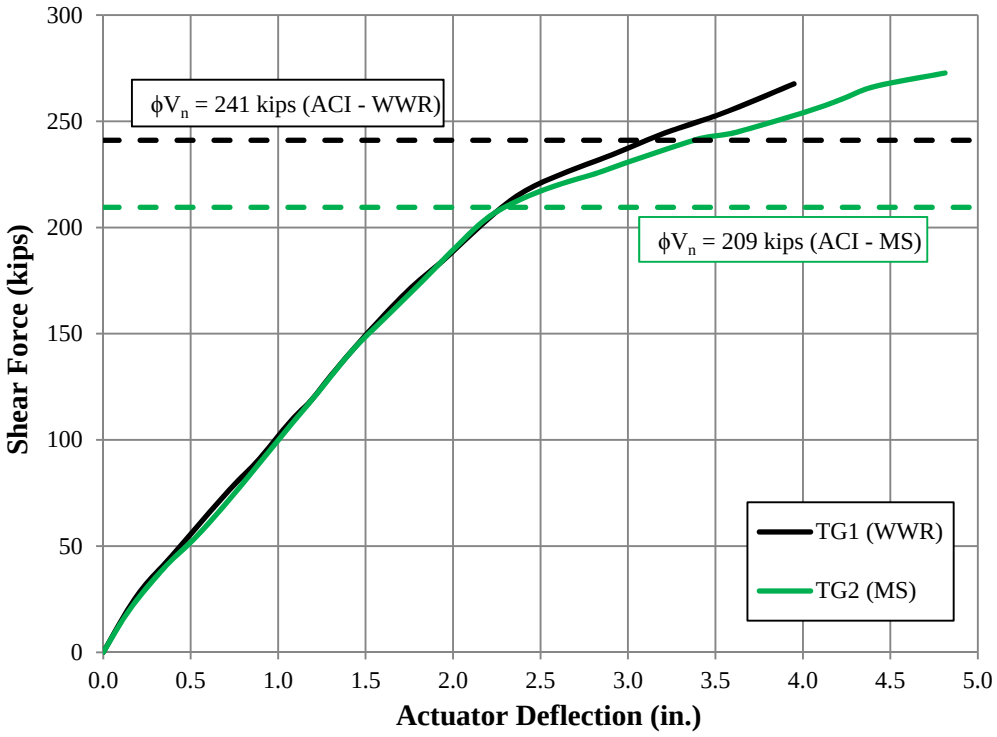

Conversions: 1 in = 25.4 mm, 1 kip = 4.44822 kN

Figure 6-23. ACI Load Deflection Response for Test #1

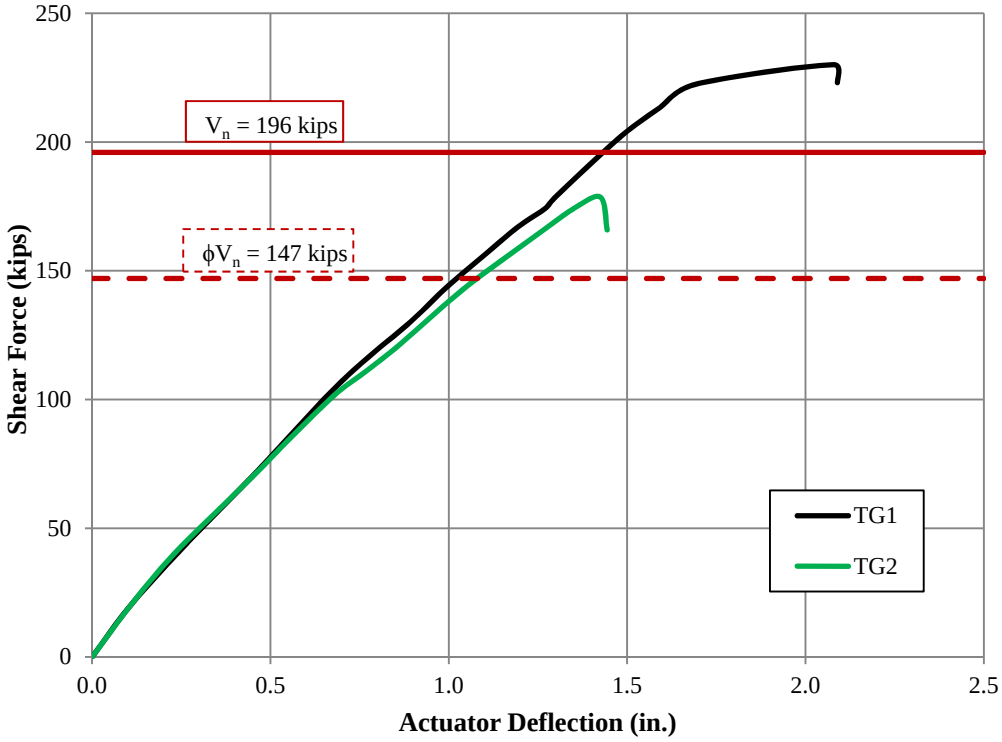

Conversions: 1 in = 25.4 mm, 1 kip = 4.44822 kN

Figure 6-24. ACI Load Deflection Response for Test #2

Table 6-24. ACI Shear Response Summary Table

	Test #1 (kips)					Test #2 (kips)			
	V_c	V_s	V_n	ϕV_n	$V_{n,test}$	V_c	ϕV_c	$V_{c,test}$	$V_{c,test}/V_{c,calc}$
TG1 (WWR)	196.0	125.4	321.4	241.1	267.6	196.0	147.0	230.0	1.17
TG2 (MS)		83.3	279.3	209.5	272.7			178.5	0.91
								Average	1.04

Conversion: 1 kip = 4.44822 kN

6.2.2.2 AASHTO.

The Missouri Department of Transportation uses their Engineering Policy Guide (EPG), Category 751 LRFD Bridge Design Guidelines for bridge design for new construction (MoDOT 2011). This document is based on the AASHTO LRFD Bridge Design Specifications. This section will refer to relevant AASHTO 2012 equations also specified in MoDOT's EPG.

The MoDOT EPG follows the general procedure from AASHTO 2012 for determination of the nominal shear resistance, V_n. This procedure is derived from the Modified Compression Field Theory (MCFT) developed by Vecchio and Collins (1986). It involves the calculation of the shear resistance at sections along the length of the member based on the applied loads. AASHTO 2012 cites a critical shear location at a distance d_v from the support. The effective shear depth, d_v, is calculated as the distance between the resultant tensile and compressive forces due to flexure. For the composite NU girder section, this value is approximately 51 in. (1.30 m). The nominal shear resistance is the summation of the contribution to shear from the concrete (V_c), transverse reinforcement (V_s), and vertical component of effective prestressing force (V_p). AASHTO also specifies a maximum limit on V_n to prevent crushing of the concrete in the web before yielding of the transverse reinforcement. The nominal shear resistance is then multiplied by the resistance factor, ϕ, to determine the factored shear resistance, ϕV_n. Unlike ACI 318-11, AASHTO 2012 uses a resistance factor of 0.9. The nominal shear resistance, maximum limit, and factored shear resistance are presented in Equations 6.55, 6.56, and 6.57, respectively. In Equation 6.56, f'_c is the compressive strength (ksi), b_v is the effective web width (in.).

$$V_n = V_C + V_S + V_p \tag{6.55}$$

$$V_{n,max} = 0.25 f'_c b_v d_v + V_p \tag{6.56}$$

$$\phi V_n \geq V_u \tag{6.57}$$

The concrete contribution to shear in the general procedure is calculated following Equations 6.58 to 6.62. The β factor, which indicates the ability of the diagonally cracked concrete to transmit tension and shear, depends on the net longitudinal strain at the section at the centroid of the longitudinal reinforcement, ε_s. Two different equations are used to determine β, depending on the presence of transverse reinforcement. When transverse reinforcement is not included, as was the case during the second test, a crack spacing parameter, s_{xe}, is included to account for the spacing of longitudinal reinforcement and maximum aggregate size; it is to be taken not less than 12.0 in. (305 mm), nor greater than 80.0 in. (2030 mm). For the following expressions,

M_u is the factored moment at the section (in.-kip.), V_u is the factored shear at the section (kip.), N_u is the factored axial force (kip.), A_{ps} is the area of prestressing steel (in.^{2}), f_{po} is the locked in difference in strain between the prestressing steel and the surrounding concrete multiplied by the modulus of elasticity of the prestressing steel (ksi), E_s is the modulus of elasticity of the non-prestressing steel (ksi), A_s is the area of non-prestressing steel (in.^{2}), E_p is the modulus of elasticity of the prestressing steel (ksi), s_x is the crack spacing parameter (in.), and a_g is the maximum aggregate size (in.).

$$V_c = 0.0316\beta\sqrt{f'_c}b_v d_v \tag{6.58}$$

$$\beta = \frac{4.8}{(1+750\varepsilon_s)} \tag{6.59}$$

$$\beta = \frac{4.8}{(1+750\varepsilon_s)}\left(\frac{51}{39+s_{xe}}\right) \tag{6.60}$$

$$\varepsilon_s = \frac{\left(\frac{|M_u|}{d_v}+0.5N_u+|V_u-V_p|-A_{ps}f_{po}\right)}{E_s A_s+E_p A_{ps}} \tag{6.61}$$

$$s_{xe} = s_x\left(\frac{1.38}{a_g+0.63}\right) \tag{6.62}$$

The contribution to shear from the transverse reinforcement from AASHTO 2012 is taken using Equation 6.63, when the transverse reinforcement is perpendicular to the longitudinal axis of the beam. The variable θ is the angle of inclination of the diagonal compressive stress in the concrete (degrees) and is shown in Equation 6.64. In Equation 6.63, A_v is the area of the transverse reinforcement (in.^{2}), f_y is the yield strength of the transverse reinforcement (ksi), and s is the transverse reinforcement spacing (in.).

$$V_s = \frac{A_v f_y d_v \cot\theta}{s} \tag{6.63}$$

$$\theta = 29 + 3500\varepsilon_s \tag{6.64}$$

The load-deflection response of the girders was presented in Figure 6-23 and Figure 6-24. The response from the second test (unreinforced region) is presented again as Figure 6-25, but compared to the nominal and factored shear resistance computed from AASHTO 2012. The response from the shear reinforced test is not graphed against

AASHTO predictions because at the conclusion of the test, they had not reached the factored shear resistance as occurred with ACI 318-11.

Both test girders exceed the nominal and factored shear resistance without transverse reinforcement as predicted by AASHTO 2012 and MoDOT EPG. The second test girder showed additional displacement ductility over the second girder, noted by the brief leveling off portion in Figure 6-25. This ductility is unique as concrete shear failures are typically very brittle. Table 6-25 summarizes ultimate shears compared to AASHTO prediction equations.

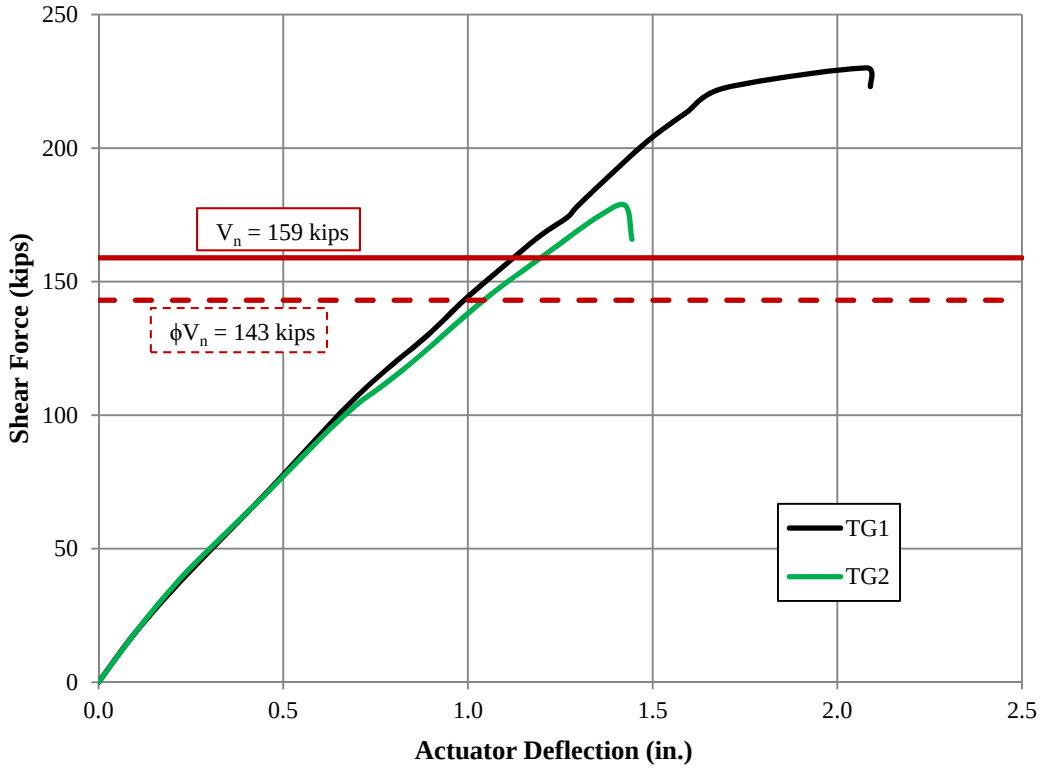

Conversions: 1 in = 25.4 mm, 1 kip = 4.44822 kN

Figure 6-25. AASHTO/MoDOT EPG Load Deflection Response for Test #2

Table 6-25. AASHTO Shear Response Summary Table

	Test #1 (kips)					Test #2 (kips)			
	V_c	V_s	V_n	ϕV_n	$V_{n,test}$	V_c	ϕV_c	$V_{c,test}$	$V_{c,test}/V_{c,calc}$
TG1 (WWR)	158.9	214.7	373.6	336.2	265.7	158.9	143.0	228.1	1.44
TG2 (MS)		142.6	301.5	271.4	270.8			176.7	1.11
								Average	1.27

Conversion: 1 kip = 4.44822 kN

6.2.2.3 Crack observations.

Crack widths and patterns were recorded throughout each test. Appendix E contains the crack patterns and widths. Five different crack width categories were considered; the first three were based off of ACI 224R-01, Table 4-1 (ACI 224 2001). Cracks less than or equal to 0.004 in. (0.10 mm) were classified as hairline cracks; less than or equal to 0.012 in. (0.30 mm) as acceptable; less than or equal to 0.016 in. (0.41 mm) as moderate; less than or equal to 0.100 in. (2.54 mm) as excessive; and greater than 0.100 in. (2.54 mm) as severe. ACI 224R-01, no longer included in the ACI 318-11 code, lists an upper limit on reasonable crack widths of 0.016 in. (0.41 mm) (ACI 224 2001).

Maximum shear crack widths during the first tests (reinforced section) measured 0.018 in. (0.46 mm) and 0.050 in. (1.27 mm) for test girders 1 and 2, respectively. The larger spacing of the transverse reinforcement in TG2 resulted in larger crack widths. Maximum crack widths during the second test (unreinforced section) measured 0.400 in. (10.2 mm) and 0.969 in. (24.6 mm) for test girders 1 and 2, respectively. The smaller crack widths at failure of TG1 could explain the increased ductility compared to TG2. The shear deformations in TG1could have been distributed among multiple cracks, reducing the observed crack width at failure. For TG2, the shear deformation was concentrated along one failure plane, resulting in a larger crack width of nearly 1.0 in. (25.4 mm).

6.2.2.4 Future analysis.

The shear behavior of the girders will be compared to results from computer models and included in the final MoDOT report. Both Response 2000 and ATENA

Engineering will be used. Response 2000 is a sectional analysis program developed by Evan Bentz and Michael Collins at the University of Toronto designed for beams and columns subject to axial load, moment and shear. ATENA Engineering was developed at Cervenka Consulting, Czech Republic as a nonlinear finite element analysis program for reinforced and prestressed concrete.

6.3. PRELIMINARY CONCLUSIONS

6.3.1. Trial Mixes.

The following conclusions were reached from the HVFAC, HS-SCC, and NS-SCC trial mixes:

1. The modulus of elasticity of the HS-SCC trial mix closely matches the Martinez et al. equation of ACI 363R 2010 while the equation suggested by Tomosawa et al. in ACI 363R 2010 provides a lower bound estimate. The ACI 318 2011 equation overestimated the modulus of elasticity.
2. The splitting tensile strength of the HS-SCC mix was overestimated by both the ACI 318 2011 and ACI 363R 2010 prediction equations. Post-test cross section images revealed that the aggregate failed before the interfacial bond zone between the paste and aggregate.
3. The modulus of elasticity of the 8,000 psi (55.2 MPa) NS-SCC trial mix was accurately estimated by both the Tomosawa et al. and Martinez et al. prediction equations in ACI 363R 2010. Both of these curves intersected at roughly 8,000 psi.
4. The ACI 318 2011 equation for the splitting tensile strength provides the best prediction for NS-SCC, while the ACI 363R 2010 equation overestimated the STS.

6.3.2. Intermediate Bents (HVFAC).

The following observations were documented regarding the HVFAC with 50% fly ash replacement:

1. Raising the level of replacement fly ash from 20% to 50% reduced the heat generated by 24-43%.
2. There was a negligible difference in the setting time of the HVFAC versus the CC mix with 20% fly ash replacement.

3. There were mixed results when analyzing the time to reach the peak hydration temperature between the CC (Class B mix) and HVFAC.

6.3.3. NU Test Girders.

The following conclusions were reached pertaining to the hardened material properties and shear testing of the HS-SCC mix in the NU 53 girder series:

1. Similar to the HS-SCC trial mix, the modulus of elasticity of the HS-SCC mix in the test girders was overestimated by ACI 318 2011, and accurately predicted by the Martinez et al. equation in ACI 363R 2010.
2. The modulus of rupture was most accurately predicted by the ACI 318 2011 and overestimated by ACI 363R 2010. Scatter on the order of 40% was observed among the testing results for the modulus of rupture.
3. The shear strength not in the presence of web reinforcement exceeds the nominal resistance predicted by the AASHTO 2012 LRFD Design Specifications. Both girders exceeded the factored shear resistance predicted by ACI 318 2011. TG1 exceeded while TG2 fell just short of the nominal shear resistance following ACI 318 2011. When compared to the nominal predicted shear strength, the average test to predicted shear strength ratio was 1.04.
4. It is recommended to use welded wire mesh over mild steel bars for transverse reinforcement. The larger spacing of the mild steel bars resulted in larger crack widths. Reducing the spacing of the reinforcement by using a smaller bar diameter increases the number of cracks per unit length, but reduces the maximum crack width. Smaller crack widths will increase the concrete contribution to shear at the interfacial transition zone due to surface roughness and aggregate interlock.

6.3.4. Implementation Program

1. The first full-scale structure implementation of high-strength self-consolidating concrete (HS-SCC) and high volume fly ash concrete (HVFAC) has been executed on the structure of Bridge A7957 through the Missouri Department of Transportation (MoDOT).
2. High volume fly ash concrete, a sustainable material, at a 50% replacement level was used within one of the interior supports of this bridge. Coupled with the use

of SCC, Bridge A7957 is expected to have a longer service life than traditional reinforced concrete structures.

3. The instrumentation phase of the project has been effectively accomplished. Currently, maturity studies are being conducted on the different concrete mixes employed in the bridge to compare the differences among the development of mechanical properties including: creep, shrinkage, thermal gradients, time dependent behavior and serviceability in the long-term.
4. A series of live load tests have been conducted to establish a benchmark that will be used to monitor any change in the structure's response and to help validate design assumptions.

6.4. OVERVIEW OF FINAL MODOT REPORT

In addition to the study reported herein, a final MoDOT report will include:

1. Instrumentation components including temperature, concrete strain, camber and deflection will be analyzed from the data acquired.
2. Prestress losses will be studied for both short term and long-term based on the concrete strain data included.
3. Data from the first series of live load tests will be included and bridge load distribution properties and overall behavior will be analyzed. The results will be compared with theoretical results based on a Finite Element Model (FEM) developed for the bridge.
4. Through field and lab tests and analysis, recommendation for MoDOT in NS-SCC, HS-SCC and HVFAC bridge design and construction will be provided.
5. The final MoDOT report is expected to be submitted to the Missouri Department of Transportation (MoDOT) in January 2016.

APPENDIX A.

DESIGN DRAWINGS

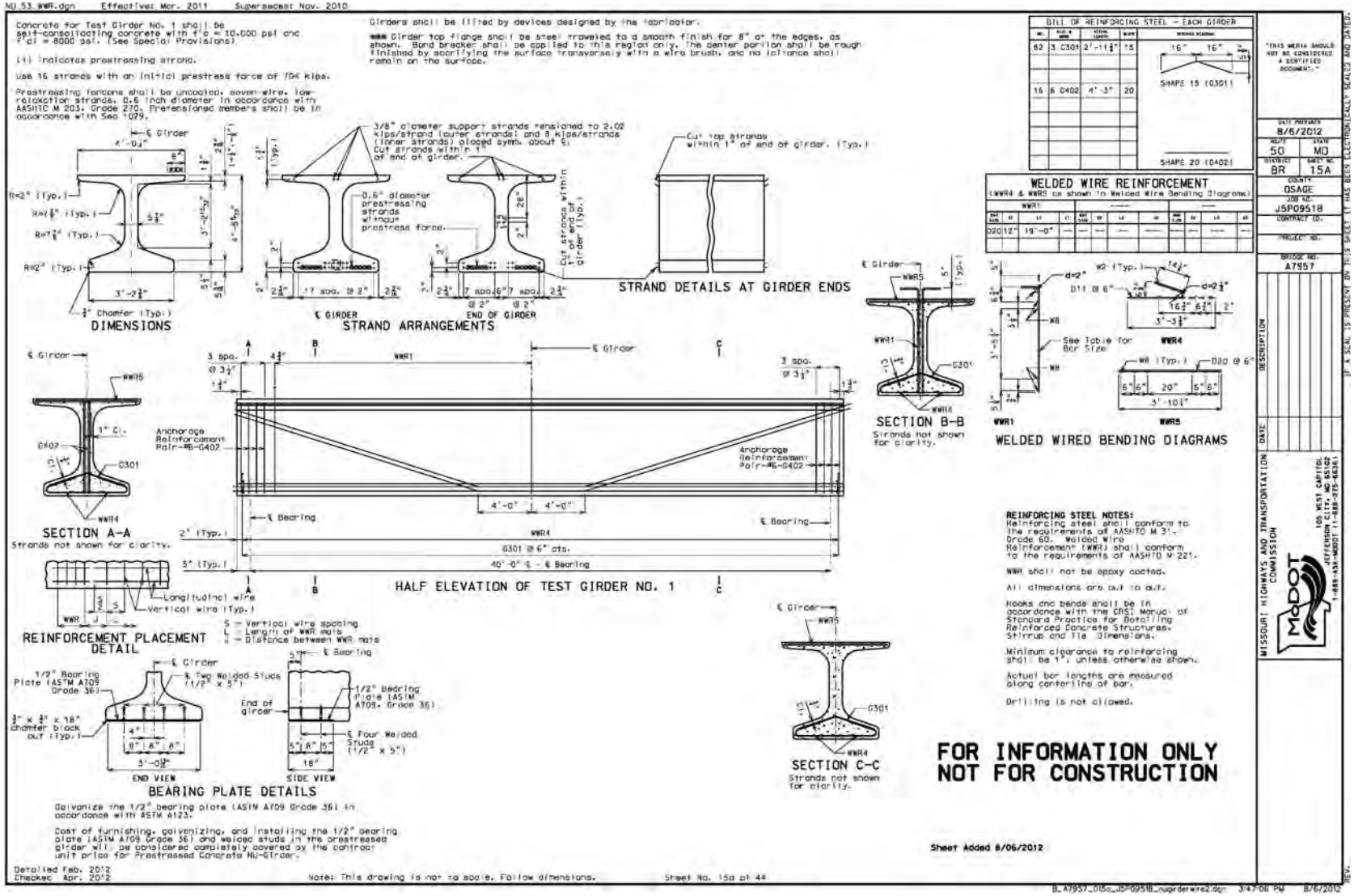
NU-53_WWR.dgn Effective: Mar. 2011 Superseded: Nov. 2010
Concrete for Test Girder No. 1 shall be self-consolidating concrete with f'ci = 10,000 psi and f'ci = 8000 psi. (See Special Provisions)
(+) Indicates prestressing strand.
Use 16 strands with an initial prestress force of 704 kips.
Prestressing tendons shall be uncoated, seven-wire, low-relaxation strands, 0.6 inch diameter in accordance with AASHTO M 203, Grade 270. Prestressed members shall be in accordance with Sec 1079.
Girders shall be lifted by devices designed by the fabricator.
Girder top flange shall be steel troweled to a smooth finish for 8" at the edges, as shown. Bond breaker shall be applied to this region only. The center portion shall be rough finished by scarifying the surface transversely with a wire brush, and no laitance shall remain on the surface.
BILL OF REINFORCING STEEL - EACH GIRDER
SHAPE 15 (G301)
SHAPE 20 (G402)
WELDED WIRE REINFORCEMENT
(WWR4 & WWR5 as shown in Welded Wire Bending Diagrams)
WWR1
DIMENSIONS
STRAND ARRANGEMENTS
STRAND DETAILS AT GIRDER ENDS
SECTION A-A
Strands not shown for clarity.
SECTION B-B
Strands not shown for clarity.
SECTION C-C
Strands not shown for clarity.
WELDED WIRED BENDING DIAGRAMS
HALF ELEVATION OF TEST GIRDER NO. 1
REINFORCING PLACEMENT DETAIL
BEARING PLATE DETAILS
END VIEW
SIDE VIEW
REINFORCING STEEL NOTES:
Reinforcing steel shall conform to the requirements of AASHTO M 31, Grade 60. Welded Wire Reinforcement (WWR) shall conform to the requirements of AASHTO M 221.
WWR shall not be epoxy coated.
All dimensions are out to out.
Hooks and bends shall be in accordance with the CRSI Manual of Standard Practice for Detailing Reinforced Concrete Structures. Stirrup and Tie Dimensions.
Minimum clearance to reinforcing shall be 1", unless otherwise shown.
Actual bar lengths are measured along centerline of bar.
Drilling is not allowed.
FOR INFORMATION ONLY
NOT FOR CONSTRUCTION
Galvanize the 1/2" bearing plate (AASTM A709 Grade 36) in accordance with ASTM A123.
Cost of furnishing, galvanizing, and installing the 1/2" bearing plate (AASTM A709 Grade 36) and welded studs in the prestressed girder will be considered completely covered by the contract unit price for Prestressed Concrete NU-Girder.
Sheet Added 8/06/2012
Detailed Feb. 2012
Checked Apr. 2012
Note: This drawing is not to scale. Follow dimensions.
Sheet No. 15a of 44
B_A7957_015a_J5P0951B_nugirderwire2.dgn 3:47:08 PM 8/6/2012
"THIS MEDIA SHOULD NOT BE CONSIDERED A CERTIFIED DOCUMENT."
DATE PREPARED 8/6/2012
ROUTE 50 STATE MO
DISTRICT 8R SHEET NO. 15A
COUNTY OSAGE
JOB NO. J5P0951B
CONTRACT ID.
PROJECT NO.
BRIDGE NO. A7957
DESCRIPTION
DATE
MISSOURI HIGHWAYS AND TRANSPORTATION COMMISSION
105 WEST CAPITOL JEFFERSON CITY, MO 65102 1-888-ASK-MODOT (1-888-275-6636)
MoDOT
IF A SEAL IS PRESENT ON THIS SHEET IT HAS BEEN ELECTRONICALLY SEALED AND DATED.
REV.

NU-53_Bent_Bars.dgn Effective: Mar. 2011 Supercedes: Nov. 2010

Concrete for Test Girder No. 2 shall be self consolidated with f'_c = 10,000 psi and f'_{ci} = 8000 psi. (See Special Provisions)

(*) Indicates prestressing strand.

Use 16 strands with an initial prestress force of 704 kips.

Prestressing tendons shall be uncoated, seven-wire, low-relaxation strands, 0.6 inch diameter in accordance with AASHTO M 203, Grade 270. Pretensioned members shall be in accordance with Sec 1029.

Girders shall be lifted by devices designed by the fabricator.

Girder top flange shall be steel troweled to a smooth finish for 8" at the edges, as shown. Bond breaker shall be applied to this region only. The center portion shall be rough finished by scarifying the surface transversely with a wire brush, and no laitance shall remain on the surface.

DIMENSIONS

STRAND ARRANGEMENTS

STRAND DETAILS AT GIRDER ENDS

SECTION A-A
Strands not shown for clarity.

SECTION B-B
Strands not shown for clarity.

ELEVATION OF TEST GIRDER NO. 2

SECTION B-B
Strands not shown for clarity.

BEARING PLATE DETAILS

Galvanize the 1/2" bearing plate (ASTM A709 Grade 36) in accordance with ASTM A123.

Cost of furnishing, galvanizing, and installing the 1/2" bearing plate (ASTM A709 Grade 36) and welded studs in the prestressed girder will be considered completely covered by the contract unit price for Prestressed Concrete NU-Girder.

Detailed Feb. 2012
Checked Apr. 2012

Note: This drawing is not to scale. Follow dimensions.

Sheet No. 17a of 44

BILL OF REINFORCING STEEL — EACH GIRDER

NO.	BAR MARK	TOTAL LENGTH	SHAPE
38	5 B1	5'-9"	19
16	6 B2	5'-2"	19
27	4 C1	3'-10"	20
54	4 D1	4'-2"	9

All dimensions are out to out.

Hooks and bends shall be in accordance with the CRSI Manual of Standard Practice for Detailing Reinforced Concrete Structures. Stirrup and tie dimensions.

Actual lengths are measured along centerline of bar to the nearest inch.

Minimum clearance to reinforcing shall be 1".

All reinforcement shall be Grade 60.

The two D1 bars may be furnished as one bar at the fabricator's option.

All B1 bars shall be epoxy coated.

At fabricator's option WWR5 bars may be used to replace C1 bars.

Drilling is not allowed.

"THIS MEDIA SHOULD NOT BE CONSIDERED A CERTIFIED DOCUMENT."

DATE PREPARED 8/6/2012
ROUTE 50 STATE MO
DISTRICT BR SHEET NO. 17A
COUNTY OSAGE
JOB NO. J5P0951B
CONTRACT ID.
PROJECT NO.
BRIDGE NO. A7957

DESCRIPTION | DATE

MISSOURI HIGHWAYS AND TRANSPORTATION COMMISSION
PO BOX 270
JEFFERSON CITY, MO 65102
1-888-ASK-MODOT (1-888-275-6636)

IF A SEAL IS PRESENT ON THIS SHEET IT HAS BEEN ELECTRONICALLY SEALED AND DATED.

FOR INFORMATION ONLY
NOT FOR CONSTRUCTION

Sheet Added 8/06/2012

REV.

B_A7957_017a_J5P0951B_nugirderbars2.dgn 3:47:11 PM 8/6/2012

APPENDIX B.

INSTRUMENTATION PLAN

Instrumentation Plan for BRIDGE A7957

Route 50

Osage County, Missouri

In Conjunction with

Research Investigation Number TRyy1236

Center for Infrastructure Engineering Studies
Department of Civil, Architectural and Environmental Engineering
Missouri University of Science and Technology
and
The Missouri Department of Transportation

Jan 25, 2013

Prepared by:

Dr. John J. Myers, P.E. (PI)
Dr. Jeffery S. Volz, P.E. (Co-PI)
Benjamin Gliha
Eli Hernandez

Department of Civil Engineering
1401 North Pine Street
325 Butler Carlton Hall
Missouri University of Science and Technology
Rolla, MO 65409-0710

Research Sponsored by:
The Missouri Department of Transportation and
The National University Transportation Center at
Missouri University of Science and Technology

Introduction:

For Bridge A7957 over the Maries River, Missouri University of Science and Technology (Missouri S&T), in conjunction with the Missouri Department of Transportation (MoDOT), will be performing research during the construction of the 3-span, NU-girder bridge. This research will include instrumentation during and after construction of the selected NU girders, Bent No. 3, Bent No. 4, and portion of the slab deck. This document outlines the instrumentation plan including locations and types of sensors as well as timing for the activities.

Goals:

The primary goals of the instrumentation plan are summarized as follows:

1. Monitor deflections from transfer through service life;
2. Compare predicted and measured deflections;
3. Monitor stresses along spans at cgs due to prestressing, applied loads, and thermal effects;
4. Develop stress blocks (strain blocks) along depth of members at support and midspan;
5. Monitor thermal gradients at similar cross-sections, for both interior and exterior spans;
6. Evaluate distribution of loading between adjacent interior and exterior sections of the same span through a live load test after construction has been completed;
7. Determine transfer length for 0.6-in diameter strands in the actual high-strength beams used in the structure;
8. Determine level of continuity (both M- and M+) provided at the intermediate bents.

Objectives:

The primary objectives of the instrumentation program are as follows:

1. Monitor components of the bridge superstructure during early-age and later-ages;
2. Identify trends in measured and observed behavior;
3. Examine applicability of current design procedures and assumptions for high performance concrete designs with 0.6-in. diameter prestressing strands. Provide recommendations for design of future Self Consolidating Concrete (SCC) and High Volume Fly Ash Concrete (HVFAC) bridges in Missouri with 0.6-in. diameter prestressing strands as warranted.

Instrumentation:

The type of sensors used in (and on) the girders and deck will include:

1. Vibrating wire strain gauges, VWSG (see Figure 1);
2. DEMEC points (see Figure 2);
3. Taut-wire deflection gauges (see Figure 3 and Figure 4);
4. Load Cell (see Figure 5);
5. Thermocouples

The research team will coordinate their activities with MoDOT engineers and MoDOT's Research Group, Construction and Materials and with personnel from the precast concrete plant and jobsite such that early-age monitoring of temperature and strain histories is possible for the girders and deck.

Three independent systems will be used to monitor concrete strains. Vibrating wire strain gauges (VWSG) will be embedded in the concrete for selected girders. To assure proper orientation after concrete placement and adequate protection during casting, the research team will attach the VWSG as illustrated in Figure 1.

Figure 1: Instrumented Vibrating Wire Strain Gauge (VWSG) on Prestressing Strand

DEMEC points will be located on the side of the girder by the research team according to the image in Figure 2.

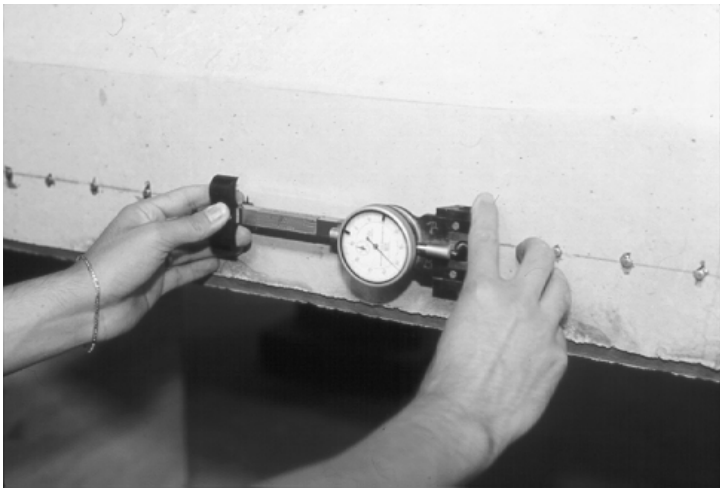

Figure 2: Illustration of DEMEC Points and DEMEC Gauge

Estimating and comparing experimental camber/deflections to measured values is often very critical for new materials particularly those where the modulus of elasticity may vary. In order to measure camber at release, a tension wire system may be used as illustrated in Figure 3 and Figure 4. This requires the use of a dead weight, piano wire, and two expansion anchors that are attached to the girder after the forms are removed, but prior to de-tensioning of the prestressing force. This will be undertaken on a representative HS-SCC girder.

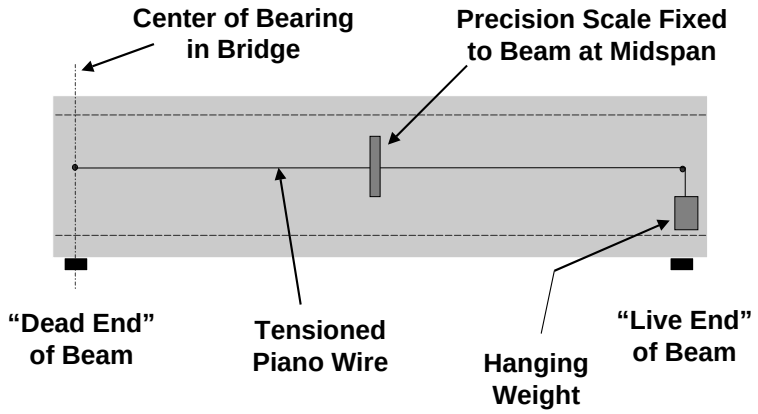

Figure 3: Schematic of Tensioned Wire System

Figure 4: Dead Weight for Tension-Wire System

In order to examine the associated prestress losses with the 0.6-in. diameter seven wire strands, a load cell and DAS will be required at the dead end of the member during fabrication. The set-up for this procedure is illustrated in Figure 5. A thermocouple will also be attached to the strand to monitor the temperature of the strand by the researchers.

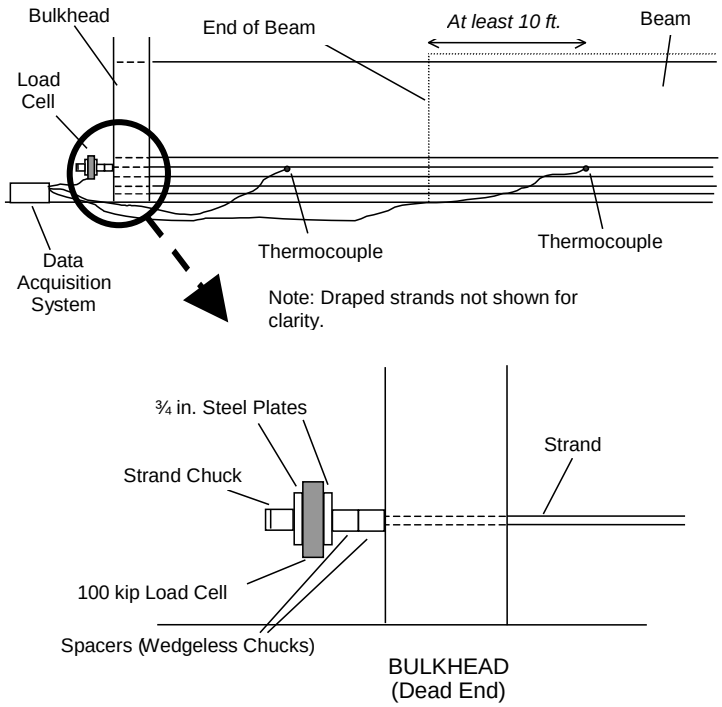

Figure 5: Set-Up for Measurement of Strand Stresses and Temperature Before Release

A single exit point for all of the instruments' cables (VWSG and thermocouples) will be provided so as to facilitate the use of a data acquisition system (DAS) which will record data from the various instruments (see their locations in Figure 6). The data will be acquired at regular intervals during the first few days after the casting. Thereafter, data will be acquired during placement of the girders and superstructure construction as described in subsequent sections of this instrumentation plan.

The cost of furnishing and placing the instrumentation systems in and on the girders and any other incidental work items shall be considered as completely covered in the research contract between Missouri S&T and MoDOT.

Location of Instrumentation:

The location of the instrumentation described above will consist of several "cluster" locations for Span (1-2), Span (2-3), and Span (3-4). These "cluster" locations occur in the prestressed / precast girders and cast-in-place deck directly above the girder instrumentation. Two data acquisition system boxes will be located and mounted along interior bents No. 2 and No. 3 as illustrated in Figure 6.

Girders:

The research team will instrument a maximum of six out of twelve girders prior to casting by the fabricator as illustrated in Figure 6. These will comprise one exterior and one interior girder for Span (1-2), Span (2-3), and Span (3-4). Within each girder of Span (1-2) and Span (3-4), the instrumentation "clusters" will be located at two cross-sections, one at midspan and one in a close proximity to the support at Bent 2

and Bent 3 respectively. For the girders of Span (2-3), the instrumentation "clusters" will be located at three cross-sections, one at midspan and one in a close proximity to each of the supports (Bents 2 and 3). Figure 7 and Figure 8 illustrate the instrumentation required at the girder cluster locations. In addition to the cluster locations described herein, a VWSG (and thermocouple) will be located at the quarter point (within the member) along the centroid of the prestressing strands for the instrumented girders on beam lines 3 and 4.

Cast-In-Place Deck*:*

The research team will instrument Span (2-3) at the same "cluster" location described for the girders at midspan in Figure 6, but within the depth of the deck above the girders and along the transverse direction (see Figure 7). There will be a total of four VWSG (two at each location according to the detail in Figure 7).

NU Girder Instrumentation for Destructive Testing:

The research team will instrument two lab test girders with strain gauges prior to casting by the fabricator. The strain gauges will be installed at midspan according to the instrument configuration shown in Figure 9.

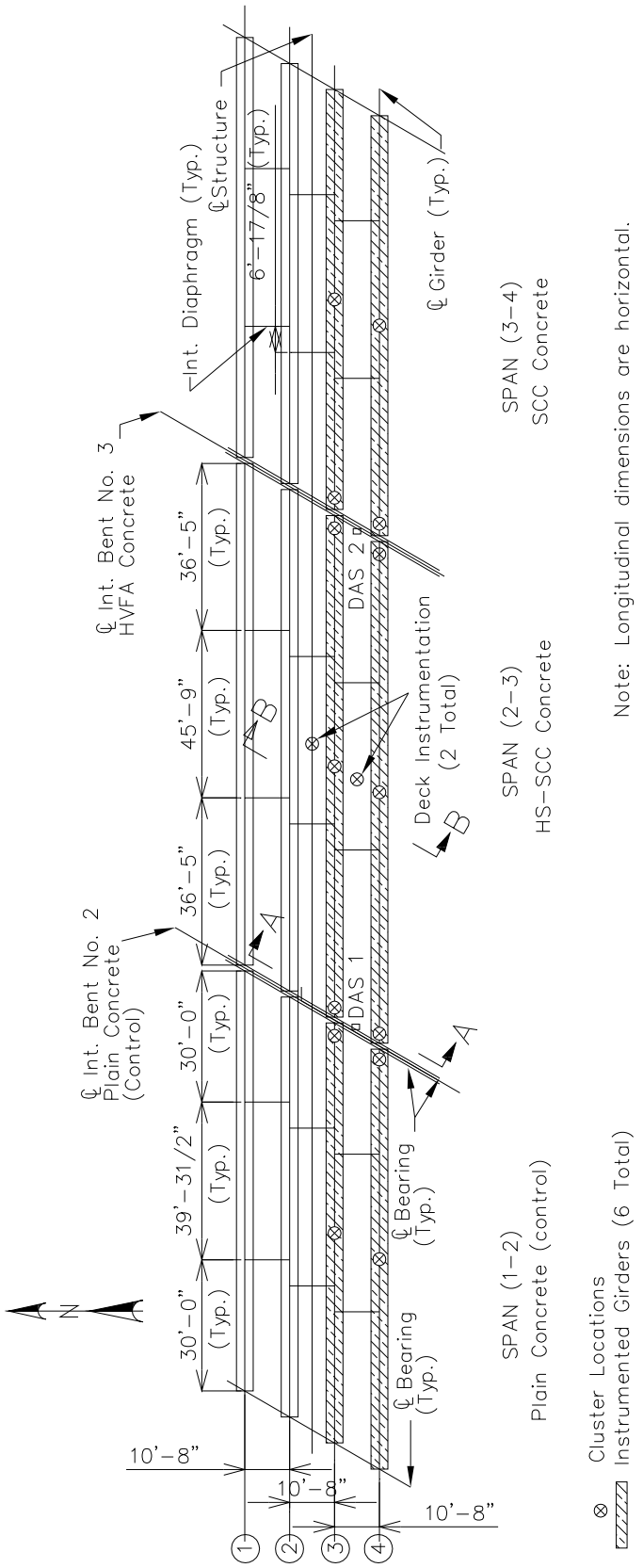

Figure 6: Plan Illustrating Girders to be Instrumented and "Cluster" Locations

Location of VWSG at Girder Line 3 and 4 "Cluster" Locations (Midspan)

***TD*:** Top Deck (2 in. Below Top Fiber of Deck)

***BD*:** Bottom Deck (2 in. Above Bottom Fiber of Deck)

***TF*:** Top Flange (2 in. Below Top Fiber)

CGC: Center of Gravity of Composite Beam Section (Midspan Only)

CGU/CGI: Center of Gravity of Noncomposite Beam Section (Midspan Only)

CGS: Center of Gravity of Pretensioned Strands

BF: Bottom Flange (2 in. Above Bottom Fiber)

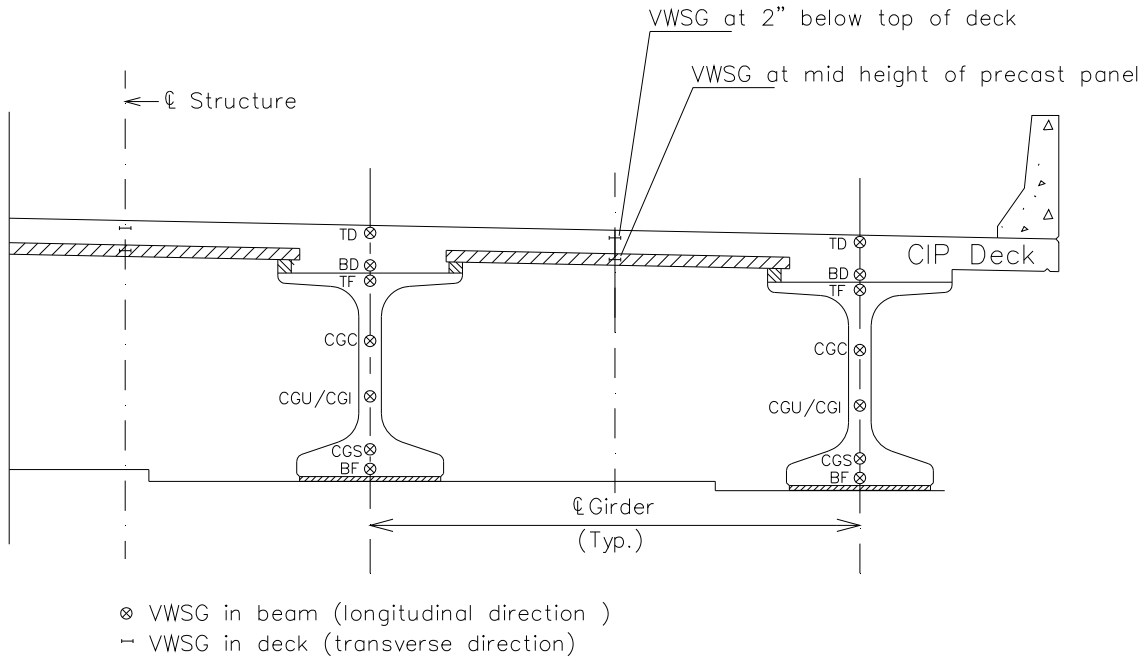

Figure 7: Cross-Section of NU Girders Illustrating Instrumentation at Midspan

Location of VWSG at Girder Line 3 and 4 "Cluster" Locations (Near Supports)

***TD*:** Top Deck (2 in. Below Top Fiber of Deck)

***TF*:** Top Flange (2 in. Below Top Fiber)

CGC: Center of Gravity of Composite Beam Section

CGS: Center of Gravity of Pretensioned Strands

BF: Bottom Flange (2 in. Above Bottom Fiber)

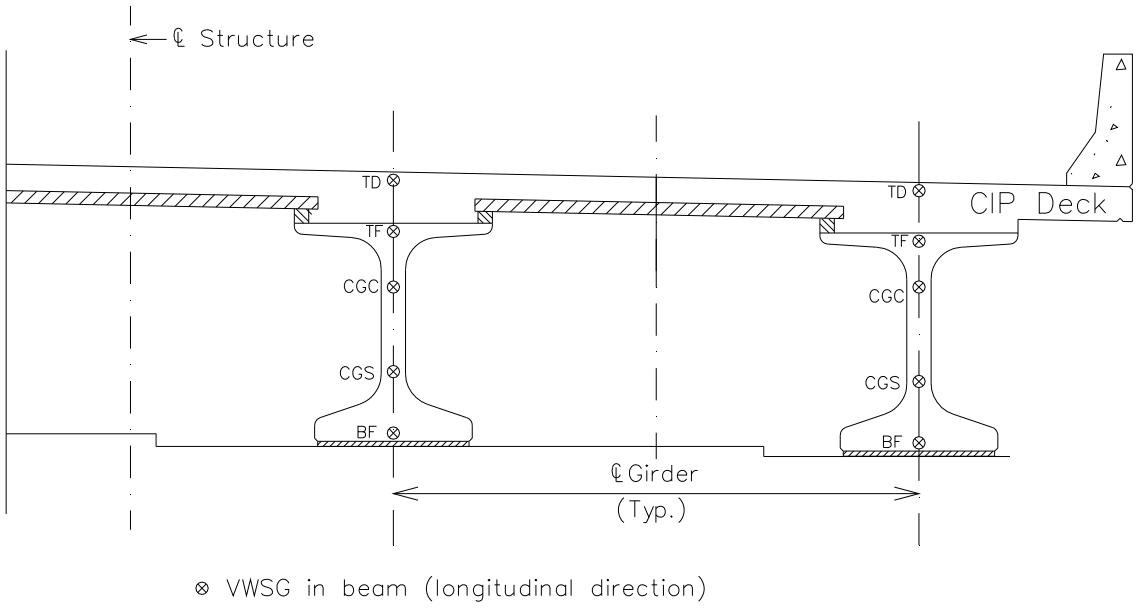

Figure 8: Cross-Section of NU Girders Illustrating Instrumentation Near Supports

Location of Gauges at NU Lab Test Girder (Midspan)

***TF*:** Top Flange (2 in. Below Top Fiber of Girder)

CGS: Center of Gravity of Pretensioned Strands

***BF*:** Bottom Flange (2 in. Above Bottom Fiber of Girder)

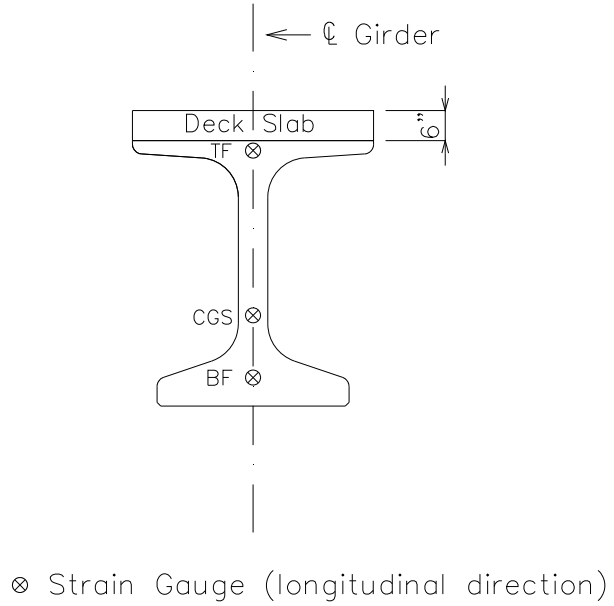

Figure 9: Cross-Section of NU Girders Illustrating Instrumentation at Midspan for Lab Destructive Testing

Bent Instrumentation:

The research team will instrument Bent Nos. 2 and 3 (see Figure 6) according to the thermocouple arrangement shown in Figure 10. For each bent, two thermocouples will be placed 3 ft from the top edge and at the center of the Web Wall (see Figure 10a, and Figure 10b). A second set of thermocouples will be installed on the bent columns, separated 3 ft. from the top of the pier (See Figure 10a, and Figure 10c). The beam cap will be instrumented with three interior thermocouples and one exterior thermocouple according to the detail shown in Figure 10d.

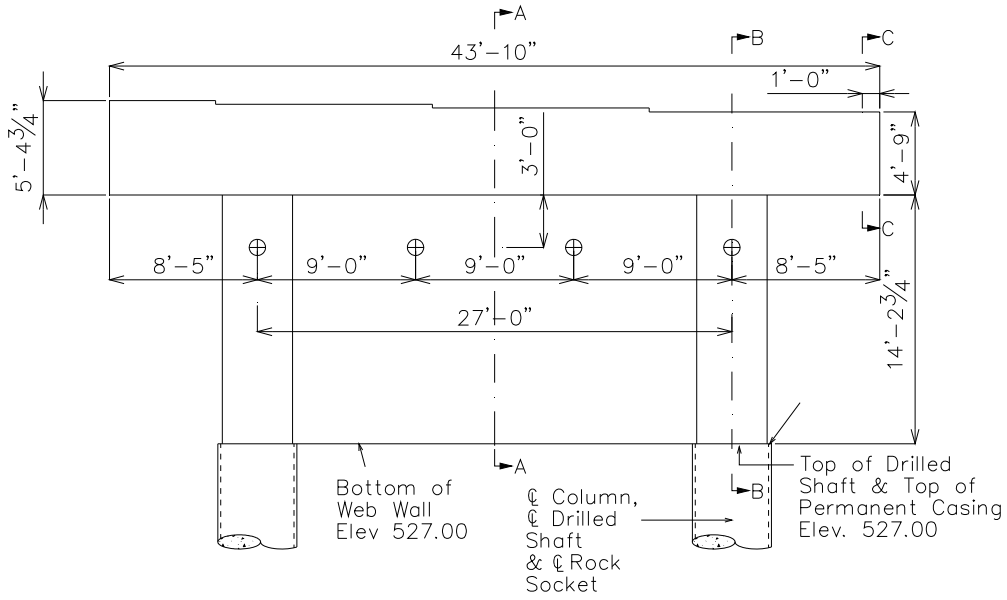

⊕ Thermocouple Location (TC)

(a) East Elevation

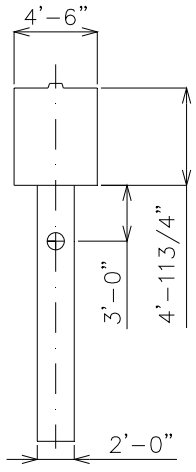

(b) Section A-A

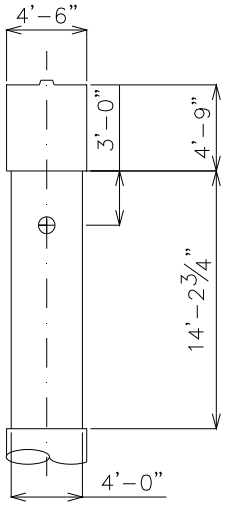

(c) Section B-B

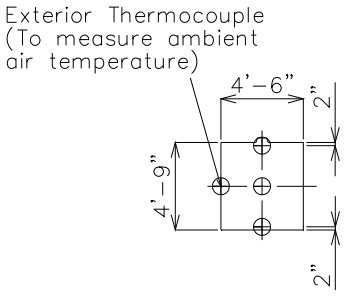

(d) Section C-C

Figure 10. Cross-Section of Bents Illustrating Thermocouple Locations

Additional Instrumentation:

A chloride detection sensor may be added to the instrumentation plan if available.

Staging of Instrumentation:

The anticipated staging of the instrumentation is as follows:

Plain Concrete / HVFA Bent – the instrumentation / research activity is in *italics*.

1. Operation – Bent forms are set by the contractor.
2. Operation – Reinforcement is placed by the contractor.
3. *The researchers will install thermocouple sensors in the locations shown in* Figure 10 *prior to casting of the web walls and columns of the bents. It is desirable that the sensors be placed as close to the casting of the web walls and columns as possible. This is to avoid potential damage to these sensors. The contractor shall allow time for this activity as part of the construction process.*
4. Operation – Concrete is placed by the fabricator.
5. *Test Specimens for the researchers are cast when the concrete is placed.*
6. Operation – Concrete attains required strength, the fabricator removes forms.
7. *The researchers will inspect the bents and record thermocouple readings before and after the forms are removed. The fabricator may note that the Data Acquisition System (DAS) will "scan" readings periodically after concrete is cast. A "cherry picker" or equivalent will be required by the researchers to acquire readings and/or data by the researchers. During construction, this access is to be provided by the contractor. After construction, MoDOT will assist with this activity.*

Prestressed / Precast Girders – the instrumentation / research activity is in *italics*.

8. Operation – Prestressing strands are stressed by the fabricator.
9. *A load cell will be installed at the dead end prior to prestressing of the tendons during the stressing operation to monitor prestress losses during stressing and release of the strands (see* Figure 5*). This load cell and DAS will be removed when the strands are released after the member has attained the required concrete release strength.*
10. *After the strands have been stressed, but before the forms have been set, the researchers will install the girder sensors in the cluster locations described herein. The fabricator shall allow time for this activity as part of the fabrication process.*
11. Operation – Precast Forms are set by the fabricator.
12. Operation – Concrete is placed by the fabricator.
13. *Test Specimens for the researchers are cast including match cured cylinders when the concrete is placed. The fabricator shall provide a covered area (preferably temperature controlled) for the*

casting and curing of match cured specimens by the researchers. The fabricator shall have a calibrated compression-testing machine on site capable of testing the concrete cylinders at release.

14. Operation – Concrete attains required release strength, the fabricator removes forms.
15. *DEMEC points are placed by the researchers near the ends of the members on each side of the lower flange with epoxy. After installation, the research team shall take baseline DEMEC readings. The fabricator shall allow time for this activity as part of the fabrication process.*
16. *Tension wire system installed by the researchers (see* Figure 3*). The fabricator shall allow time for this activity as part of the fabrication process.*
17. Operation – Pretensioning strands are released by the fabricator.
18. *The load cell is removed by the researchers in conjunction with release of the pretensioning strands.*
19. *The researchers will inspect the member, record DEMEC readings, and deflection readings (while the member is still on the bed). The fabricator may note that the Data Acquisition System (DAS) will "scan" readings periodically throughout the fabrication process.*
20. Operation – Place the member in storage at the precasting yard. (The support points for the members in storage should be similar to the final centerline of bearing after the member is erected.)
21. *Additional readings will be taken by the researchers periodically, but of note to the fabricator and contractor is that readings will be taken prior to shipment, at 28 days, at 56-days (optional to the researchers), after erection (before the formwork is set), after erection (before the slab is placed), after the slab is placed, during a live load test, and at later-ages (i.e. six months, 1 year, etc:).*

Cast-In-Place (CIP) Deck – the instrumentation / research activity is in *italics*.

1. Operation – Girders are erected and braced by the contractor.
2. Operation – CIP deck forms are set by the contractor.
3. Operation – Reinforcement is placed by the contractor.
4. *The researchers will install the CIP sensors in the cluster locations prior to casting that section of the deck. It is desirable that the sensors be placed as close to the casting of the deck as possible. This is to avoid potential damage to sensors. The contractor shall allow time for this activity as part of the construction process. In addition, the contractor may note that a "PVC" type or equivalent sleeve will be installed through the deck by the researchers near Bent No. 2. This will be of adequate size for the bundle of instrumentation wiring that will feed into the data acquisition system / data logging box. The researchers will coordinate the location of this sleeve with the contractor before the instrumentation is installed.*
5. Operation – Concrete is placed by the contractor.
6. *Test Specimens for the researchers are cast when the concrete is placed.*
7. *Additional readings will be taken by the researchers periodically, but of note to the contractor is that readings will be taken at the erection of the girders (before the deck is placed), after the slab is placed, during a live load test, and at later-ages (i.e. six months, 1 year, etc.). A "cherry picker" or equivalent*

will be required by the researchers to acquire readings and/or data by the researchers. During construction, this access is to be provided by the contractor. After construction, MoDOT will assist with this activity.

Damage to Instrumentation:

Many of the sensors that will be installed in the girders, bents, and CIP deck are sensitive to the construction process. Jobsite and plant workers must be aware of the location of the instrumentation to avoid damage. Equipment in particular that may cause damage to sensors or wiring includes hand held vibrators, foot traffic, and construction equipment. During any handling, transportation and erection of the prestressed girders, the contractor shall make provisions to prevent damage to the instrumentation installed during the fabrication of the prestressed / precast girders. The contractor shall also make provisions to prevent damage to the instrumentation placed in the bents and deck during fabrication / casting of the cast-in-place elements.

Any damage sustained to the instrumentation installed in or on the prestressed / precast girders, bents, or CIP deck as a result of the contractor's operations shall be the responsibility of the contractor. All costs of repair and/or replacement shall be as determined by the researchers.

Representative Test Specimens:

Additional specimens for the purpose of research testing will be collected by the researchers during fabrication of the prestressed girders, casting of the HVFAC web walls and bents, and casting of the deck. Fabrication of research specimens and the associated testing will require a maximum of 0.50 cubic yard of additional concrete to be provided per casting date where concrete is sampled. The researchers will be required to cast test specimens to monitor the mechanical and material performance of the in-place concrete. Figure 11 illustrates representative quality control test specimens that may be required by the researchers.

The contractor shall notify both the researchers [Dr. John Myers and Dr. Jeffery Volz] and the MoDOT Research Group, Construction and Materials, Division [Ms. Jennifer Harper and Mr. William Stone] with written notice four weeks prior to the commencement of fabrication of the prestressed girders, bents, and CIP deck. It is most desirable that the tentative fabrication / production schedule be sent to the researchers as soon as feasible since the preparation of instrumentation can be very time consuming. If possible, it is recommended that the instrumented beams be fabricated last to allow the greatest lead-time.

Figure 11: Representative QC/QA Test Specimens

During fabrication / casting of the girders, bents, and CIP deck, the contractor's fabricator and site crew shall be required to allow access to the work as required by the researchers. Specimen collection activities including use of equipment provided by research personnel will be accomplished with the minimum disturbance to the fabricator's and contractor's operations.

For any additional questions about this instrumentation plan, Dr. John Myers can be reached at (573) 341-6618 and Dr. Jeffery Volz can be reached at (573) 341-6280.

Dr. John J. Myers, P.E.
CIES / Department of Civil Engineering
1401 North Pine Street
325 Butler Carlton Hall
Missouri University of Science and Technology
Rolla, MO, 65409-0710
Phone: (573) 341-6618
Fax: (573) 341-4729
Email: jmyers@mst.edu

Dr. Jeffery S. Volz, P.E.
CIES / Department of Civil Engineering
1401 North Pine Street
331 Butler Carlton Hall
Missouri University of Science and Technology
Rolla, MO 65409-0710
Phone: (573) 341-6280
Fax: (573) 341-4729
Email: volzj@mst.edu

APPENDIX C

INSTRUMENTATION LABELING

Date: 7/29/2013
Span: 1-2
Member: Girder 4 (S1-G4)
Stage: **Fabrication**

Location	S/N	Begin #	End #	Chanel #	DAS	MODULE
S1-G4-M1	114013049	9244	9269	17	1	2
S1-G4-M2	114013040	9920	9945	18	1	2
S1-G4-M3	114013039	9893	9918	19	1	2
S1-G4-M4	114013034	10325	10351	20	1	2
S1-G4-M5	114013068	9784	9810	21	1	2
S1-G4-M6	114013033	10352	10377	N/A	N/A	N/A
S1-G4-M7	114013056	10109	10135	N/A	N/A	N/A
S1-G4-E1	114013080	7243	7251	23	1	2
S1-G4-E2	114013110	7595	7603	24	1	2
S1-G4-E3	114013111	7386	7394	25	1	2
S1-G4-E4	114013112	7585	7594	26	1	2
S1-G4-E5	114013114	7319	7327	N/A	N/A	N/A

Date: 8/1/2013
Span: 1-2
Member: Girder 3 (S1-G3)
Stage: **Fabrication**

Location	S/N	Begin #	End #	Chanel #	DAS	MODULE
S1-G3-M1	114013037	10244	10270	60	2	2
S1-G3-M2	114013036	10271	10297	61	2	2
S1-G3-M3	114013053	9162	9188	62	2	2
S1-G3-M4	114013055	9514	9540	63	2	2
S1-G3-M5	114013035	10298	10324	64	2	2
S1-G3-M6	114013067	9757	9783	N/A	N/A	N/A
S1-G3-M7	114013042	10190	10216	N/A	N/A	N/A
S1-G3-E1	114013116	7329	7337	70	2	2
S1-G3-E2	114013117	7348	7356	71	2	2
S1-G3-E3	114013118	7338	7346	72	2	2
S1-G3-E4	114013115	7405	7412	73	2	2
S1-G3-E5	114013081	7252	7260	N/A	N/A	N/A

Date: 8/3/2013
Span: 3-4
Member: Girder 4 (S3-G4)
Stage: **Fabrication**

Location	S/N	Begin #	End #	Chanel #	DAS	MODULE
S3-G4-W1	114013091	7452	7460	72	2	2
S3-G4-W2	114013092	7300	7308	73	2	2
S3-G4-W3	114013086	7290	7297	74	2	2
S3-G4-W4	114013093	7433	7441	75	2	2
S3-G4-W5	114013103	7548	7556	N/A	N/A	N/A
S3-G4-M1	114013050	7604	7630	60	2	2
S3-G4-M2	114013041	10217	10243	61	2	2
S3-G4-M3	114013065	9703	9729	62	2	2
S3-G4-M4	114013045	9270	9296	63	2	2
S3-G4-M5	114013062	9460	9485	64	2	2
S3-G4-M6	114013063	9487	9512	N/A	N/A	N/A
S3-G4-M7	114013061	9433	9458	N/A	N/A	N/A

Date: 8/5/2013
Span: 3-4
Member: Girder 3 (S3-G3)
Stage: **Fabrication**

Location	S/N	Begin #	End #	Chanel #	DAS	MODULE
S3-G3-W1	114013083	7262	7267	66	2	2
S3-G3-W2	114013098	7519	7527	67	2	2
S3-G3-W3	114013084	7271	7279	68	2	2
S3-G3-W4	114013085	7281	7289	69	2	2
S3-G3-W5	114013082	7415	7423	N/A	N/A	N/A
S3-G3-M1	114013078	9568	9593	60	2	2
S3-G3-M2	114013074	9838	9864	61	2	2
S3-G3-M3	114013059	10055	10081	62	2	2
S3-G3-M4	114013070	10020	10052	63	2	2
S3-G3-M5	114013058	9542	9567	64	2	2
S3-G3-M6	114013073	9947	9972	N/A	N/A	N/A
S3-G3-M7	114013060	9407	9431	N/A	N/A	N/A

Date: 8/8/2013
Span: 2-3
Member: Girder 4 (S2-G4)
Stage: **Fabrication**

Location	S/N	Begin #	End #	Chanel #	DAS	MODULE
S2-G4-W1	114013102	7557	7565	60	2	2
S2-G4-W2	114013094	7443	7450	61	2	2
S2-G4-W3	114013107	7576	7584	62	2	2
S2-G4-W4	114013105	7538	7545	63	2	2
S2-G4-W5	114013104	7367	7375	N/A	N/A	N/A
S2-G4-M1	114013077	9595	9621	1	1	1
S2-G4-M2	114013044	9297	9323	2	1	1
S2-G4-M3	114013066	9730	9755	3	1	1
S2-G4-M4	114013076	9622	9648	4	1	1
S2-G4-M5	114013075	9676	9702	5	1	1
S2-G4-M6	114013043	9352	9377	N/A	N/A	N/A
S2-G4-M7	114013047	10136	10162	N/A	N/A	N/A
S2-G4-E1	114013095	7424	7432	11	1	1
S2-G4-E2	1140130101	7500	7508	12	1	1
S2-G4-E3	114013100	7510	7518	13	1	1
S2-G4-E4	114013097	7529	7537	14	1	1
S2-G4-E5	114013099	7309	7317	N/A	N/A	N/A

Date: 8/13/2013
Span: 2-3
Member: Girder 3 (S2-G3)
Stage: **Fabrication**

Location	S/N	Begin #	End #	Chanel #	DAS	MODULE
S2-G3-W1	114013113	7395	7404	72	2	2
S2-G3-W2	114013088	7491	7499	73	2	2
S2-G3-W3	114013087	7481	7489	74	2	2
S2-G3-W4	114013079	7234	7242	75	2	2
S2-G3-W5	114013109	7376	7385	N/A	N/A	N/A
S2-G3-M1	114013057	10083	10108	60	2	2
S2-G3-M2	114013048	9326	9350	61	2	2
S2-G3-M3	114013052	9189	9215	62	2	2
S2-G3-M4	114013046	10163	10189	63	2	2
S2-G3-M5	114013054	9379	9404	64	2	2
S2-G3-M6	114013051	9217	9242	N/A	N/A	N/A
S2-G3-M7	114013069	9811	9837	N/A	N/A	N/A
S2-G3-E1	114013090	7462	7470	11	1	1
S2-G3-E2	114013106	7568	7573	12	1	1
S2-G3-E3	114013096	7357	7365	13	1	1
S2-G3-E4	114013108	9153	9161	14	1	1
S2-G3-E5	114013089	7471	7479	N/A	N/A	N/A

Date: 8/21/2013
Panels (Mid-span 2-3 between girders 2 and 3, Mid-span 2-3 between girders 3 and 4)
Stage: **Fabrication**

Location	S/N	Begin #	End #	Chanel #	DAS	MODULE
S2-D23-M1	114013064	9651	9675	10	1	1
S2-D23-M2	114013071	10001	10027	N/A	N/A	N/A
S2-D34-M1	114013072	9975	10200	50	2	1
S2-D34-M2	114013038	9865	9891	N/A	N/A	N/A

Date: 9/24/2013
Span: 2-3
Member: Girder 4 (S2-G4)
Stage: **Erection**

Location	S/N	Begin #	End #	Chanel #	DAS	MODULE
S2-G4-W1	114013102	7557	7565	N/A	N/A	N/A
S2-G4-W2	114013094	7443	7450	N/A	N/A	N/A
S2-G4-W3	114013107	7576	7584	N/A	N/A	N/A
S2-G4-W4	114013105	7538	7545	N/A	N/A	N/A
S2-G4-W5	114013104	7367	7375	N/A	N/A	N/A
S2-G4-M1	114013077	9595	9621	17	1	2
S2-G4-M2	114013044	9297	9323	18	1	2
S2-G4-M3	114013066	9730	9755	19	1	2
S2-G4-M4	114013076	9622	9648	20	1	2
S2-G4-M5	114013075	9676	9702	21	1	2
S2-G4-M6	114013043	9352	9377	N/A	N/A	N/A
S2-G4-M7	114013047	10136	10162	N/A	N/A	N/A
S2-G4-E1	114013095	7424	7432	33	1	3
S2-G4-E2	1140130101	7500	7508	34	1	3
S2-G4-E3	114013100	7510	7518	35	1	3
S2-G4-E4	114013097	7529	7537	36	1	3
S2-G4-E5	114013099	7309	7317	N/A	N/A	N/A

Date: 9/25/2013
Span: 3-4
Member: Girder 4 (S3-G4)
Stage: **Erection**

Location	S/N	Begin #	End #	Chanel #	DAS	MODULE
S3-G4-W1	114013091	7452	7460	33	1	3
S3-G4-W2	114013092	7300	7308	34	1	3
S3-G4-W3	114013086	7290	7297	35	1	3
S3-G4-W4	114013093	7433	7441	36	1	3
S3-G4-W5	114013103	7548	7556	N/A	N/A	N/A
S3-G4-M1	114013050	7604	7630	17	1	2
S3-G4-M2	114013041	10217	10243	18	1	2
S3-G4-M3	114013065	9703	9729	19	1	2
S3-G4-M4	114013045	9270	9296	20	1	2
S3-G4-M5	114013062	9460	9485	21	1	2
S3-G4-M6	114013063	9487	9512	N/A	N/A	N/A
S3-G4-M7	114013061	9433	9458	N/A	N/A	N/A

Date: 10/15/2013 (Connected to CR800 DAS)
Span: 1-2
Member: Girder 3 (S1-G3)
Stage: **Deck Placement**

Location	S/N	Begin #	End #	Chanel #	DAS	MODULE
S1-G3-M1	114013037	10244	10270	1	1	1
S1-G3-M2	114013036	10271	10297	2	1	1
S1-G3-M3	114013053	9162	9188	3	1	1
S1-G3-M4	114013055	9514	9540	4	1	1
S1-G3-M5	114013035	10298	10324	5	1	1
S1-G3-M6	114013067	9757	9783	6	1	1
S1-G3-M7	114013042	10190	10216	7	1	1
S1-G3-E1	114013116	7329	7337	8	1	1
S1-G3-E2	114013117	7348	7356	9	1	1
S1-G3-E3	114013118	7338	7346	10	1	1
S1-G3-E4	114013115	7405	7412	11	1	1
S1-G3-E5	114013081	7252	7260	12	1	1

Date: 10/15/2013 (Connected to CR800 DAS)
Span: 1-2
Member: Girder 4 (S1-G4)
Stage: **Deck Placement**

Location	S/N	Begin #	End #	Chanel #	DAS	MODULE
S1-G4-M1	114013049	9244	9269	13	1	1
S1-G4-M2	114013040	9920	9945	14	1	1
S1-G4-M3	114013039	9893	9918	15	1	1
S1-G4-M4*	114013034	10325	10351	16	1	1
S1-G4-M5	114013068	9784	9810	17	1	2
S1-G4-M6	114013033	10352	10377	18	1	2
S1-G4-M7	114013056	10109	10135	19	1	2
S1-G4-E1	114013080	7243	7251	20	1	2
S1-G4-E2	114013110	7595	7603	21	1	2
S1-G4-E3	114013111	7386	7394	22	1	2
S1-G4-E4	114013112	7585	7594	23	1	2
S1-G4-E5	114013114	7319	7327	24	1	2

*: VWSG did not work properly

Date: 10/15/2013 (Connected to CR800 DAS)
Span: 2-3
Member: Girder 3 (S2-G3)
Stage: **Deck Placement**

Location	S/N	Begin #	End #	Chanel #	DAS	MODULE
S2-G3-W1	114013113	7395	7404	25	1	2
S2-G3-W2	114013088	7491	7499	26	1	2
S2-G3-W3	114013087	7481	7489	27	1	2
S2-G3-W4	114013079	7234	7242	28	1	2
S2-G3-W5	114013109	7376	7385	29	1	2
S2-G3-M1	114013057	10083	10108	35	1	2
S2-G3-M2	114013048	9326	9350	36	1	3
S2-G3-M3	114013052	9189	9215	37	1	3
S2-G3-M4	114013046	10163	10189	38	1	3
S2-G3-M5*	114013054	9379	9404	39	1	3
S2-G3-M6	114013051	9217	9242	40	1	3
S2-G3-M7	114013069	9811	9837	41	1	3
S2-G3-E1	114013090	7462	7470	51	2	1
S2-G3-E2	114013106	7568	7573	52	2	1
S2-G3-E3	114013096	7357	7365	53	2	1
S2-G3-E4	114013108	9153	9161	54	2	1
S2-G3-E5	114013089	7471	7479	55	2	1

*: VWSG did not work properly

Date: 10/15/2013 (Connected to CR800 DAS)
Span: 2-3
Member: Girder 4 (S2-G4)
Stage: **Deck Placement**

Location	S/N	Begin #	End #	Chanel #	DAS	MODULE
S2-G4-W1	114013102	7557	7565	30	1	2
S2-G4-W2	114013094	7443	7450	31	1	2
S2-G4-W3	114013107	7576	7584	32	1	2
S2-G4-W4	114013105	7538	7545	33	1	3
S2-G4-W5	114013104	7367	7375	34	1	3
S2-G4-M1	114013077	9595	9621	44	2	1
S2-G4-M2	114013044	9297	9323	45	2	1
S2-G4-M3	114013066	9730	9755	46	2	1
S2-G4-M4	114013076	9622	9648	47	2	1
S2-G4-M5	114013075	9676	9702	48	2	1
S2-G4-M6	114013043	9352	9377	49	2	1
S2-G4-M7	114013047	10136	10162	50	2	1
S2-G4-E1	114013095	7424	7432	56	2	1
S2-G4-E2	1140130101	7500	7508	57	2	1
S2-G4-E3	114013100	7510	7518	58	2	1
S2-G4-E4	114013097	7529	7537	59	2	1
S2-G4-E5	114013099	7309	7317	60	2	2

Date: 10/15/2013 (Connected to CR800 DAS)
Span: 3-4
Member: Girder 3 (S3-G3)
Stage: **Deck Placement**

Location	S/N	Begin #	End #	Chanel #	DAS	MODULE
S3-G3-W1	114013083	7262	7267	61	2	2
S3-G3-W2	114013098	7519	7527	62	2	2
S3-G3-W3	114013084	7271	7279	63	2	2
S3-G3-W4	114013085	7281	7289	64	2	2
S3-G3-W5	114013082	7415	7423	65	2	2
S3-G3-M1	114013078	9568	9593	66	2	2
S3-G3-M2	114013074	9838	9864	67	2	2
S3-G3-M3	114013059	10055	10081	68	2	2
S3-G3-M4	114013070	10020	10052	69	2	2
S3-G3-M5	114013058	9542	9567	70	2	2
S3-G3-M6	114013073	9947	9972	71	2	2
S3-G3-M7	114013060	9407	9431	72	2	2

Date: 10/15/2013 (Connected to CR800 DAS)
Span: 3-4
Member: Girder 4 (S3-G4)
Stage: **Deck Placement**

Location	S/N	Begin #	End #	Chanel #	DAS	MODULE
S3-G4-W1	114013091	7452	7460	73	2	2
S3-G4-W2	114013092	7300	7308	74	2	2
S3-G4-W3	114013086	7290	7297	75	2	2
S3-G4-W4	114013093	7433	7441	76	2	3
S3-G4-W5	114013103	7548	7556	77	2	3
S3-G4-M1	114013050	7604	7630	78	2	3
S3-G4-M2	114013041	10217	10243	79	2	3
S3-G4-M3	114013065	9703	9729	80	2	3
S3-G4-M4	114013045	9270	9296	81	2	3
S3-G4-M5	114013062	9460	9485	82	2	3
S3-G4-M6	114013063	9487	9512	83	2	3
S3-G4-M7	114013061	9433	9458	84	2	3

APPENDIX D

LIVE LOAD TEST (LOAD STOPS)

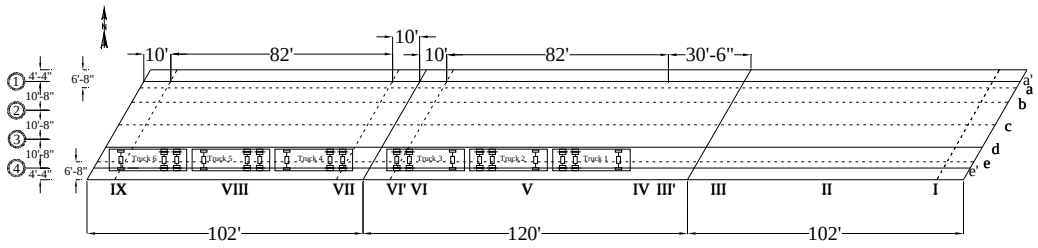

Stop 1

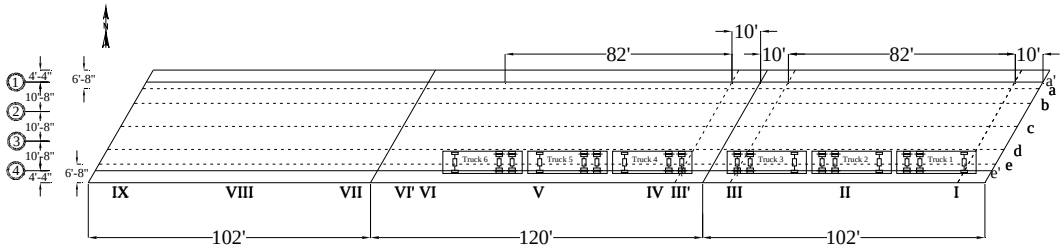

Stop 2

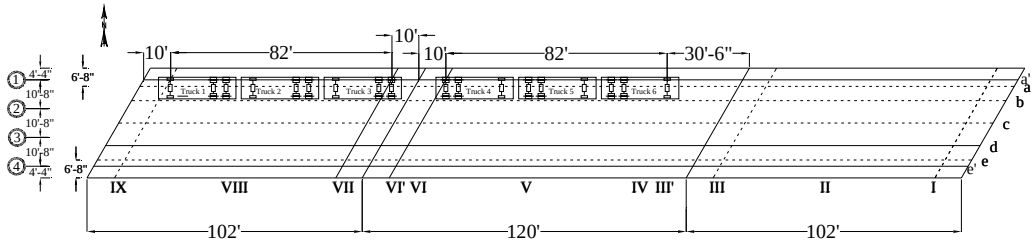

Stop 3

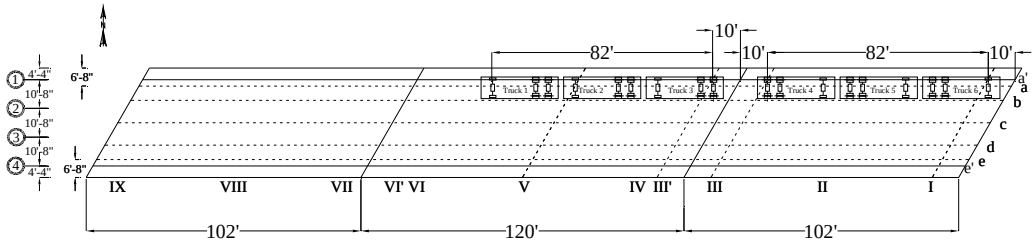

Stop 4

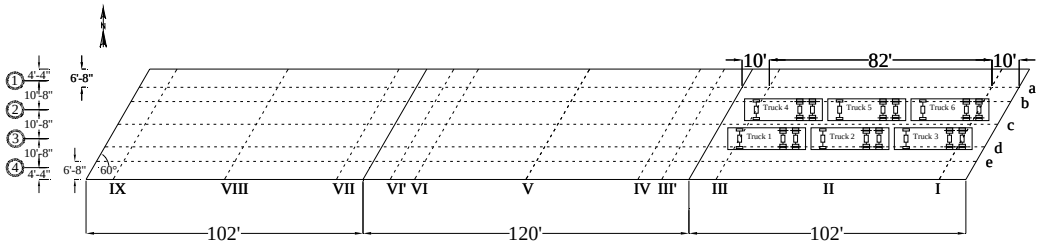

Stop 5

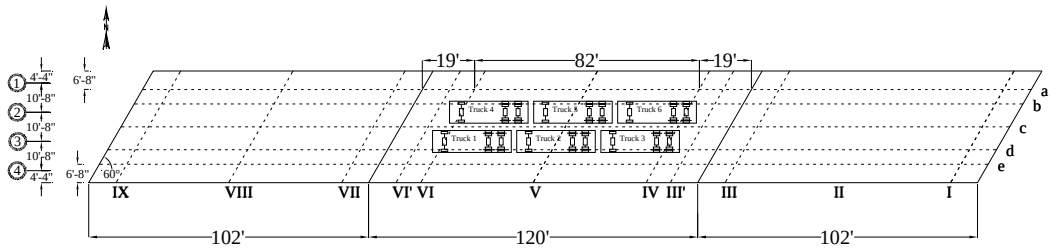

Stop 6

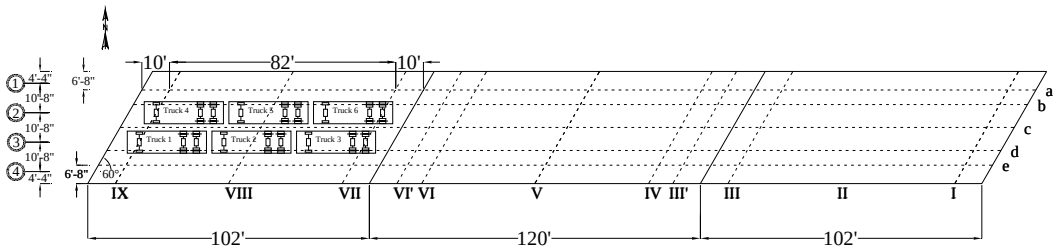

Stop 7

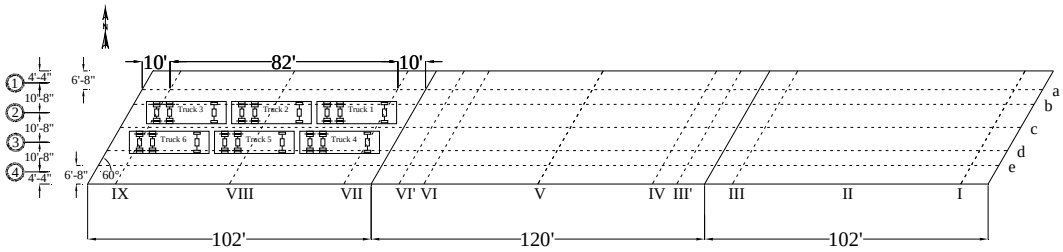

Stop 8

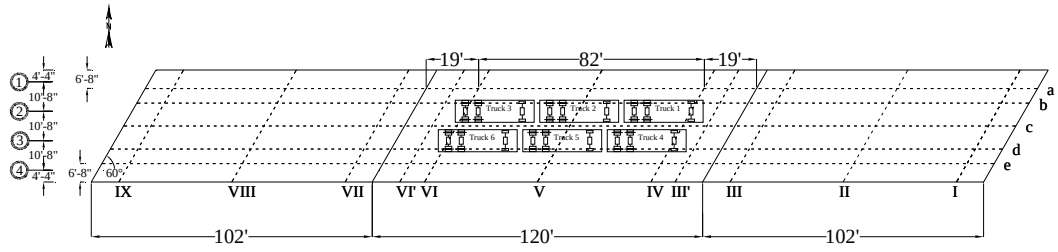

Stop 9

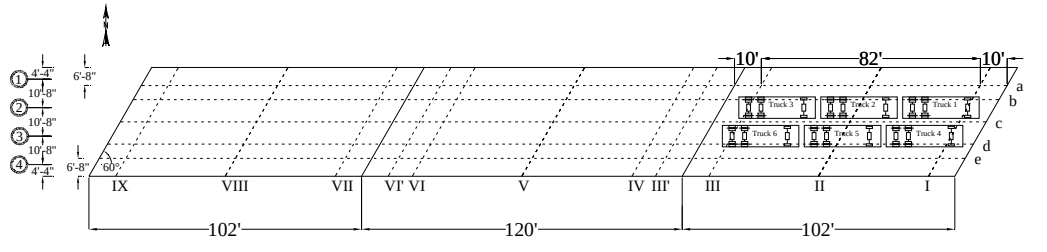

Stop 10

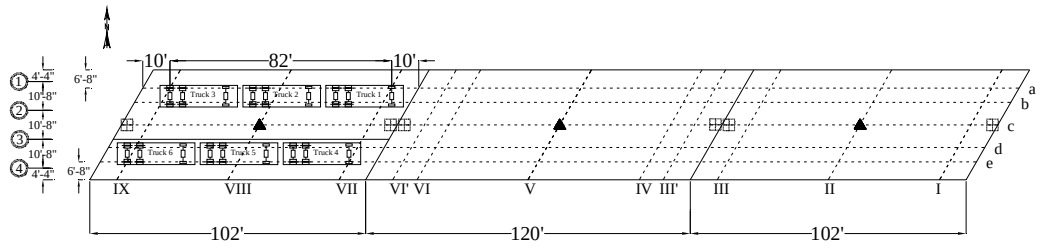

Stop 11

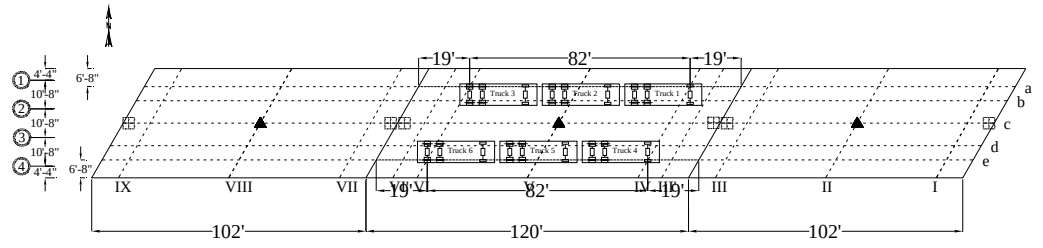

Stop 12

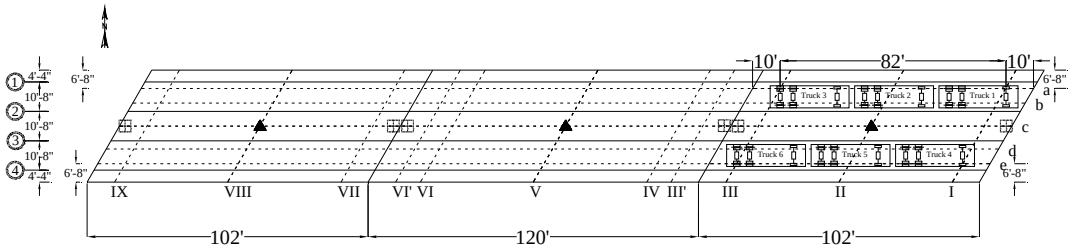

Stop 13

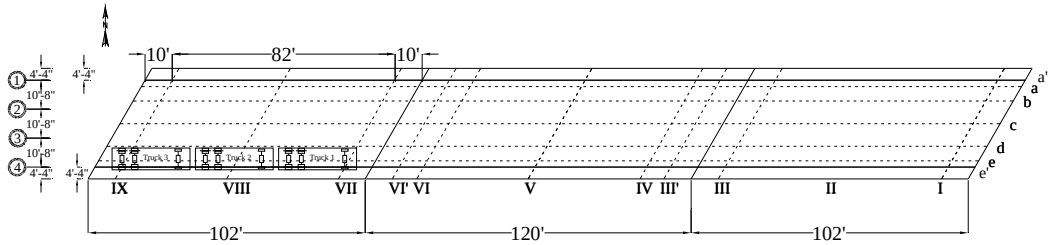

Stop 14

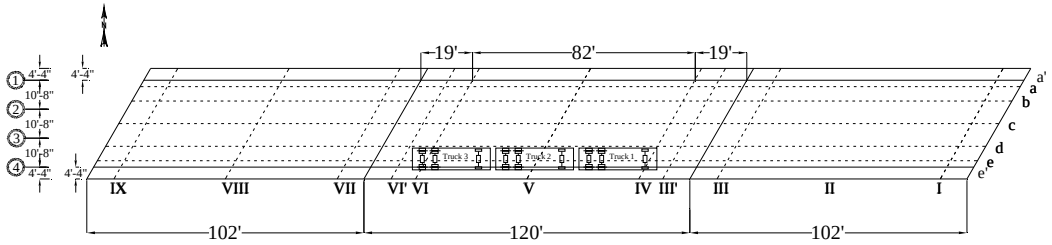

Stop 15

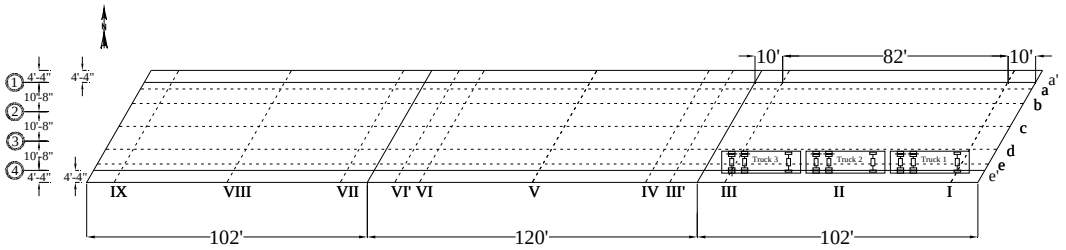

Stop 16

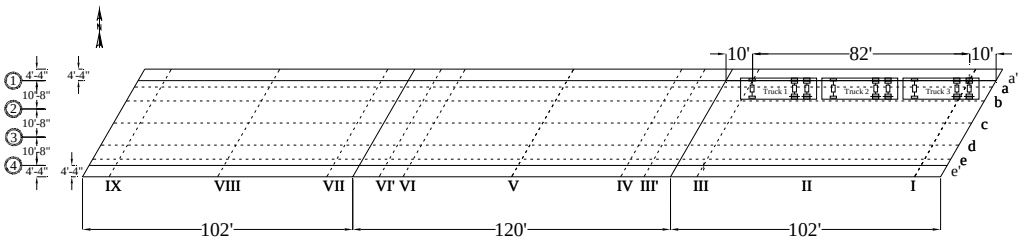

Stop 17

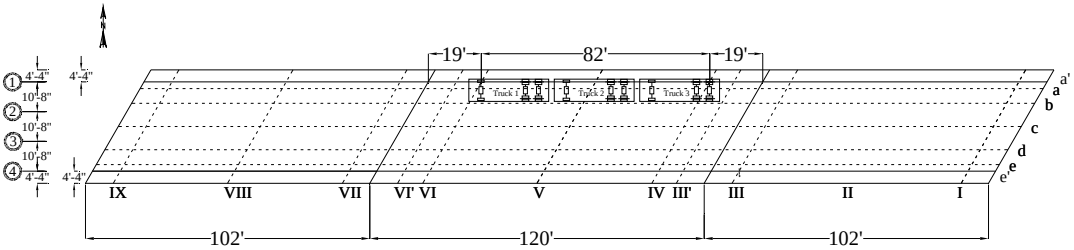

Stop 18

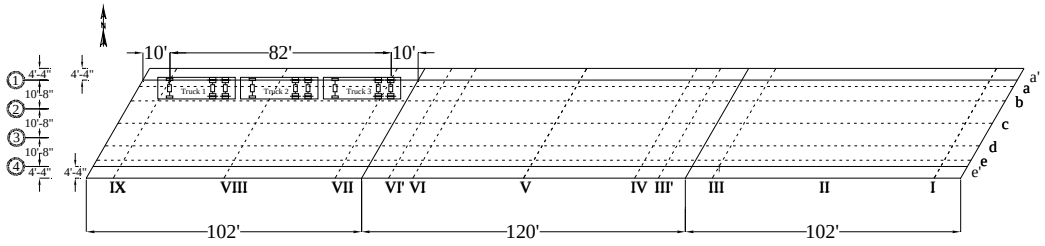

Stop 19

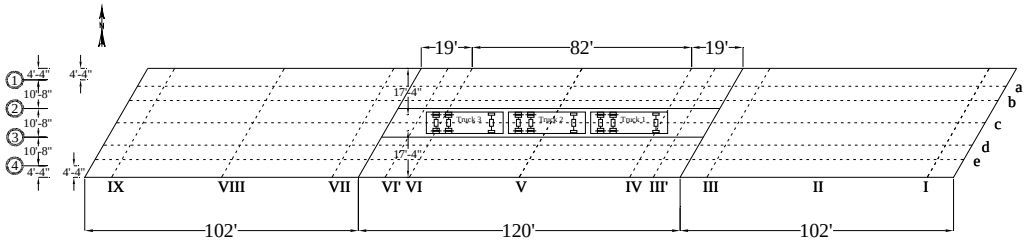

Stop 20

APPENDIX E

NU TEST GIRDER CRACK DOCUMENTATION

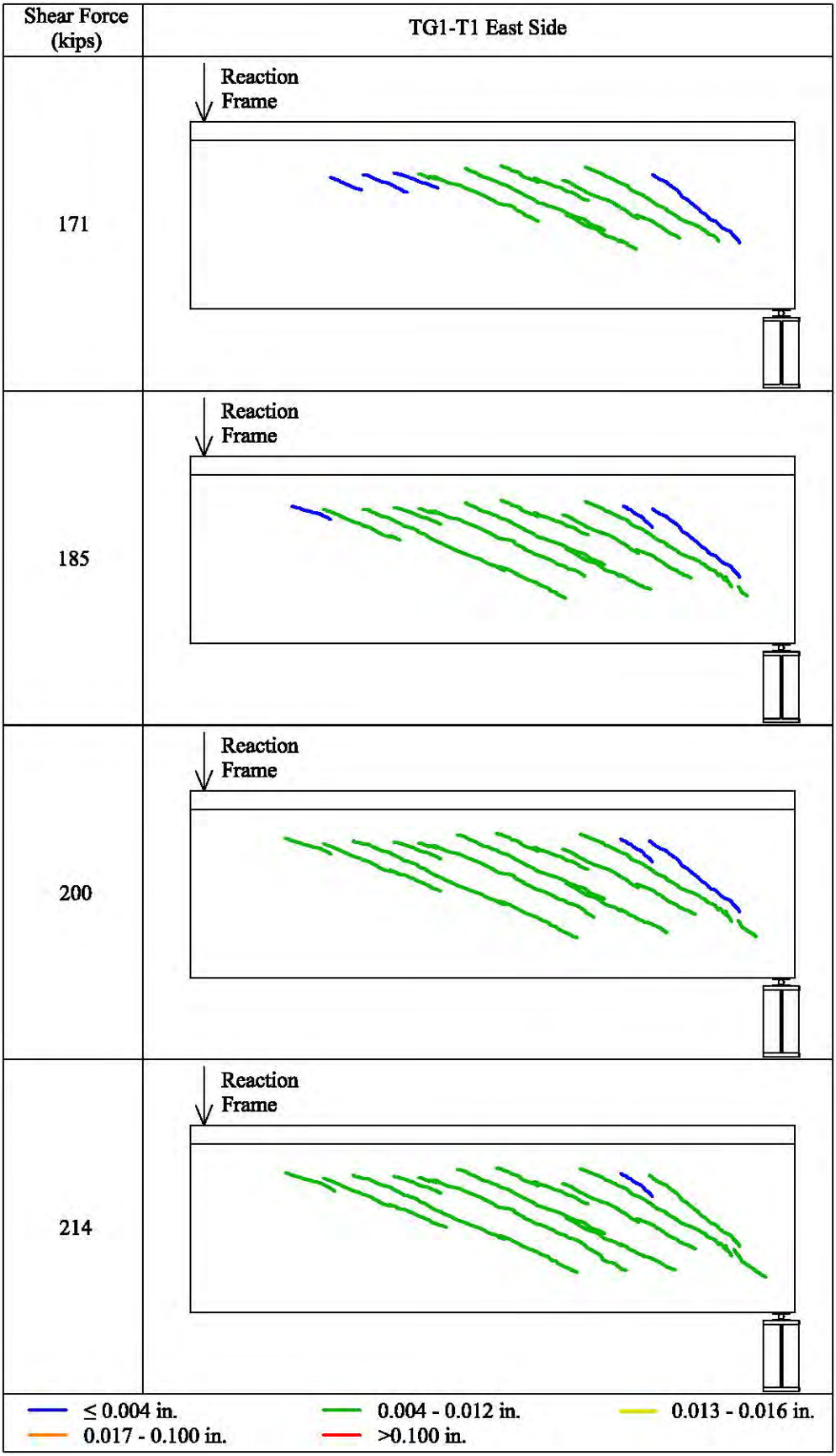
Shear Force (kips)
TG1-T1 East Side
171
185
200
214
Reaction Frame
≤ 0.004 in.
0.004 - 0.012 in.
0.013 - 0.016 in.
0.017 - 0.100 in.
>0.100 in.

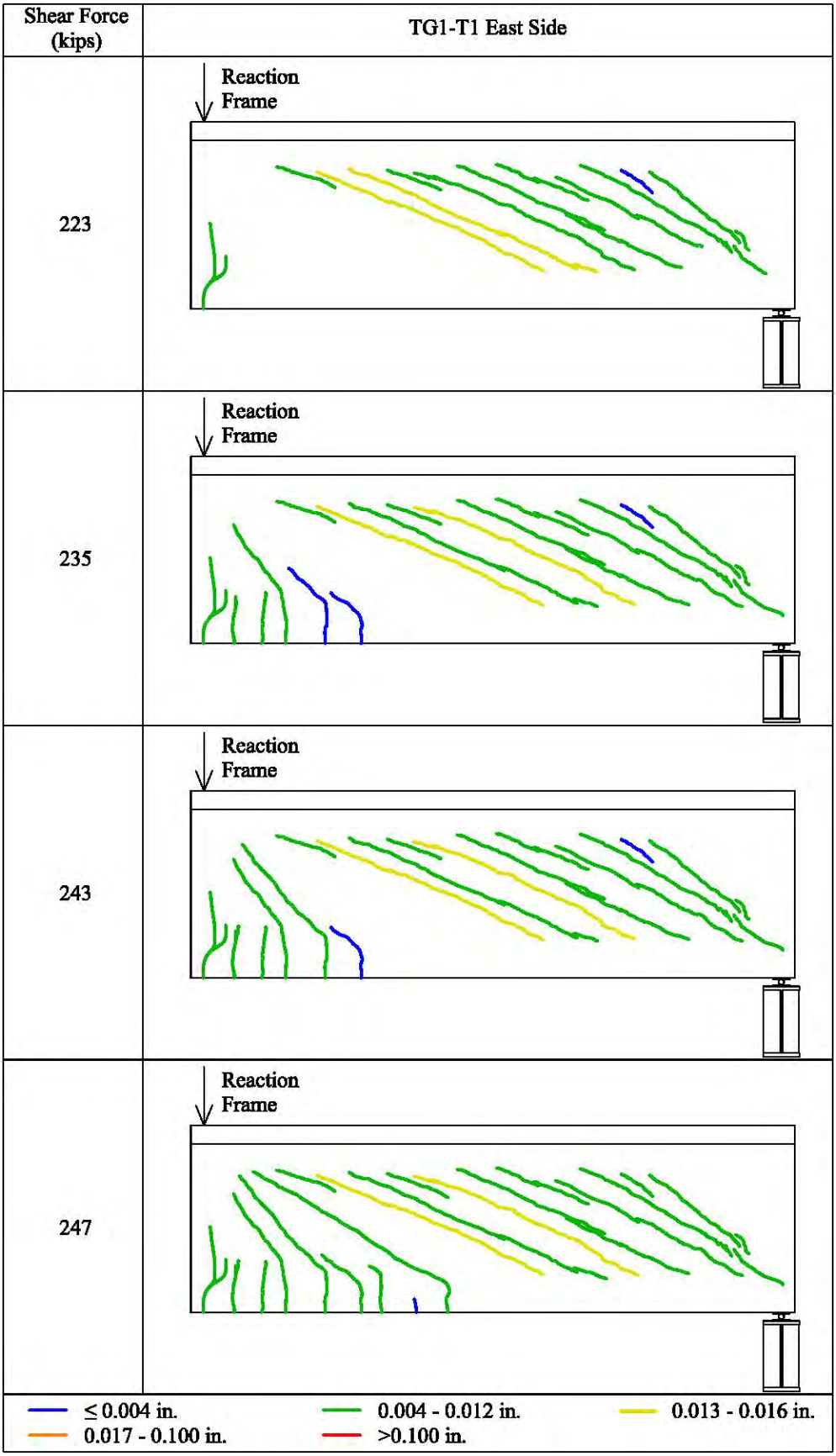
Shear Force (kips)
TG1-T1 East Side
223
235
243
247
Reaction Frame
≤ 0.004 in.
0.004 - 0.012 in.
0.013 - 0.016 in.
0.017 - 0.100 in.
>0.100 in.

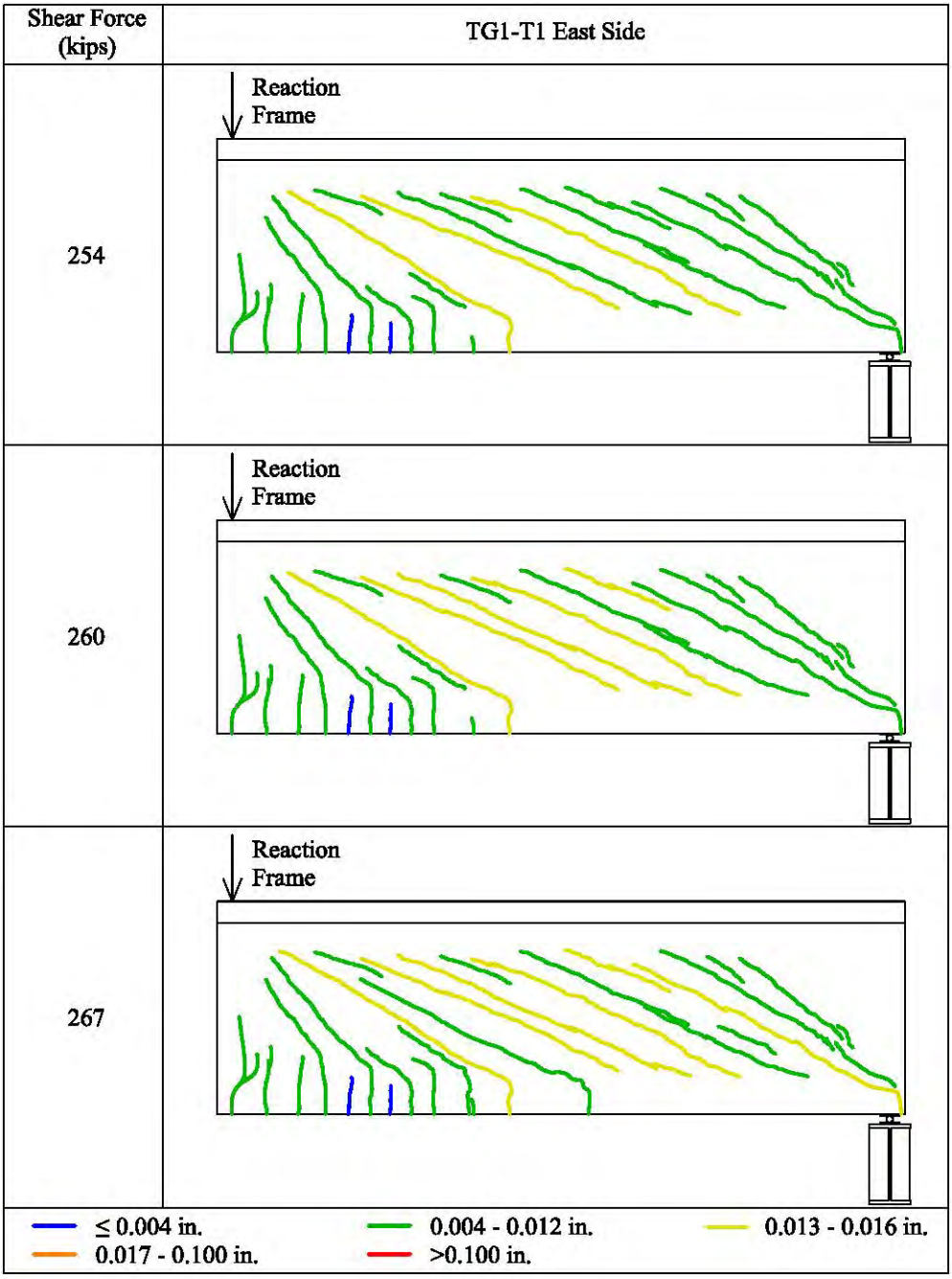
Shear Force (kips)
TG1-T1 East Side
254
260
267
Reaction Frame
Reaction Frame
Reaction Frame
≤ 0.004 in.
0.004 - 0.012 in.
0.013 - 0.016 in.
0.017 - 0.100 in.
>0.100 in.

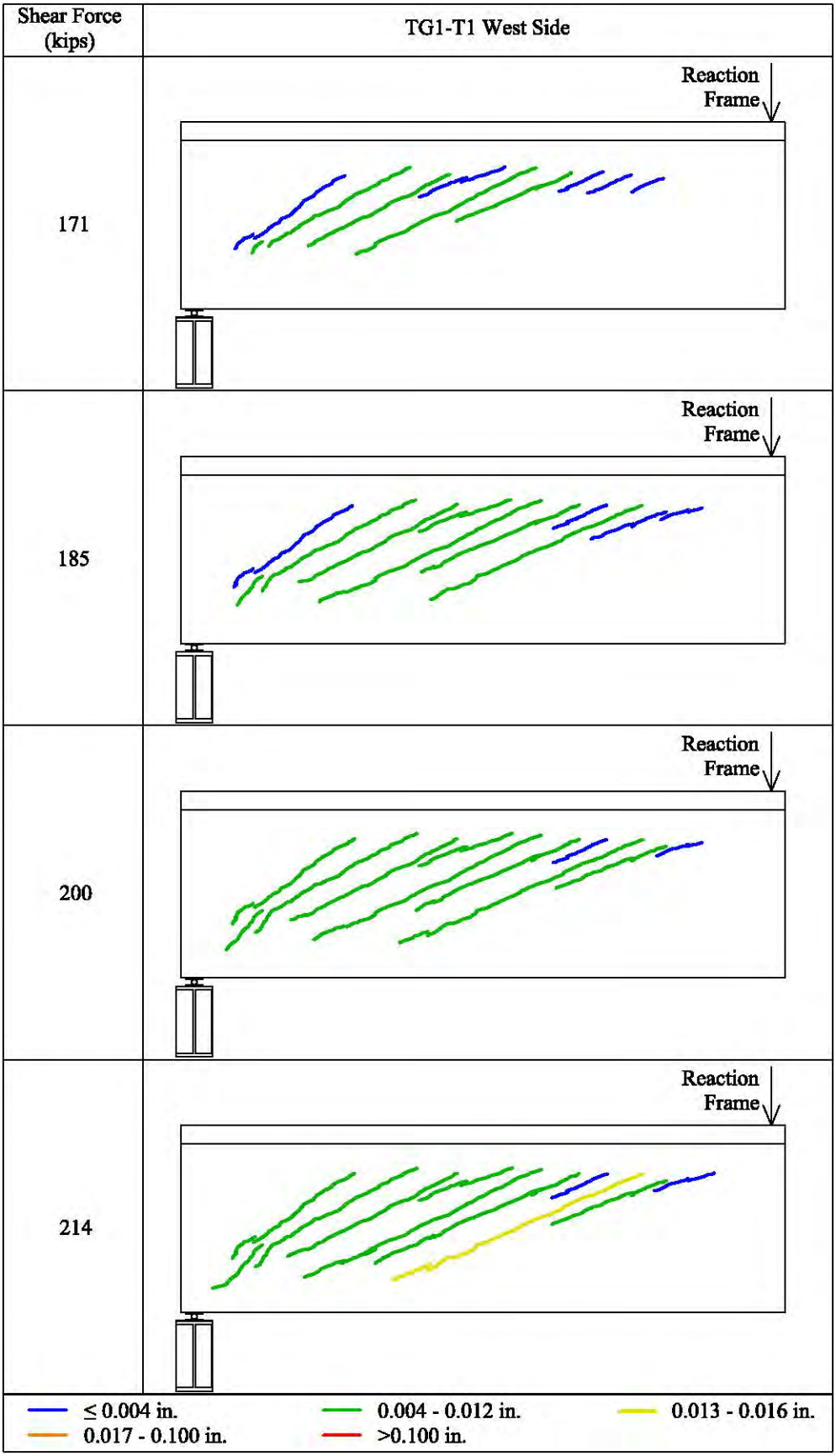
Shear Force (kips)
TG1-T1 West Side
171
185
200
214
Reaction Frame
≤ 0.004 in.
0.004 - 0.012 in.
0.013 - 0.016 in.
0.017 - 0.100 in.
>0.100 in.

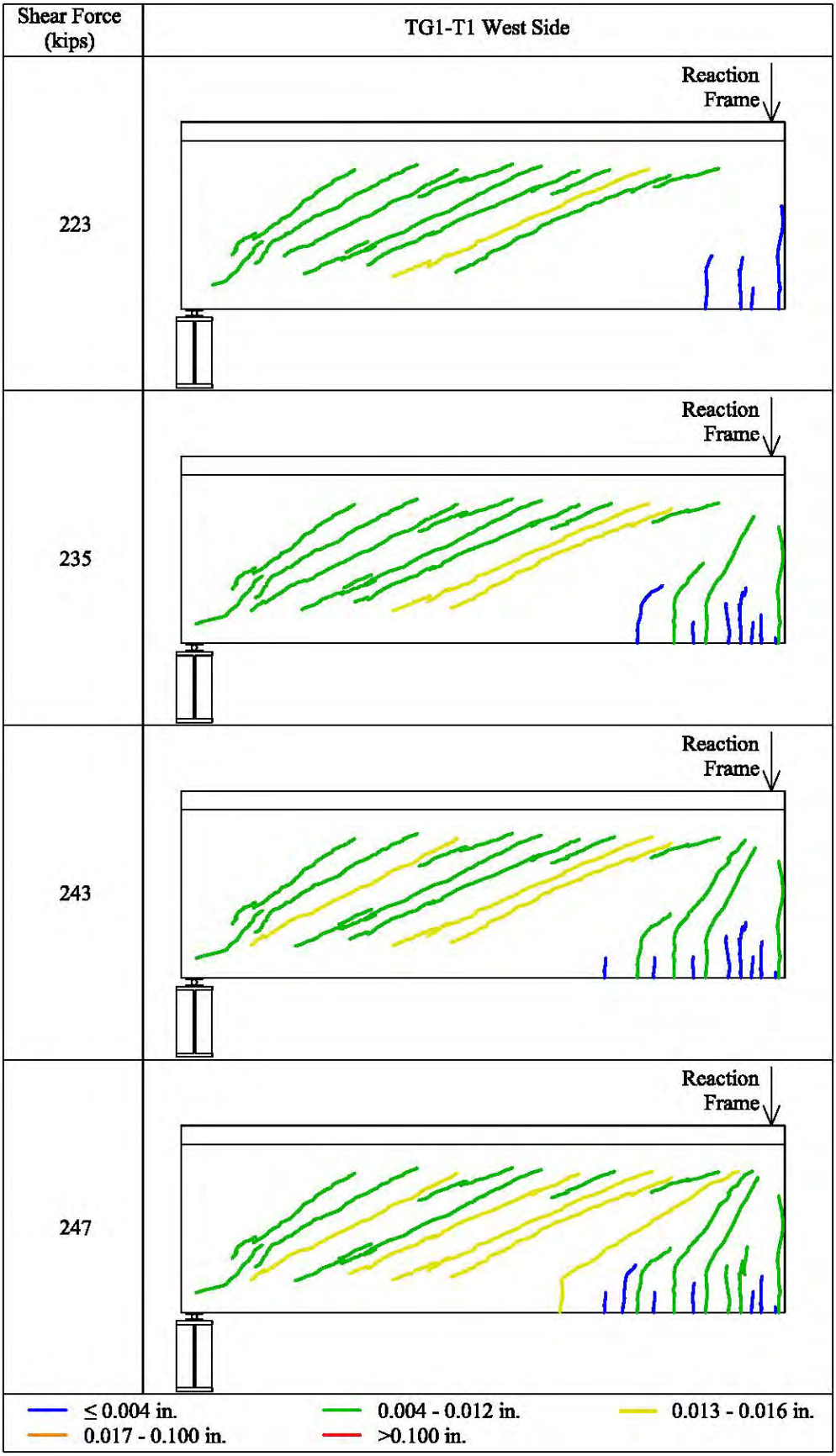
Shear Force (kips)
TG1-T1 West Side
223
235
243
247
Reaction Frame
≤ 0.004 in.
0.004 - 0.012 in.
0.013 - 0.016 in.
0.017 - 0.100 in.
>0.100 in.

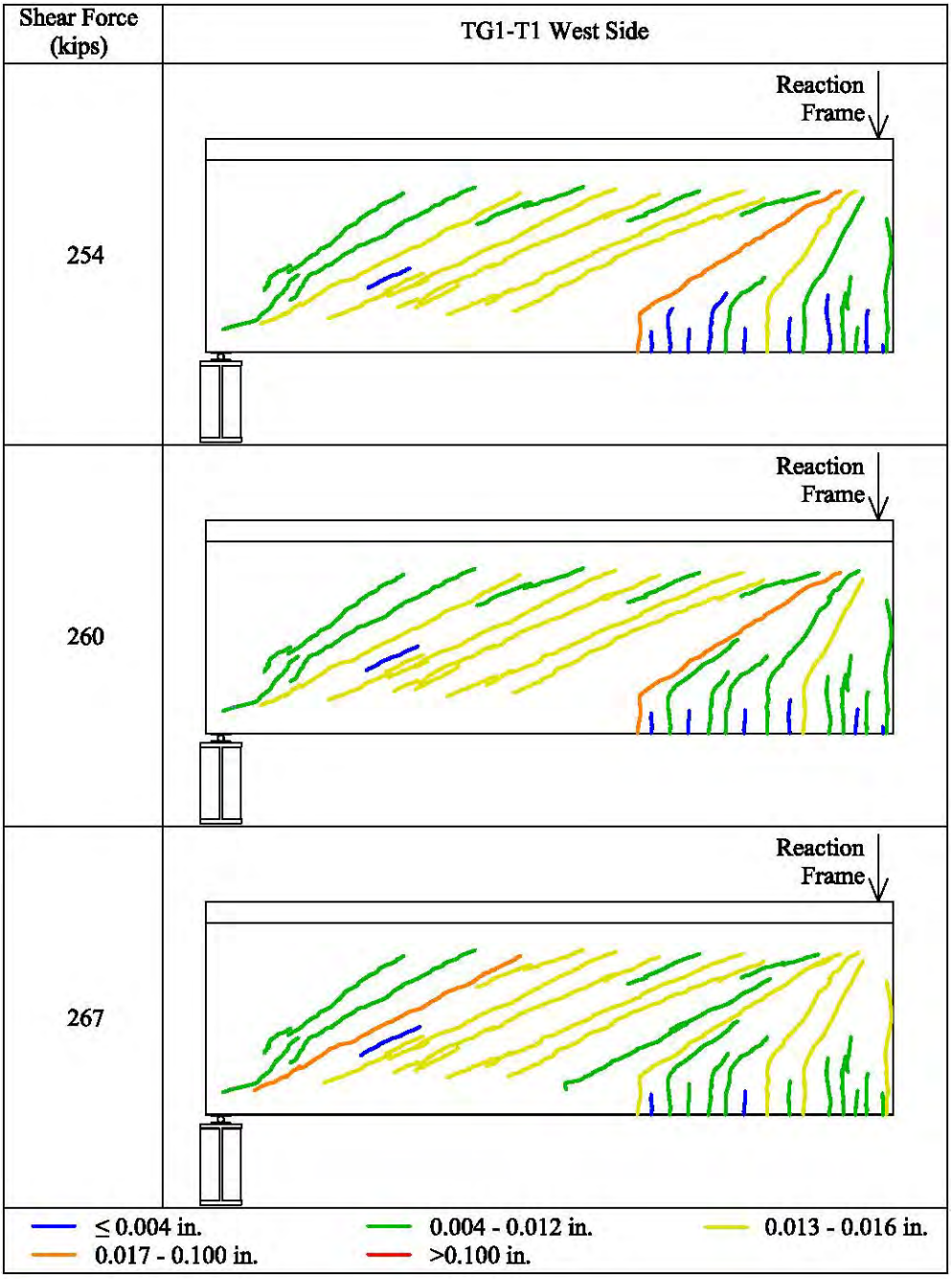
Shear Force (kips)
TG1-T1 West Side
254
260
267
Reaction Frame
Reaction Frame
Reaction Frame
≤ 0.004 in.
0.004 - 0.012 in.
0.013 - 0.016 in.
0.017 - 0.100 in.
>0.100 in.

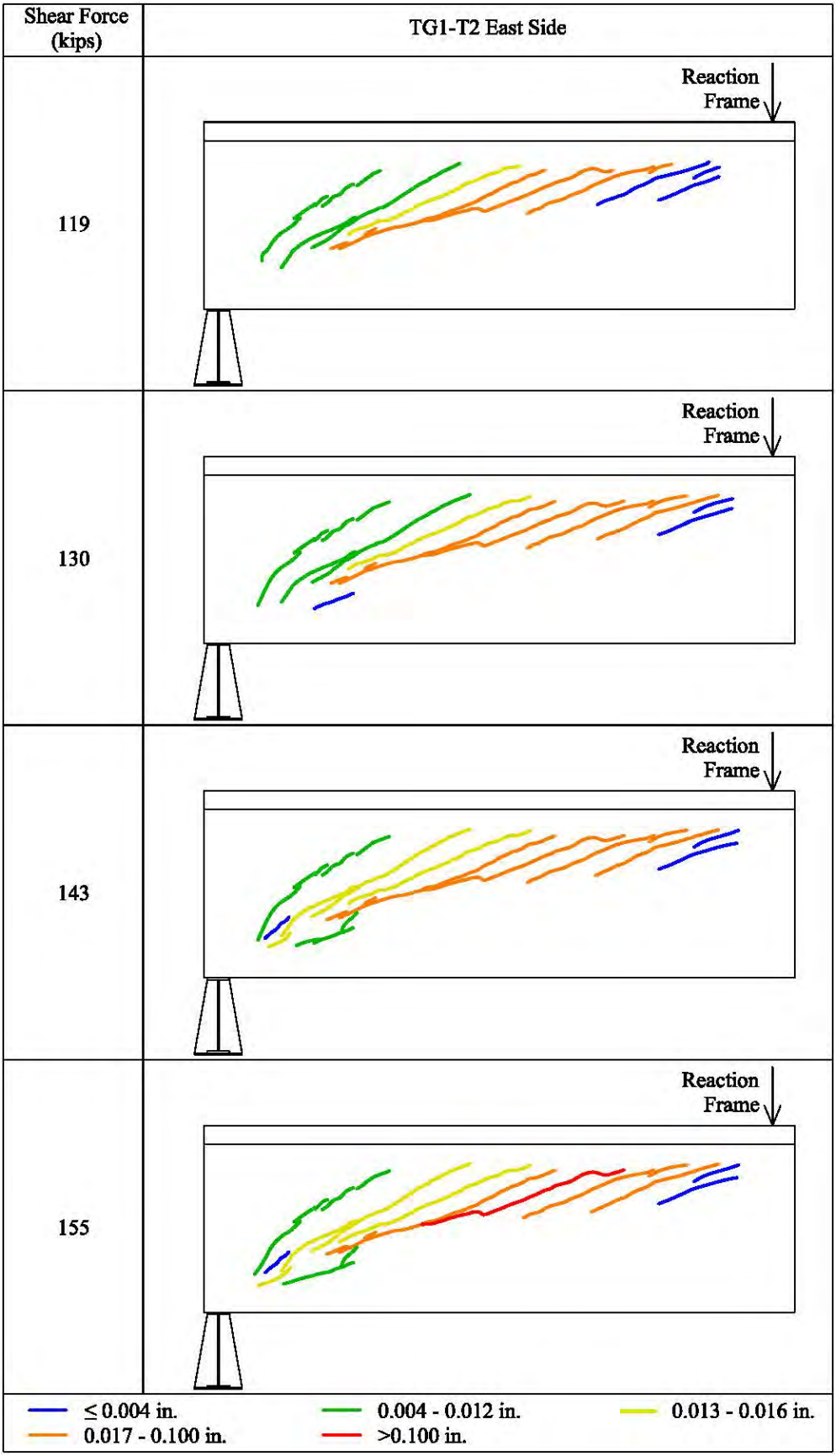
Shear Force (kips)
TG1-T2 East Side
119
130
143
155
Reaction Frame
≤ 0.004 in.
0.004 - 0.012 in.
0.013 - 0.016 in.
0.017 - 0.100 in.
>0.100 in.

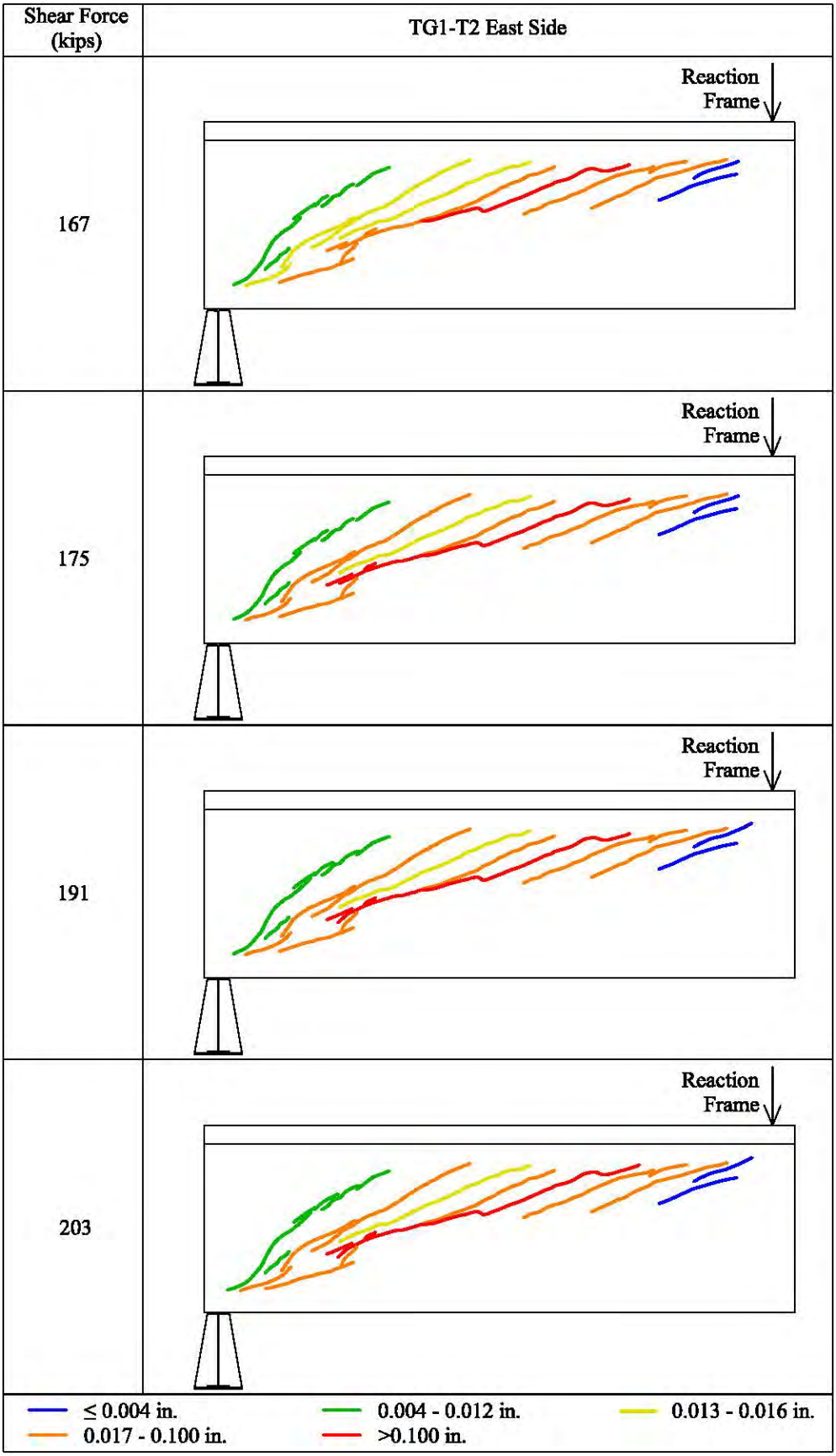
Shear Force (kips)
TG1-T2 East Side
167
175
191
203
Reaction Frame
≤ 0.004 in.
0.004 - 0.012 in.
0.013 - 0.016 in.
0.017 - 0.100 in.
>0.100 in.

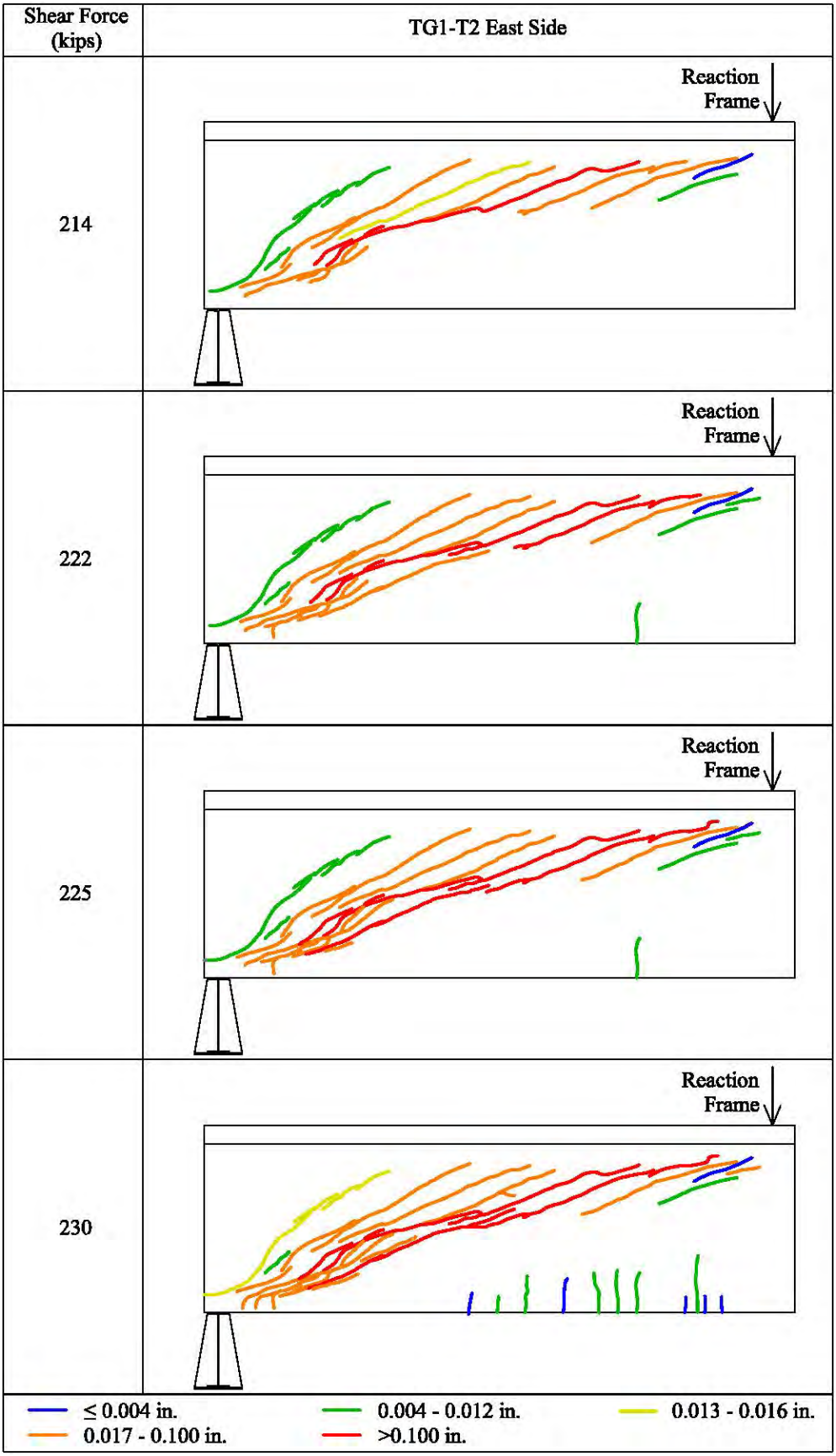
Shear Force (kips)
TG1-T2 East Side
214
222
225
230
Reaction Frame
≤ 0.004 in.
0.004 - 0.012 in.
0.013 - 0.016 in.
0.017 - 0.100 in.
>0.100 in.

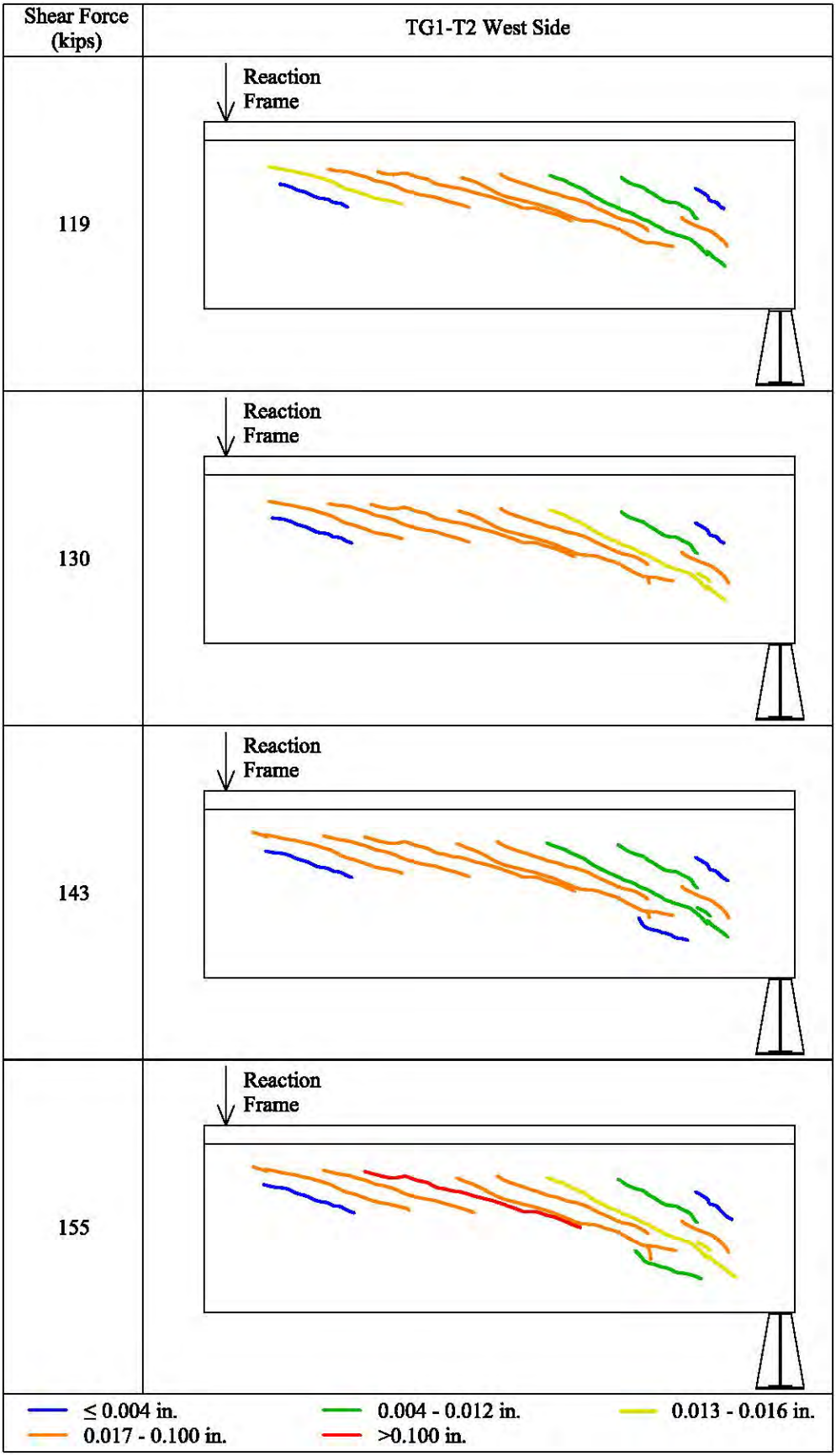
Shear Force (kips)
TG1-T2 West Side
119
130
143
155
Reaction Frame
Reaction Frame
Reaction Frame
Reaction Frame
≤ 0.004 in.
0.004 - 0.012 in.
0.013 - 0.016 in.
0.017 - 0.100 in.
>0.100 in.

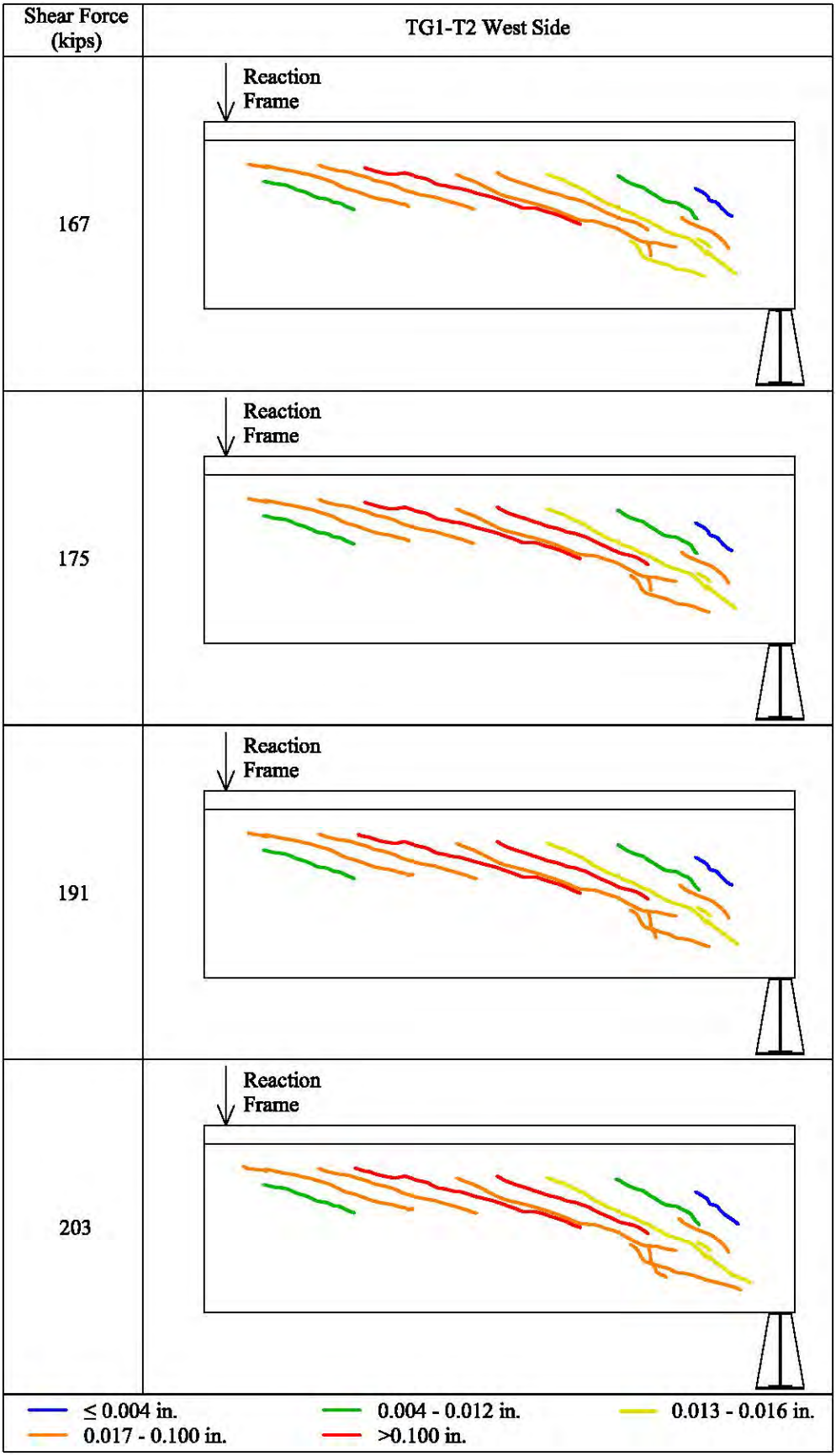
Shear Force (kips)
TG1-T2 West Side
167
175
191
203
Reaction Frame
≤ 0.004 in.
0.004 - 0.012 in.
0.013 - 0.016 in.
0.017 - 0.100 in.
>0.100 in.

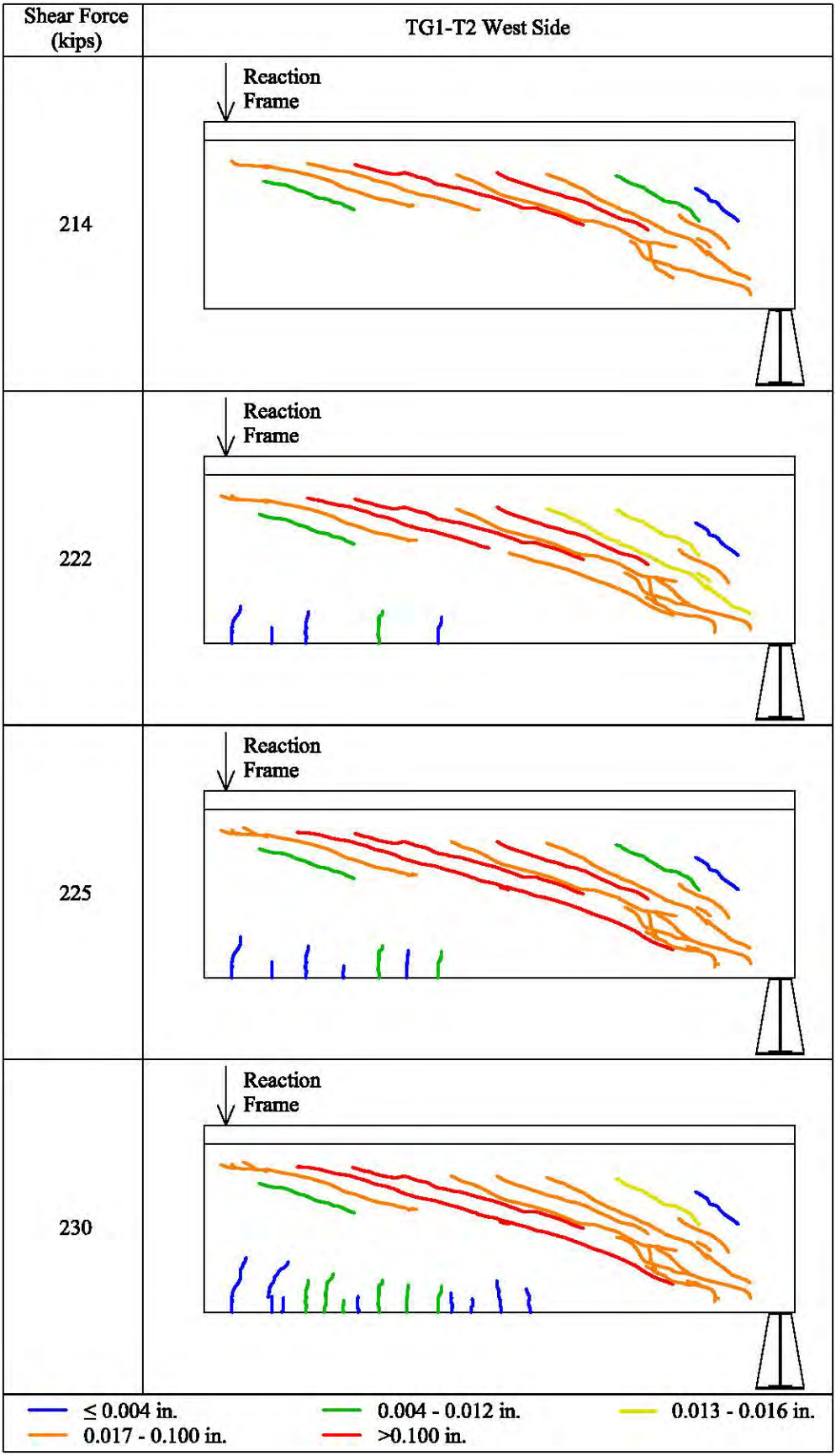
Shear Force (kips)
TG1-T2 West Side
214
222
225
230
Reaction Frame
≤ 0.004 in.
0.004 - 0.012 in.
0.013 - 0.016 in.
0.017 - 0.100 in.
>0.100 in.

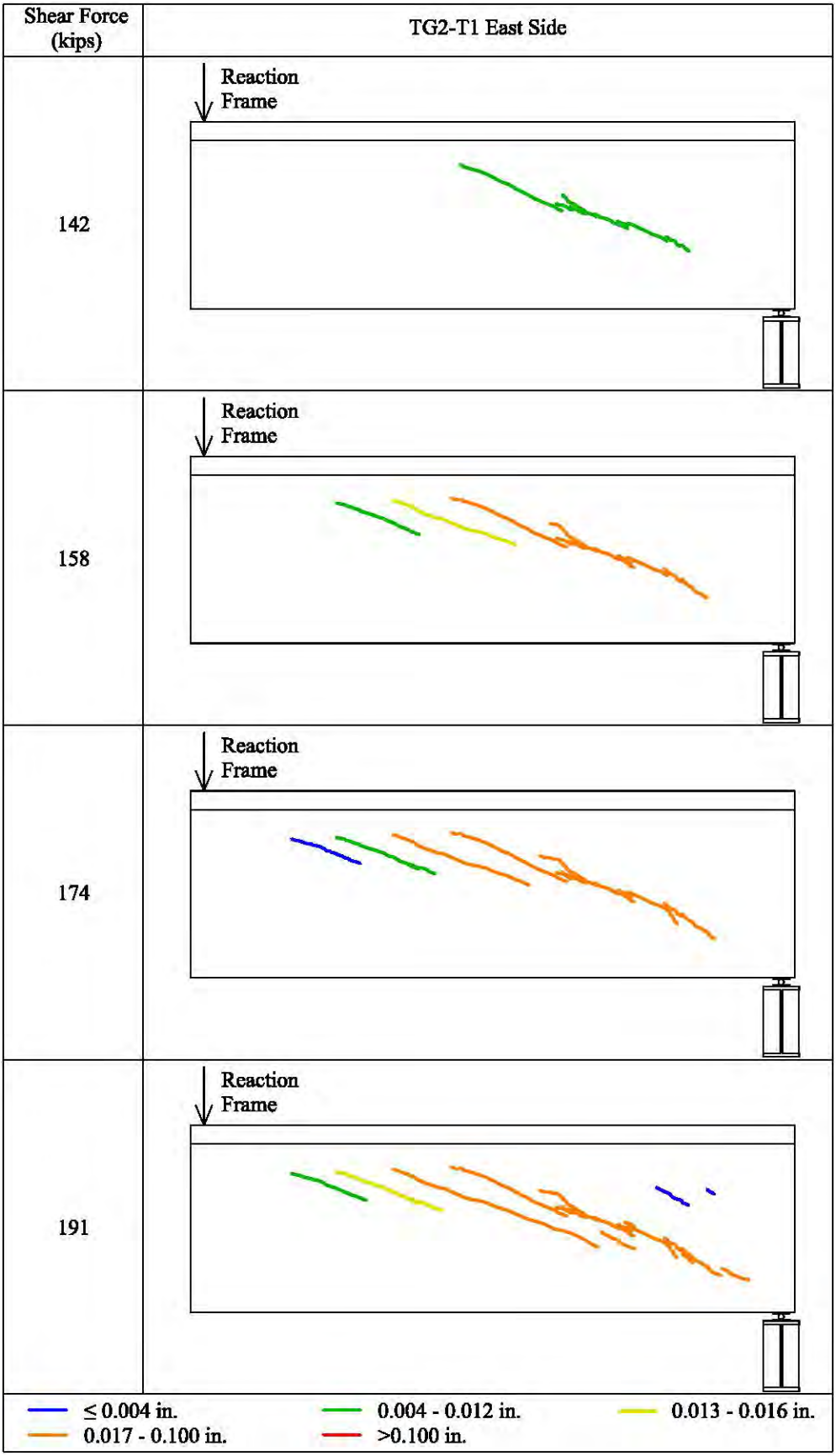
Shear Force (kips)
TG2-T1 East Side
142
158
174
191
Reaction Frame
≤ 0.004 in.
0.004 - 0.012 in.
0.013 - 0.016 in.
0.017 - 0.100 in.
>0.100 in.

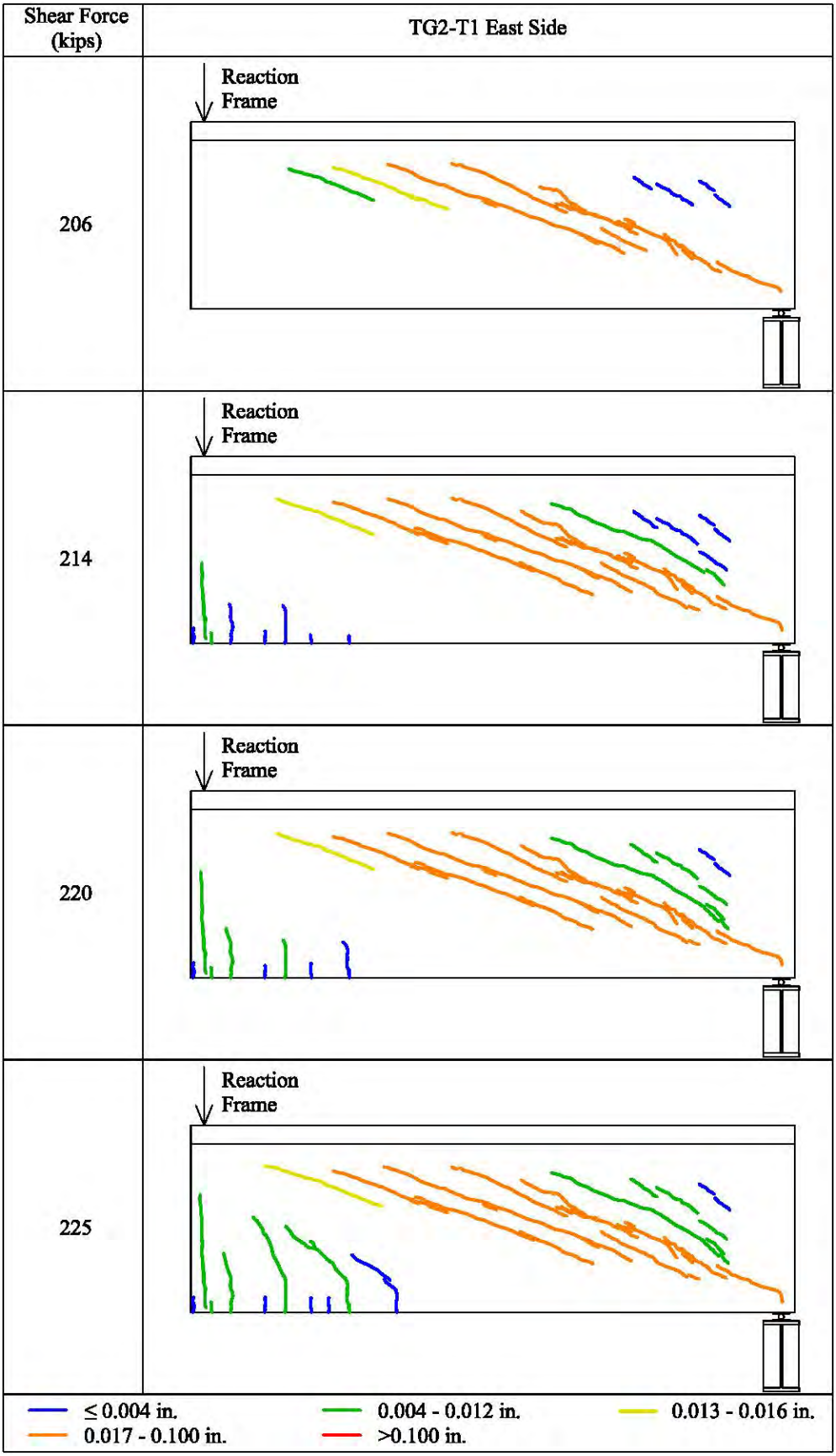
Shear Force (kips)
TG2-T1 East Side
206
214
220
225
Reaction Frame
Reaction Frame
Reaction Frame
Reaction Frame
≤ 0.004 in.
0.004 - 0.012 in.
0.013 - 0.016 in.
0.017 - 0.100 in.
>0.100 in.

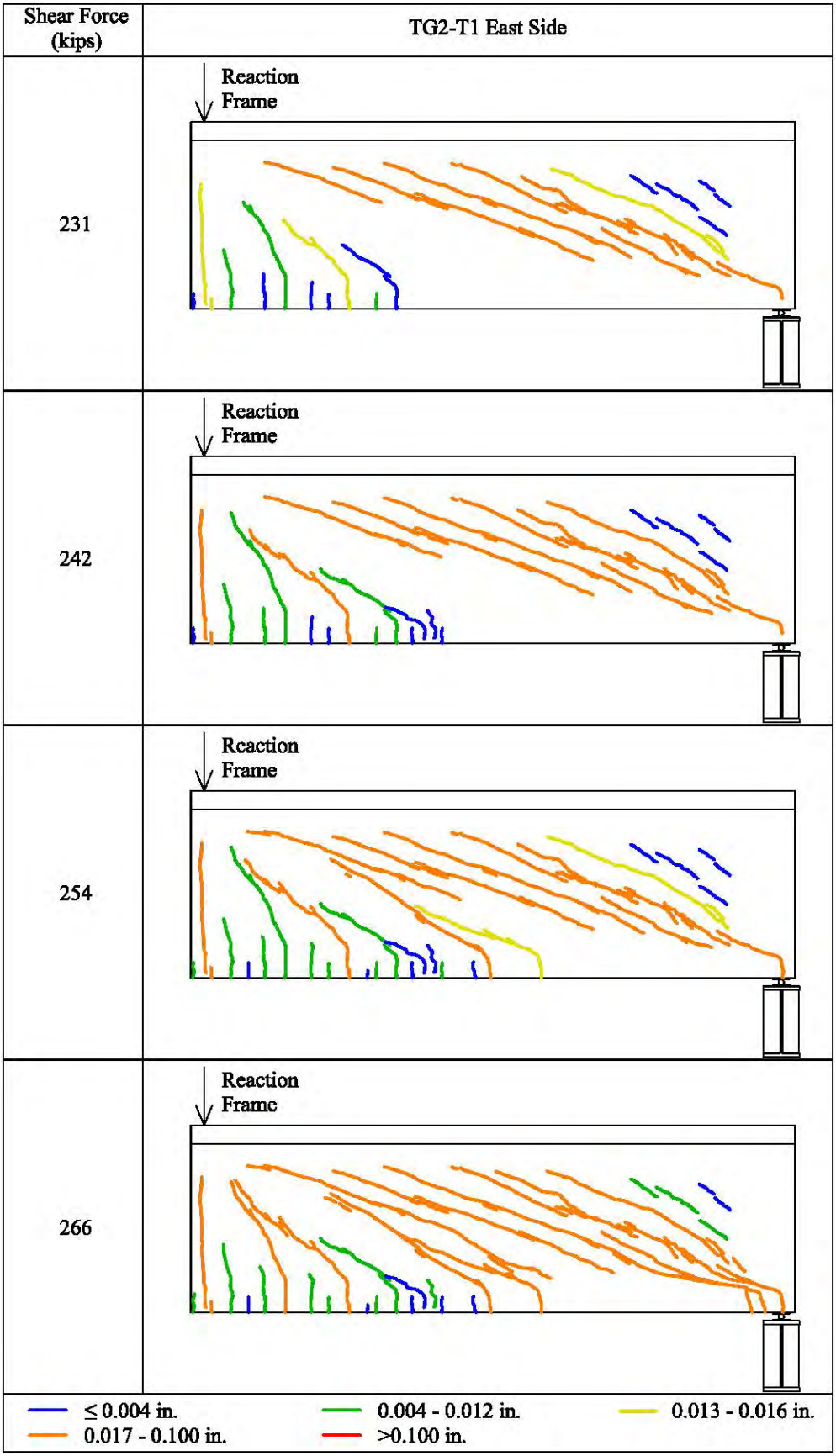
Shear Force (kips)
TG2-T1 East Side
231
242
254
266
Reaction Frame
≤ 0.004 in.
0.004 - 0.012 in.
0.013 - 0.016 in.
0.017 - 0.100 in.
>0.100 in.

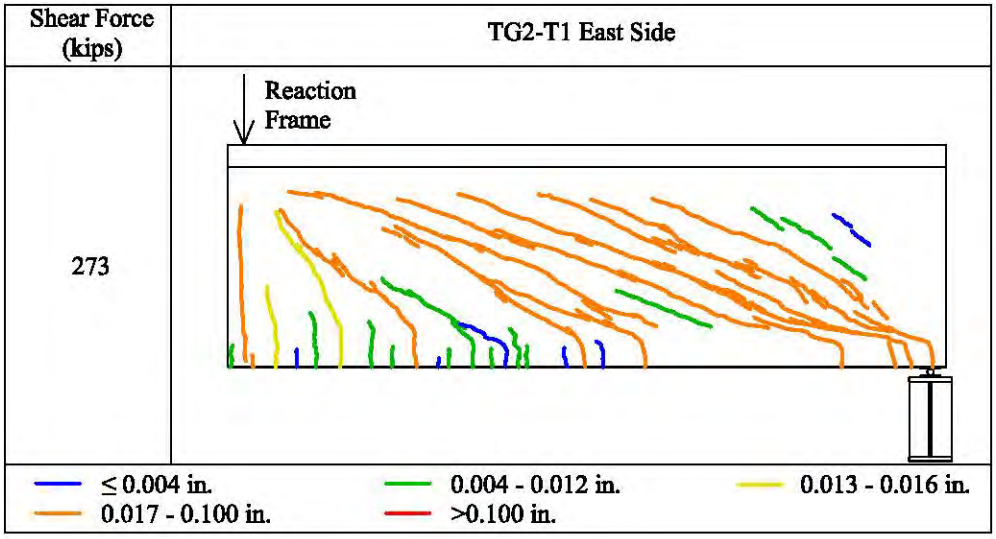
Shear Force (kips)
TG2-T1 East Side
Reaction Frame
273
≤ 0.004 in.
0.004 - 0.012 in.
0.013 - 0.016 in.
0.017 - 0.100 in.
>0.100 in.

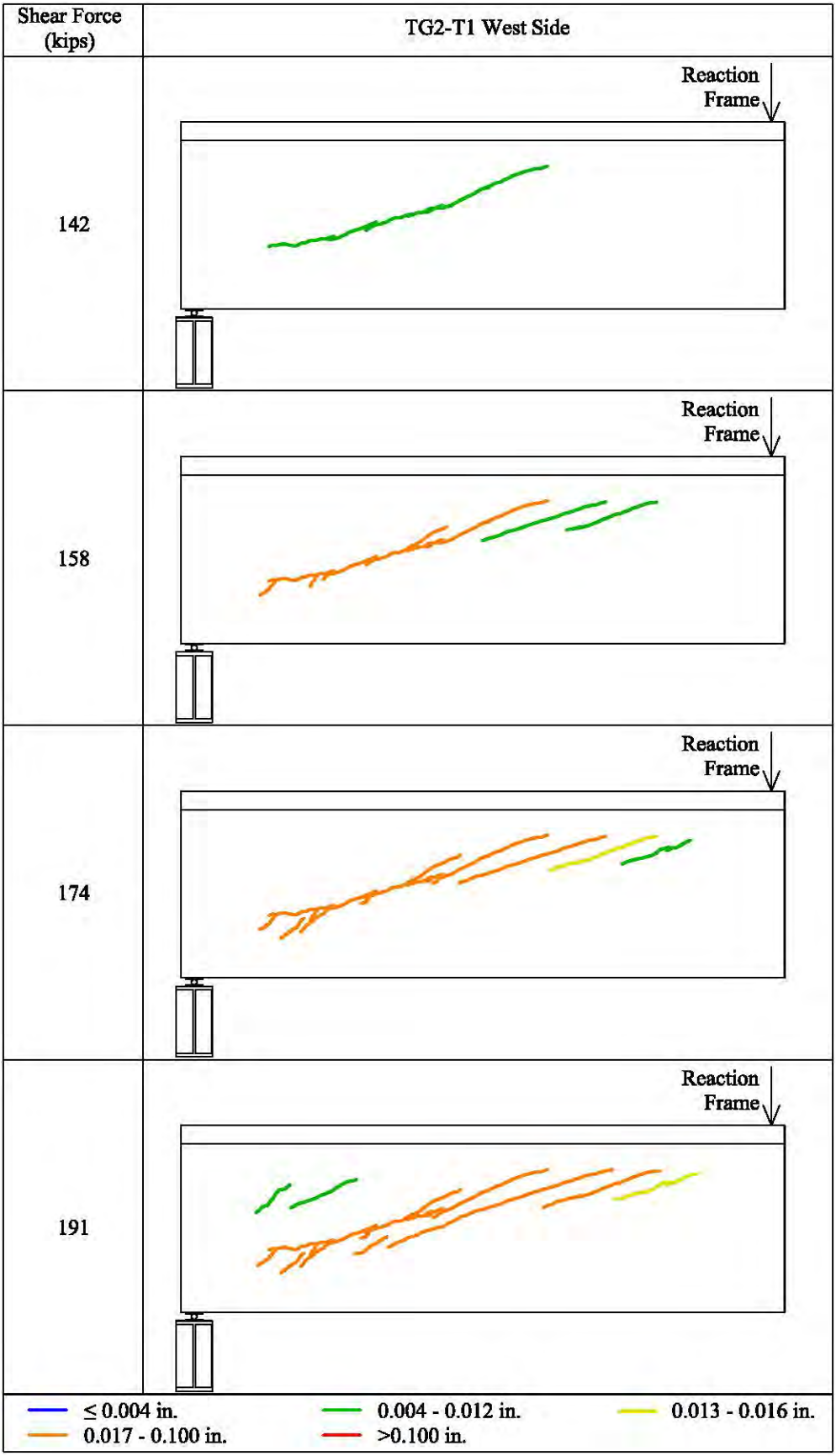
Shear Force (kips)
TG2-T1 West Side
142
158
174
191
Reaction Frame
≤ 0.004 in.
0.004 - 0.012 in.
0.013 - 0.016 in.
0.017 - 0.100 in.
>0.100 in.

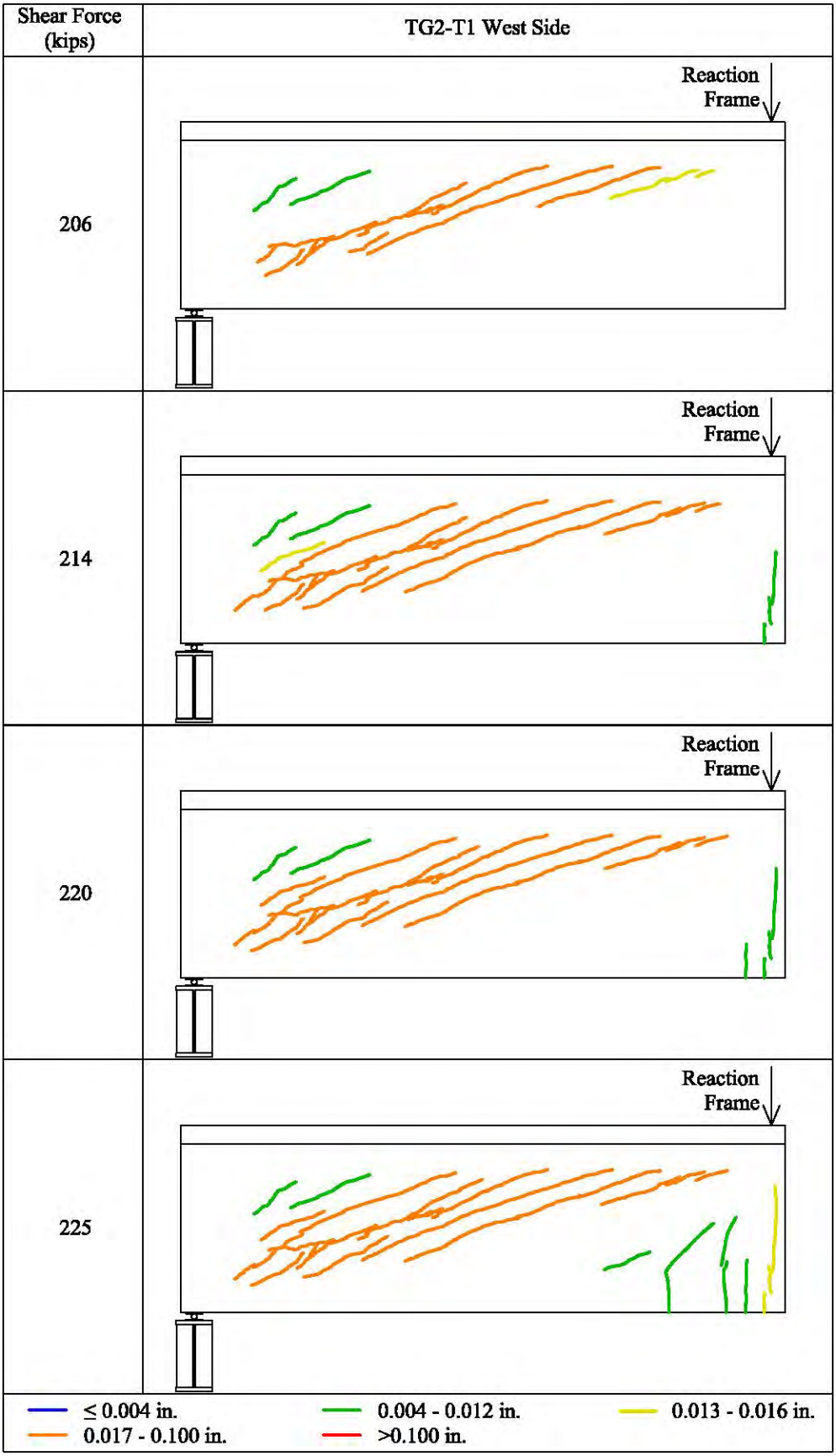
Shear Force (kips)
TG2-T1 West Side
206
214
220
225
Reaction Frame
≤ 0.004 in.
0.004 - 0.012 in.
0.013 - 0.016 in.
0.017 - 0.100 in.
>0.100 in.

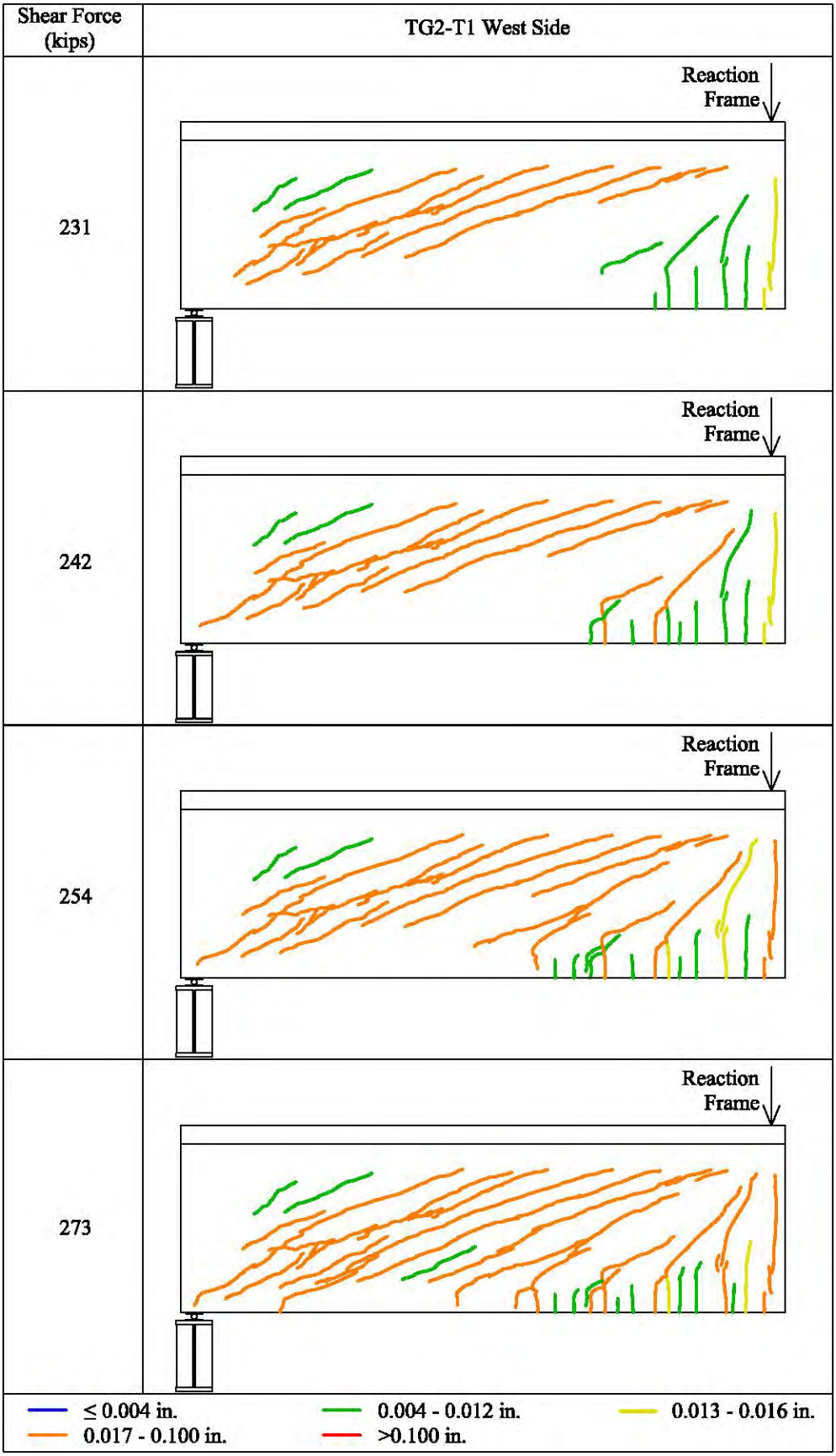
Shear Force (kips)
TG2-T1 West Side
231
242
254
273
Reaction Frame
≤ 0.004 in.
0.004 - 0.012 in.
0.013 - 0.016 in.
0.017 - 0.100 in.
>0.100 in.

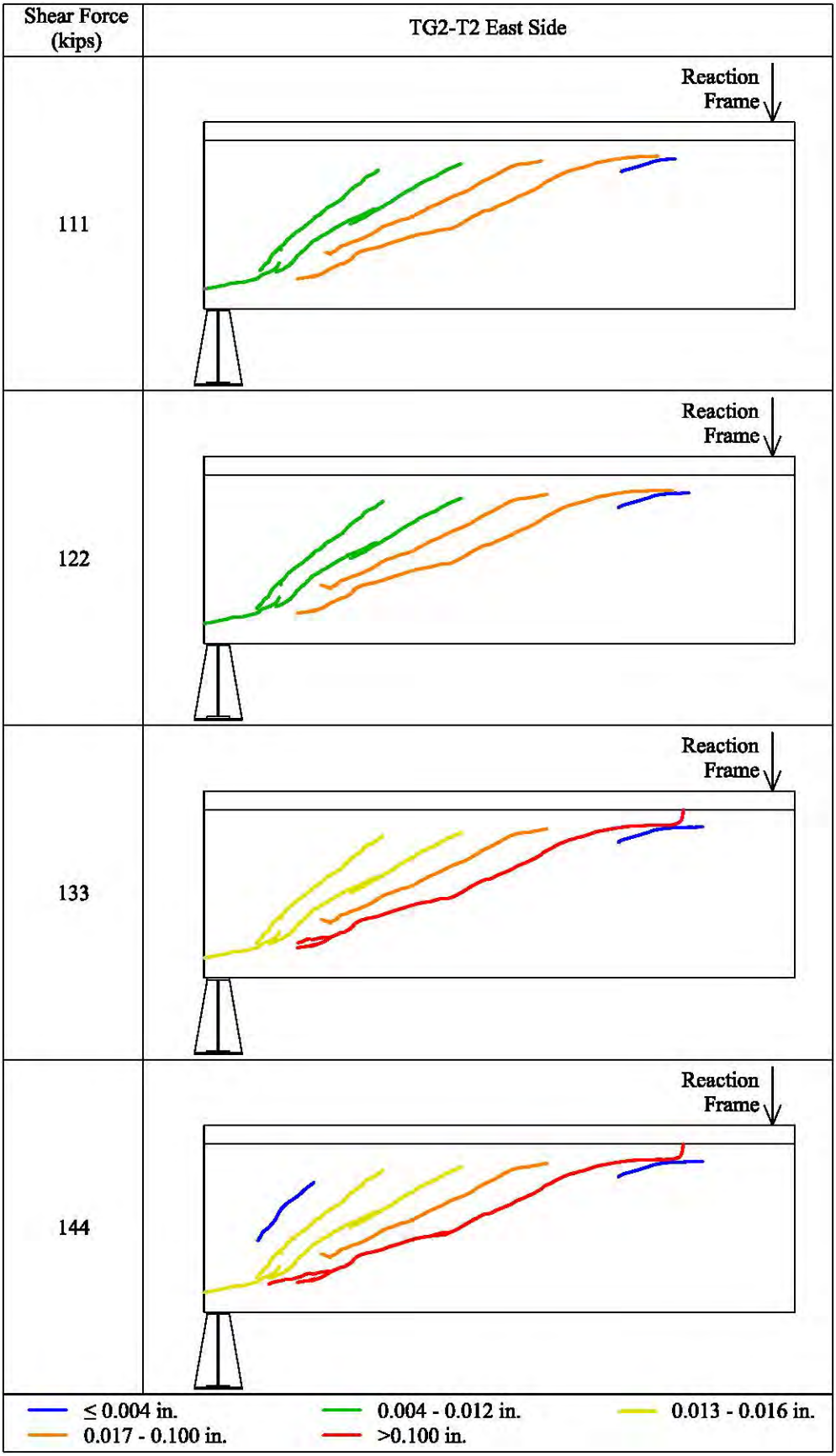
Shear Force (kips)
TG2-T2 East Side
111
122
133
144
Reaction Frame
≤ 0.004 in.
0.004 - 0.012 in.
0.013 - 0.016 in.
0.017 - 0.100 in.
>0.100 in.

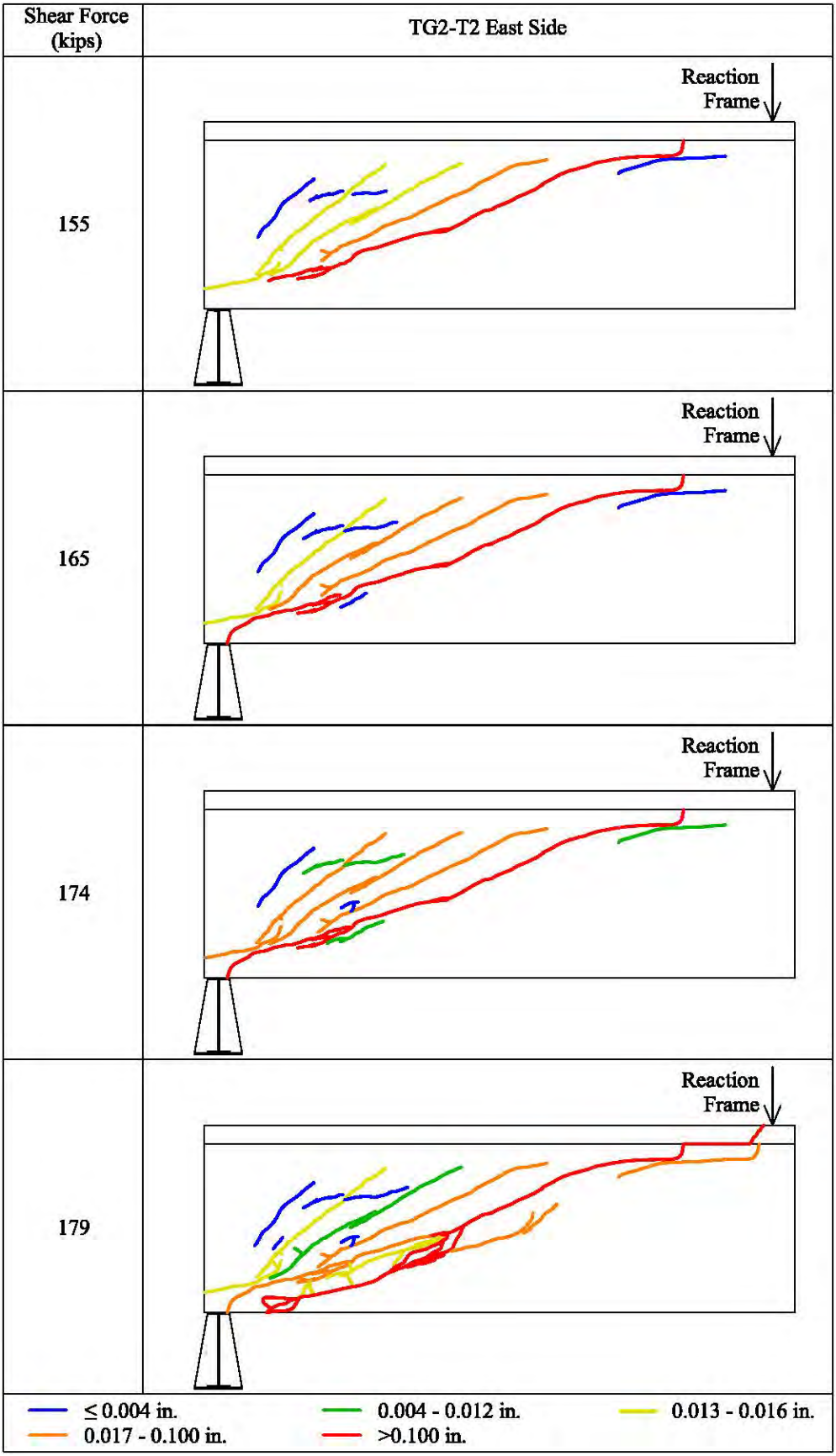
Shear Force (kips)
TG2-T2 East Side
155
165
174
179
Reaction Frame
≤ 0.004 in.
0.004 - 0.012 in.
0.013 - 0.016 in.
0.017 - 0.100 in.
>0.100 in.

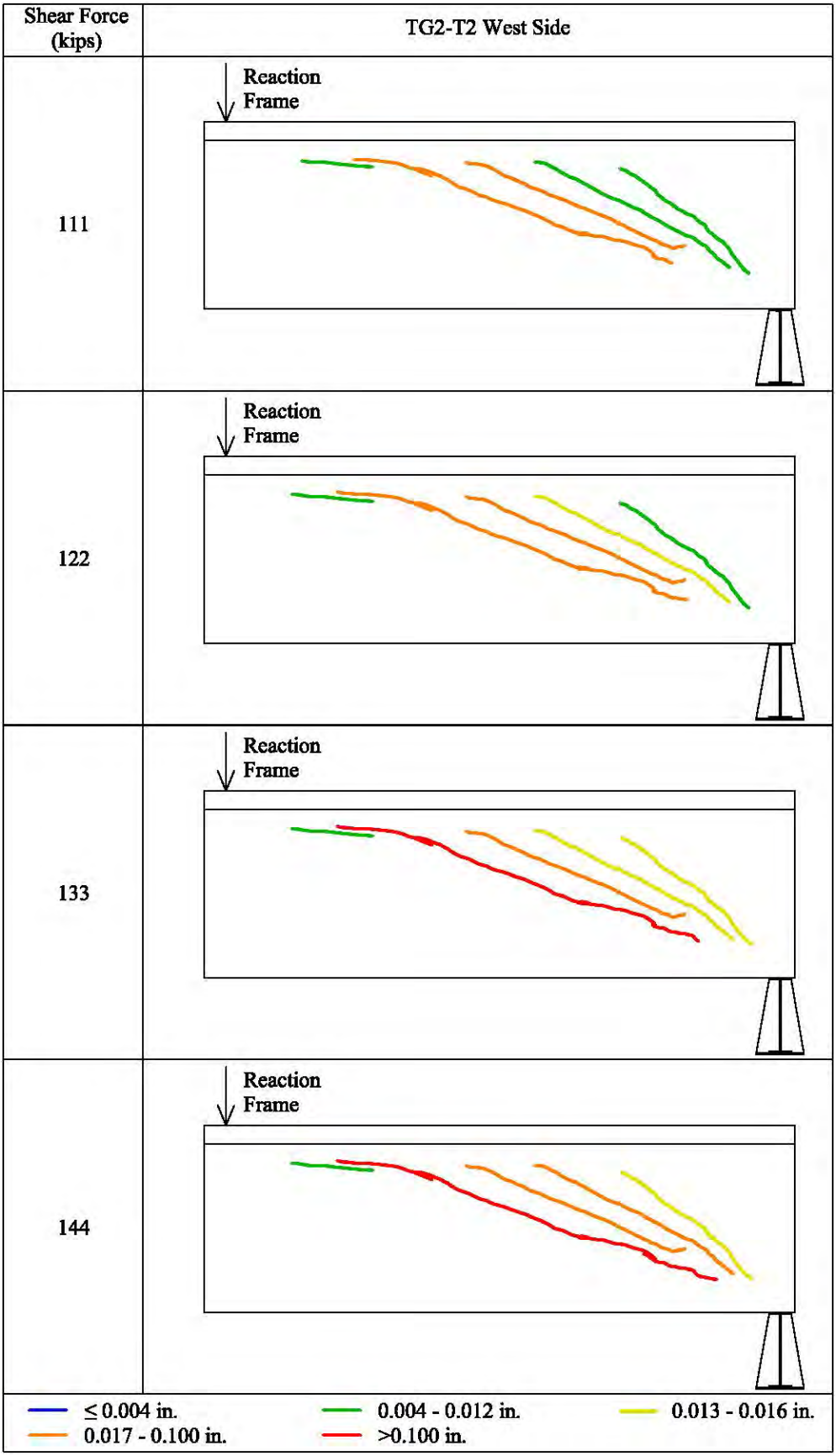
Shear Force (kips)
TG2-T2 West Side
111
122
133
144
Reaction Frame
≤ 0.004 in.
0.004 - 0.012 in.
0.013 - 0.016 in.
0.017 - 0.100 in.
>0.100 in.

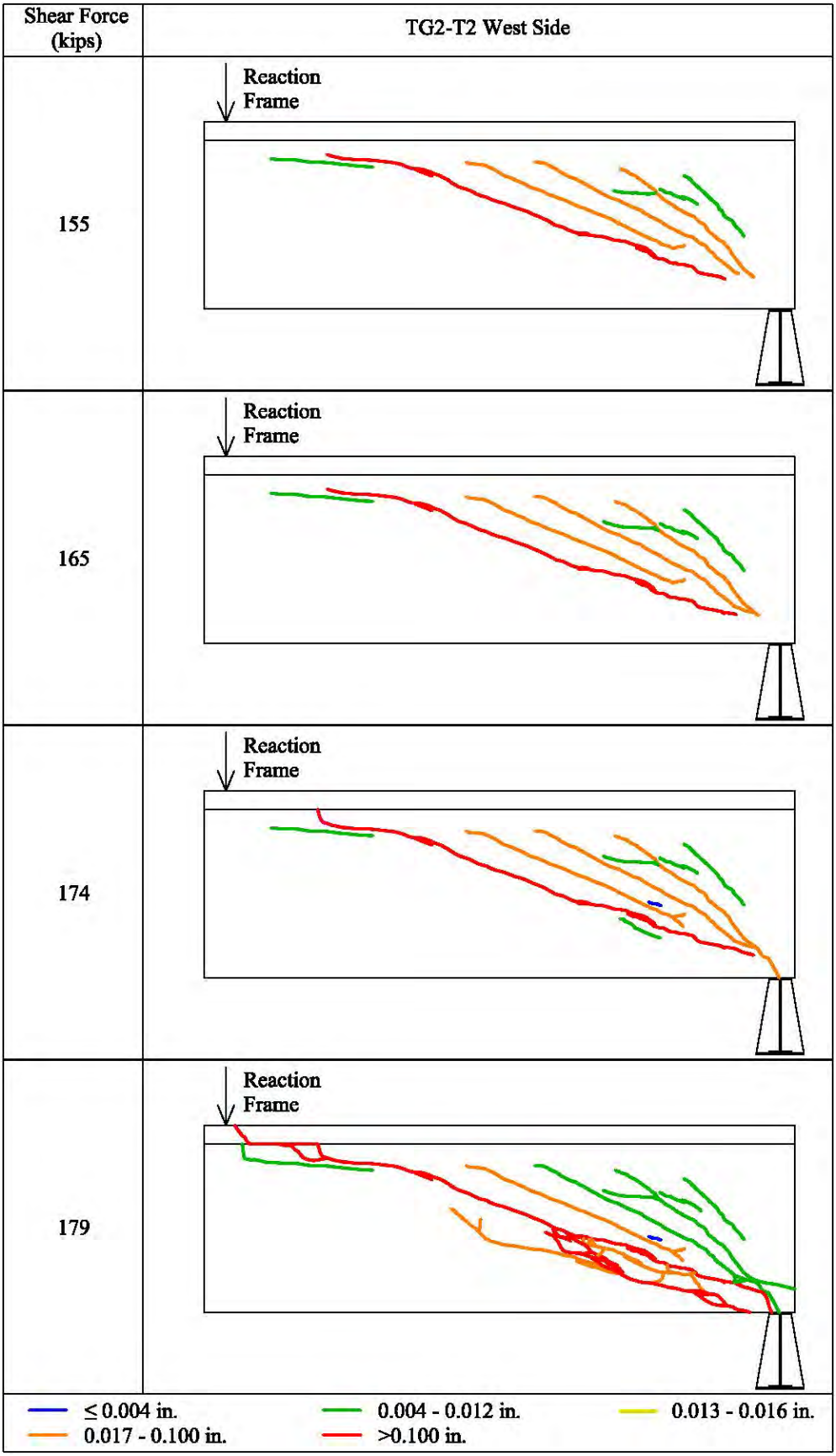
Shear Force (kips)
TG2-T2 West Side
155
165
174
179
Reaction Frame
≤ 0.004 in.
0.004 - 0.012 in.
0.013 - 0.016 in.
0.017 - 0.100 in.
>0.100 in.

TG1 - T1 East Side

Crack Label	Shear Force (kips)										
Shear Cracks	171	185	200	214	223	235	243	247	254	260	267
1	0.004	0.004	0.004	0.006	0.008	0.008	0.010	0.010	0.010	0.010	0.010
1'	--	0.002	0.002	0.002	0.004	0.004	0.004	0.006	0.006	0.006	0.006
2	0.006	0.006	0.006	0.008	0.008	0.010	0.010	0.010	0.010	0.010	0.010
3	0.008	0.008	0.008	0.008	0.010	0.012	0.012	0.012	0.012	0.012	0.014
4	0.006	0.006	0.006	0.006	0.008	0.012	0.012	0.012	0.012	0.014	0.014
5	0.008	0.008	0.008	0.010	0.010	0.012	0.012	0.012	0.012	0.012	0.012
6	0.006	0.006	0.008	0.012	0.012	0.014	0.014	0.014	0.014	0.014	0.014
7	0.004	0.006	0.006	0.008	0.010	0.010	0.010	0.010	0.010	0.010	0.010
8	0.004	0.006	0.008	0.012	0.014	0.012	0.012	0.012	0.012	0.014	0.014
9	0.002	0.006	0.008	0.010	0.014	0.014	0.014	0.016	0.016	0.016	0.016
10	--	0.004	0.006	0.008	0.008	0.010	0.010	0.012	0.012	0.012	0.012
11	--	--	--	--	--	--	--	--	--	--	0.008

Crack Label	Shear Force (kips)										
Flexure/Flexure-Shear Cracks	171	185	200	214	223	235	243	247	254	260	267
F1	--	--	--	--	0.006	0.010	0.010	0.010	0.012	0.012	0.012
F2	--	--	--	--	0.002	0.004	0.006	0.006	0.008	0.008	0.010
F3	--	--	--	--	0.002	0.004	0.004	0.004	0.004	0.004	0.004
F4	--	--	--	--	0.006	0.008	0.010	0.010	0.012	0.012	0.012
F5	--	--	--	--	0.002	0.002	0.002	0.002	0.002	0.002	0.002
F6	--	--	--	--	0.002	0.008	0.010	0.010	0.012	0.014	0.014
F7	--	--	--	--	0.002	0.004	0.004	0.004	0.004	0.004	0.004
F8	--	--	--	--	0.002	0.002	0.004	0.004	0.004	0.004	0.004
F9	--	--	--	--	--	0.004	0.004	0.010	0.010	0.010	0.012
F10	--	--	--	--	--	0.004	0.006	0.008	0.008	0.012	0.012
F11	--	--	--	--	--	0.006	0.006	0.010	0.010	0.012	0.012
F12	--	--	--	--	--	0.006	0.006	0.008	0.008	0.010	0.010
F13	--	--	--	--	--	0.006	0.006	0.006	0.006	0.010	0.010
F14	--	--	--	--	--	0.010	0.012	0.014	0.016	0.016	0.016
F15	--	--	--	--	--	0.004	0.004	0.006	0.008	0.008	0.010
F16	--	--	--	--	--	--	0.002	0.006	0.006	0.008	0.008
F17	--	--	--	--	--	--	0.004	0.008	0.008	0.008	0.008
F18	--	--	--	--	--	--	--	0.012	0.014	0.016	0.016
F19	--	--	--	--	--	--	--	0.004	0.006	0.008	0.010
F20	--	--	--	--	--	--	--	0.006	0.006	0.006	0.006
F21	--	--	--	--	--	--	--	0.014	0.018	0.018	0.016
F22	--	--	--	--	--	--	--	--	0.004	0.006	0.008
F23	--	--	--	--	--	--	--	--	0.004	0.004	0.004
F24	--	--	--	--	--	--	--	--	0.004	0.004	0.004
F25	--	--	--	--	--	--	--	--	--	0.010	0.010
F26	--	--	--	--	--	--	--	--	--	0.002	0.002
F27	--	--	--	--	--	--	--	--	--	0.002	0.002
F28	--	--	--	--	--	--	--	--	--	--	0.012

TG1 - T1 West Side

Crack Label	Shear Force (kips)										
Shear Cracks	171	185	200	214	223	235	243	247	254	260	267
1	0.002	0.004	0.008	0.008	0.006	0.008	0.008	0.008	0.006	0.008	0.008
1'	0.006	0.006	0.008	0.008	0.006	0.008	0.010	0.010	0.010	0.010	0.012
2	0.008	0.010	0.012	0.012	0.012	0.012	0.014	0.016	0.016	0.016	0.018
3	0.004	0.005	0.006	0.006	0.007	0.008	0.010	0.010	0.012	0.012	0.014
4	0.006	0.008	0.010	0.010	0.012	0.012	0.012	0.012	0.014	0.016	0.016
5	0.006	0.006	0.011	0.012	0.012	0.012	0.012	0.014	0.014	0.014	0.014
6	0.004	0.004	0.004	0.004	0.006	0.006	0.008	0.006	0.008	0.008	0.010
7	0.002	0.006	0.012	0.014	0.014	0.014	0.014	0.016	0.016	0.016	0.016
8	0.001	0.004	0.008	0.010	0.012	0.014	0.015	0.014	0.016	0.016	0.014
9	--	0.002	0.002	0.004	0.006	0.006	0.008	0.008	0.008	0.010	0.010
10	--	--	--	--	--	--	--	--	0.004	0.004	0.002
11	--	--	--	--	--	--	--	--	--	--	0.012

Crack Label	Shear Force (kips)										
Flexure/Flexure-Shear Cracks	171	185	200	214	223	235	243	247	254	260	267
F1	--	--	--	--	0.004	0.008	0.010	0.010	0.012	0.016	0.014
F2	--	--	--	--	0.004	0.004	0.004	0.006	0.006	0.006	0.008
F3	--	--	--	--	0.002	0.002	0.002	0.004	0.006	0.004	0.006
F4	--	--	--	--	0.004	0.008	0.010	0.010	0.012	0.010	0.014
F5	--	--	--	--	0.002	0.002	0.004	0.004	0.004	0.002	0.006
F6	--	--	--	--	0.002	0.004	0.010	0.012	0.014	0.014	0.014
F7	--	--	--	--	0.002	0.002	0.004	0.004	0.006	0.004	0.006
F8	--	--	--	--	--	0.004	0.008	0.008	0.012	0.012	0.010
F9	--	--	--	--	--	0.006	0.010	0.012	0.014	0.012	0.014
F10	--	--	--	--	--	0.001	0.002	0.004	0.004	0.004	0.006
F11	--	--	--	--	--	0.002	0.002	0.006	0.004	0.006	0.006
F12	--	--	--	--	--	0.002	0.004	0.004	0.004	0.006	0.006
F13	--	--	--	--	--	0.001	0.002	0.004	0.004	0.004	0.006
F14	--	--	--	--	--	0.004	0.004	0.006	0.006	0.008	0.008
F15	--	--	--	--	--	0.002	0.004	0.004	0.006	0.006	0.006
F16	--	--	--	--	--	0.006	0.012	0.012	0.014	0.014	0.012
F17	--	--	--	--	--	0.001	0.002	0.002	0.002	0.002	0.002
F18	--	--	--	--	--	--	0.002	0.004	0.004	0.004	0.006
F19	--	--	--	--	--	--	0.001	0.002	0.002	0.002	0.002
F20	--	--	--	--	--	--	0.002	0.004	0.004	0.004	0.004
F21	--	--	--	--	--	--	0.001	0.002	0.002	0.002	0.006
F22	--	--	--	--	--	--	--	0.014	0.018	0.018	0.016
F23	--	--	--	--	--	--	--	0.004	0.004	0.006	0.006
F24	--	--	--	--	--	--	--	--	0.002	0.002	0.002
F25	--	--	--	--	--	--	--	--	0.004	0.008	0.010
F26	--	--	--	--	--	--	--	--	0.004	0.004	0.004
F27	--	--	--	--	--	--	--	--	0.004	0.006	0.004
F28	--	--	--	--	--	--	--	--	0.002	0.006	0.010
F29	--	--	--	--	--	--	--	--	--	0.002	0.008
F30	--	--	--	--	--	--	--	--	--	0.002	0.004

* F27 and 11 connected at 254 k

TG1 - T2 East Side

Crack Label	Shear Force (kips)											
Shear Cracks	119	130	143	155	167	175	191	203	214	222	225	230
1	0.010	0.010	0.010	0.010	0.012	0.012	0.012	0.012	0.012	0.012	0.012	0.014
2	0.010	0.010	0.014	0.014	0.016	0.018	0.018	0.020	0.020	0.020	0.020	0.020
3	0.015	0.015	0.015	0.016	0.016	0.016	0.016	0.016	0.016	0.018	0.018	0.020
4	0.050	0.050	0.075	0.075	0.100	0.125	0.125	0.125	0.125	0.125	0.125	0.125
4a	0.025	0.030	0.030	0.035	0.035	0.035	0.050	0.075	0.100	0.100	0.100	0.100
4b	0.075	0.075	0.100	0.125	0.125	0.188	0.188	0.188	0.188	0.250	0.250	0.250
5	0.035	0.035	0.050	0.050	0.050	0.075	0.075	0.075	0.075	0.125	0.125	0.313
6	0.002	0.020	0.022	0.028	0.032	0.050	0.050	0.050	0.050	0.050	0.050	0.050
7	0.002	0.002	0.002	0.004	0.004	0.004	0.004	0.004	0.004	0.004	0.004	0.004
8	0.002	0.002	0.002	0.004	0.004	0.004	0.004	0.004	0.006	0.006	0.006	0.006
9	--	0.002	0.008	0.012	0.018	0.026	0.026	0.030	0.032	0.032	0.032	0.040
10	--	--	0.004	0.004	0.008	0.008	0.008	0.008	0.008	0.008	0.008	0.008
11	--	--	--	--	--	--	--	--	--	0.012	0.012	0.018
12	--	--	--	--	--	--	--	--	--	0.075	0.125	0.188
13	--	--	--	--	--	--	--	--	--	--	--	0.040

Crack Label	Shear Force (kips)											
Flexure/Flexure-Shear Cracks	119	130	143	155	167	175	191	203	214	222	225	230
F1	--	--	--	--	--	--	--	--	--	0.006	0.006	0.006
F2	--	--	--	--	--	--	--	--	--	--	--	0.002
F3	--	--	--	--	--	--	--	--	--	--	--	0.006
F4	--	--	--	--	--	--	--	--	--	--	--	0.010
F5	--	--	--	--	--	--	--	--	--	--	--	0.004
F6	--	--	--	--	--	--	--	--	--	--	--	0.006
F7	--	--	--	--	--	--	--	--	--	--	--	0.006
F8	--	--	--	--	--	--	--	--	--	--	--	0.004
F9	--	--	--	--	--	--	--	--	--	--	--	0.010
F10	--	--	--	--	--	--	--	--	--	--	--	0.002
F11	--	--	--	--	--	--	--	--	--	--	--	0.002

TG1 - T2 West Side

Crack Label	Shear Force (kips)											
Shear Cracks	119	130	143	155	167	175	191	203	214	222	225	230
1	0.001	0.001	0.002	0.002	0.002	0.002	0.002	0.002	0.002	0.004	0.002	0.004
2	0.006	0.008	0.008	0.008	0.010	0.010	0.012	0.012	0.012	0.014	0.012	0.014
3	0.018	0.020	0.020	0.024	0.026	0.030	0.030	0.030	0.030	0.030	0.030	0.030
4	0.012	0.014	0.012	0.016	0.014	0.014	0.014	0.016	0.018	0.016	0.022	0.022
4a	0.032	0.050	0.075	0.075	0.100	0.125	0.125	0.125	0.125	0.125	0.125	0.075
4b	0.020	0.026	0.026	0.028	0.028	0.028	0.028	0.035	0.035	0.035	0.050	0.050
5	0.075	0.100	0.100	0.125	0.125	0.125	0.188	0.188	0.188	0.250	0.250	0.400
6	0.030	0.035	0.050	0.050	0.050	0.050	0.075	0.075	0.100	0.125	0.125	0.313
7	0.016	0.022	0.022	0.026	0.032	0.035	0.040	0.050	0.050	0.050	0.075	0.040
8	0.004	0.004	0.004	0.004	0.006	0.006	0.006	0.006	0.006	0.006	0.008	0.012
9	--	--	0.004	0.010	0.014	0.018	0.024	0.030	0.032	0.032	0.032	0.032
10	--	--	--	--	--	--	--	--	--	0.075	0.125	0.250

Crack Label	Shear Force (kips)											
Flexure/Flexure-Shear Cracks	119	130	143	155	167	175	191	203	214	222	225	230
F1	--	--	--	--	--	--	--	--	--	0.004	0.006	0.006
F2	--	--	--	--	--	--	--	--	--	0.006	0.006	0.006
F3	--	--	--	--	--	--	--	--	--	0.004	0.004	0.008
F4	--	--	--	--	--	--	--	--	--	0.002	0.002	0.006
F5	--	--	--	--	--	--	--	--	--	0.004	0.004	0.006
F6	--	--	--	--	--	--	--	--	--	--	0.002	0.004
F7	--	--	--	--	--	--	--	--	--	--	0.002	0.004
F8	--	--	--	--	--	--	--	--	--	--	--	0.004
F9	--	--	--	--	--	--	--	--	--	--	--	0.004
F10	--	--	--	--	--	--	--	--	--	--	--	0.002
F11	--	--	--	--	--	--	--	--	--	--	--	0.004
F12	--	--	--	--	--	--	--	--	--	--	--	0.002
F13	--	--	--	--	--	--	--	--	--	--	--	0.006
F14	--	--	--	--	--	--	--	--	--	--	--	0.004
F15	--	--	--	--	--	--	--	--	--	--	--	0.002

TG2 - T1 East Side

Crack Label	Shear Force (kips)												
Shear Cracks	142	158	174	191	206	214	220	225	231	242	254	266	273
1	0.010	0.020	0.026	0.024	0.028	0.028	0.026	0.026	0.026	0.026	0.026	0.032	0.040
2	--	0.014	0.018	0.020	0.026	0.028	0.030	0.026	0.026	0.030	0.028	0.032	0.075
3	--	0.006	0.010	0.016	0.016	0.026	0.026	0.024	0.026	0.030	0.032	0.035	0.035
4	--	--	0.004	0.008	0.010	0.014	0.016	0.016	0.018	0.018	0.032	0.035	0.040
5	--	--	--	0.002	0.002	0.002	0.002	0.002	0.002	0.002	0.002	0.002	0.002
6	--	--	--	0.004	0.004	0.004	0.006	0.006	0.004	0.004	0.004	0.006	0.006
7	--	--	--	--	--	0.012	0.012	0.012	0.014	0.018	0.016	0.018	0.018
8	--	--	--	--	--	--	--	--	--	--	--	--	0.008

Crack Label	Shear Force (kips)												
Flexure/Flexure-Shear Cracks	142	158	174	191	206	214	220	225	231	242	254	266	273
F1	--	--	--	--	--	0.002	0.004	0.012	0.016	0.022	0.028	0.032	0.035
F2	--	--	--	--	--	0.002	0.002	0.004	0.004	0.004	0.006	0.006	0.006
F3	--	--	--	--	--	0.004	0.006	0.010	0.008	0.012	0.012	0.018	0.014
F4	--	--	--	--	--	0.002	0.002	0.004	0.004	0.006	0.006	0.008	0.010
F5	--	--	--	--	--	0.004	0.006	0.008	0.010	0.010	0.012	0.012	0.014
F6	--	--	--	--	--	0.008	0.010	0.010	0.014	0.020	0.024	0.030	0.028
F7	--	--	--	--	--	0.002	0.002	0.004	0.002	0.004	0.006	0.006	0.008
F8	--	--	--	--	--	--	0.006	0.008	0.006	0.008	0.008	0.008	0.010
F9	--	--	--	--	--	--	0.004	0.004	0.004	0.004	0.006	0.006	0.006
F10	--	--	--	--	--	--	0.008	0.010	0.010	0.012	0.012	0.014	0.020
F11	--	--	--	--	--	--	0.002	0.004	0.004	0.006	0.006	0.006	0.008
F12	--	--	--	--	--	--	--	0.004	0.004	0.004	0.006	0.008	0.008
F13	--	--	--	--	--	--	--	0.004	0.004	0.006	0.008	0.008	0.010
F14	--	--	--	--	--	--	--	0.008	0.010	0.014	0.018	0.016	0.020
F15	--	--	--	--	--	--	--	0.004	0.010	0.018	0.020	0.012	0.024
F16	--	--	--	--	--	--	--	--	0.006	0.006	0.006	0.008	0.008
F17	--	--	--	--	--	--	--	--	0.002	0.004	0.006	0.006	0.010
F18	--	--	--	--	--	--	--	--	0.002	0.008	0.010	0.016	0.006
F19	--	--	--	--	--	--	--	--	0.010	0.014	0.020	0.016	0.018
F20	--	--	--	--	--	--	--	--	--	0.002	0.006	0.004	0.006
F21	--	--	--	--	--	--	--	--	--	0.004	0.004	0.006	0.006
F22	--	--	--	--	--	--	--	--	--	0.002	0.002	0.004	0.004
F23	--	--	--	--	--	--	--	--	--	0.004	0.004	0.004	0.010
F24	--	--	--	--	--	--	--	--	--	0.002	0.006	0.006	0.008
F25	--	--	--	--	--	--	--	--	--	0.002	0.002	0.004	0.004
F26	--	--	--	--	--	--	--	--	--	--	0.016	0.024	0.032
F27	--	--	--	--	--	--	--	--	--	--	0.032	0.032	0.032
F28	--	--	--	--	--	--	--	--	--	--	--	0.008	0.010
F29	--	--	--	--	--	--	--	--	--	--	--	0.002	0.004
F30	--	--	--	--	--	--	--	--	--	--	--	--	0.022
F31	--	--	--	--	--	--	--	--	--	--	--	--	0.002

TG2 - T1 West Side

Crack Label	Shear Force (kips)												
Shear Cracks	142	158	174	191	206	214	220	225	231	242	254	266	273
1	0.010	0.020	0.035	0.040	0.040	0.035	0.035	0.035	0.035	0.035	0.035	0.045	0.050
2	--	0.010	0.025	0.035	0.035	0.035	0.035	0.040	0.040	0.040	0.040	0.040	0.080
3	--	0.005	0.015	0.020	0.025	0.035	0.035	0.035	0.040	0.040	0.040	0.035	0.040
4	--	--	0.010	0.015	0.015	0.020	0.020	0.020	0.025	0.030	0.040	0.045	0.050
5	--	--	--	0.010	0.010	0.010	0.010	0.005	0.005	0.005	0.005	0.005	0.005
6	--	--	--	0.005	0.010	0.010	0.010	0.010	0.010	0.010	0.010	0.010	0.010
7	--	--	--	--	--	0.015	0.020	0.020	0.020	0.025	0.025	0.030	0.030
8	--	--	--	--	--	--	--	0.005	0.010	0.020	0.025	0.025	0.025
9	--	--	--	--	--	--	--	--	--	--	0.025	0.035	0.045
10	--	--	--	--	--	--	--	--	--	--	--	--	0.010

Crack Label	Shear Force (kips)												
Flexure/Flexure-Shear Cracks	142	158	174	191	206	214	220	225	231	242	254	266	273
F1	--	--	--	--	--	0.005	0.010	0.015	0.015	0.015	0.020	0.020	0.020
F2	--	--	--	--	--	0.005	0.010	0.010	0.010	0.010	0.015	0.020	0.020
F3	--	--	--	--	--	0.005	0.005	0.005	0.005	0.005	0.005	0.010	0.010
F4	--	--	--	--	--	0.010	0.010	0.010	0.015	0.015	0.015	0.010	0.015
F5	--	--	--	--	--	0.005	0.010	0.015	0.015	0.020	0.025	0.030	0.030
F6	--	--	--	--	--	--	0.005	0.005	0.010	0.010	0.010	0.010	0.015
F7	--	--	--	--	--	--	0.010	0.010	0.015	0.020	0.020	0.020	0.020
F8	--	--	--	--	--	--	0.005	0.005	0.005	0.005	0.005	0.010	0.010
F9	--	--	--	--	--	--	--	0.005	0.005	0.010	0.010	0.005	0.010
F10	--	--	--	--	--	--	--	0.010	0.010	0.010	0.015	0.015	0.015
F11	--	--	--	--	--	--	--	0.010	0.010	0.005	0.005	0.005	0.005
F12	--	--	--	--	--	--	--	0.005	0.005	0.010	0.015	0.015	0.020
F13	--	--	--	--	--	--	--	0.005	0.005	0.005	0.005	0.010	0.005
F14	--	--	--	--	--	--	--	0.005	0.010	0.005	0.010	0.010	0.010
F15	--	--	--	--	--	--	--	--	0.005	0.020	0.035	0.035	0.050
F16	--	--	--	--	--	--	--	--	0.005	0.005	0.005	0.005	0.010
F17	--	--	--	--	--	--	--	--	0.005	0.005	0.005	0.010	0.010
F18	--	--	--	--	--	--	--	--	0.005	0.005	0.005	0.005	0.005
F19	--	--	--	--	--	--	--	--	0.010	0.015	0.020	0.020	0.020
F20	--	--	--	--	--	--	--	--	--	0.005	0.005	0.005	0.010
F21	--	--	--	--	--	--	--	--	--	0.005	0.005	0.005	0.010
F22	--	--	--	--	--	--	--	--	--	--	0.010	0.005	0.005
F23	--	--	--	--	--	--	--	--	--	--	0.005	0.010	0.010
F24	--	--	--	--	--	--	--	--	--	--	0.010	0.010	0.020
F25	--	--	--	--	--	--	--	--	--	--	0.005	0.005	0.010
F26	--	--	--	--	--	--	--	--	--	--	0.005	0.005	0.005
F27	--	--	--	--	--	--	--	--	--	--	0.005	0.005	0.005
F28	--	--	--	--	--	--	--	--	--	--	0.005	0.010	0.010
F29	--	--	--	--	--	--	--	--	--	--	0.005	0.005	0.005
F30	--	--	--	--	--	--	--	--	--	--	0.005	0.010	0.005
F31	--	--	--	--	--	--	--	--	--	--	0.005	0.005	0.005
F32	--	--	--	--	--	--	--	--	--	--	0.005	0.005	0.005

TG2 - T2 East Side

Crack Label	Shear Force (kips)							
Shear Cracks	111	122	133	144	155	165	174	179
1	0.012	0.012	0.014	0.014	0.014	0.016	0.020	0.014
2	0.010	0.012	0.014	0.016	0.016	0.018	0.022	0.008
3	0.024	0.030	0.030	0.030	0.032	0.032	0.032	0.026
4	0.075	0.100	0.125	0.125	0.188	0.188	0.250	0.938
5	0.002	0.002	0.002	0.004	0.004	0.004	0.008	0.020
6	--	--	--	0.004	0.004	0.004	0.004	0.004
7	--	--	--	--	0.002	0.004	0.006	0.004
8	--	--	--	--	--	0.004	0.012	0.016
9	--	--	--	--	--	--	--	0.750

Crack Label	Shear Force (kips)							
Flexure/Flexure-Shear Cracks	111	122	133	144	155	165	174	179
F1	No flexural cracks							

TG2 - T2 West Side

Crack Label	Shear Force (kips)							
Shear Cracks	111	122	133	144	155	165	174	179
1	0.010	0.012	0.014	0.016	0.018	0.022	0.022	0.012
2	0.012	0.014	0.016	0.020	0.022	0.022	0.022	0.010
3	0.026	0.028	0.030	0.032	0.035	0.040	0.040	0.026
4	0.075	0.100	0.125	0.125	0.156	0.188	0.219	0.969
5	0.006	0.006	0.006	0.008	0.010	0.010	0.010	0.012
6	--	--	--	--	0.008	0.008	0.010	0.010
7	--	--	--	--	0.006	0.010	0.010	0.006
8	--	--	--	--	--	--	0.002	0.001
9	--	--	--	--	--	--	0.006	0.040
10	--	--	--	--	--	--	--	0.600

Crack Label	Shear Force (kips)							
Flexure/Flexure-Shear Cracks	111	122	133	144	155	165	174	179
F1	No flexural cracks							

BIBLIOGRAPHY

ACI Committee 209 (2008). "Prediction of Creep, Shrinkage, and Temperature Effects in Concrete Structures;" *American Concrete Institute*, Farmington Hills, Michigan.

ACI Committee 224 (2001). "Control of Cracking in Concrete Structures." A*merican Concrete Institute*, Farmington Hills, Michigan.

ACI Committee 237 (2007). "Self-Consolidating Concrete." *American Concrete Institute*, Farmington Hills, Michigan.

ACI Committee 318 (2011). "Building Code Requirements for Structural Concrete and Commentary." *American Concrete Institute*, Farmington Hills, Michigan.

ACI Committee 363 (2010). "State of the Art Report on High Strength Concrete." *American Concrete Institute*, Farmington Hills, Michigan.

American Association of State Highway and Transportation Officials (2012). "AASHTO LRFD Bridge Design Specifications, 6th Edition." *American Association of State Highway and Transportation Officials*, Washington, D.C.

ASTM A 615 (2012). "Standard Specification for Deformed and Plain Carbon-Steel Bars for Concrete Reinforcement." *American Society for Testing and Materials (ASTM) International*, West Conshohocken, Pennsylvania.

ASTM A 1064 (2012). "Standard Specification for Carbon-Steel Wire and Welded Wire Reinforcement, Plain and Deformed, for Concrete." *American Society for Testing and Materials (ASTM) International*, West Conshohocken, Pennsylvania.

ASTM C 39 (2012). "Standard Test Method for Compressive Strength of Cylindrical Concrete Specimens." *American Society for Testing and Materials (ASTM) International*, West Conshohocken, Pennsylvania.

ASTM C 78 (2010). "Standard Test Method for Flexural Strength of Concrete." *American Society for Testing and Materials (ASTM) International*, West Conshohocken, Pennsylvania.

ASTM C 496 (2011). "Standard Test Method for Splitting Tensile Strength of Cylindrical Concrete Specimens." *American Society for Testing and Materials (ASTM) International*, West Conshohocken, Pennsylvania.

EFNARC (2006). "Guidelines for Viscosity Modifying Admixtures for Concrete." Retrieved March 18, 2014, from http:www.efnarc.org.

Bilodeau, A., Sivasundaram, V., Painter, K. E., and Malhotra, V. M. (1994). Durability of concrete incorporating high volumes of fly ash from sources in the U.S. *ACI Materials Journal, 91(1),* 3-12.

Bouzoubaa, N., Bilodeau, A., Sivasundaram, V., and Chakraborty, A. (2007). Mechanical Properties and Durability Characteristics of High Volume Fly Ash Concrete Made with Ordinary Portland Cement and Blended Portland Fly Ash Cement." *ACI Special Publication 242,* American Concrete Institute, Farmington Hills, MI, 303-320.

Bouzoubaa, N., Zhang, M. H., Malhotra, V. M., and Golden, D. M. (2001). Mechanical Properties and Durability of Laboratory Produced High-Volume Fly Ash Blended Cements. *ACI Special Publication 199,* American Concrete Institute, Farmington Hills, MI, 55-82.

Domone, P. (2007). A review of hardened mechanical properties of self-compacting concrete. *Cement and Concrete Composites, 29(1),* 1-12.

Frosch, R. and Wolf, T. (2003). *Simplified Shear Design of Prestressed Concrete Members (*Report FHWA/IN/JTRP-2003/5). Purdue University, West Lafayette, Indiana.

Galeota, D., Giammatteo, M. and Marino, R. (1995). Structural Concrete Incorporating High Volume of Fly Ash. *ACI Special Publication 153,* American Concrete Institute, Farmington Hills, MI, 25-42.

Hassan, A., Hossain, K., and Lachemi, M. (2010). Strength, cracking and deflection performance of large-scale self-consolidating concrete beams subjected to shear failure. *Engineering Structures, 32,* 1262-1271.

Hernandez, E., Galati, N., Myers, J. and Nanni, A. (2006), Long-term monitoring of bridges using a robotic tacheometry system. *Proceeding for the 2006 NDE Conference on Civil Engineering, 113-120*.

Hwang, S., Khayat, K. H., and Bonneau, O. (2006). Performance-based specifications of self-consolidating concrete used in structural applications. *ACI Material Journal, 103(2),* 121-129.

Khayat, K. H., and Mitchell, D. (2009); "Self-Consolidating Concrete for Precast, Prestressed Concrete Bridge Elements." National Cooperative Highway Research Program Report No. 628 (NCHRP 628), *Transportation Research Board*, Washington, DC.

Kim, Y., Hueste, M., Trejo, D. and Cline, D. (2010). Shear characteristics and design for high-strength self-consolidating concrete. *ASCE Journal of Structural Engineering, 136 (8),* 989-1000.

Lachemi, M., Hossain, K., and Lambros, V. (2005). Shear resistance f self-consolidating concrete beams – experimental investigations. *Canadian Journal of Civil Engineering, 32(6),* 1103-1113.

Laplante, P., Aifcin, P.C., and Vezina (1991). Abrasion resistance of concrete. *Journal of Materials in Civil Engineering, 3(1),* 19-30.

Lin, C. and Chen, J. (2012). Shear behavior of self-consolidating concrete beams. *ACI Structural Journal, 109(3),* 307-315.

Long, W., Khayat, K. H., and Hwang, S (2013). Mechanical properties of prestressed self-consolidating concrete. *Materials and Structures, 46,* 1473-1487.

McSaveney, L., Papworth, F., and Khrapko, M. (2011). Self-Compacting Concrete for Superior Marine Durability and Sustainability. *Concrete in Australia, 37(2),* 69-64.

Mehta, P., and Montiero, P. J. (1993). *Concrete Microstructure, Properties, and Materials*. McGraw-Hill.

Mindess, S., Young, J. F., Darwin, D. (2003). "*Concrete-Second Edition*." Prentice Hall, Upper Saddle River, New Jersey.

Missouri Department of Transportation (MoDOT) (2011). "Engineering Policy Guide, Category 751 LRFD Bridge Design Guidelines." MoDOT, Jefferson City, Missouri.

Myers, J. and Bloch, K. (2011) Accelerated Construction for Pedestrian Bridges: A Comparison between High Strength Concrete (HSC) and High-Strength Self Consolidating Concrete (HS-SCC). *Design, Construction, Rehabilitation, and Maintenance of Bridges*: 129-136. doi: 10.1061/47630(409)17.

Myers, J., and Carrasquillo, R. (1998). *Production and Quality Control of High Performance Concrete in Texas Bridge Structures (*Report 9-580/589-1). University of Texas at Austin, Austin, Texas.

Myers, J. J., and Hernandez, E. S. (2014). *"Implementation of Radio Frequency Identification (RFID) Sensors for Monitoring of Bridge Deck Corrosion in Missouri." Retrieved May 5, 2014, from* http://transportation.mst.edu/media/research/transportation/documents/R351%20Final%20Report.pdf.

Myers, J., Volz, J., Sells, E., Porterfield, K., Looney, T., Tucker, B., and Holman, K. (2012). *Self-Consolidating Concrete (SCC) for Infrastructure Elements*, (Report cmr 13-003). Missouri University of Science and Technology, Rolla, Missouri.

Nagi, M. and Whiting, D. (1994). "Determination of water content of fresh concrete using a microwave oven." *Cement, Concrete and Aggregates, 16(2),* 125-131.

Naik, T. R., Ramme, B. W., Krauss, R. N., and Siddique, R. (2003). "Long-term performance of high-volume fly ash concrete pavements." *ACI Materials Journal, 100(2)*, 150-155.

Naik, T. R., Ramme, B. W., and Tews, J. H. (1995). "Pavement construction with high-volume Class C and Class F fly ash concrete." *ACI Materials Journal, 92(2),* 200-210.

Nanni, A., "Abrasion resistance of roller compacted concrete", *ACI Materials Journal, 86(53)*, 1989, 559-565 pp.

Okamura, H. and Ouchi, M. (2003). Self-compacting concrete. *Journal of Advanced Concrete Technology, 1(1)*, 5-15.

Ouchi, M., Nakamura, S., Osterberg, T., Hallberg, S., and Lwin, M. (2003). "Applications of Self-Compacting Concrete in Japan, Europe, and the United States." Federal Highway Administration. ISHPC.

Pauw, A. (1960). Static modulus of elasticity of concrete as affected by density. *Journal of the American Concrete Institute, 32(6)*, 769-687.

Reiner, M. and Rens, K. (2006). High-volume fly ash concrete: Analysis and application. *Practice Periodical on Structural Design and Construction, 11(1)*, 58-64.

Rivets, M., Bouzoubaa, N., and Malhotra, V. (2004). Strength development and temperature rise in high-volume fly ash and slag concretes in large experimental monoliths." *ACI Special Publication 221*, 859-878.

Sells, E. (2012). "Self-Consolidating Concrete for Infrastructure Elements Shear Characterization." Master's Thesis, Civil Engineering, Missouri University of Science and Technology, Rolla, Missouri.

Stark, D. (1989). "Durability of Concrete in Sulfate-Rich Soils," Research and Development Bulletin RD097, Portland Cement Association, Skokie, Illinois, 14.

Tadros, M.K.; Al-Omaishi, N.; Seguirant, S.J.; and Gallt, J.G. (2003). *Prestress Losses in Pretensioned High-Strength Concrete Bridge Girders*, National Cooperative Highway Research Program Report 496 (NCHRP 496). Transportation Research Board, National Research Council, Washington, DC.

Trejo, D., Hueste, M., Kim, Y., and Atahan, H. (2008). *Characterization of Self-Consolidating Concrete for Design of Precast Prestressed Bridge Girders* (Report 0-5134-2). Texas A&M University, College Station, Texas.

Vecchio, F., and Collins, M. (1986). The modified compression-field theory for reinforced concrete elements subjected to shear. *ACI Journal, 83(2)*, 219-231.

Volz, J., Myers, J., Richardson, D., Arezoumandi, M., Beckemeier, K., Davis, D., Tucker, B. (2012). *Design and Evaluation of High-Volume Fly Ash (HVFA) Concrete Mixes* (Report cmr 13-008). Missouri University of Science and Technology, Rolla, Missouri.

Wang, H., Qi, C., Farzam, H., and Turici, J. (2006). Interaction of materials used in concrete. *Concrete International, 28(4)*, 47-52.

Wang, K. (2006a). "Monitoring Heat Evolution of Concrete Mixtures." *National Concrete Pavement Technology Center. Retrieved July 1, 2014, from* http://www.intrans.iastate.edu/publications/_documents/t2summaries/calorimetry.pdf.

Wei Sun, Ru Mu, Xin Luo, Changwen Miao, (2002). Effect of chloride salt, freeze-thaw cycling and externally applied load on the performance of the concrete, *Cement and Concrete Research, 32,* 1859-1864.

Wight, K. and MacGregor, J. (6^{th} Ed.). (2005). Reinforced *Concrete Mechanics and Design*. Upper Saddle River, New Jersey: Pearson Education, Inc.